AEC RESEARCH AND DEVELOPMENT REPORT

HW-73337
0.44

RESEARCH AND DEVELOPMENT ACTIVITIES IN THE RADIOLOGICAL SCIENCES

PHYSICAL SCIENCES PORTION

JANUARY THROUGH DECEMBER, 1961

Edited by

R. L. JUNKINS and J. E. BROWN

JANUARY 15, 1962

HANFORD LABORATORIES

HANFORD ATOMIC PRODUCTS OPERATION
RICHLAND, WASHINGTON

GENERAL ELECTRIC

HW-73337

UC-48, Biology and Medicine
(TID-4500, 18th Ed.)

RESEARCH AND DEVELOPMENT ACTIVITIES IN THE RADIOLOGICAL SCIENCES

Physical Sciences Portion

January Through December, 1961

By

Staff Members of
Hanford Laboratories Operation

Edited by

R. L. Junkins and J. E. Brown

January 15, 1962

FIRST UNRESTRICTED DISTRIBUTION MADE JAN 2 '63

HANFORD ATOMIC PRODUCTS OPERATION
RICHLAND, WASHINGTON

Work performed under Contract No. AT(45-1)-1350 between the Atomic Energy Commission and General Electric Company

Printed by/for the U. S. Atomic Energy Commission

Printed in USA. Price $4.00. Available from the

Office of Technical Services
Department of Commerce
Washington 25, D. C.

TABLE OF CONTENTS

Page

Page

Page

Page

RESEARCH AND DEVELOPMENT ACTIVITIES IN THE RADIOLOGICAL SCIENCES

ATMOSPHERIC PHYSICS

Atmospheric Diffusion and Transport - C. L. Simpson, C. E. Elderkin, J. J. Fuquay, P. W. Nickola, and M. F. Scoggins

Dispersion data, which heretofore had not stratified according to customary meteorological variables, were found to separate into two groups according to the presence or absence of wind direction trend. Whether the dispersion arises primarily from diffusion or from meander depends on the spectrum of eddy sizes relative to the plume dimensions. Eddies smaller than the plume dimensions cause the diffusion while the larger eddies only contribute to meander. Within the first 2 miles of travel, the meander effect became less significant and, as the distance increased, the increased plume dimensions embraced larger and larger eddies. At 16 miles, the difference in the mean width between the plume initially dominated by diffusion and the mean width of the plume initially dominated by meander is very small, although within 2 miles from the source their widths differed by a factor of two.

A diffusion model which accounts for the wind direction shear with height in the lower layers of the atmosphere is described. The shearing effect is evident from both visual observation of tracer plumes and from exposure data gathered from many experiments. Dosage measurements made on the cylindrical surface formed by the vertical and horizontal sampling grids at a given arc distance were found to exhibit maxima in the vertical which changed in height with azimuth angle. The line joining peak dosages sloped upwards to the right or left depending upon the sense of the wind direction shear. To account for the tilted appearance of the observed isolines, a normal frequency function of two variables is hypothesized, with correlation between the horizontal and vertical positions of the particles on the surface.

Micrometeorological research has continued on problems associated with predicting the dosage levels and concentrations in the environment of contaminant materials released to the atmosphere. Results of these studies not only provide insight into the basic processes of diffusion and deposition in the lower atmosphere, but also provide important information applicable

to immediate practical problems such as (1) determination of the effort required to ensure adequate containment of fission products through examination of the hazards produced by their release to the atmosphere and (2) evaluation of potential hazards resulting from planned or accidental release of radioactive material to the air. A particularly significant application of the research findings was the evaluation of the hazards of shipping gross quantities of radionuclides to various locations in the country.

Field experiments on the dispersion and deposition of materials released to the atmosphere have continued, extending the measurements over greater ranges of wind speed and atmospheric stability. The Hanford sampling grids and the general methodology of experimentation were reported last year.[1] In addition to the Hanford diffusion experiments, support of field trials by the Air Force Geophysical Research Laboratories has permitted extensive studies of the diffusive properties at Cape Canaveral, Florida, and Vandenberg Air Force Base, California. These latter studies have provided data on diffusion in the East coast sea breeze regime and the rugged coastal region of the Pacific coast which will supplement the Hanford data for determining the effect of vegetation, terrain, and climatological regimes on the diffusion patterns.

The Hanford data were analyzed for diffusion characteristics according to the Gaussian model.[1] As had been found in previous studies, power function relationships for the increase of lateral dispersion and decrease of maximum exposure with distance represented the gross behavior of the data fairly well. However, contrary to simple theory, no vivid correlation between the over-all width of the plume and thermal stability was found in the early analyses. Figure 1 shows the plume width, represented by the standard deviation of the arcwise dosage distribution as a function of distance for selected experiments. Runs 5 and 15 from the Green Glow series are associated with very great thermal stability, but yet they represent the narrowest and broadest plumes, respectively, of the 26 tests of the series. Runs 41 and 45 were tests from the "30 series" conducted during very unstable daytime conditions and here again are very narrow and

broad plumes. The mean growth curves for both series are also shown and, in general, approximate a power function with a slope near 0.85, although there is some evidence to support curvature in the region between 3200 meters and 12,800 meters where a marked elevation change with irregular topography existed.

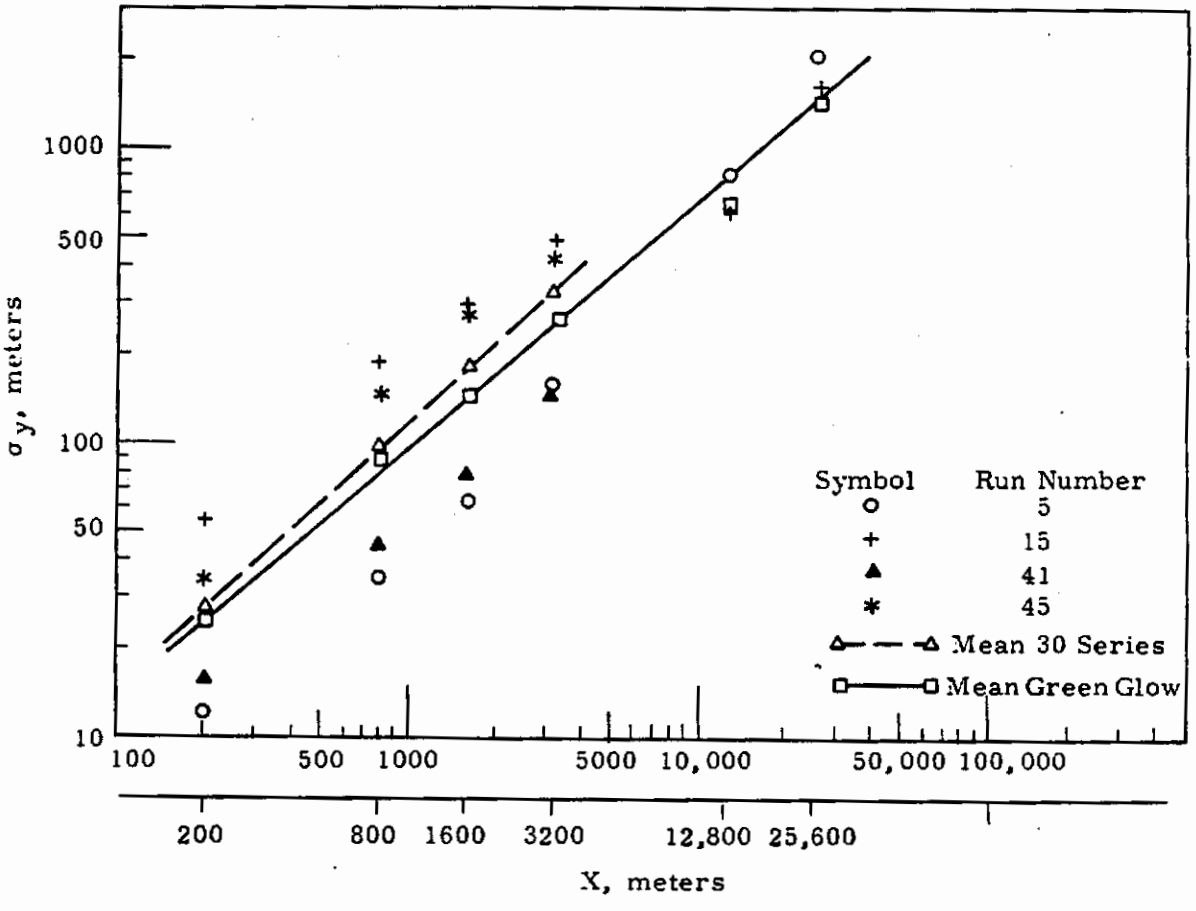

FIGURE 1

Horizontal Plume Growth as a Function of Distance for Selected Green Glow and 30 Series Runs and for the Mean of all Green Glow and 30 Series Runs

Since the data clearly demonstrate that knowledge of thermal stability alone is insufficient for prediction of the time mean plume width, a serial analysis of the wind was examined for the existence of trends and cycles. Figure 2 shows the standard deviation plotted as before as a function of distance from the source. Here, however, some stratification of the data is obtained with the defining of two subclasses. The open circle points are Green Glow and "30 series" tests associated with winds characterized by meander or trend, whereas the plus points are runs that were conducted under fairly steady state conditions. Analytically, this determination was made by computing the standard deviation of the 20-second averages of the wind directions observed at 2 meters through the one-half hour period of tracer release. The direction standard deviation, $\sigma(A)$ degrees, of 6 degrees appeared to differentiate the two classes.

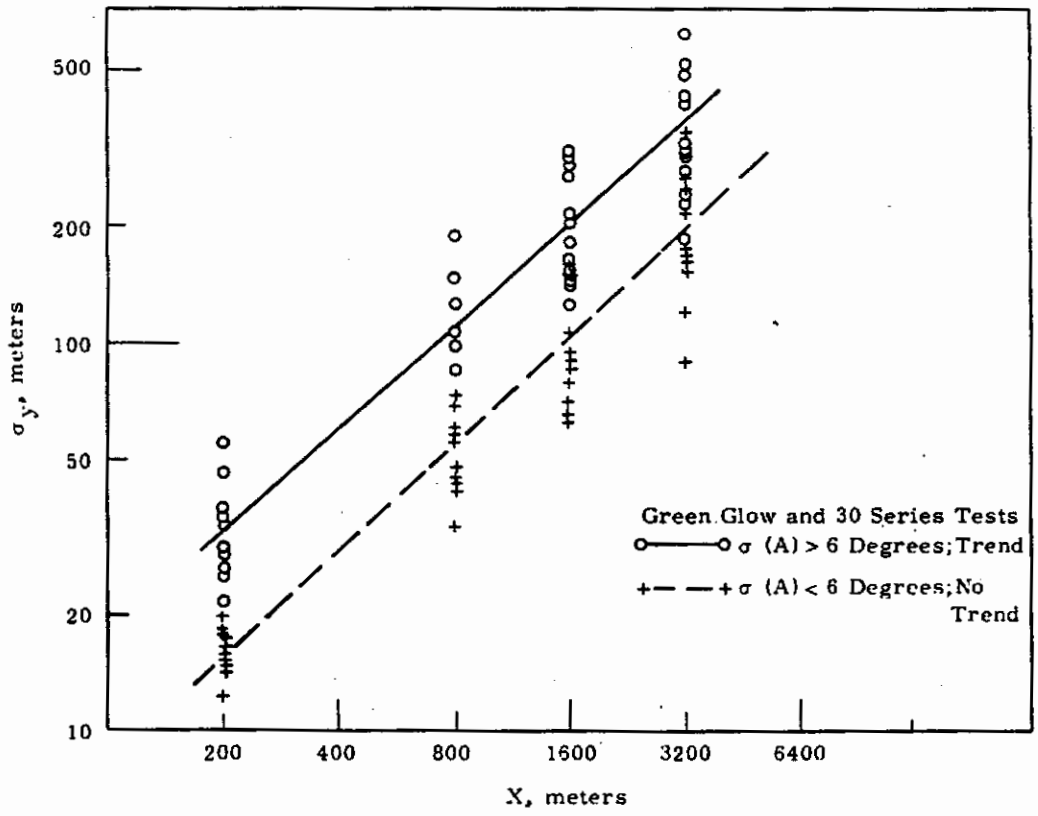

FIGURE 2

Horizontal Plume Growth as a Function of Distance and the Standard Deviation of the Surface Wind Direction over a 30 Minute Period for Green Glow and 30 Series Runs

The dispersion of the time mean plume generated from a continuous point source, as measured by our experimental technique, is the result of both diffusion and transport of the "instantaneous" plume elements. Whether the dispersion arises primarily from diffusion or from meander depends on the spectrum of turbulent eddy sizes relative to the plume dimensions; eddies smaller than the plume dimensions cause the diffusion while the larger eddies only contribute to meander. Within the first 2 miles of travel, the meander effect became less significant as the distance increased, so the increased plume dimensions embraced larger and larger eddies. The result was that at 16 miles the difference in the mean width between the plume initially dominated by diffusion and the mean width of the plume initially dominated by meander was very small, although within 2 miles of the source their widths differed by a factor of two.

In a large number of the diffusion experiments conducted at Hanford during very strong temperature inversions, it was found that the vertical distributions of tracer dosage deviated considerably from theoretical expectations. Competitive mechanisms of deposition on the surface and vegetation, vertical diffusion, and wind shear resulted in a characteristic maximum above ground. In addition, the wind direction shear with height resulted in greater horizontal diffusion and a sloping axis of the maximum in the vertical, when compared with less stable experiments.

In a homogeneous, turbulent medium, one would expect that isolines of dosage in a vertical plane perpendicular to the mean flow would be an ellipse, with the axes horizontal and vertical. To account for the tilted appearance of the observed isolines, it was hypothesized that the dosage in the cylindrical surface formed by the horizontal and vertical sampling grids at a given arc distance was given by the normal frequency function of two variables, with correlation between the horizontal and vertical positions of the particles on the cylinder. The fundamental equation may be written as follows:[2]

$$D(z, y) = \frac{\exp\left\{-\frac{1}{2(1-\rho^2)}\left[\left(\frac{y'}{\sigma_y}\right)^2 - \frac{2\rho y' z'}{\sigma_y \sigma_z} + \left(\frac{z'}{\sigma_z}\right)^2\right]\right\}}{2\pi\sigma_y\sigma_z\sqrt{1-\rho^2}} \quad (1)$$

where D is the dosage;

y and z are the lateral and vertical coordinates in the cylindrical surface, respectively,

y' and z' are deviations from the respective mean values y and z,

ρ is the correlation coefficient between the y and z positions of the particles on the cylinder, and

σ_y and σ_z are the respective standard deviations of dosage.

For $\rho \neq 0$ the axis of the elliptical isolines of dosages are inclined with respect to the horizontal. When the correlation is zero, the model becomes the conventional diffusion formula.

The conditional distribution at a fixed value of y, say at a tower location, is given by

$$D\,\frac{z}{y} = \frac{\left\{\exp -\frac{1}{2}\left[z' - \rho\,\frac{\sigma_z}{\sigma_y}\,y'\right]^2\right\}}{\sqrt{2\pi}\,\sigma_z\sqrt{1-\rho^2}} . \quad (2)$$

This expression shows that the vertical distribution at a fixed y has a mean

$$\overline{z'} = \rho\,\frac{\sigma_z}{\sigma_y}\,y' \quad (3)$$

and represents the locus of all mean values of z'. This line is referred to as the regression line. The standard deviation of the conditional vertical distribution is given by

$$\sigma_z^* = \sigma_z\sqrt{1 - \rho^2} \tag{4}$$

and that of the horizontal distribution by

$$\sigma_y^* = \sigma_y\sqrt{1 - \rho^2} \ . \tag{5}$$

Table I summarizes the values of the model parameters found in one experiment. H is the estimated height of maximum dosage on each tower.

TABLE I

VALUES OF MODEL PARAMETERS

Arc Arc Distance (m)	Tower Tower	σ_z^* (m)	σ_y^* (m)	$\rho\frac{\sigma_z}{\sigma_y}$ (Slope)	ρ	σ_z (m)	σ_y (m)	H (m)
200	3							2.8
	4	6.9	19.1	0.059	0.16	7.0	19.3	4.5
	5	6.1						6.1
800	3							
	4	11.5	52.4	0.047	0.21	11.8	53.6	4.5
	5	9.0						11.6
1600	3	9.5						2.8
	4	14.1	85.7	0.041	0.25	14.6	88.5	10.0
	5	9.4						21.0
3200	3	12.4						1:55
	4	10.4	153.0	0.053	0.78	16.6	244.0	20.0
	5	12.1						49.0

The model realistically describes the distributions observed on the vertical sampling surface during the experiment. The parameters which define the distribution are a direct consequence of the cross-correlations

of the velocity fluctuations and, therefore, have a fundamental basis. Investigation, continuing with this model and utilizing other experimental data, will include deposition effects as they become clearer.

Deposition of Airborne Materials - C. L. Simpson, J. J. Fuquay, and M. F. Scoggins

Results of recent deposition experiments at Hanford are summarized along with a general introduction to the deposition problem. Deposition of ZnS tracer material was determined by calculating the mass of tracer material that passed through successive vertical surfaces downwind of the release point near ground level and attributing the loss of material to deposition. The fraction of the released mass that was deposited within 3200 meters of travel ranged from 80 to 97 percent in the four stable experiments analyzed. A method for determining the deposition by direct measurement on vegetation is described and results of a deposition study over cheat grass are presented.

Matter that is being transported and dispersed by the atmosphere in the vicinity of a surface (the ground, vegetation, or a building) may actually deposit and remain on the surface long after the transient cloud has passed. This process will lower the concentration of matter remaining in the air and must be accounted for if reasonable results are to be derived from diffusion models. For small particles and vapors, deposition during nonprecipitation conditions is believed to be limited by the meteorological parameters which define the diffusion in the atmosphere, and the processes of impaction and sticking to objects on the ground, rather than by the settling of particles through the influence of gravity. Particles brought through the boundary layer to the ground by the turbulent diffusion process deposit on vegetation or other objects by inertial impaction and diffusion and stick by electrostatic forces, chemical attraction, or other means.

Chamberlain[3] recognized the significance of the deposition process in reactor accident calculations and has contributed considerably to the understanding of all processes that lead to the removal of particulates from the air. He also has taken the first steps to modify Sutton's[4] diffusion equations to account for deposition. Fuquay[5] again points to this problem with the general Gaussian dispersion formula, accounting for the scavenging effects in the manner of Chamberlain, and gives experimental values of

parameters obtained at Hanford and in Great Britain. Healy[6] has incorporated the latter developments in his calculations of environmental consequences of reactor accidents. These results indicate that deposition can have a significant effect on the dispersion of particulates in the atmosphere, and further estimates of the magnitude of that effect are needed. More recent deposition experiments have been conducted at Hanford and the results of these were reported by Simpson[7] and will be summarized here, along with some later data.

Deposition of ZnS particulate tracer material was determined by calculating the mass of tracer material that passed through successive vertical surfaces downwind of the release point, and attributing any loss of material to deposition. The total flux through a given vertical surface can be represented by the equation of continuity and solved for the deposition as follows:

$$\text{Total Deposition} = Q_t - \int_0^T \int_{-\infty}^{\infty} \int_{-\infty}^{\infty} \overline{U X}\, dy\, dz\, dt \qquad (1)$$

where Q_t is the total amount of material released,
U is the ambient wind speed,
X is the ambient concentration,
T is the duration of the experiment, and
y and z are the horizontal and vertical coordinates of the surface, respectively.
The bar represents the average value.

The value of the triple integral is determined approximately from total dosage or exposure measurements on the sampling grid described earlier.[1] Exposure, E, is defined here as the product of the average concentration and the time duration of release. Four experiments in the Green Glow series were selected for analysis on the basis of having fairly well defined vertical and horizontal distributions of exposure to 3200 meters distance from the source. Because the sampling towers were only 62 meters high, all four experiments necessarily utilized ground sources during stable atmospheric conditions so the plume would be

completely contained. A detailed description of the sampling grids, supporting meteorological measurements, and exposure data tabulations can be found in references 8 and 9.

Isopleths of exposure multiplied by the wind speed, $E\ \overline{U}$ (g m^{-2}), were drawn for each of the four vertical surfaces defined by the horizontal and vertical sampling grids, and the area inclosed between isopleths was measured with a planimeter. The product of $E\ \overline{U}$ and the Area gives the mass of material transported, and when summed for the entire cross-section, yields the total mass transported. Results of the analysis are summarized in Table II, where the subscript on Q indicates the distance from the source to the sampling surface. Q_o (grams) is the total mass released from the source during the 1/2 hour emission period.

TABLE II

INTEGRATED MASS FOR SUCCESSIVE VERTICAL SURFACES

Experiment Run No.	Q_o	Q_{200}	Q_{800}	Q_{1600}	Q_{3200}
1	1728	1228	914	599	339
2	1699	1381	1021	---	381
3	3173	1742	1427	1070	520
4	3420	1872	516	249	118

Run 4, characterized by extreme stability, has deposited 97 percent of its source mass within 3200 meters. Run 3, also very stable, shows heavy deposition, but the rate is less than that of Run 4 beyond 200 meters. Runs 1 and 2 show the least deposition (moderately stable), but even so, 80 percent of the initial mass has been removed and deposited. The settling rate of ZnS tracer is negligible, so these figures represent only deposition brought about by turbulent diffusion carrying the particles to the vegetation and soil.

The results indicate that the rate of deposition is dependent on the height of the plume above ground. The height of release of the particles from the dispenser was 0.5 meter, but the effective height determined by

both visual observations of the vapor near the point of release and examination of vertical cross-sections indicates there is a relationship between plume height, wind speed, and stability. The plume height has a very significant effect on prediction of deposition; the height varies with distance, oftentimes in a most irregular manner as shown in Table III.

TABLE III

PLUME HEIGHT AS A FUNCTION OF DISTANCE (METERS)

	Distance			
Run Number	200	800	1600	3200
1	0.6	2.0	5.0	6.0
2	0.8	1.0	1.2	12.0
3	0.8	3.7	3.7	4.0
4	0.5	0.5	0.5	0.5

The effect of the plume rising as it travels downwind is evident in a comparison of Runs 2 and 4. The plume height of Run 4 remained constant and deposition proceeded in a regular manner. On the other hand, the plume of Run 3 continued to ascend, resulting in a decreased rate of deposition with distance.

Prediction of the distribution of exposure at downwind points was attempted, using the Gaussian interpolation formula, modified to account for deposition. The crosswind dispersion parameters, σ_y^2, were computed directly from exposure data. However, the vertical variance, σ_z^2, could not be computed directly from observations, because the derivation requires values determined in the absence of deposition. Therefore, σ_z^2 was determined from the derived mass flux and exchange coefficient principles. (See section on Vertical Exchange Coefficients.) Values of the computed and observed centerline exposure are shown in Table IV for three experiments.

TABLE IV

OBSERVED AND CALCULATED PEAK EXPOSURES
($g\ sec\ m^{-3}$)

Run Number		Distance from Source (meters) 200	800	1600	3200
1	Calculated	2.90	0.53	0.15	0.026
	Observed	1.70	0.24	0.090	0.021
2	Calculated	1.15	0.19	0.074	0.021
	Observed	1.40	0.21	0.067	0.013
3	Calculated	5.17	0.31	0.057	0.011
	Observed	4.88	0.24	0.055	0.012

Run 4 was unique in that the plume height was invariant with distance, providing a classical check on the formulation of the problem. Parameters derived from data taken within 3200 meters of the source were used to extend the calculations to 12,800 meters' distance. Results of this extension are compared with observed values in Table V.

TABLE V

OBSERVED AND CALCULATED EXPOSURES FOR RUN 4
($g\ sec\ m^{-3}$)

Distance (meters)	Calculated Maximum	Observed Maximum
200	4.32	4.87
800	0.33	0.24
1600	0.059	0.055
3200	0.0093	0.012
12800	0.000021	0.000016

The agreement between predicted and observed values in this instance is encouraging, in light of the large extension involved.

Returning to Equation (1), the term under the integral represents the total flux through the vertical surface, and is made up of a mean flux,

plus an eddy flux given by

$$\overline{U X} = \overline{U}\,\overline{X} + \overline{U' X'} \quad . \tag{2}$$

where the primed quantities represent deviations from the mean values. The eddy flux is due to the turbulent transfer of material in the downwind direction. Experimentally, we have deduced the average concentration and average wind speed, and have so far determined the mean flux, $\overline{U}\,\overline{X}$. Estimates of the eddy flux, $\overline{U' X'}$, by various investigators have ranged from negligible to possibly as high as 20 percent of the mean flux. Consequently, in the absence of eddy flux measurements, deposition determined by mean flux calculations can only be tentative.

In order to substantiate the earlier findings, a direct determination of the amount of material deposited on the surface was attempted. Such measurements are difficult because of the sampling problem introduced by the character of the surface itself. At Hanford, the surface consists of a variety of bushes and grasses of varying thickness and height. Furthermore, the vegetative cover is not uniform, but heterogeneously dispersed with intervening sand. To simplify the vegetation sampling problem, a flat field uniformly and densely covered with dry cheat grass was selected over which to conduct a deposition experiment. The grass was about 30 cm in height and resembled a wheat field, with only small areas of earth exposed between stalks. Actually, the ground surface was covered with cheat burrs that had fallen from the plants and matted to form a surface that could easily be removed from the soil surface.

The experiment was conducted in the same manner as other Hanford experiments. A continuous plume of ZnS particles was dispersed for 1/2 hour over the grid during stable atmospheric conditions. Samples of grass were then taken at specified grid points along arcs at distances of 10, 50, 100, and 200 meters from the source. At each sampling point, all the grass within a unit area was removed and chopped in a container. A second sample was obtained at the grid point by carefully scraping the matted burrs from the ground surface and placing them in a second container. Over 100 samples were taken, to yield the density distribution of grass in the field.

Smaller samples were extracted from these and analyzed for ZnS. The method of analysis is reported in the Radiological Chemistry section of this document (J. D. Ludwick, page 137).

The mass of ZnS determined for the mat under surface was added to the mass determined for the grass to yield the total mass per unit area at each grid point. In general, the matted burrs contained an order of magnitude less tracer than the standing grass. With the mass distribution represented graphically, isopleths of deposition ($g\ m^{-2}$) were drawn and the area inclosed within isopleths measured, to determine the total mass deposited. Integration to a distance of 100 meters from the source showed that 22 percent of the initial release had been deposited on the vegetation. Integration beyond 200 meters was not possible because the 200 meter samples had masses too near the background to be significant.

The magnitude of the deposition measured on the vegetation agrees with that determined from the earlier flux measurements, which showed about 20 percent deposited in 100 meters of travel. Deposition velocities taken from the ratio of exposure values obtained from air samples at 1 meter height and deposition per unit area below the sample varied between 0.5 and 1.0 cm/sec, only slightly lower than those calculated from flux considerations.

Vertical Exchange Coefficients and the Vertical Flux of Matter - C. L. Simpson, J. J. Fuquay, and C. E. Elderkin

A method is described for determining vertical exchange coefficients for matter in the surface layer of the atmosphere by using results of diffusion and deposition experiments. Exchange coefficients for matter determined from Hanford experiments are compared to coefficients for heat, momentum, and water vapor found by other investigators. The Hanford data, based on the flux of particulate matter, are in the region of high stability values obtained by other investigators and two of the points are associated with higher stability than previously reported in the literature. The general relation inferred from the combined data is maintained by the Hanford data into the higher stabilities.

Results of diffusion and deposition experiments can be used to determine vertical exchange coefficients for matter in the surface layer of the atmosphere. The exchange coefficients can then be compared to those

derived by other investigators and can thereby determine if the deposition results are reasonable. It must be remembered that the Hanford results are for particulate matter, whereas the other investigations deal with heat, momentum, and water vapor.

Assuming steady state conditions, it has been shown[4] that the mean flux of matter (per unit area per unit time) through a plane parallel to a horizontal surface is directly proportional to the concentration gradient.

$$\text{Mean Flux} = K_m \frac{\partial \bar{X}}{\partial z} \tag{1}$$

where $\bar{X}$ is the mean concentration and K_m is the vertical exchange coefficient for matter. In integrating Equation (1) over the period of the experiment, the assumption that K_m is invariant with time yields

$$\frac{\text{Mean Mass Transport}}{\text{Unit Area}} = K_m \frac{\partial E}{\partial z} \tag{2}$$

If Equation (2), in turn, is integrated over θ, degrees azimuth along a sampling arc, the result is the total mass transport through a strip of 1 meter width, in the downwind direction, x, which parallels an arc, is proportional to the gradient of exposure averaged over the arc times the arc length L, or

$$\text{Total Vertical Mass Transport} = K_m \frac{\partial E}{\partial z} L. \tag{3}$$

Rearranging terms, the exchange coefficient is defined as

$$K_m = \frac{\text{Total Vertical Mass Transport}}{L \frac{\overline{\partial E}}{\partial z}}, \tag{4}$$

taking the surface where K_m is defined to be the average height of the desert vegetation, 1 meter. Assuming the vegetation is a perfect sink, this is equivalent to equating the downward flux to deposition at the surface 1 meter above ground. Then the total arc-wise flux per unit distance (x) at 1 meter is equal to $\frac{\partial Q}{\partial x}$, the mass of particulate deposited per unit length (x) integrated over the azimuth (θ) as determined from the deposition data. $\frac{\overline{\partial E}}{\partial z}$ is the

average vertical gradient over the same arc, as determined from exposure data. Values of K_m are listed in Table VI, along with other parameters to be explained later.

Priestly[10] has summarized the results of several determinations of exchange coefficients and their relation to atmospheric stability as determined from the Richardson Number, R_i. So that independent investigations can be compared, the effects of the height at which the measurement was obtained and the characteristics of the wind have been removed by defining the dimensionless quantity

$$K^* = \frac{K_m}{U^* Z} \tag{5}$$

where K_m is the exchange coefficient, U^* is the frictional velocity, and Z is the height of the surface considered. Figure 3, which has been extracted from Priestly's book, gives the results obtained by Rider[11] from stress measurements with a floating plate, by Swinbank[12] from gustiness components and humidity fluctuations measured at 1.5 meters with a hot wire anemometer, and by Cramer and Record[13] from gustiness measurements with a bivane and hot wire anemometer. The solid line is an empirical fitted curve to Swinbank's data as given by Holzman. Added to the graph are the four Hanford calculations from mass considerations.

TABLE VI

SUMMARY OF OBSERVED AND CALCULATED STATISTICS OF SELECTED STABLE EXPERIMENTS

	Run Number			
	1	2	3	4
$K_m \left(\frac{m^2}{sec}\right)$	0.1235	0.0343	0.0343	0.0501
$U^* \left(\frac{m}{sec}\right)$	0.378	0.398	0.473	0.468
K^*	0.327	0.354	0.073	0.107
R_i (1.5-3.0 m)	0.046	0.095	0.139	0.223
Z_o (m)	0.330	0.246	0.467	0.467

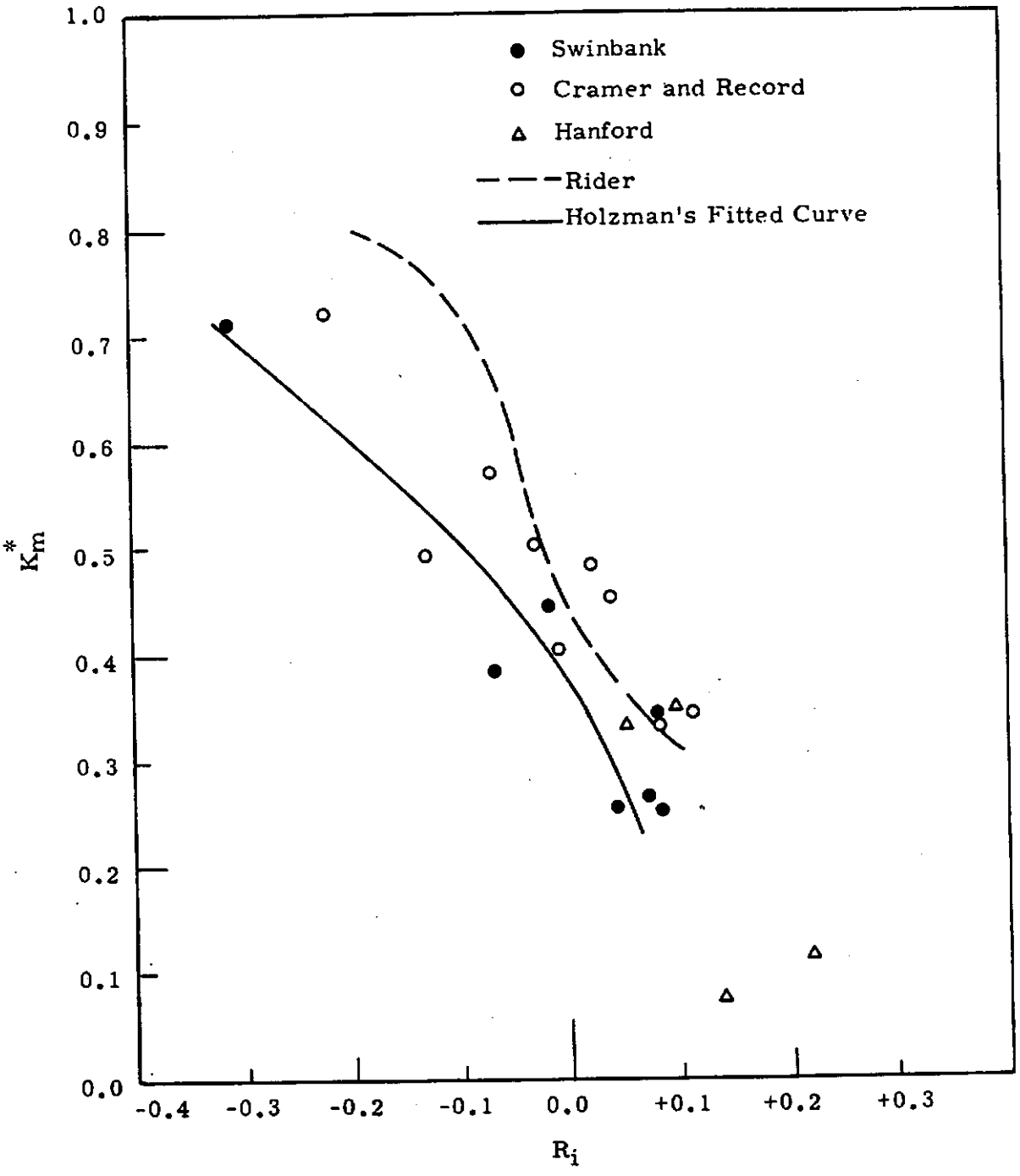

FIGURE 3

Dependence of the Exchange Coefficient on Atmosphere Stability

AEC-GE RICHLAND, WASH.

The parameters U* and R_i are very sensitive to the height and height interval over which they are derived. So that the Hanford data might be directly comparable to other data, the height intervals were chosen to be as close as possible to the others. In evaluation of U*, the Deacon profile was assumed in the interval 1.5 to 8 meters, whereas the reference heights for the computation of the Richardson Number were 1.5 and 3.0 meters. These derived values are listed in Table VI, along with Z_o, the roughness parameter.

The Hanford data, based on the flux of particulate matter, lie in the region of high stability values obtained by other investigators and two of these points are associated with higher stability than previously represented. The general relation inferred from the combined data is maintained by the Hanford data into the higher stabilities.

Precipitation Scavenging Processes - R. J. Engelmann and J. J. Fuquay

The probable mechanisms by which microscopic particles are scavenged from the air are reviewed. It is concluded that the interception process can be studied using tracer techniques and equipment already available at Hanford. Data collected at Hanford are compared with the theoretical collection efficiencies predicted by Langmuir's theory. Differences found between Langmuir's predictions, the Hanford data, and results reported by other investigators require further clarification. The raindrop sampler used in the Hanford experiments is described and raindrop spectra presented.

The cleansing of the air by rain is an everday experience, and it has been found that washout by rain accounts for most of the deposition of atomic bomb debris (except for the initial fallout). In an analysis of rain-scavenging of radioactive particulate matter from the atmosphere, Greenfield[14] found that the direct interaction of raindrops and particles does not account for the efficient removal of material whose diameter is below approximately 1 micron. However, he was able to explain the removal of smaller particles by allowing them to mix with the water cloud before the rain starts. The small particles that are scavenged by coagulation are then placed in a position to be more efficiently removed by the rain.

Our present knowledge is still inadequate to provide anything beyond a suggestion of the scavenging processes in the atmosphere for such finely

divided material as radioactive debris. Evidence from world-wide fallout studies suggests that the very small fission products become attached to the natural aerosol particles and then have a history in the atmosphere similar to that of the host. The time required for such a coalition to near completion is not known, but one would not expect it to be as rapid as the coagulation with larger water droplets because of the relative differences in mean free paths. Junge[15] suggests that the predominant cause of the modification in size-distribution of the stratospheric aerosols on the way down through the troposphere is the repeated cycle of condensation and evaporation of clouds, a process requiring considerable time. Thus, the scavenging mechanism for small particles is enivsaged as cloud-droplet-scavenging coupled with later scavenging of the cloud droplets by larger raindrops.[16] The amount of activity that will fall out as rain will depend upon the time of mixing of the contaminant and the cloud elements and the rate at which the cloud droplets are swept from the cloud by larger raindrops.

Calculations for precipitation scavenging of materials released in the lower layers of the atmospheres usually consider only a modified mechism of interaction between the falling raindrop and the contaminant particles. This aspect of the problem was studied by Chamberlain[3] using Langmuir's theory[17] of the formation of raindrops by coalescence with smaller raindrops and Best's relationship[18] between raindrop size and rainfall rate. However, the computed values correspond only approximately to the actual conditions, as the size of the drops always show a spectral distribution. Best's curve contains mean values. Large deviations from this curve are found in individual rains with the extreme range in rainfall rate for a given mean drop size about a factor of two. In addition, the Langmuir theory is applicable to coalescence of water drops, with certain restrictions, and particle interception could be quite different, depending on the physical and chemical nature of the particulate.

In an effort to clarify the scavenging process in the lower layers of the atmosphere, a part of the total scavenging problem, the feasibility of studying the rain scavenging process under field conditions was investigated

utilizing the Hanford Fluorescent Tracer Technique. Results of the study indicated that, since the scavenging efficiency of a raindrop is a function of drop size as well as the scavenged particulate size, the collection of individual droplets for assay of particulate content was preferable to the collection of bulk samples of mixed drop sizes. A light rainfall rate would be preferred to a heavier rate, simplifying the task of collecting single drops. Therefore, the low precipitation rates at Hanford seemed to be advantageous. Using calculated collection efficiencies and field measurements of particle concentrations from the diffusion experiments, it was determined that sufficient particles would be collected during a normal rain to permit analysis of individual drop content.

The raindrop sampler shown schematically in Figure 4 was developed to collect individual drops and permit determination of the particulate content of the drops. The drops are collected on a moving strip of Ozalid Diazo paper to provide time resolution of the drop collection. Each drop falling on the paper leaves a spot uniquely related to the drop's size. A tight box houses the chart-drive, hot air ducts for drying the collected drops, a developer section, and a filtered air source for reducing predevelopment contamination. Both the chart speed and the size of the rain entrance are adjustable, permitting satisfactory sampling over a range of rainfall rates. Toweling placed around the entrance nearly eliminates collection of splash-drops from outside the sampler, and water-soluble blue dye placed around the opening permits identification of drops that struck the edge of the sampler entrance upon entering. Dry deposition on the paper is reduced to a low value by introducing a small positive pressure in the entry chamber.

The Diazo paper used in the instrument has been calibrated for the drop size range 0.25 to 4.6 mm equivalent diameter.

The 95 percent confidence intervals for the logarithm of the drop diameter, given the spot diameter, are 0.918 and 1.091.

The general methodology of the experimentation is as follows. The tracer material is released upwind of a tower fitted with membrane filters. At the base of the tower the sampler collects raindrops, natural or artificial,

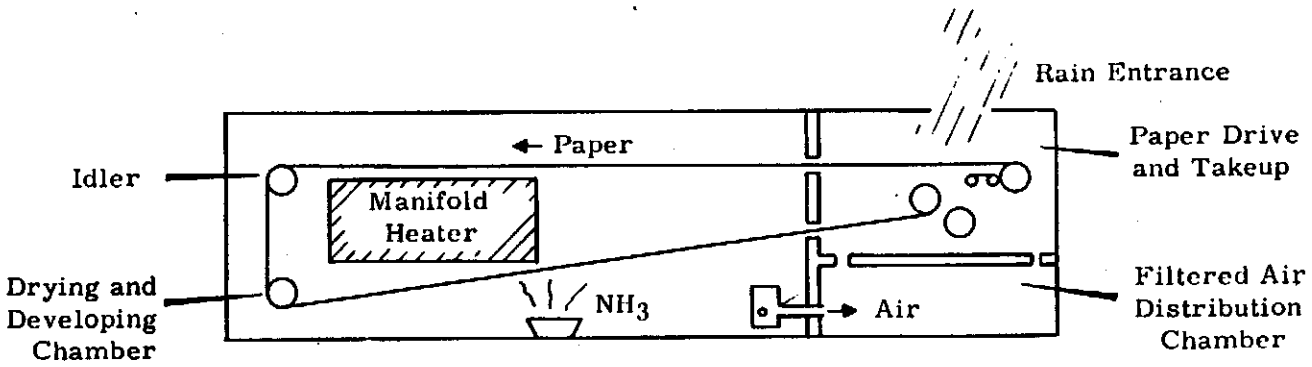

Side View, Side Removed

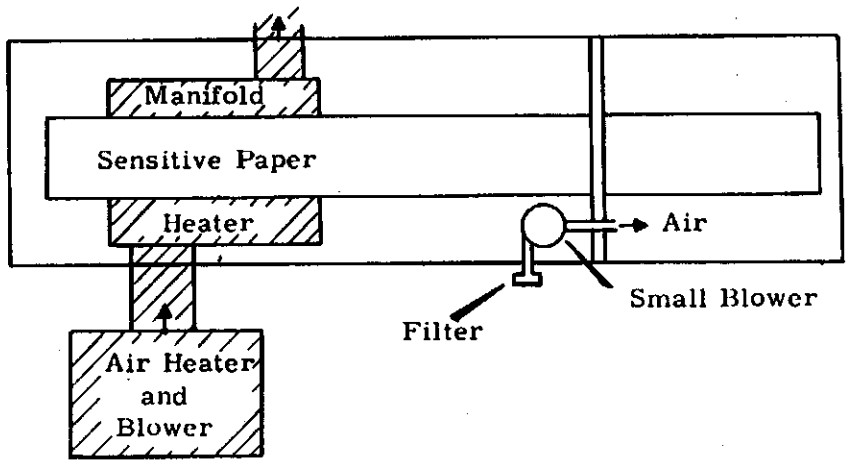

Top View, Cover Removed

FIGURE 4

Hanford Raindrop Sampler

that have fallen through the tracer plume. After termination of the release, the filters are assayed by microscope to determine the integrated concentration of tracer material through which the raindrops passed. The droplet diameter is determined by measuring the spot size on the Diazo paper. The number of scavenged tracer particles of a given size is obtained by counting the tracer particles within the drop autograph and correcting for background.

The efficiency with which a raindrop of a given size collects tracer particles of a given size is calculated as follows. The number of particles, N_d, collected by a raindrop in falling a distance, Δz, is given by the expression

$$N_d = E_d \frac{\pi d^2}{4} X \Delta z$$

where E_d is the scavenging efficiency of the drop for the particulate,
d is the diameter of the drop, and
X is the concentration of tracer of the given size in the drop path.

The data collected on the vertical sampling grid provides the time-integrated concentration, or dosage, rather than an instantaneous concentration is used and the equation is applied in the following form.

$$\overline{N}_d = E_d \frac{\pi d^2}{4} \frac{n}{F T} \int_o^z M \, d z$$

where n is the number of particles per unit mass of zinc sulfide,
F is the volumetric flow rate through the filter,
T is the time interval of tracer release,
M is the mass of zinc sulfide collected on the filter, and
z is the vertical coordinate.

Results of an early pilot-experiment indicated a peak collection efficiency for the ZnS tracer at a drop diameter somewhat below 0.8 mm. Kinzer and Cobb[19] have published data showing a maximum in collection efficiency for water drops in the range 0.2 to 0.4 mm when scavenging 4 to 10 micron water droplets. Such results are not in accord with the Langmuir

theory, which predicts a very flat maximum at diameters greater than 1.2 mm. Since small drops are far more numerous than larger ones in natural rainfall, this deviation from theory would later considerably interception predictions.

The differential equation for interception can be written in dimensionless form to yield the definition of an "impaction parameter", K, of the form

$$K = \frac{2}{9} \frac{a^2 \rho U}{\mu S},$$

where U is the terminal velocity,
s is the radius of the raindrop,
μ is the fluid viscosity,
a is the particle radius, and
ρ is the particle density.

To the extent that the differential equation describes the motion, the impaction parameter determines the scavenging efficiency.

Figure 5 shows a summary of selected determinations of scavenging efficiency as a function of the parameter, K. The Langmuir curves represent his predictions for very large and very small Reynold's numbers (potential and viscous flow, respectively) and two intermediate Reynold's numbers of 43 and 269 (corresponding to droplet diameters of 0.4 and 1.0 mm). It is generally accepted that the efficiencies at intermediate Reynold's numbers should fall between the viscous and potential flow curves. However, Pearcey and Hill[20] have predicted the curve shown for a 0.34 mm drop that lies outside this range. The Hanford curve, labeled experiment R-3, was determined from droplet collection of ZnS tracer No. 2210. A similar curve for the same tracer was published by McCully, et al.[21] as determined from bulk rain samples. McCully reasoned that the low scavenging efficiency for No. 2210 was due to "nonwettability" and he obtained a higher efficiency for the "wettable" tracer No. 2230. Thus, the chemical nature of the particles appears important.

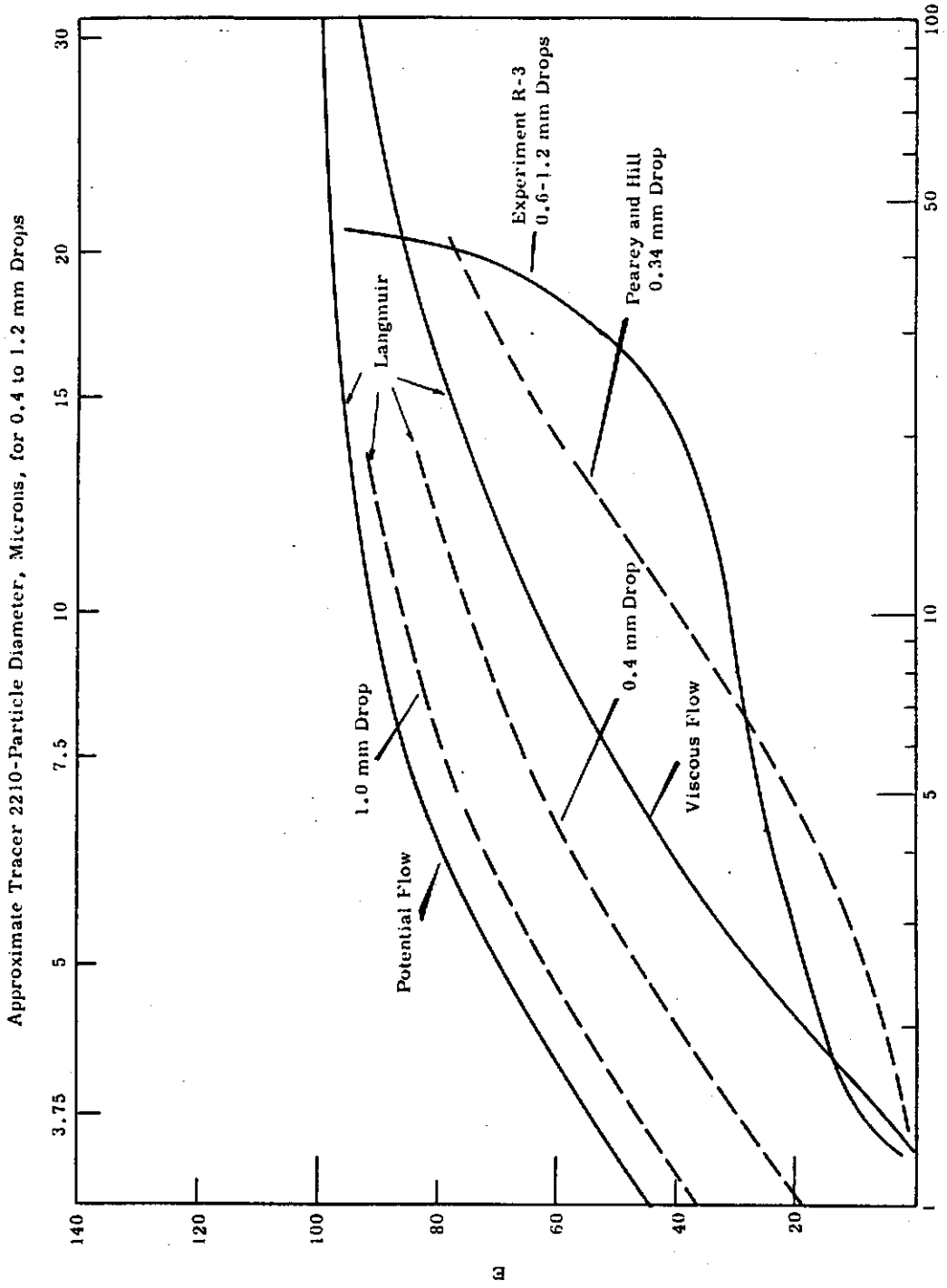

FIGURE 5

Rain Scavenging Efficiency as a Function of the Particle Parameter "K"

Figure 6 shows sample raindrop spectra taken at Hanford with the sampler described earlier. The sampler actually permits determination of the flux of raindrops to the ground, in contrast to air volume samplers, which only provide an estimate of the spatial density of droplets. For comparison, a raindrop spectrum reported by Hardy and Dingle[22] as measured by their raindrop spectrometer is shown. Numerous other raindrop spectra have been obtained at Hanford in an effort to characterize the rainfall.

The Hanford experiments have demonstrated the feasibility of determining scavenging efficiency by measurements on individual drops from either natural or artificial rain. They have also raised the question again as to whether small drops have a greater scavenging efficienty than the larger drops, and whether the collision efficiency for intermediate Reynold's numbers may not lie outside the range of efficiencies calculated between potential and viscous flows.

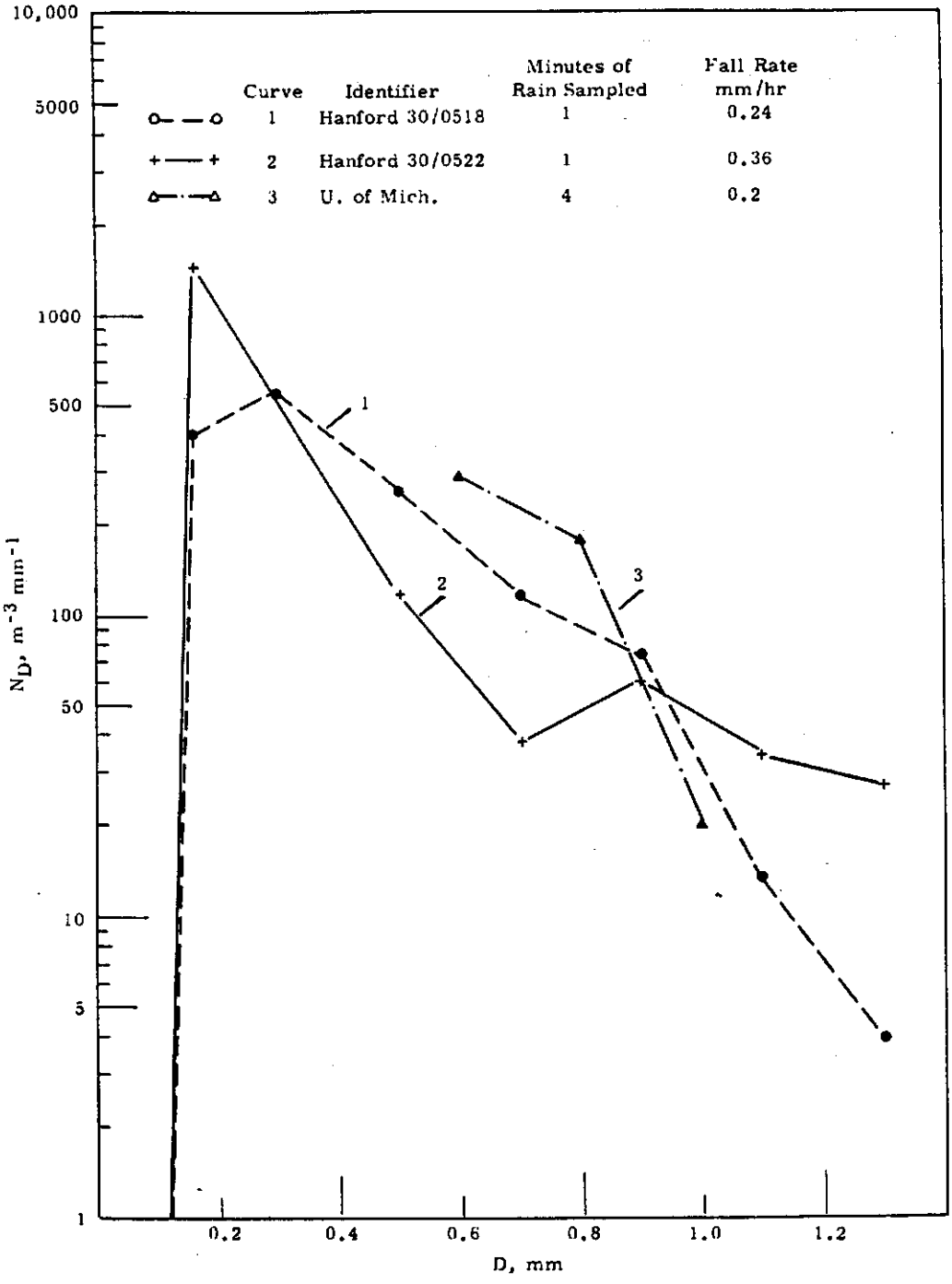

FIGURE 6

Number of Raindrops Per Volume of Air Per Diameter Class Width Versus Drop Diameter, for Selected Light Rains

REFERENCES

1. Simpson, C. L., et al. "Atmospheric Dispersion Measurements," Research and Development Activities in the Radiological Sciences - Physical Sciences Portion - January Through December, 1960, HW-70050. January 16, 1961.
2. Barad, M. L. and J. J. Fuquay. "Diffusion in Shear Flow," 1961. Submitted to the Journal of Applied Meteorology.
3. Chamberlain, A. C. Aspects of Travel and Deposition of Aerosol and Vapor Clouds, AERE-HP-R-1261. September, 1953.
4. Sutton, O. G. Micrometeorology, New York: McGraw-Hill, 1953.
5. Fuquay, J. J. Meteorology as Related to Waste Disposal and Weapons Tests, HW-47721 A. January, 1957.
6. Healy, J. W. Calculations on Environmental Consequences of Reactor Accidents, HW-54128. December, 1957.
7. Simpson, C. L. Some Measurements of the Deposition of Matter and its Relation to Diffusion from a Continuous Point Source in a Stable Atmosphere, HW-69292 REV. April, 1961.
8. Barad, M. L. and J. J. Fuquay (eds.). The Green Glow Diffusion Studies, HW-71400 VOL1. December, 1961.
9. Barad, M. L. and J. J. Fuquay (eds.). The Green Glow Diffusion Studies, HW-71400 VOL2. (In press.)
10. Priestly, C. H. B. Turbulent Transfer in the Lower Atmosphere, Chicago: University of Chicago Press, 1959.
11. Rider, N. E. "Eddy Diffusion of Momentum, Water Vapor, and Heat Near the Ground," Phil. Trans. Roy. Soc. London. 246A: 481-501. 1954.
12. Swinbank, W. C. "The Measurement of Vertical Transfer of Heat and Water Vapor by Eddies in the Lower Atmosphere," J. of Meteorology, 8: 135-145. 1951.
13. Cramer, H. E. and F. A. Record. "The Variation with Height of the Vertical Flux of Heat and Momentum," J. of Meteorology, 10: 219-226. 1953.
14. Greenfield, S. M. "Rain Scavenging of Radioactive Particulate Matter From the Atmosphere," J. of Meteorology, Vol. 14, No. 2, pp. 115-125. 1957.
15. Junge, C. E. "Atmospheric Chemistry," Advances in Geophysics, Vol. 4, Ch. I, Academic Press, 1958.

16. Barad, M. L., D. A. Haugen, and J. J. Fuquay. "A Diffusion-Deposition Model for In-Flight Release of Fission Fragments," Air Force Surveys in Geophysics, No. 123. June 1960. (TN-60-60-400).

17. Langmuir, I. "The Production of Rain by a Chain Reaction in Cumulus Clouds at Temperatures Above Freezing," J. of Meteorology, 5: 175-192. 1948.

18. Best, A. C. "The Size Distribution of Raindrops," Quart. J. Royal Soc. 76: 16-36. 1950.

19. Kinzer, G. D. and W. E. Cobb. "Laboratory Measurements of the Growth and Collection Efficiency of Raindrops," J. of Meteorology, 13: 295-301. 1956.

20. Pearcey, T. and G. W. Hill. "A Theoretical Estimate of the Collection Efficiencies of Small Droplets," Quart. J. Royal Meteorological Soc., 83: 77-92. 1957.

21. McCully, C. R., et al. "Scavenging Action of Rain on Airborne Particulate Matter," Ind. and Eng. Chem., 48: 1512-1516. 1956.

22. Hardy, K. R. and A. N. Dingle. "Raindrop-size Distributions in a Cold Frontal Shower," Contrib. 43 from Met. Lab., U. of Mich.

sensitivities of different detectors. Ten nanocuries of I^{131} were placed at the thyroid position in the neck phantom. The source and the phantom then were counted with five different detectors. The background at the neck of a subject was measured with each detector. The detectors tried were:

1. a 3- by 3-inch NaI(T1) crystal positioned directly in front of and in contact with the neck at the position of the thyroid lobes;
2. two 2- by 2-inch NaI(T1) crystals, each centered over a lobe of the thyroid and in contact with the neck;
3. two 3- by 3-inch NaI(T1) crystals, each centered over a lobe of the thyroid and in contact with the neck;
4. two 1/4- by 2-1/2-inch NaI(T1) crystals, each centered over a lobe of the thyroid and in contact with the neck; and
5. a 4- by 9-3/8-inch crystal located directly in front of and as close to the neck as possible and centered opposite the thyroid lobes.

The results of these trials are listed in Table II.

TABLE II

SENSITIVITY OF SEVERAL DETECTORS FOR COUNTING I^{131} IN THE THYROID

Detector Number	Count/5 min from source in Neck Phantom	Background Count 5 min at the Neck of a Subject	Minimum Detectable Amount* for 5 min, pc
1	11,390	181	15
2	13,274	172	17
3	28,822	362	13
4	5,478	40	23
5	75,884	1,388	9.8

* The minimum detectable amounts were calculated from the equation:

$$MDA = \frac{K}{C}\sqrt{B} ,$$

where:

K = probability constant, taken to be 1;

C = counts/picocurie in the counting time;

B = background count in the counting time; and

MDA = minimum detectable amounts.

The minimum detectable amounts in Table II are figure of merit values rather than actual values, since the conditions around the source are not exactly the same as that of a human thyroid. Detector 5 gives the lowest MDA using the neck phantom. In counting a subject, however, the value will not be as low. The 9-3/8-inch-diameter crystal cannot be placed close to the thyroid because it first touches the chin or chest. The 3- by 3-inch or 2- by 2-inch detectors yield the best practical MDA. It was anticipated that the 1/4- by 2-1/2-inch crystals would give the best sensitivity, since they absorb most of the I^{131} gamma rays but count less background because of their reduced thickness. The resolution of these detectors was half that of the 2- by 2 inch and 3- by 3 inch detectors, however, and the smaller thickness resulted in fewer counts in the photopeak. These two factors greatly reduce the sensitivity of the thin crystals.

Two sources of near background activity were placed over the two lobes of the thyroid of a subject. The subject was counted with Detectors 2, 3, 4, and 5. Figure 3 shows the 0.36-Mev peak visible above the background of the subject. The peak of Cs^{137}, Zn^{65}, and K^{40} are also present. The results confirmed the previous experiment--Detectors 2 and 3 gave the best sensitivity, Detector 5 was less sensitive, and Detector 4 was so insensitive that the peak was not visible.

The single 3- by 3-inch crystal (Detector 1) was selected for use. The arrangement of two 3- by 3-inch crystals was only slightly more sensitive and for routine counting was much more trouble to set up geometrically and electrically. The detector was calibrated by use of an Alderson Research Laboratory Remab phantom. The phantom was filled with water and the two lobes of the thyroid that were built into the neck were filled with

RADIOLOGICAL PHYSICS

The Shadow Shield Whole Body Counter - H. E. Palmer

The calibration of the shadow shield counter is independent of body size for potassium, Zn^{65}, and Cs^{137}. The sensitivity is approximately two-thirds that of the Hanford Whole Body Counter.

The background characteristics and some of the whole body-counting characteristics of the shadow shield counter were described previously.[1] This report describes the calibration and further testing of the counter.

Figure 1 shows the experimental model of the shadow shield counter. The subject lies on a low bed which has rollers on the bottom. A chain drive attached to the bed moves the subject slowly through the counter at a constant speed. The direction of movement can be reversed. The bed is stopped at either end of travel by a microswitch. Figure 2 shows cross sections of the counter.

A good whole body counter requires a calibration which is independent of body size. Four subjects with known body burdens of potassium were counted in the shadow shield counter. The results of these counts are shown in Table I.

TABLE I

COMPARISON OF COUNTING EFFICIENCY WITH BODY SIZE FOR POTASSIUM

Subject	Weight	Height	Count/min-Gram K in Body
1	185	5 ft 7 in.	0.500
2	160	5 ft 11 in.	0.497
3	195	6 ft 0 in.	0.507
4	200	6 ft 6 in.	0.505
		Average	0.502
		Deviation from Average	± 1 %

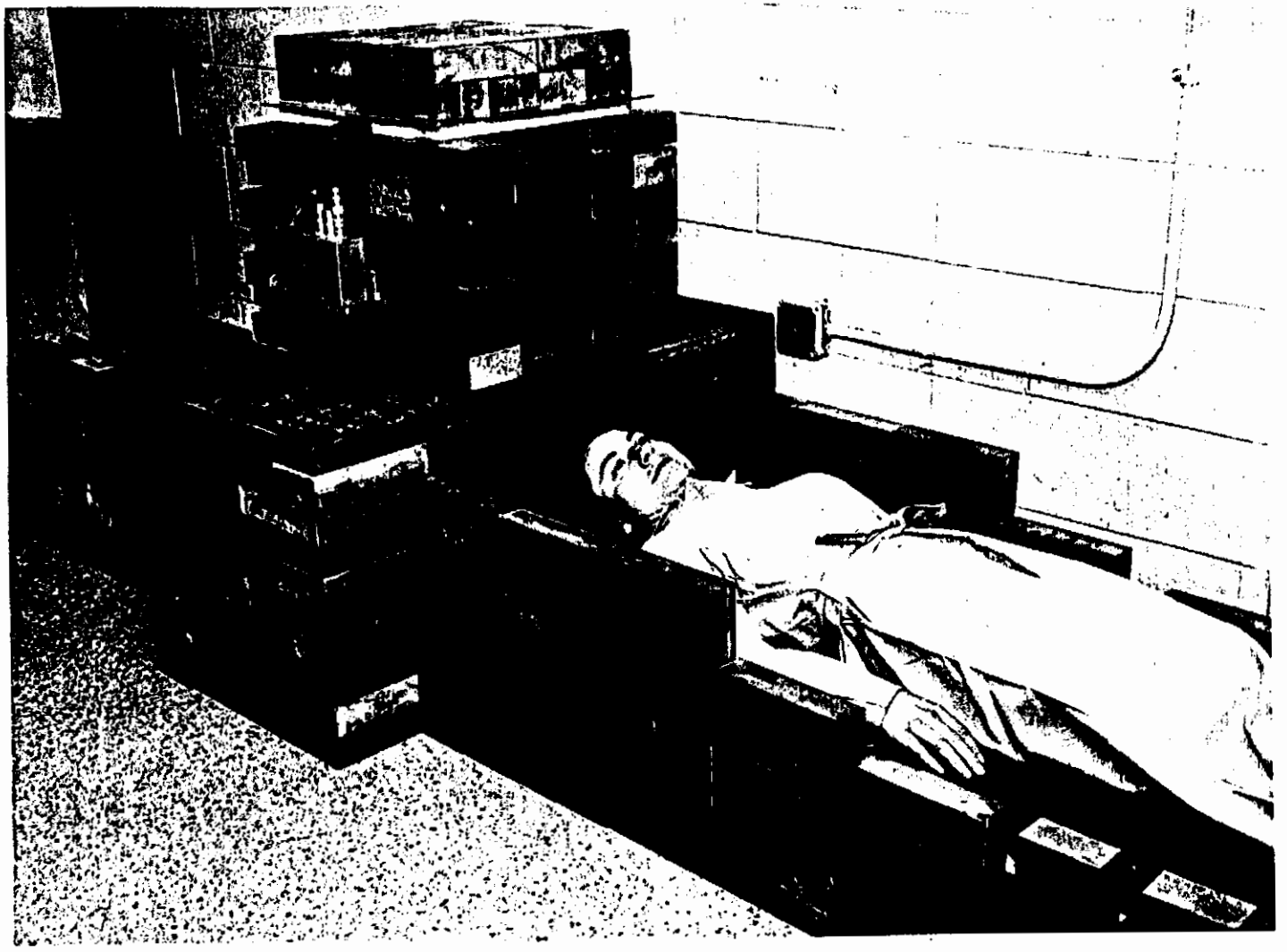

Figure 1

Experimental Model of Shadow Shield Counter

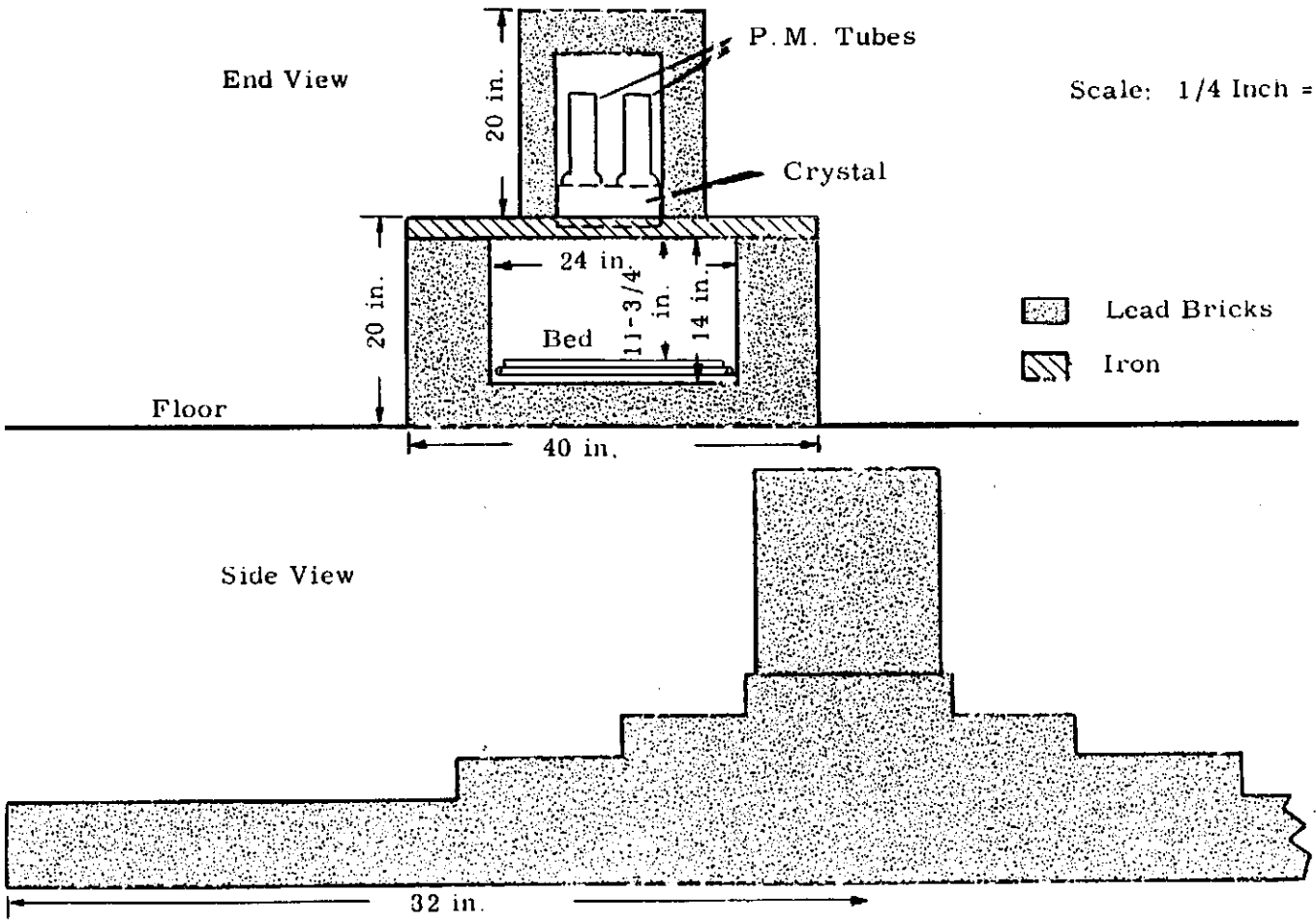

FIGURE 2

Total Weight of Shadow Shield is 5 Tons

Table I shows that the counts per minute per gram of potassium in the body show negligible variation over the range of body sizes indicated. Therefore, the shadow shield counter should be useful in determining the amount of potassium in any adult person. Calibrations for Cs^{137} have not been done yet. Since Cs^{137} and potassium are similarly distributed in the body, no problems are expected. A scanning method[2] has been satisfactorily demonstrated for measuring Zn^{65}; therefore, the shadow shield counter can be used to measure this isotope also.

A disadvantage of the shadow shield counter is its lower counting efficiency. The 0.502-count per minute per gram of potassium in the body is 29 percent lower than that of the chair geometry. The routine counting time for the chair position is 20 minutes. Thirty minutes would be required to get the same number of counts with the shadow shield counter.

Determination of Low Level I^{131} in Human Thyroids Resulting from Nuclear Test Fallout - H. E. Palmer and F. Swanberg, Jr.

A 3- by 3-inch NaI scintillation counter was proven capable of detecting as low as approximately 17 nc of I^{131} in the human thyroid. Following the U.S.S.R. nuclear tests in the fall of 1961, I^{131} was detected in subjects who regularly drank fresh milk. The body burdens were 18 to 150 pc.

Extensive work has been done in the measurement of I^{131} in the thyroid gland after administration of the radionuclide to subjects for diagnostic and therapeutic purposes.[3] Far less work has been done in measuring very small amounts of I^{131} in the thyroid. Burch[4] measured nanocurie amounts (10^{-9} curies) in residents in the vicinity of Windscale following the reactor accident there and Comar, et al.[5] measured I^{131} in the thyroid originating from the fallout of weapons debris.

A study was made to find a sensitive detector and calibrate it for measuring picocurie (10^{-6} μc) quantities of I^{131} in the thyroid gland. A small pressed-wood neck phantom was made for measuring the relative

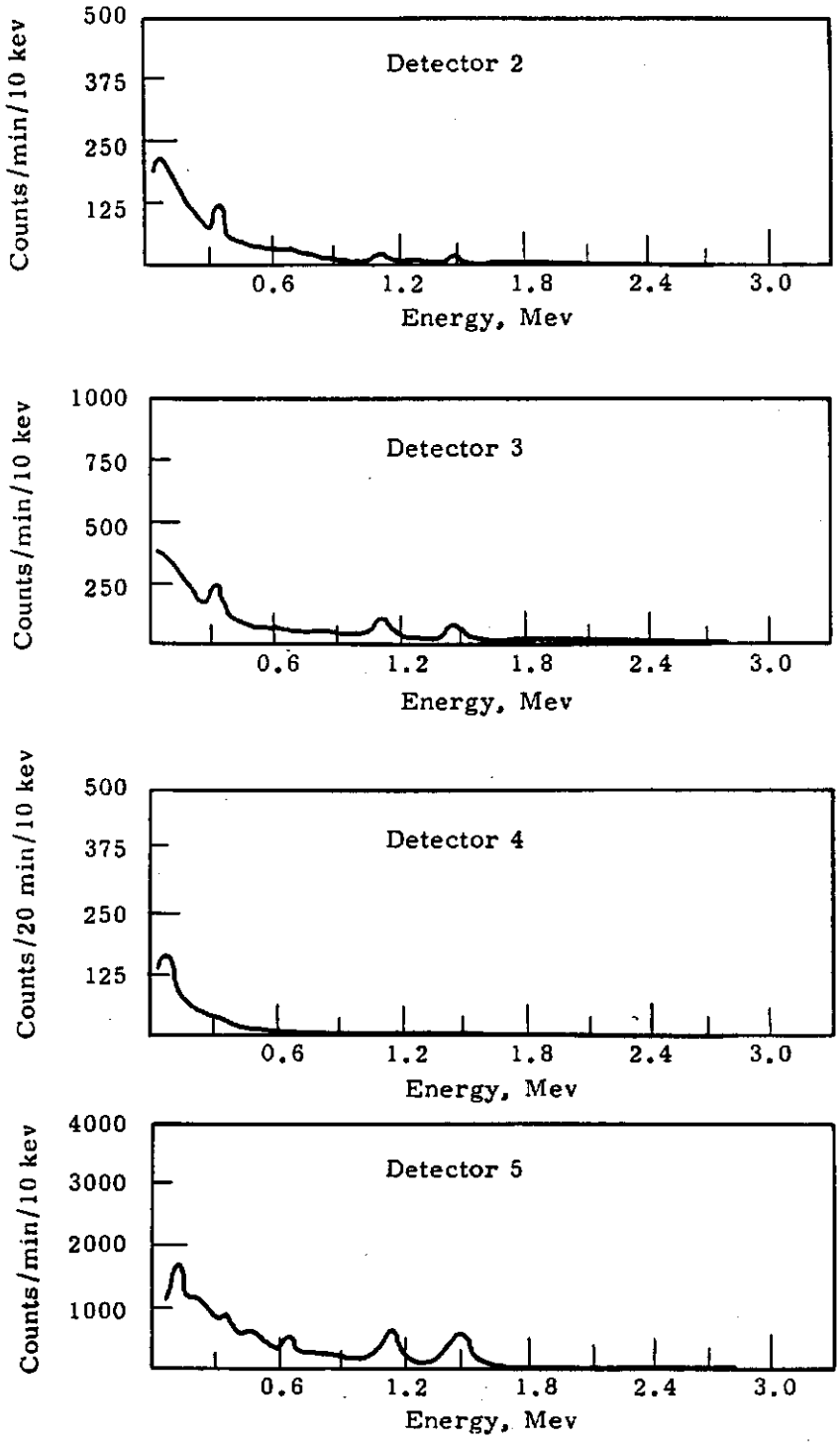

FIGURE 3

Tests of I^{131} Counters

a calibrated solution of I^{131}. The thyroid I^{131} was then measured with the detector directly in front of and in contact with the neck to obtain a calibration factor. This factor was 3.72 counts/30 min/picocurie in the thyroid gland. With the detector very close to the thyroid, some errors will occur due to variations in the size, shape, and location of thyroid glands. Maximum sensitivity is attained by positioning the detector as close as possible to the thyroid gland. The difference observed in measuring I^{131} in the thyroid gland of the Remab phantom with the thyroid one-third full compared to measurements with the gland completely filled was less than 3 percent. This indicates that gland sizes and shapes have small effect on the measurement of I^{131} in man.

Detection of I^{131} in Residents of the Northwest

In the fall of 1961, the fallout debris from the U.S.S.R. nuclear tests raised the I^{131} content in milk. During October of 1961 the concentration of I^{131} in a sample of milk produced in a Washington coastal area was reported as 840 picocuries/liter.(6) Shortly after that the cold weather began; cows were taken off pasture and fed stored hay. The I^{131} content in milk dropped to an almost undetectable level by early December of 1961.

The measurement of I^{131} taken up from fallout of weapons debris in the thyroid of subjects began in November. At that time I^{131} was detected in all subjects who regularly drank fresh milk but could not be detected in subjects who did not drink milk or who drank reconstituted dry milk. The thyroid burdens ranged from 18 to 150 picocuries. Table III lists the results obtained from examination of 11 subjects.

One subject who did not drink milk and in whom I^{131} could not be detected began drinking 1 quart of milk per day. This milk was purchased from local commercial supplies, but was produced in the Washington coastal area and its I^{131} content was known to be higher than the local average. Table IV shows the amounts of I^{131} detected in the thyroid of this subject.

TABLE III

DETERMINATION OF I^{131} IN SEVERAL SUBJECTS

Subject Number	Amount of Milk Consumed Per Day	I^{131} in Thyroid, Picocuries
1	None	Not Detectable
2	1 Quart	75
3	1 Quart	138
4	3 Glasses	135
5	1 Quart	54
6	1 Quart	63
7	None	Not Detectable
8	1 Quart	18
9	None	Not Detectable
10	2 Glasses Nonfat Milk	Not Detectable
11	None	Not Detectable

TABLE IV

I^{131} INCREASE IN THE THYROID DUE TO CONSUMPTION OF 1 QUART OF MILK PER DAY

Time Interval After Beginning Milk Diet	I^{131} Detected in the Thyroid, Picocuries	Remarks
0	Not Detectable	
2 Hours	24	
20 Hours	54	Stopped drinking milk after 5 days
4 Days	108	
6 Days	99	
8 Days	69	
11 Days	27	
14 Days	18	
22 Days	Not Detectable	

The milk consumed on the first day was analyzed and contained 80 picocuries/quart. Milk on succeeding days was not analyzed, but it appears that the I^{131} content was probably lower. The gamma spectrum of the subject's neck on 3 days during the experiment is shown in Figure 4. The background has not been subtracted from these spectra. Several other subjects drank the same brand of milk at the rate of 1 quart per day. The results were similar to the ones described. After December 15, 1961, the I^{131} concentration in milk was so low that it could not be detected in local residents. The detection limit of the method described is about 17 picocuries. The average background assumed was 1000 counts/30 min. over the energy range of 0.33 to 0.39 Mev for a subject containing no I^{131}. Using a probability constant of 2, the minimum detectable amount is

$$\text{MDA} = \frac{2}{3.72 \text{ counts/picocuries}} \times \sqrt{1000 \text{ background counts}} = 17 \text{ picorcuries}$$

This value is reasonable in the opinion of the operators of the counter.

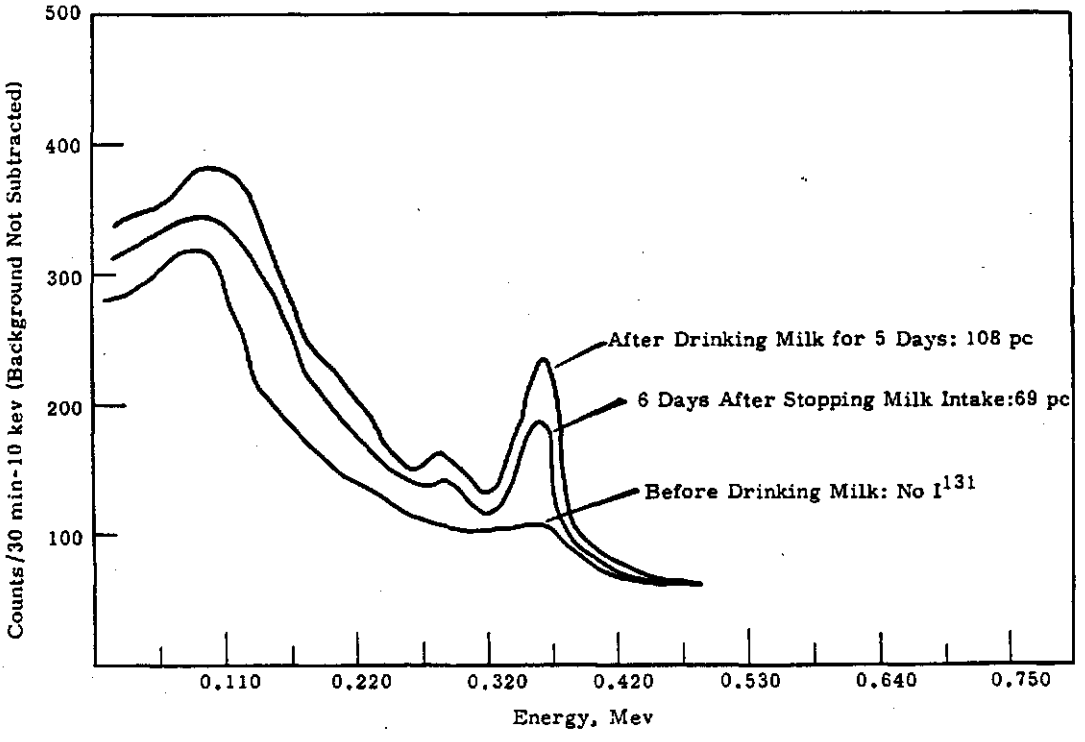

FIGURE 4

Differences of I^{131} in the Thyroid Due to Changes in Milk Intake

Factors Influencing Measurement of Plutonium in Wounds -
H. E. Palmer and N. E. Erickson

In X-ray counting of plutonium in wounds, a lack of allowance for the wound depth will cause less than about 20 percent error for depths up to 3mm. No correction is necessary for lateral size or a displacement of less than 7 mm from the center of the counter. Measurements of plutonium in large particles may be inaccurate because of self-absorption in the source.

The efficiency and accuracy of plutonium measurement in wounds by thin crystal X-ray scintillation spectrometry depends on a number of factors, among which are: depth and area of contamination in the wound; position of the wound with respect to the crystal; and self-absorption of the 17-kev X-rays by the contaminating material.

A plutonium-contaminated wound is counted by placing it directly on top of the detector and comparing the count rate with that of a standard source placed in the same position.[7] Increases in the depth of contamination decrease the count rate, because of absorption by the flesh and the increased distance from the crystal. The effect of increased distance cannot be calculated from the simple inverse square law when a source is close to the crystal. The distance effect for both a point and a spread source was measured experimentally and is shown in Figure 5. The spread source has a diameter of 1.2 cm; the diameter of the 1-mm-thick crystal was 4.5 cm. The difference between the effects with a point and with a spread source is negligible. When the depth of the wound is 5 mm or less, the error caused by neglecting the distance from the crystal is less than 10 percent. The decrease in counting rate from absorption by the flesh was determined by measuring the transmission of several thicknesses of tissue-equivalent styrene plastic. The absorption curve is shown in Figure 6. From Figures 5 and 6 the total reduction in count rate due to distance and absorption can be estimated for any depth of wound contamination up to 1 cm. The total decrease for several depths is listed in Table V.

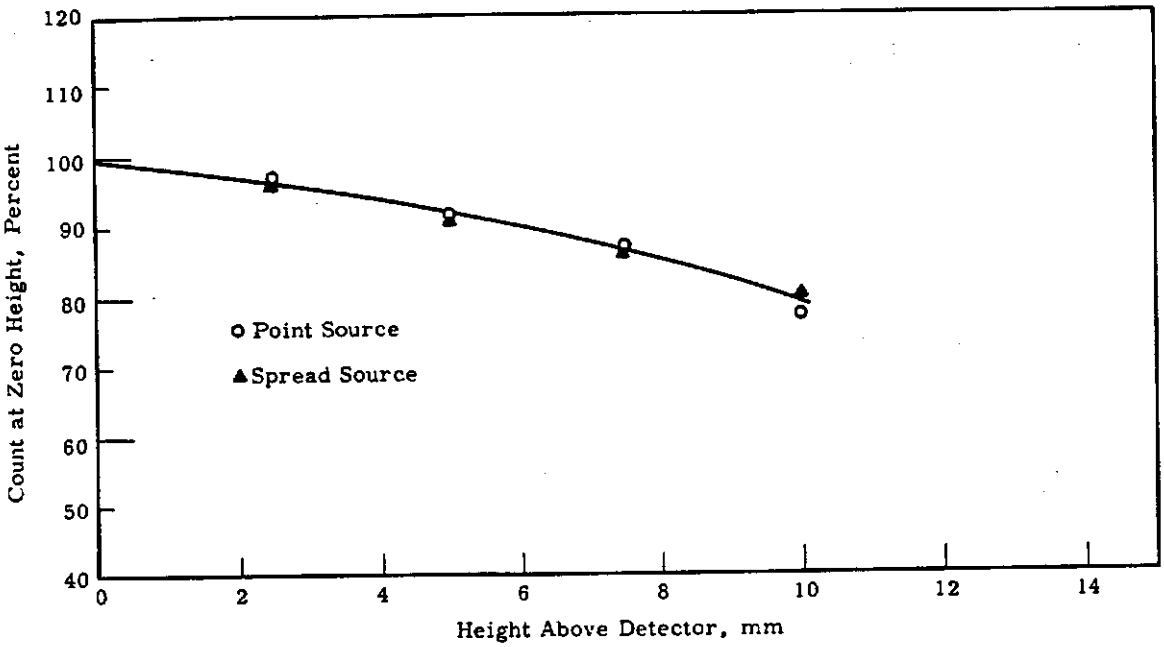

FIGURE 5

The Decrease in Counting Rate of Point and Spread Sources Due to Distance From the Detector

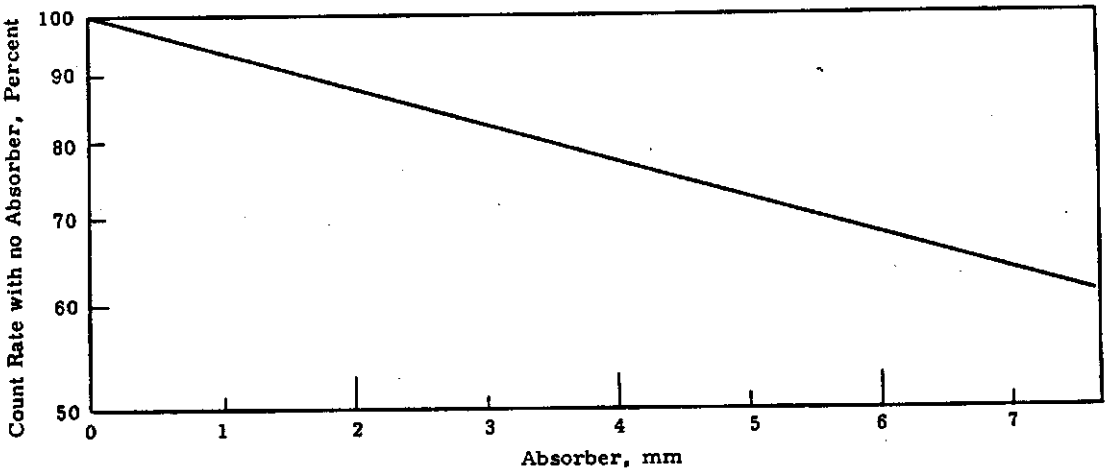

FIGURE 6

Absorption of Pu^{239} X-rays By Tissue Equivalent Plastic

TABLE V

REDUCTION IN WOUND COUNT RATE AS A FUNCTION OF DEPTH

Depth, mm	Percent By Absorption	Percent By Distance	Total Percent
1	6.4	1.5	7.8
2	12.6	3.0	15.0
3	17.5	4.5	21.0
4	22.6	6.5	28.0
5	27.5	8.5	34.0
6	32.0	10.5	39.0
7	36.0	12.5	44.0

To use the values in Table V, the depth of the plutonium contamination in the wound must be known. The depth of the wound is easily measured, but it is extremely difficult to measure the position of the plutonium inside the wound. In most instances the wound depth is shallow (1 to 3mm). Neglect of the depth correction will produce errors of up to 20 percent.

If the position of the wound is not near the center of the crystal, an error in the count rate will result from the smaller solid angle subtended by the crystal. A point source was counted at several positions between the center and the outside edge of a 1-mm by 4.5-cm-diameter crystal. From the center out to a distance of 7 mm, the counting rate remained constant. The count rate decreased at greater distances; at 20 mm from the center the count rate was reduced 33 percent.

Another source of error in measuring plutonium in wounds is self-absorption by the contaminated particles. As an example, a small particle of plutonium was removed from a wound and counted with the thin crystal detector. The amount of plutonium was estimated from these counts. The particle was dissolved, and a small aliquot of the solution was evaporated on a steel disk and counted in an alpha proportional counter. The activity of the particle was 15 times higher than that estimated by the thin crystal

detector. Of course, if the particle is plutonium there will always be enough activity to indicate that the tissue around the wound must be excised. However, if a small amount of plutonium is adsorbed on another type of metal particle, the absorption by the particle could cause an erroneous decision concerning removal of the tissue around the wound. Especially for this reason, the wound should be thoroughly cleaned.

Retention of Isotopes - H. E. Palmer

The retention and distribution of Co^{60} and of Sb^{125} arising in particular contamination incidents are described.

Two radioactive contamination incidents during 1961 contributed to the study of retention of isotopes in the body.

A subject inhaled some radioactive particles of Co^{60} while grinding a pipe that had previously been used in a heat exchanger at a reactor. In the Whole Body Counter the radioactivity was identified as Co^{60} and the location of the activity was pinpointed in the left lung. The amount of Co^{60} was estimated at about 4 nc. Two weeks later, the activity had decreased by only 7 percent and thereafter the decrease was very slow. After one year, 1 to 2 nc were still present and the activity was still located in the left lung. Apparently the activity is in a quite insoluble form If the particle had been soluble, it would have had an effective half life in the body of only 9.5 days.(8)

During a routine whole body count, 20 nc of Sb^{125} were detected in a subject. The characteristic gamma ray peaks of 0.61, 0.43, and 0.17 Mev were identified. To further confirm the presence of Sb^{125}, the 27-kev X-ray peak was identified by use of a 1-mm by 2-inch NaI(T1) crystal. The activity was found in the area of the lower right lung or the liver. The source of this subject's contamination is still unknown. Subsequent counts showed that activity was leaving this area very slowly. After 71 days the activity had decreased almost 50 percent. About 20 percent of the activity

still remained after 9 months. This retention of Sb^{125} is in good agreement with the Report of I. C. R. P. Committee II On Permissible Dose for Internal Radiation which gives an effective half-life in the lung of 90 days.

Detection of P^{32} in Vivo* - H. E. Palmer

A 3-mm-thick, 4-1/2-inch-diameter NaI scintillation counter was used to detect bremsstrahlung from P^{32} in human subjects. The counter was calibrated by measuring the bremsstrahlung from two subjects who were given known amounts of P^{32} for therapy by Dr. E. E. Osgood of the University of Oregon Medical School. The counter can detect quantities of P^{32} in the body that are relevant for radiation protection purposes. If no background count is available for a given subject before acquisition of the P^{32}, then uncertainties in the background correction limit the sensitivity to about 0.25 μc.

The Precision Long Counter - J. De Pangher

The effect on the sensitivity of the precision long counter was investigated for the secular variation of source emission rates, the asymmetries in source emissions, and the properties of different BF_3 tubes. Some variations in sensitivity are attributed to differences in construction of the BF_3 tubes and to changes in their operation produced by intense gamma ray exposure.

When a precision long counter[9, 10] is calibrated in one laboratory against external neutron sources of strength Q (neutrons/sec) and geometrical factors ϵ, and the characteristic rate $\dot{A}_c$ (counts/min) is measured for the internal Pu-Be neutron standard, then a second precision long counter in another laboratory may, in principle, be readily calibrated by simply making measurements with a second internal standard calibrated against the first internal standard and omitting the external calibrations. However, six effects may arise which could cast doubt on the accuracy of this simple calibration procedure:

---

* Published in Radiology 78: 115. 1962.

1. energy dependence on flux sensitivity S (counts per minute per unit of flux) because of the choice of counter or BF_3 tube;
2. energy dependence on room-scattering corrections because of the choice of counter, tube, or room;
3. energy dependence for the variation of the location of the effective center inside the counter because of the choice of counter, tube, or room;
4. position errors in locating the internal source or small inhomogeneities in the polyethylene core between the internal source and the BF_3 tube;
5. lack of precise knowledge about the decay or buildup in Q as a function of time; and
6. different source-holder geometry.

Studies of these various effects have been made in one particular room—the low-scattering room in the building which contains the Hanford positive ion Van de Graaff accelerator. This room contains an 8-foot-deep pit covered with a light aluminum grating floor. The pit covers an area 20- by 21-feet in the center of the room enclosing an area 28- by 29-feet. The ceiling is about 20 feet high. Two of the walls are plasterboard; the other two contain considerable concrete. Most of the measurements were made 42 inches above the grating floor with the source on its stand near the center of the room. The long counter was hung by wires from an overhead trolley. The position of the trolley is controlled manually by setting a 25-turn potentiometer in the accelerator control room or automatically by a string of precision resistors wired to a stepping switch. The source holder was designed to uncover the source as much as possible and still be rigid enough for accurate positioning.

The procedure for studying these various effects was to measure the constants a, b, and c by making "inverse square runs" and then fitting the data by least squares to the equation.[11, 12]

$$\dot{A} = a + \frac{b}{(x + c)^2} \quad (1)^*$$

where $\dot{A}$ (count/minute) is the counting rate as a function of the source-detector separation distance x(cm). The data processing, which is done by an IBM 7090 digital computer, minimizes the sums of the fractional deviations of the counting rates from the fitted values.

The flux sensitivity S is defined by the equation

$$S = \frac{4\pi b}{\varepsilon Q} \quad (2)$$

and may be related to the characteristic rate $\dot{A}_c$ for the internal PuBe source by the equation

$$S = \frac{\alpha \dot{A}_c}{1 + \beta t} \quad (3)$$

where α is a constant to be determined for a source with a particular neutron energy spectrum and $1 + \beta t$ is an approximate time-correction factor which allows for the buildup of the neutron emission rate t days after January 1, 1961.

Considerable effort has been expended in measuring the reproducibility of α for different arrangements by employing three particular sources: the small internally-used source, Pu–Be M-246; the externally used source, Pu–Be M-199 containing about 80 grams of plutonium; and a second externally used source, Pu–Be M-590.** Other sources were used, too, but will not be mentioned here. The time-correction factors for these neutrons sources will be discussed in more detail in another paper in this report.

The work reported previously was concerned with the reproducibility of α given by

$$\alpha = \frac{4\pi b\,(1 + \beta t)}{\dot{A}_c\ \varepsilon Q} \quad (4)$$

---

* Anderson in reference 12 states that $A = (1 - kx)\,a + b(x + c)^{-2}$ gives a better fit than $A = a + b(x + c)^{-2}$ to the data obtained in a smaller room than was used at Hanford.

** On loan from M. E. Anderson, Monsanto Research Corporation, Mound Laboratory, Miamisburg, Ohio.

for different counters and various calibrated sources but with a particular BF_3 tube. It was desirable to extend this work to different BF_3 tubes like the original brass BF_3 tube employed for the earlier work and, also, for aluminum and copper (oxygen-free) BF_3 tubes to find the best possible BF_3 tube for use in the precision long counters. Operating characteristics of these different kinds of tubes will be discussed in another paper in this section. (J. De Pangher. Page 48)

An additional piece of equipment had to be developed to improve the accuracy in the measurements of the ϵ's for the various sources employed. The quantity ϵ is measured by placing the source horizontally on a stand and then measuring the counting rate $\dot{A}$ at some value of x (usually about 87.8 cm) between the center of the source and the front polyethylene face of a precision long counter as a function of the angle θ for the source ($\theta = 0°$ or $180°$ when the axes of the source and counter lie on the same line). The equipment consisted of an automated source-holder stand that advanced in $5°$ steps. Counts were recorded on a digital recorder until the full $360°$ span was covered. The relation between $\dot{A}(\theta)$ and ϵ is given, when cylindrical symmetry is assumed for the source, by

$$\epsilon = \frac{2\,\dot{A}(90°)}{\int_0^{\pi} \dot{A}(\theta) \sin\theta \, d\theta} \qquad (5)$$

The use of automatic equipment allowed long unattended running times and, hence, greater statistical accuracy in the measurements of ϵ than was formerly achieved with manually operated equipment. The error was reduced from about 1 percent to about 0.2 percent.

The data on α for various BF_3 tubes tested inside the precision long counter, PLC-H-1, are shown in Table VI. These data exhibit fluctuations from one BF_3 tube to another that extend beyond the standard statistical errors calculated by the IBM 7090 digital computer. Even the data for repeat measurements on a particular tube G-14023 have large fluctuations. To explain the large deviation from $\alpha = 4645 \times 10^{-6}$ on

August 27, 1960 to $\alpha = 4599 \times 10^{-6}$ on March 6, 1961, this writer blames radiation damage from the "gamma-ray" effect for causing a change in the tube. The tube was subjected to intense X-radiations a number of times during, but not after, that period. Tubes G-14511 and G-13911 were only exposed once in this way, and then used only infrequently in the calibration of the precision long counters. Some of the variations in α for the different tubes may be due to a lack of reproducibility in the absorption of thermal neutrons from 1 tube to another. A 3 percent deviation had been found previously in the reproducibility of the brass tube pockets which were once used to contain the BF_3 tubes. These were replaced with aluminum tube pockets which reduced the deviations to ±0.1 percent.

TABLE VI

α FOR VARIOUS BF_3 TUBES INSIDE PLC-H-1

Source	Run Number	Tube	Tube Material	$10^6 \alpha$	Date
M-199	39	G-14023	Brass*	4645 ± 10	8-27-60
M-199	62	G-14023	Brass	4599 ± 13	3- 6-61
M-199	65	G-14023	Brass	4701 ± 23	8-31-61
M-590	71	G-14023	Brass	4661 ± 21	11- 5-61
M-590	76	G-14023	Brass	4728 ± 33	12-21-61
M-590	78	G-14023	Brass	4707 ± 21	12-25-61
M-199	67	G-16412	Brass	4631 ± 19	9- 7-61
M-590	72	G-14511	Brass	4668 ± 18	11-18-61
M-590	73	G-14123	Brass	4662 ± 18	11-20-61
M-590	74	G-15872	Brass	4670 ± 21	11-21-61
M-590	75	F-14492**	Brass	4631 ± 36	11-26-61
M-590	77	G-13911	Brass	4713 ± 21	12-23-61
M-199	66	C-672	Aluminum†	4625 ± 30	9- 6-61
M-590	79	TCE-1	Copper††	4636 ± 21	1- 5-62

* Made by N. Wood Counter Laboratory, 1525 East 53rd Street, Chicago 15, Illinois.

** Filled with depleted BF_3 gas at a pressure of 25 cm Hg, sensitivity relative to all other tubes filled with enriched BF_3 gas at a pressure of 25 cm Hg about 1/7.

† Made by Reuter-Stokes Electronics Components, Inc., 2149 Hamilton Avenue, Cleveland 14, Ohio.

†† Made by 20th Century Electronics, Ltd., King Henry's Drive, New Addington, Croydon, Surrey, England.

Radiation Effects in BF_3 Tubes - J. De Pangher

Gamma ray irradiation produced changes in the pulse height distribution and the counting rates from brass BF_3 tubes used in the precision long counter work. Changes in counting rates were about 1 percent. Some of the changes disappeared after about one week. BF_3 tubes made of oxygen-free copper were found to be quite free from these effects.

The BF_3 tube is an important part of the precision long counter. High stability in the count rates over long periods of time is required to demonstrate the reproducibility of different copies of this instrument. Early in the work with the precision long counters, a BF_3 tube called the "type B" tube was designed and a number of tubes following this design were made at Hanford. They proved to have better pulse height distributions, and, hence, better plateaus than a number of commercial BF_3 tubes tested. These tubes had brass walls. Subsequently, a tube manufacturer* built several "type B" tubes according to specifications. One of these tubes (G-14023), which at times gave a pulse height resolution of 7 percent, was used for a large part of the past work with the precision long counters. The reason this tube did not always give the same resolution is now apparent--the resolution depends on the recent past exposure of the tube to neutron and to gamma radiation. Figure 7 shows, in the upper left corner, the pulse height distribution for this tube obtained with a 256-channel analyzer when the tube was giving 9 percent resolution.

Although G-14023 and others like it gave good results in most measurements with the precision long counters, there was one situation where a difficulty arose. It was noticed that whenever the precision long counter was exposed to the neutron source Ra-Be68B (containing 500 mg of radium) in a fixed position during an overnight run, the count rate would gradually increase until it was about 1 percent higher at the end than at the start of the run. Furthermore, if this source was then removed and replaced with the

---

N. Wood Counter Laboratory, 1525 East 53rd Street, Chicago 15, Ill.

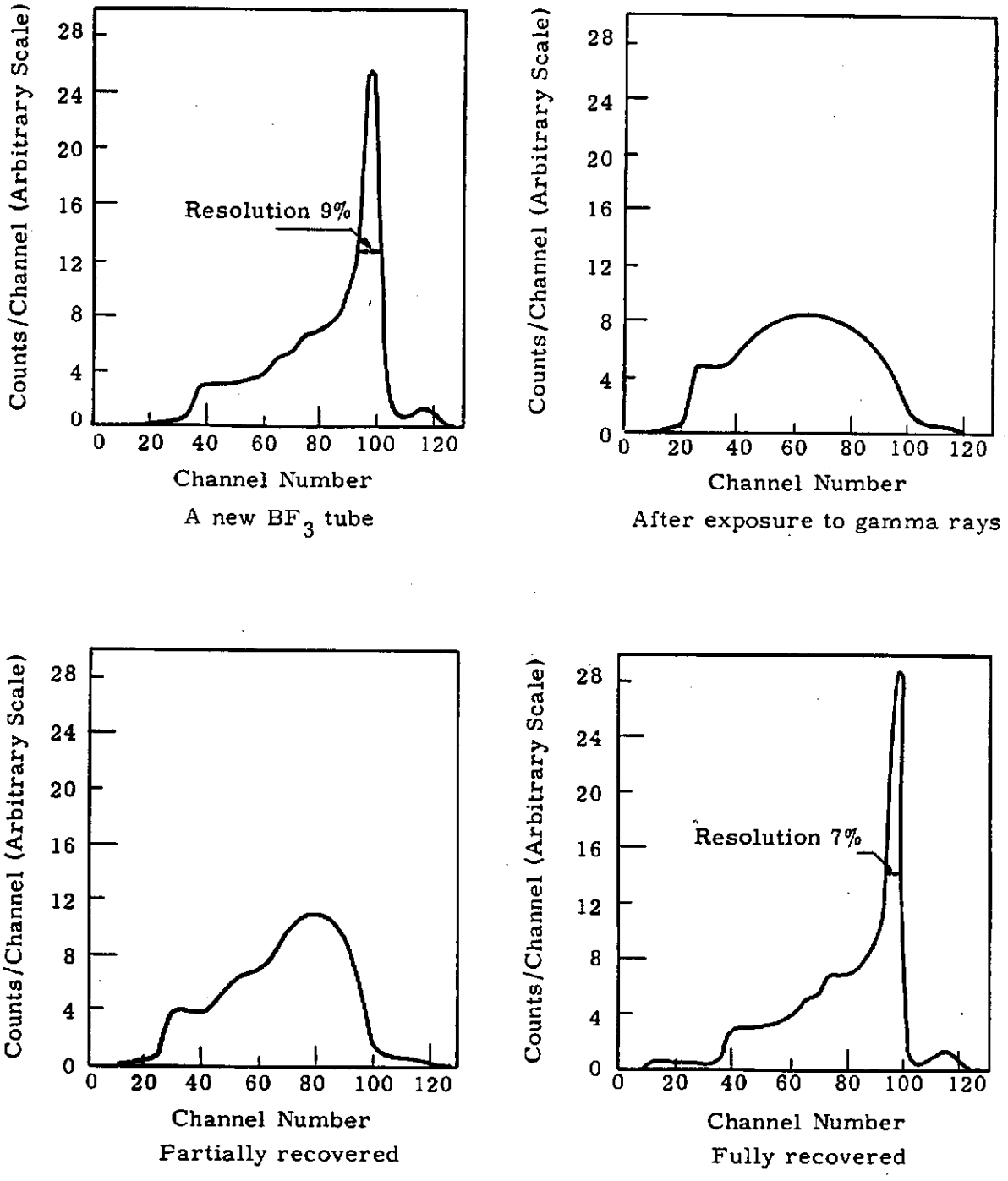

FIGURE 7

BF_3 Tube Pulse Height Spectra

source Pu-Be M-199, or the counter was calibrated with the internal Pu-Be standard, the count rates were about 1 percent higher than expected. These rates with the Pu-Be sources would gradually fall toward their expected values and would reach them in about a week. During a study of this effect, which is now termed the "gamma ray" effect, it was noted that the pulse height resolution was also affected by gamma radiation.

To study the gamma ray effect, G-14023 was exposed to X-radiations from the Hanford 2-Mev electron accelerator. The distortion and recovery from the distortion are shown in Figure 7. Just after the curve shown in the upper left corner was obtained, the tube was exposed to 600 r of X-radiation in 20 minutes. During the exposure the voltage on the center wire was kept at a positive potential of about 1450 volts, the normal working voltage. The other curves show the deterioration and recovery of the pulse height distribution of the tube.

The presence of the "gamma-ray" effect limited the accuracy obtained with the brass "type B" BF_3 tubes when used with the Ra-Be68B source or with the radium-gamma beryllium source NBS II borrowed from the National Bureau of Standards. Although the nature of this effect was not understood, it was thought the tube walls might play a role in the phenomenon; consequently, tubes made with aluminum walls and with copper walls were obtained and tested. Two tubes made according to the Hanford specification for the "type B" tube but with aluminum walls were supplied by a commercial manufacturer.* They gave excellent pulse height distributions, but gave count rates which changed by about 1 percent overnight for exposure just to Pu-Be sources. Measurements on the pulse height distributions after one of these tubes was exposed to 600 r of X-radiations showed smaller distortions than for the brass tubes. Recovery from the distortions was complete in about a week.

The search for a tube which did not exhibit the "gamma-ray" effect was rewarded when the copper-wall tube was investigated. This tube,

---

* Reuter-Stokes Electronic Components, Inc., 2149 Hamilton Avenue, Cleveland 14, Ohio

borrowed from the National Bureau of Standards, was originally obtained from a manufacturer* of BF_3 tubes in England for work with the precision long counter. It was not made according to the "type B" design but did happen to be the right size for the precision long counter. The copper is designated as "oxygen-free" copper. To test for the "gamma-ray" effect, two precision long counters were set up facing one another about 89 cm apart with a source holder stand half way between them. One counter contained a brass tube; the other counter contained the copper tube. The measurements, which took five days, were made by placing either the Ra-Be68B source or the Pu-Be M-590 source on the stand and recording count rates and pulse distributions simultaneously (the latter on a 400-channel analyzer). The results of the measurements are shown Tables VII and VIII as functions of the time elapsed from the start of the experiment. Unaccounted time in Table VIII was used for calibrations of the long counters with the internal Pu-Be standard. The sensitivity of the brass tube to gamma radiation is apparent. In addition, a small effect is shown on the resolution and on the time-stability for neutrons from the Pu-Be source. The quite small effect for the copper tube is striking.

TABLE VII

RESULTS OF RESOLUTION CHECKS ON BRASS TUBE AND ON COPPER TUBE

Time from Start of Exposure, min	Source	Resolution for Brass Tube, %	Resolution for Copper Tube, %
165	Pu-Be M-590	10.4	7.5
1543	Pu-Be M-590	13.0	7.7
1612	Ra-Be68B	15.3	9.6
2852	Ra-Be68B	25.1	10.1
2912	Pu-Be M-590	22.9	8.0
4638	Pu-Be M-590	21.3	8.3
6157	Pu-Be M-590	20.8	7.7
7130	Pu-Be M-590	17.6	7.7

* 20th Century Electonics, Ltd., King Henry's Drive, New Addington, Croyden, Surrey, England

TABLE VIII

RESULTS OF TIME-STABILITY CHECKS
ON BRASS TUBE AND ON COPPER TUBE

Time from Start of Exposure min	Source	Change in Counting Rate for Brass Tube, %	Change in Counting Rate for Copper Tube, %
350-1270	Pu-Be M-590	0.28	-0.02
1600-2900	Ra-Be68B	1.69*	0.06
2900-6150	Pu-Be M-590	-1.38**	-0.04

* Starting from the 0.28% level and ending at the 1.69% level.

** Starting from the (1.69 + 0.28) % level; consequently the tube finally gave essentially the same count rate as at the end of the 0.28% level.

Neutron Energy Degradation in Plutonium-Beryllium Sources - J. De Pangher

Recent data show directly the neutron energy degradation in a Pu-Be source and show the presence of a low energy group in the Pu-Be neutron spectrum.

Three developments have helped the study of neutron energy degradation in plutonium-beryllium sources: (1) development of an automated source holder stand that advances the angular position of the source in 5-degree steps in synchronization with a clock-controlled double moderator,[11] (2) discovery at the Rice Institute* of a fairly intense low-energy neutron group in the yield of the $Be^9(\alpha, n)$ reaction for alpha particles with energies above 4.3 Mev, and (3) development of a computer program for calculating double-moderator ratios from published neutron energy spectra.

The results of the application of (1) to the measurement of the double moderator ratio, R, of the 80-gram Pu-Be source, M-199, are shown in Figure 8. The fact that R is larger at 0 and 180 degrees than it is

* On loan from M. E. Anderson, Monsanto Research Corporation, Mound Laboratory, Miamisburg, Ohio.

at 90 and 270 degrees means that the neutrons coming from the ends of the source are higher in energy on the average than the neutrons from the side of the source. The possibility that the change in the ratio from R(0 degree) = 0.915 to R(90 degree) = 0.895, a 2.2 percent effect, might be due to a change in the mean source-detector distance rather than caused by energy changes was excluded by showing that a decrease in R of only 0.2 percent results when the source is moved from 98 to 102 cm from the detector.

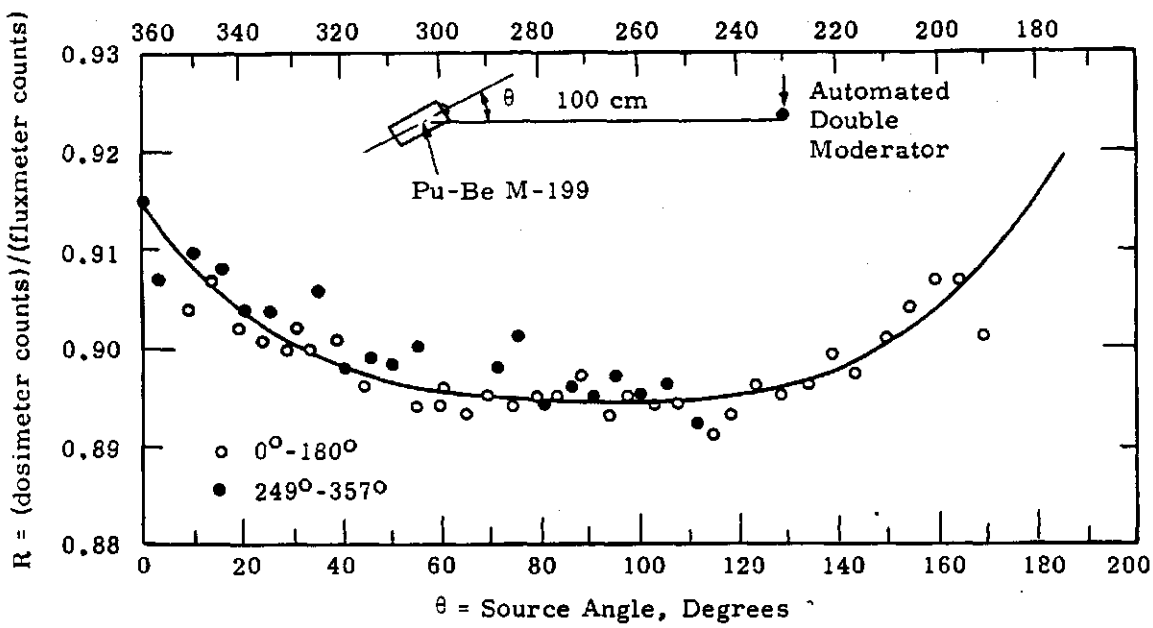

FIGURE 8

Double Moderator Ratio Vs. Direction of Emission

The studies of the group at Rice Institute[14] have indicated the presence of an intense group of low energy fast neutrons from α particle bombardment of beryllium. For simplicity in working with Pu-Be sources they assume these neutrons have 300 kev energy. Previous attempts[15] at Hanford to find this low-energy group with a Perlow neutron spectrometer gave suggestive but inconclusive results because of the masking effect caused by higher-energy neutrons room-scattered back into the spectrometer. This new development requires new calculations of double moderator ratios from published data, which leave out this normally undetectable low-energy group. The IBM program was prepared to facilitate these studies.

Secular Variation in Neutron Emission from Plutonium-Beryllium Sources - J. De Pangher

Estimates of the rate of increase of neutron emission are reported for four Pu-Be sources. Two methods are described for providing sources whose rates of emission change are known.

The problem involved in standardizing neutron counters with Pu-Be neutron sources whose emission rates are increasing with time is best demonstrated by describing our sketchy knowledge for a number of Pu-Be sources of a quantity β defined by the approximate equation

$$Q(t) = Q_o (1 + \beta t)$$

where Q_o is the source strength on January 1, 1961, and Q(t) is the source strength t days later. Table IX gives values of β for six different Pu-Be neutron sources along with the approximate Pu^{239} content in grams, the source strength Q_o in neutrons/sec, and 36,500 β (the percent increase per year in the neutron emission rate). The methods for measuring β are also briefly indicated.

The complete formula for the variation of the neutron emission rate was given by Hertz:[16]

$$Q(t)/Q(0) = \left[2.85\ P_1\ e^{-2.85 \times 10^{-5}\ t} + 10.5\ P_2\ e^{-1.05 \times 10^{-4} t} + 194\ P_3\ (e^{-1.51 \times 10^{-3} t} - e^{-5.25 \times 10^{-2}\ t})\right] \div \left[2.85\ P_1 + 10.5\ P_2\right] \quad (6)$$

where P_1 is the atomic fraction of the Pu^{239} isotope,
P_2 is the atomic fraction of the Pu^{240} isotope, and
P_3 is the atomic fraction of the Pu^{241} isotope.

The time, t, in this formula is in years after the preparation of the source. At t = o the source is assumed to be free from the isotopes Pu^{238}, Am^{241}, and Pu^{242}. The buildup in the neutron emission rate is caused by the buildup in the Am^{241} isotope. If one assumes a source has $P_1 = 0.934$,

TABLE IX

VALUES OF β FOR VARIOUS Pu-Be NEUTRON SOURCES

Source	Approximate Pu^{239} Content, grams	Source Strength Q_o, neutrons/sec	10^7 β	Increase Per Year, %	Method for Determing β
M-246	1	$\sim 10^5$	575	2.1	(1), (5)
M-710	1	$\sim 10^5$	575	2.1	(2)
M-199	80	8.20×10^6	139	0.5	(3), (5)
M-590	80	8.92×10^6	338	1.2	(4)

(1) Calculation based on the somewhat uncertain knowledge of the isotopic composition of the source: 93.4% Pu^{239}, 5.9% Pu^{240}, and 0.7% Pu^{241}

(2) Comparison with M-246 inside the precision long counter

(3) Comparison with NBS-I on 8/27/58 and then with M-590 on 10/31/61 after the latter had been calibrated against NBS-I on 7/14/61 (manganese sulfate bath technique at the National Bureau of Standards on 8/27/58 and 7/14/61 and precision long counter method on 10/31/61)

(4) Calorimetric method at Mound Laboratory[17]

(5) Short term comparison with precision long counters against NBS-II and Ra-Be68B at Hanford

$P_2 = 0.059$, and $P_3 = 0.007$, then Hertz states that the initial buildup rate is 2.1 percent/year and that the neutron emission rate will rise to a maximum 36.3 percent above its initial value in 69.5 years.

One source, M-590, now on loan from Mound Laboratory to Hanford, was measured calorimetrically[17] and from the rate of change of its heat output the law for neutron emission rate buildup was deduced and is expressed approximately in the following equation

$$Q(t) = 8.98 \times 10^6 + 2.11 \times 10^6 (1 - e^{-1.438 \times 10^{-4} t}) \quad (7)$$

where t is measured in days since the calibration at the National Bureau of Standards made on July 14, 1961. When referred to January 1, 1961, this equation gives approximately

$$Q(t) = 8.92 \times 10^6 (1 + 0.0000338t) \quad (8)$$

Accurate records of isotopic compositions for most of the sources given in Table IX are unavailable. Thus, accurate application of Hertz's formula for determining β is not possible. Nevertheless, probably the best value of β for the source M-246 is the value stated in Table IX because application of Method (5), which makes use of the precision long counter, is probably affected by the "gamma-ray" effect described in a previous paper. (Method (5) gave a buildup rate of 2.6 ± 0.5%/year compared to the calculated value of 2.1%/year for 36,500 β).

The two 1-gram Pu-Be neutron sources listed in Table IX are mounted in special holders for use with the precision long counters and cannot be removed from these holders and then returned without recalibration in terms of one of the undisturbed sources.

Two quantities are of interest regarding these small sources:

$$r(x) = \frac{\text{count rate for source x inside a precision long counter}}{\text{count rate for M-246 inside the same long counter}}$$

and

$$q(x) = \frac{\text{count rate for source x in "reversed" orientation in counter}}{\text{count rate for source x in "normal" orientation in counter}}$$

"Normal" orientation occurs when a scribed mark on the end of the source-holder rod is facing toward the BF_3 tube and a pin through the rod is locked in place in the end of the aluminum liner containing the rod inside the counter. The "reversed" orientation occurs for the other possible locking position 180 degrees from the "normal" position.

Figure 9 gives a plot of the measured values of r(M-710). The data show two things: (1) the stability of the mountings of the two sources, M-246 and M-710, and (2) the sources have the same buildup rates in their neutron emission rates. The near symmetry of the neutron emission from M-246 is demonstrated by the measured q(M-246) = 0.9992 ± 0.0010 because it is so close to unity. The quantity a(x) was not measured for M-710 before it was returned to Mound Laboratory for recanning as part of a general recanning program for old Pu-Be sources.

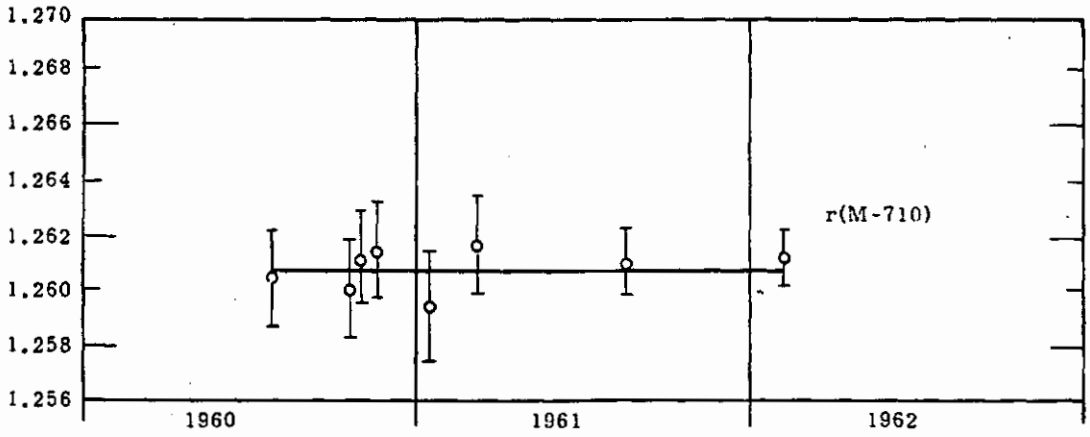

FIGURE 9

Secular Variation of Source M-710

Figure 10 shows a plot of the measured values of r(m-596). The presence of the one point (open circle) below the rest of the data and the fact that q(M-596) = 0.9919 ± 0.0010 deviates appreciably from unity suggests the possibility that r(x) might have been measured in the "reversed" position; however, the "corrected" point (solid circle) lies above the rest of the data. Instability in the mounting of M-596 is indicated.

The data presented in Figures 9 and 10 have not been corrected for dead-time loss in counting. The estimated dead time is 4.7 microseconds. A typical counting rate for M-246 is about 44,000 counts/min.

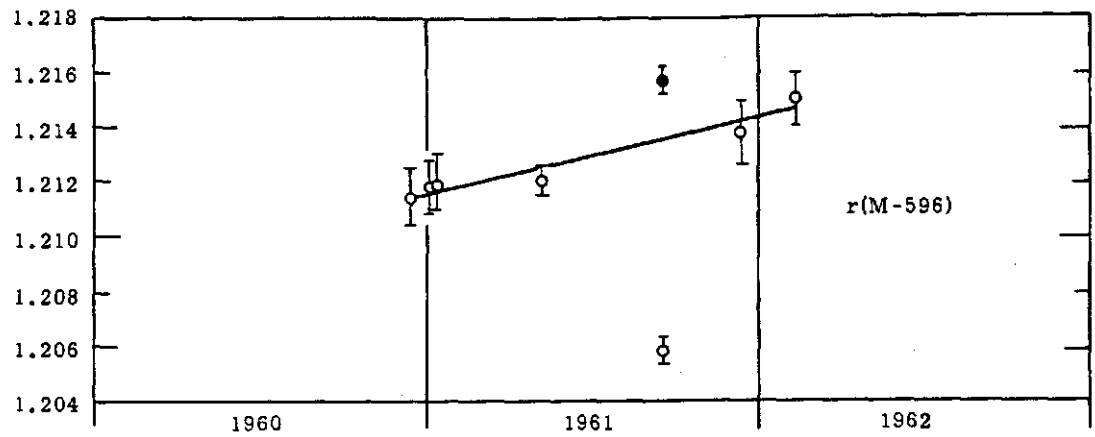

FIGURE 10
Secular Variation of Source M-596

Two solutions have been offered to the problem of obtaining Pu-Be neutron sources whose ε's are known. The first one, offered by the author, is to set up a stockpile of plutonium, extract the Am^{241}, mix the remaining plutonium thoroughly, make accurate isotopic analyses, and, finally, check samples calorimetrically. Future standard Pu-Be neutron sources would then be made from this stockpile. However, such a procedure is costly and would have to be undertaken by an appropriate national or international agency.

A second solution[18] was suggested by Geiger, who first focused attention[19] on the problem of unknown buildup rates from Pu-Be sources: Pu-Be sources would be made of pure Pu^{238} instead of Pu^{239} and its companion isotopes. This type of neutron source would have a noticeable decay rate. On the other hand it would yield a high specific activity and, hence, would be small in size, thus avoiding excessive scattering within the source. Finally, it would not undergo neutron induced fission. The spontaneous fission rate, however, is appreciable.

A Large Neutron Moderator - J. De Pangher and P. E. Bramson

A large moderator is described that can be used for studying neutron emission from (α, n) or (γ, n) sources or for obtaining a small flux of thermal neutrons.

A large neutron moderator (3 feet long, 3 feet in diameter) was constructed to be used to (1) measure neutron yields of plutonium compounds, and (2) produce thermal neutrons from the fast neutrons generated in a thick beryllium target bombarded by deuterons from the Van de Graaff accelerator. The moderator was mounted with wheels on a track for easy conversion from the 4π mode of operation [function (1)] to the neutron activation mode of operation [function (2)].

Figure 11 shows a sketch of the large moderator. It was made of an aluminum container filled with paraffin except for 17 holes defined by aluminum tubing and usually containing polyethylene inserts. Table X gives the locations and the sizes of these 17 tubes.

TABLE X

TUBE LOCATIONS AND DIAMETERS

Distance From Tube Center to the Moderator Center, in.	Number of Tubes	Inside Diameter, in.	Tube Designation
14	8	1.5	Outer Small
12	4	2.5	Outer Large
7	4	2.5	Inner Large
0	1	9.0	Central

The central polyethylene insert is made of 3 cylinders placed end to end with lengths 12 inches and diameters 9 inches. The cylinder on the end of the moderator facing the beryllium target contains a 1.75-inch diameter polyethylene insert which is removed when the moderator is used in the neutron activation mode. Two different cylinders are used for the middle cylinder in the central insert, one for the 4π mode of operation, the other for the neutron activation mode of operation. The cylinder for the 4π mode

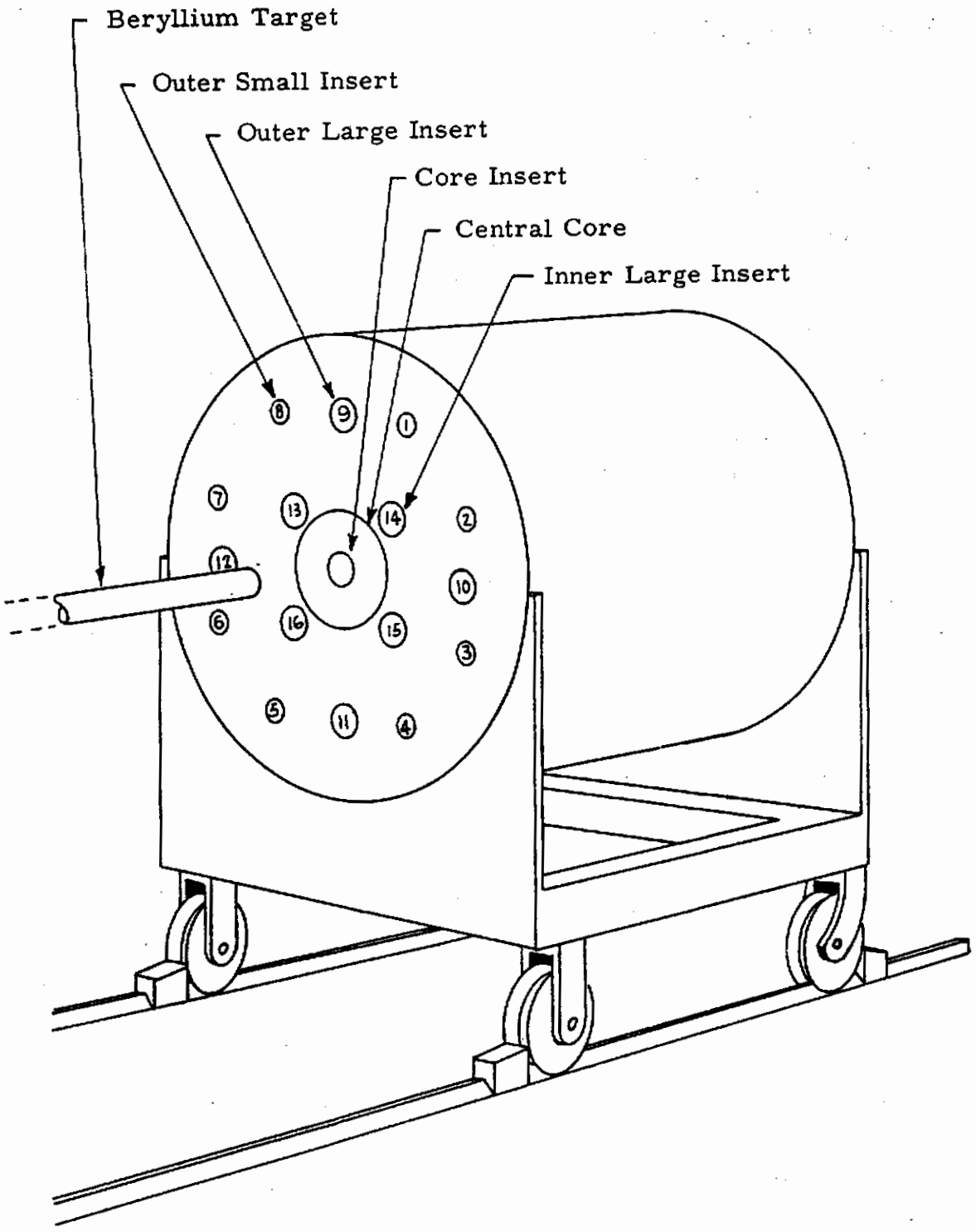

FIGURE 11

A Large Neutron Moderator

of operation contains a large cavity measuring 4-1/2 inches in diameter and 6 inches in length in which plutonium compounds can be placed. The cylinder for the neutron-activation mode contains slots for the activation foils.

A preliminary investigation of the 4π mode of operation of the large moderator was completed. The objective was to arrange a set of BF_3 tubes to minimize the effect of radial or axial displacements of a source in the central cavity so that samples of a particular compound could be counted with little concern about their shape or size. Only 8 BF_3 tubes were available at the start of these studies. These tubes contain 25 cm mercury pressure of enriched (96 percent B^{10} and 4 percent B^{11}) gas, have a sensitive length of 10-3/8 inches, and are 1-1/2 inches in diameter. Four of these were arranged in holes 1, 3, 5, and 7 (Figure 11), with the centers of the sensitive regions at a distance of 6-13/16 inches from one end of the moderator while the other four tubes were put into holes 2, 4, 6, and 8 at the same distance from the other end of the moderator. The counting rates for the two sets of tubes were then equalized by moving one set of tubes slightly. For these tests a rather large Pu-Be neutron source, containing about 80 grams of plutonium, was centered in the cavity on styrofoam spacers. The sum pulse height spectrum for these 8 tubes is shown in Figure 12 as measured on a 400-channel pulse height analyzer.

To test the sensitivity of the arrangement to the location of the Pu-Be source in the cavity, the source was moved to different positions and the counting rates were observed. The maximum variation of this sensitivity from from the sensitivity for a centrally positioned source amounted to 8 percent. Probably this variation could be reduced by using the full quota of 16 BF_3 tubes which are now on hand. Several plutonium metal disks of different thicknesses were counted to estimate the effect of multiplication in the disks on the emission measurements. The energy sensitivity of this arrangement was found to be very poor, as expected from the results of other workers.[20]

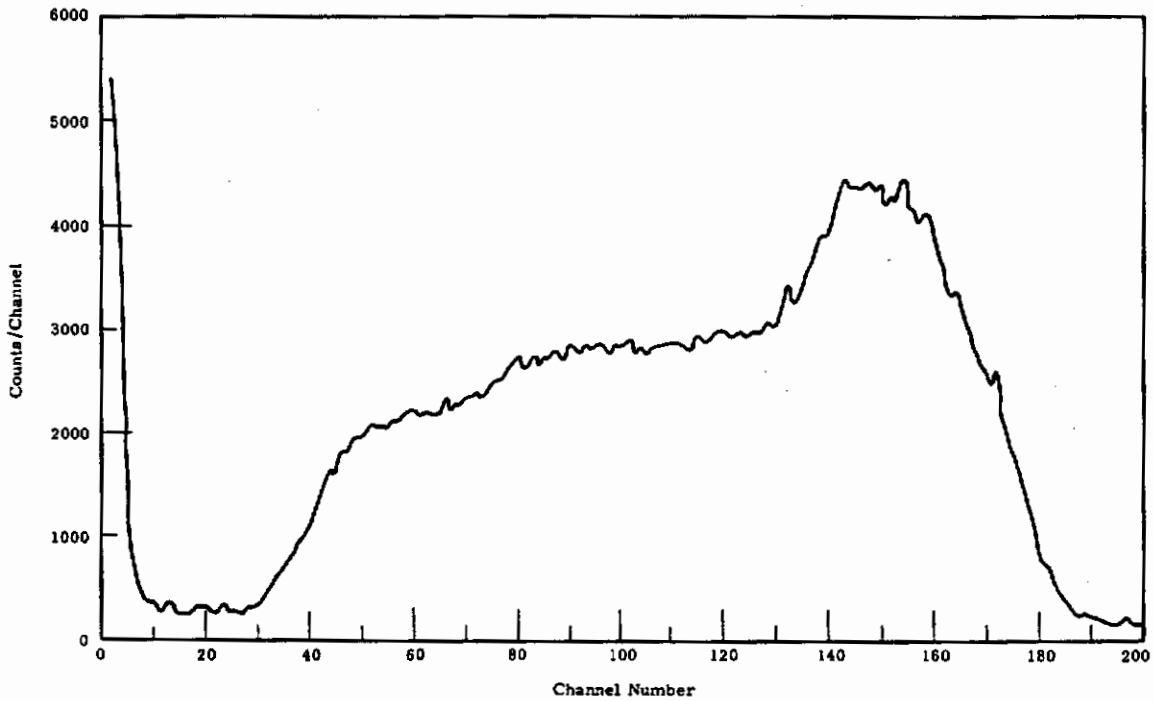

FIGURE 12

Sum Pulse Height Spectrum from Large Moderator

The moderator has not been used for activation work yet. Its position was adjusted so that it can be moved to surround a Van de Graaff target, and a thick, water-cooled beryllium target for this application was prepared and found to be satisfactory.

Improved Technique for Preparation of Carbon Targets - B. I. Griffin and R. D. McCormick

The durability of carbon targets for Van de Graaff use in considerably improved if the target backing material is kept hot while depositing the carbon.

Carbon targets made by the evaporation technique described by McCormick and McCormack[21] appeared, before bombardment, to be durable, i.e., they withstood normal handling procedures without apparent damage. However, almost immediately upon bombardment with positive

ions from a 2-Mev Van de Graaff accelerator the carbon coatings peeled or cracked on nearly every target backing, thus shortening the useful life of the target.

A method was found which produced very good adherence between the carbon film and the backing material (in this case tantalum). The improvement in technique consists of keeping the target backing material hot during the evaporation of the carbon.

The following technique proved best for evaporating carbon onto target backing material. The target backings are sanded smooth, cleaned in benzene and alcohol, outgassed at about 1100 C, and weighed. The target backing are mounted in the target holder so that they are close to the graphite electrodes. A current of 60 amperes is passed through the electrodes to outgas them and to heat the target backing material. When outgassing is completed, an arc is drawn between the electrodes. The evaporation is done as rapidly as possible. The targets are removed from the bell jar and weighed to determine the amount of carbon deposited.

One target from each batch of 5 targets in a recent lot was tested for endurance by placing it in a vacuum furnace tube and heating it to 1000 C. No noticeable damage resulted. One target was bombarded for a total of 15 hours in the positive ion accelerator with beam currents of from 8 to 14 μa and particle energies of from 0.5 to 1.5 Mev without any visible damage. There have been several target failures during routine use of the targets; usually the carbon film came completely loose from the backing material. The performance of these newly prepared targets, even with the failures, is far superior to the targets prepared by the original technique.

Target Contamination - J. De Pangher and J. S. Loomis, Jr.

The time-of-flight system was used to examine neutron spectra from deuteron bombardment of zirconium or titanium targets loaded with deuterium or tritium. Carbon contamination and surface and interior deuterium contamination were detected. A gas target that is free of contamination is described.

A number of attempts to calibrate a polyethylene version of the double moderator[11] with D(d, n) or T(d, n) neutrons produced in solid targets failed to yield reproducible ratios of counts. These targets were made by loading thin layers of zirconium or titanium evaporated on platinum disks. Even the use of previously unused targets failed to solve the problem. Consequently, studies of these types of targets were made by measuring the neutron energy spectra from them with the aid of the Hanford time-of-flight system when these targets were bombarded with 2-Mev deuterons.

The targets were made by evaporating zirconium or titanium to thicknesses in the range of 200 to 600 $\mu g/cm^2$. The deposit was confined to a 3/8-inch diameter, centrally located area on the 3/4-inch platinum disk so the uncoated remaining annulus could be used to seat an O-ring near the periphery of the disk. The platinum disks were made from 0.010-inch-thick platinum sheet. The same glass system was employed in the filling operation for both gases. The tritium gas was stored in an uranium bed and was not new. The deuterium gas was relatively new and was stored in the cylinder provided by the vendor.* The filling procedure consisted of inductively heating the disk in vacuum up to a dull red heat and then letting it cool gradually in a few millimeters pressure of the filling gas. Filling ratios of 0.5 to 1.0 gas atoms to metal atoms were obtained.

The advantage of using the time-of-flight system rather than other types of neutron spectrometers for a study of target contaminants is its high efficiency for neutron detection and, consequently, the small amount of

* Stuart Oxygen Company, San Francisco, California

integrated current required at the target for the study. Small interior loading of the platinum metal with the beam during the spectrum measurement is not expected to add appreciably to previous contamination by the beam.

The detector was a 1-1/2-inch diameter, 1/2-inch thick stilbene crystal mounted on the end face of an RCA 6810A photomultiplier. It was placed 96 cm from the target of the Hanford 2-Mev positive ion Van de Graaff accelerator. Substantial reduction of detector response to gamma radiation was achieved by employing pulse-shape discrimination. The gamma rays which "leaked" through the pulse-shape discrimination circuit were used as time markers in the time-of-flight system. The pulse beam current for a burst width of about 4 ns averaged about 0.3 μa and was directed on the target for only 10 minutes in each run.

A typical spectrum is shown in Figure 13 for Target P-88 (tritium-titanium target). The carbon contamination and the interior deuterium contamination were expected,[22] but the surface deuterium contamination came as a surprise. Apparently either the tritium bed or the gas-filling system had become contaminated with deuterium. Another surprise was that moving the beam to different parts of the target changed the neutron-energy spectrum--a result which denies an experimenter an opportunity to correct for target contamination. Table XI lists the results for 11 runs on various tritium-loaded targets.

A few deuterium-loaded targets were tested by the time-of-flight system in the same way as were the tritium-loaded targets. All runs showed carbon contamination but interior deuterium loading was not observed. (Probably the failure to observe interior deuterium loading can be attributed to the limited amount of data or to the fact that by the time the deuterons reach the interior, the energy, and hence the cross section for neutron production, is much lower than it is at the surface. In the case of the tritium-loaded targets, the cross section for neutron production from the interior deuterium is comparable to the cross section for neutron production from the surface tritium.)

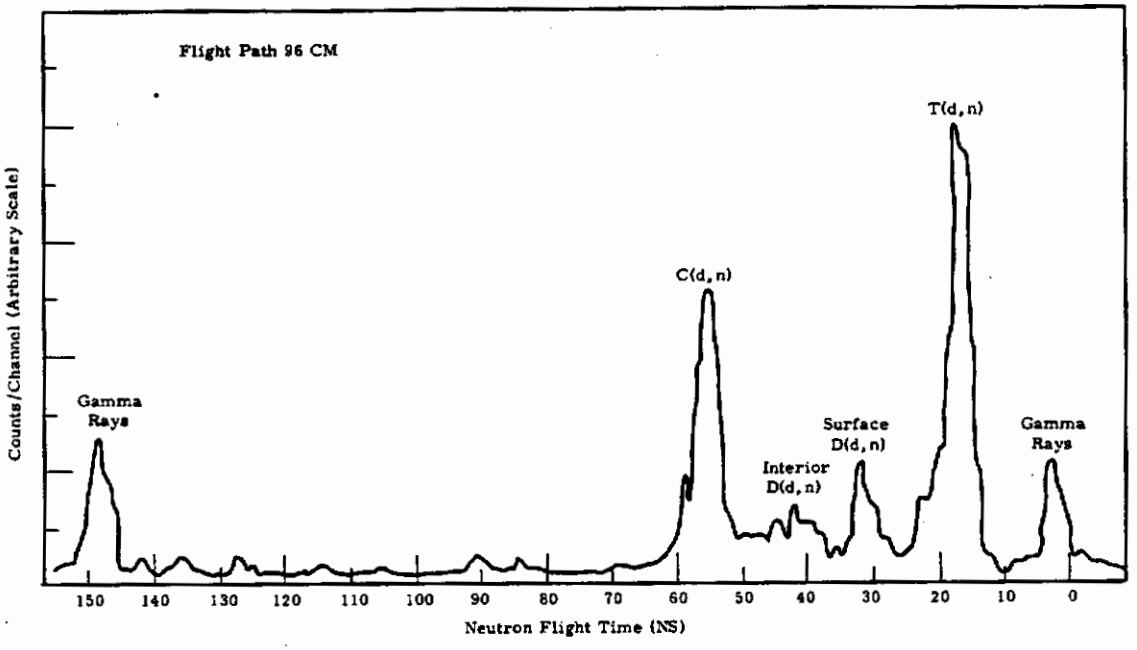

FIGURE 13

T(d, n) Target Spectrum Showing Contamination

TABLE XI

PERCENTAGE OF NEUTRONS FROM DEUTERON REACTIONS VARIOUS TRITIUM-LOADED TARGETS

Target Number	Run Number	T(d, n)	D(d, n) (Surface)	D(d, n) (Interior)	C(d, n) (Surface)
P-88	1	68	6	6	19
P-88	2	64	17	3	26
P-88	3	57	15	5	23
P-88	4	52	15	4	29
P-93	5	59	11	4	26
P-88	6	81	0	0	19
P-92	7	38	49	0	19
P-98	8	77	0	0	23
P-98	9	75	5	0	20
P-95	10	89	5	0	16
P-95	11	97	0	0	3

In the D(d, n) reaction the contamination problem has been substantially reduced by employing a gas target[23] instead of a solid target. A double gas cell is employed. The first cell, separated from the accelerator vacuum system by a thin nickel foil, contains deuterium gas at atmospheric pressure. The foil is cooled by a jet of gas directed upon it when the gas in the cell is circulated in a closed system. The beam passes through the deuterium gas, makes neutrons, passes through a second nickel foil, and stops in the second cell through which is flowing helium gas. The circulating system for the helium gas is identical to the circulating system for the duete-rium gas and provides cooling for the second nickel foil. No neutrons are made in the helium gas. High neutron yields free from contamination, as demonstrated with the time-of-flight system, result. Beam currents up to several microamperes can be maintained for several hours before the nickel foils have to be replaced. Probably the contamination of the tritium targets can be reduced by using gas instead of solid targets, although a gas flow system in this case would not be practical.

Calorimetric Determination of the Half-Life* of Antimony-124 - D. M. Fleming and I. T. Myers

An improved value for the half-life of Sb^{124} was determined using a high precision calorimeter. A 31-gram cylinder of 99.999 percent pure antimony was irradiated in a graphite moderated reactor to an activity of about 40 curies. The data, which extended over two half-lives, were least-squares-fitted using an IBM 7090 computer. The resulting value of half-life, using the 103 data points available at present, is 60.24 days, with a standard deviation of 0.02 days.

* Presented at the American Physical Society Meeting, Washington, D. C., April, 1962.

W (Air) for Cobalt-60 Gamma Ray Secondaries - I. T. Myers

A value for W (air) for Co^{60} secondaries was obtained by combining high pressure free air ionization chamber measurements and calorimetric source strength measurements of the same source. The result was 33.86 ± 0.34 ev/ion pair. This is in good agreement with other recent determinations.

The energy required to produce an ion pair in air was determined from a combination of calorimetric and ionization measurements. The equation expressing the fact that charged particle equilibrium exists in a free air chamber can be solved for W,

$$W = \frac{I \mu_a}{J} , \tag{9}$$

where I = gamma ray intensity in ev/cm^2 sec,

μ_a = energy absorption coefficient of air in cm^2/g,

J = ion current in ion pairs/g sec.

The value of $I \mu_a$ was calculated from the inverse square law,

$$I \mu_a = \frac{Q (h\nu_1 + h\nu_2) (\bar{\mu}_a) (3.7 \times 10^{10})}{4\pi r^2} , \tag{10}$$

where Q is the activity of the source in curies and $\bar{\mu}_a$ is the average mass energy absorption coefficient for the two gamma rays given off by Co^{60}. The distance r was taken as 100 cm, since the measurement of J was taken at that distance. The value of Q was determined as 0.5012 curies with a gamma ray calorimeter.[24] The NBS Handbook 62 value of $\bar{\mu}_a$ (air) is 0.02670 cm^2/g.

$$\text{The value of } I \mu_a = \frac{0.5012 (3.7 \times 10^{10}) (2.5053 \times 10^6) (0.02670)}{4\pi (100)^2}$$

$$= 9.871 \times 10^9 \text{ ev/g sec} \tag{11}$$

The value of J, the ionization per gram second, was determined with a high pressure free air ionization chamber by H. O. Wyckoff of the United States National Bureau of Standards.[25] Measurements were made at 10.75 and 12.27 atmospheres and gave a value of 0.756 r/hr at a meter. From this,

$$J = \frac{0.756 \text{ r/hr}}{0.001293 \text{ g/cm}^3 \, (3600 \text{ sec/hr}) \, 4.80288 \times 10^{-10} \text{ esu/ip}}$$

$$= 3.382 \times 10^8 \text{ ip/g sec} \quad . \tag{12}$$

The calorimetric measurement of I was made on August 1, 1960, while the free air chamber measurement was made on February 22, 1959, making a decay correction necessary. The half-life for Co^{60} was taken to be 5.264 years. The decay correction was 1.2081, with an error in this correction of less than 0.1 percent. It was also necessary[31] to make a correction of 1.011 for absorption in the source wall and a correction of 1.030 for absorption in the source. The source had a diameter of 1/8 inch and was encased in an aluminum holder.

The calculation for W (air) is then:

$$W = \frac{I \mu_a}{J}$$

$$= \frac{9.871 \times 10^8}{3.382 \times 10^8} \, \frac{(1.2081)}{(1.011)(1.030)}$$

$$= 33.86 \text{ ev/ip.} \tag{13}$$

The estimates of the uncertainties of the different measurements and quantities were: calorimeter, 0.4 percent; free air chamber, 0.6 percent; energy absorption coefficient, 0.5 percent; decay correction, 0.1 percent; absorption corrections, 0.4 percent. The total rms uncertainty was 1 percent.

These results are in excellent agreement with the recent results of Reid and Johns.[26] They obtained an average value of W for Co^{60} of 33.85 ev/ip. However, the present result is slightly higher than the average they derived from from a selected list of published work (33.86 vs 33.7 ev/ip).

One of the principal advantages of the present method of measuring W is that, since a free air ion chamber was used, the need for calculating a wall stopping power correction was eliminated, with its consequent possibility of error.

From the preceding measurements it is possible to compute the gamma ray dose rate constant for Co^{60}. The value obtained was

$\Gamma = 1.300 \pm 0.013$ r/hr at 1 meter from a 1 curie source. (14)

Ozone Hazards Incurred by Electron Van De Graaff Operation -
J. S. Loomis, I. T. Myers, H. V. Larson, and D. E. Wisehart

Examples of ozone production during experiments with a Van de Graaff electron accelerator are described. If liquid nitrogen containing even quite small amounts of dissolved oxygen is deliberately or accidentally exposed to the electron beam, hazardous amounts of ozone are often produced.

During normal operation of a Van de Graaff electron accelerator, the principal potential hazard is the high radiation level produced. Hence, adequate shielding and radiation safety measures are universally employed to prevent the accidental overexposure of personnel. For experiments in which the electron beam itself is used to irradiate materials outside the accelerator vacuum system, additional problems may be created. The possible generation of ozone during the course of an experiment is of special interest due to the relatively high yields of ozone which may be obtained if oxygen is subjected to electron irradiation and due to the toxic and explosive characteristics of ozone.

Liquid nitrogen as obtained from the manufacturer is usually relatively pure. However, unless elaborate precautions are taken, the liquid nitrogen comes into contact with air in the course of its use in experiments. Due to its lower boiling point, oxygen from the air is condensed and becomes dissolved in the liquid nitrogen. If continuous exposure of the liquid nitrogen to air is permitted, the oxygen content will increase. Some liquid nitrogen was analyzed by mass spectrographic techniques. As delivered to the laboratory from the bottling area, it was found to be quite pure. Oxygen content was generally found to be less than 0.2 percent in nitrogen which had been

used for cooling in experiments. Thus the total quantity of liquid oxygen present in experimentally employed liquid nitrogen is quite small. However, its presence is of significance if the liquid gas is subjected to electron irradiation. The obvious possibilities are the production of ozone and of oxides of nitrogen. The former process is enhanced by the low temperature of the liquid nitrogen; the latter process is retarded by low temperature.

Ozone boils at -111.9 C, and melts at -192.7 C. The melting point was determined accurately only within the last few years and a value of -251 C is still listed in many modern references. Both solid and liquid forms of ozone are blue. Since liquid nitrogen boils at -195.8 C, small quantities of ozone formed in it by electron irradiation will remain in solution as a dissolved solid.

The following events were observed when liquid nitrogen was exposed to the action of high energy electrons:

(1) After a brief irradiation the liquid nitrogen solution turned a faint but distinct blue due to the generation of ozone.
(2) If the liquid nitrogen was allowed to evaporate at room temperature, the coloration of the solution intensified since, due to vapor pressure differences, ozone was almost completely retained in solution.
(3) After complete evaporation of the liquid nitrogen a bright blue residue (ozone) appeared but evaporated within a few seconds.

Ozone dissolved in liquid nitrogen is quite stable and dilute solutions have been kept for long periods of time without an apparent decrease in dissolved ozone content.

Measurements of air concentrations of ozone were made when liquid nitrogen in a glass container was irradiated for 5 minutes with a 15 μa beam of 2.0 Mev electrons. Air samples taken in the vicinity of the container shortly after evaporation of the liquid nitrogen showed ozone concentrations of greater than 75 ppm. In view of the toxicity of ozone, even brief exposure of personnel to such concentrations is obviously to be avoided.

In another measurement a 100 μa beam of 2.0 Mev electrons was allowed to dissipate its energy for 1 hour in the room air. With the forced air ventilation in use, the ozone air concentration at the end of the run was 0.011 ppm. For another run without forced air ventilation the ozone air concentration was 0.054 ppm. A rough estimate of the total quantity of ozone generated during this latter run may be obtained by assuming uniform distribution of the ozone throughout the room volume at the time of sample collection. In this case approximately 45.9 mg of ozone were produced for a total beam energy dissipation of 200 watt-hours. The dissipation of a given electron beam energy in air apparently produces roughly 1/1000th the ozone that would result from a similar irradiation of liquid oxygen and 1/50th the ozone that would result from the irradiation of a 0.1 percent solution of oxygen in liquid nitrogen.

In the preceding measurements air samples were also collected and analyzed for oxides of nitrogen. The production of oxides of nitrogen normally does not create a hazardous condition since, relative to ozone, production yields are an order of magnitude lower and tolerance limits are an order of magnitude higher.

In performing electron irradiations a number of ozone-induced explosions were noted. When electron irradiated liquid nitrogen is placed in a glass container and allowed to evaporate, brief flashes are observed on the side of the container resulting from the decomposition of minute quantities of ozone which remain as residue as the level of the solution recedes. If a piece of masking tape or other organic material is immersed in the solution a small detonation may result after evaporation of the liquid nitrogen. The most violent detonation observed occurred when a piece of masking tape was placed in an open 400 ml beaker containing liquid nitrogen which had been subjected to irradiation by 20 μa of 2.0 Mev electrons for 4 minutes. After evaporation of the liquid nitrogen, the resulting explosion completely shattered the beaker. Ozone content of the solution in this case was estimated at less than 13 mg. Thus, the accumulation of quite small quantities of ozone in a liquid nitrogen cooling apparatus can create a serious explosion hazard if the liquid nitrogen in such a system is allowed to evaporate.

Electron irradiation of liquid nitrogen containing less than 0.2 percent dissolved oxygen will result in the generation of significant quantities of ozone. The total ozone generation is not directly proportional to the dissolved oxygen content. Thus a substantial reduction in oxygen content will not necessarily result in a similar decrease in ozone production. Ozone generated during repeated irradiations of the liquid nitrogen will tend to concentrate in the cooling system and subsequent evaporation of the liquid nitrogen may create an acute personnel exposure and explosion hazard.

The Heat Amplifier--A New Technique in Calorimetry* - I. T. Myers and D. M. Fleming

Amplification is a process in which a small signal is used to control larger amounts of power from an auxiliary source. The technique of amplification by electronic means is, of course, of immense importance. Similarly, light amplification techniques are expected to be very valuable. This paper describes a method of amplifying heat, a method of using a small source of heat to cause a much larger change in an auxiliary heat source.

The apparatus used resembles an isothermal calorimeter. The submarine jacket was made of brass and the insulation was Styrofoam. The water bath was held constant to within ± 0.001 C. Washer thermistors which had a negative temperature coefficient (the resistance decreases as the temperature increases) made up the large heat source whose amplitude was changed by the input heat signal. If a source of heat power, P, is added to the calorimeter, with a constant voltage E applied to the washer thermistors, the temperature rise will be greater than if the thermistors were not there. The change in thermistor power is simply $E^2/F_o - E^2/R$ where R is the thermistor resistance with P applied to the calorimeter and R_o is the thermister resistance when P = 0. Heat amplification could also be accomplished with positive temperature coefficient resistors with this same arrangement of components if a constant current source were used instead of a constant voltage source.

---

* Published in Radiology 78: 111. 1962.

Operation of the amplifier is started with the calorimeter at bath temperature. When voltage is applied to the washer thermistors, the calorimeter temperature rises to a new equilibrium level. The time constant for this rise was about 90 minutes. With the calorimeter at this new equilibrium level, a small amount of additional heat power (unknown or for calibration) is added. The temperature of the calorimeter then rises to a final equilibrium value.

Amplification was measured as a function of the voltage applied to the thermistors. The amplification increased up to 6.5 at 10 volts. Above this voltage, measurements were hampered by instabilities of the power supply.

Field Equations in Dosimetry* - H. H. Rossi** and W. C. Roesch

In electricity and magnetism, elasticity, etc., field equations have been developed to express fundamental properties of the field studied and to serve as the basis for theoretical development of the subjects. Such equations are developed here for fields of ionizing radiations. These equations have been useful in clarifying and more rigorously defining dosimetric concepts.

The absorbed dose D in a medium of density ρ is given by

$$D = -(1/\rho)\,\nabla \cdot \vec{G} + E - Q \qquad (14)$$

where $\vec{G}$ is the vector rather than the scalar sum of the energy flux density (intensity) components in different directions, and E and Q are the mass-densities of energy emitted by radiation sources and of the energy equivalent of any rest mass changes. The relation of this definition to such quantities as exposure dose, stopping power, and specialized absorption coefficients used in dosimetry, is shown by means of energy balance relations or by means of development from basic transport equations.

---

* Accepted for publication by Radiation Research

** Radiological Research Laboratory, Columbia University, New York, N. Y.

REFERENCES

1. Roesch, W. C. and H. E. Palmer. "Shadow Shields," Research and Development Activities in the Radiological Sciences - 1960, HW-70050. January 16, 1961.
2. Palmer, H. E. and W. C. Roesch. "Scanning Counter," Research and Development Activities in the Radiological Sciences - 1960, HW-70050. January 16, 1961.
3. Brucer, M. Thyroid Radioiodine Uptake Measurement, ORINS-19. June, 1959.
4. Burch, P. R. J. "Measurements at Leeds Following the Windscale Reactor Accident--Iodine-131 in Human Thyroids and Iodine-131 and Caesium-137 in Milk," Nature 183: 515-517. 1959.
5. Comar, C. L., et al. "Thyroid Radioactivity after Nuclear Weapons Test," Science 126: 16-18. 1957.
6. Foster, R. F. Evaluation of Radiological Conditions in the Vicinity of Hanford for 1961, HW-71999. March 1, 1962.
7. McCall, R. C. "Measurement of Plutonium in Wounds," presented at the Symposium on the Acute Radiation Syndrome, U. S. Naval Medical School, National Naval Medical Center, Bethesda, Maryland, May, 1959.
8. International Commission of Radiological Protection. Recommendations of the International Commission on Radiological Protection; Report of Committee 2 on Permissible Dose for Internal Radiation, ICRP Publication No. 2, page 167. London: Pergamon Press, 1959.
9. De Pangher, J. "A Reproducible Precision Polyethylene Long Counter for Measuring Fast Neutron Flux," Research and Development Activities in the Radiological Sciences - 1960, HW-70050. January 16, 1961.
10. De Pangher, J. "A Reproducible Precision Long Counter for Measuring Fast-Neutron Flux," Bull. Am. Phys. Soc. Series II, 6: 252-253. 1961.
11. De Pangher, J. "Double Moderator Neutron Dosimeter," Nucl Inst. and Methods 5: 61-74. 1959.
12. Anderson, M. E. Personal communication, Monsanto Research Corp., Miamisburg, Ohio. January 24, 1962.
13. St. Romain, F. A., et al. "Low Energy Neutrons from the (α, n) Reaction in Be^9," Bull. Am. Phys. Soc. Series II, 6: 369. 1961.
14. St. Romain, F. A., et al. To be published in Physical Review.
15. Loomis, J. S. An Investigation of the Operational Characteristics of the Perlow Spectrometer, HW-69471. May 2, 1961.
16. Hertz, M. R. Personal communication, Monsanto Research Corp., Miamisburg, Ohio. January 26, 1961.

17. Anderson, M. E. Personal communication, Monsanto Research Corp., Miamisburg, Ohio. January 31, 1962.

18. Geiger, K. W. Personal communication, National Research Council, Ottowa, Ontario, Canada. June 15, 1961.

19. Geiger, K. W. "Measurement of Neutron Flux and Spectra for Physical and Biological Applications," NBS Handbook 72, page 9. 1960.

20. Marion, J. B., et al. University of Maryland Physics Department Technical Report 172. April, 1960.

21. McCormick, R. D., and J. D. McCormack. Hydrogen and Carbon Target Preparation for a Positive Ion Accelerator, HW-67797. October 26, 1960.

22. Coon, J. H. "Low Scatter High Current Gas Target for D-D Neutrons," Fast Neutron Physics, Part 1, Chapter IV, pp. 677-720. New York: Interscience Publishers. 1960.

23. Richardson, A. C. B. "Targets for the Production of Neutrons," Rev. Sci. Inst. 31: 1202-1203. 1960.

24. Le Blanc, W. H., I. T. Myers, and D. M. Fleming. An Intercomparison of Adiabatic Calorimetry and Coincidence Counting for the Activity Determination of a Cobalt-60 Source, HW-66262. July 29, 1960.

25. Wyckoff, H. O. "Measurement of Cobalt-60 and Cesium-137 Gamma Rays with a Free-Air Chamber," J. Res. NBS 64C: 87-97. 1960.

26. Reid, W. B., and H. E. Johns. "Measurement of Absorbed Dose with a Calorimeter and Determination of W," Radiation Research 14: 1-16. 1961.

RADIOLOGICAL CHEMISTRY

Analytical and Counting Methods

The Separation of Scandium-46 from Aqueous Samples by a Tri-n-Octyl Phosphine Oxide-Coated Microbead Column - C. W. Thomas

A procedure was developed to determine Sc^{46} in water samples. Scandium is removed from two liter samples by passing the sample through a column of tri-n-octyl phosphine oxide-coated micro-beads. Ethanol is used to remove the tri-n-octyl phosphine oxide and adsorbed scandium. Interference from contaminants is eliminated by radioactive decay and gamma counting. The 2.0 Mev addition peak is used to measure the concentration of Sc^{46}.

Scandium-46 is produced by activation of the stable Sc^{45} present in the coolant stream of the Hanford reactors. One of the notable characteristics of scandium is its ability to readily adsorb on surfaces of the coolant system. This characteristic coupled with the 85-day half-life presents a condition which makes Sc^{46} one of the significant radioisotopes in the effluent stream, even though the concentration in the water is relatively small. During investigations of the use of tri-n-octyl phosphine oxide (TOPO) to remove uranium using a modified procedure of Dietrick, Caylor and Johnson,[1] it was noted that considerable amounts of Sc^{46} were present with the uranium. It seemed that the uranium procedure using TOPO-coated beads in a column form might also be useful to concentrate Sc^{46}.

An investigation was initiated to measure Sc^{46} in reactor coolant water and the downstream Columbia River water, using the high adsorptive characteristics of the isotope and the versatility of TOPO. The concentration of Sc^{46} in these waters was such that large sample aliquots were required to obtain the desired sensitivity. Consequently, the use of solvent extraction methods required the evaporation of 2 to 10 liter aliquots to a size which could easily be handled in the laboratory. In many cases, the time consumed in reduction of the volume and/or the possible loss of the sample on the glassware was critical and alternate methods were desired. To determine if scandium and any other reactor coolant radioisotope would

be adsorbed onto a column of TOPO-coated microbeads, a 2-liter sample of reactor effluent water was acidified with HNO_3, passed through the column, and the gamma spectrum was measured. This initial sample was 8 days old and showed mainly the photopeaks of 85-day Sc^{46}, 27-day Cr^{51}, and 2.33-day Np^{239}. Under these conditions, only a small percentage of the Np^{239} is held. Maximum hold-up of Np^{239} would require much higher acid strengths and oxidization to the NpVI state. The hold-up of Cr^{51} also represented only a small percent of the total. Fortunately, neither of these isotopes interferes with the measurement of Sc^{46}. Samples a few hours old showed the hold-up of shorter half-life isotopes such as Mn^{56} and traces of Na^{24}. The spectra from these samples are presented in Figures 1 and 2.

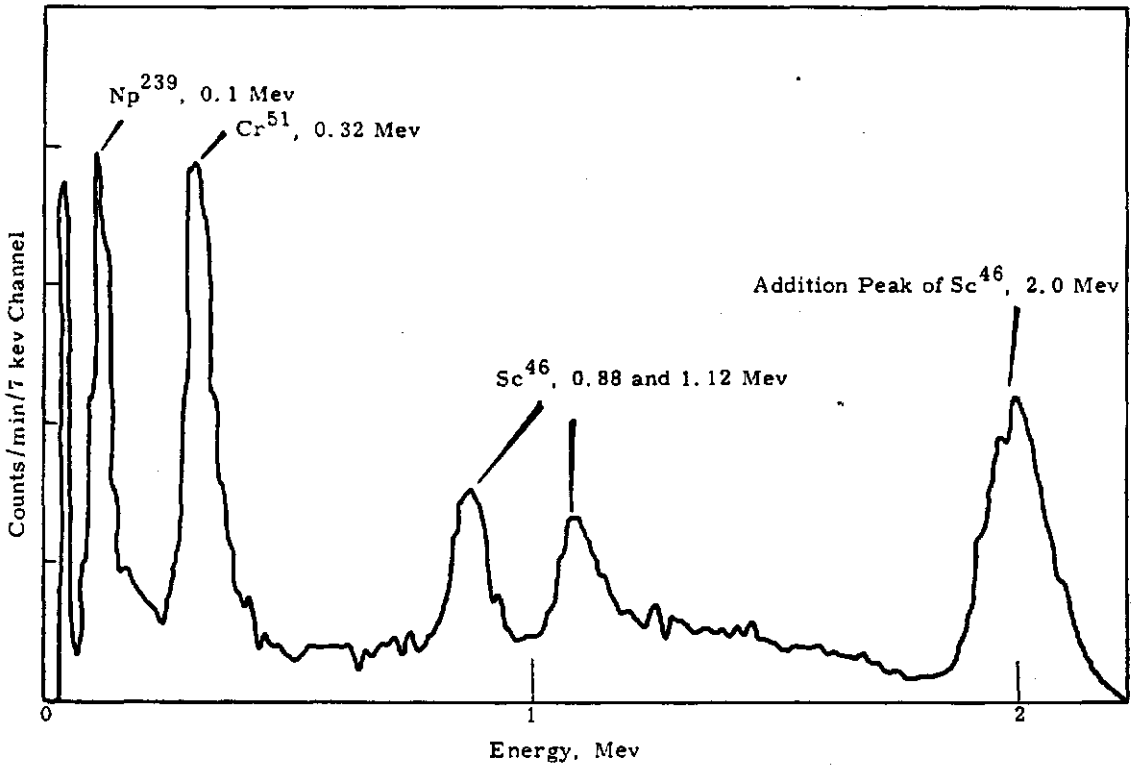

FIGURE 1

Gamma Spectrum of Eight-Day Old Effluent Water Adsorbed on Tri-n-Octyl Phosphine Oxide Column

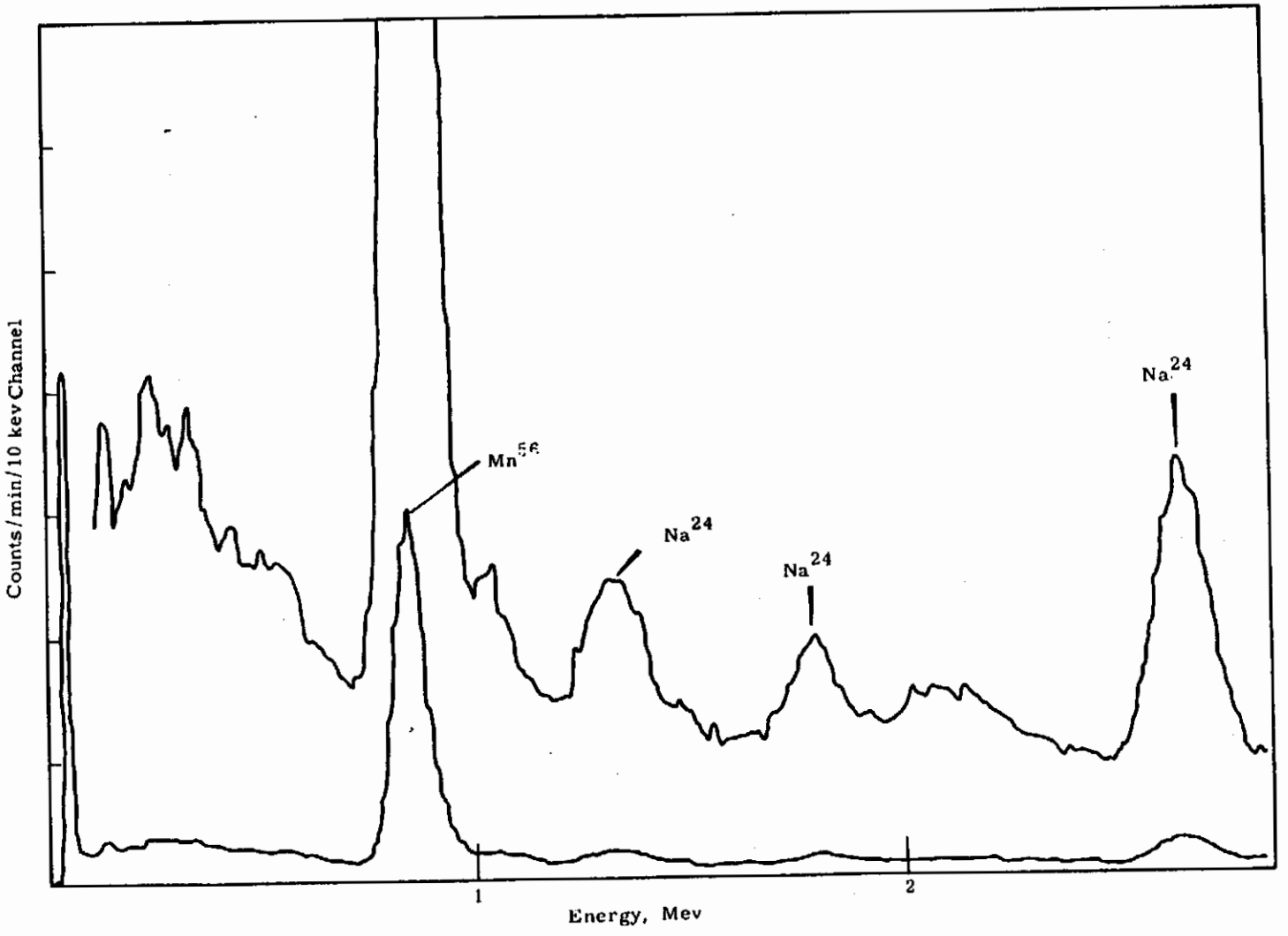

FIGURE 2

Gamma Spectrum of Four-Hour Old Effluent Water
Adsorbed on Tri-n-Octyl Phosphine Oxide Column

To determine the effects of acid concentration on the Sc^{46} removal, 2-liter samples were acidified with HNO_3 to cover the range of 0 to 6M and passed through columns at flow rates of 10 ml/min. These results are graphically illustrated in Figure 3. The removal efficiency abruptly increased to a maximum of 97 percent at a concentration of 0.5M, remained relatively stable to 1M, then slowly decreased until at 6M the efficiency was 94 percent. To determine the effects of the flow-rate on the removal efficiency, 2-liter samples were made 1M with HNO_3 (a concentration near maximum removal efficiency but sufficiently removed from the abrupt rise of the acid curve in Figure 3) and passed through the columns at flow-rates of from 1 to 50 ml/min. Pressure was required to maintain flow rates through the column greater than 30 ml/min. These data are presented in Figure 4. At low flow-rates the yield was 97 percent and relatively constant up to a flow-rate of 10 ml/min before gradually decreasing to a minimum of near 89 percent at a flow-rate of 50 ml/min. In all cases the columns were eluted with 4 column volumes of ethanol. The elution rate was adjusted initially to 0.25 ml/min but was increased rapidly as the TOPO was removed. The elution curve is presented in Figure 5. For measurement of the Sc^{46}, the eluant was placed in 9 oz. jars and measured in a 400 channel gamma spectrometer using a 9- by 9-in. NaI well crystal. The 2.0 Mev gamma addition peak was used to calculate the Sc^{46} recovery.

In summary, the adsorbent characteristics of TOPO coated on beads can be used to concentrate Sc^{46} from sample volumes up to 2 liters. Yields of 97 percent can be obtained at an acidity of 1M and a flow rate of 10 ml/min. These data suggest that conditions can probably be found where other isotopes can be similarly concentrated.

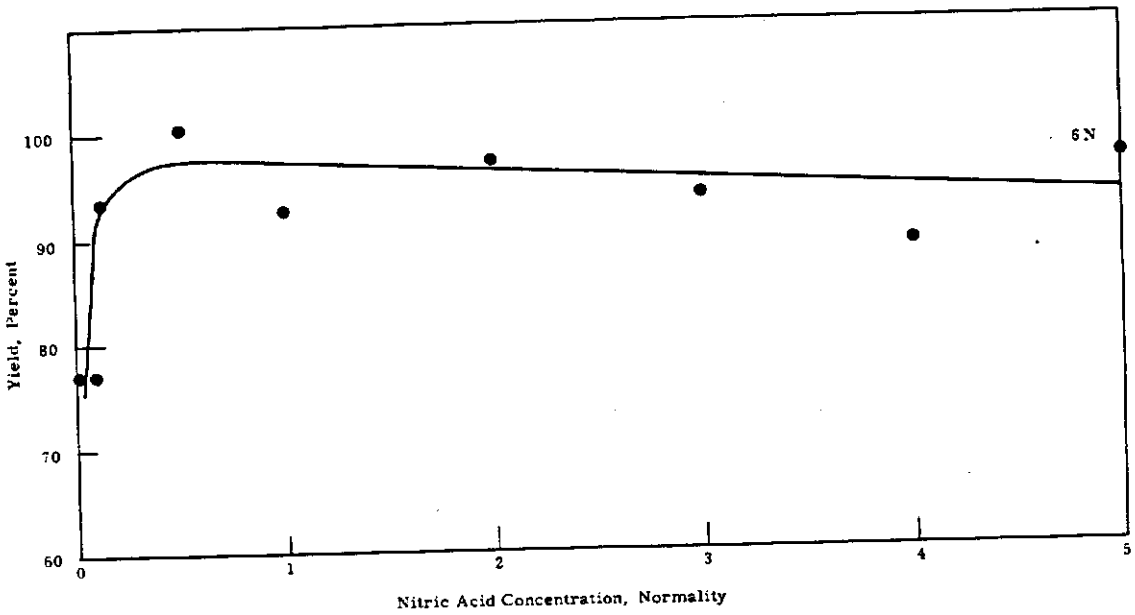

FIGURE 3

Yield Versus HNO_3 Concentration
(Flow Rate = 10 ml/min)

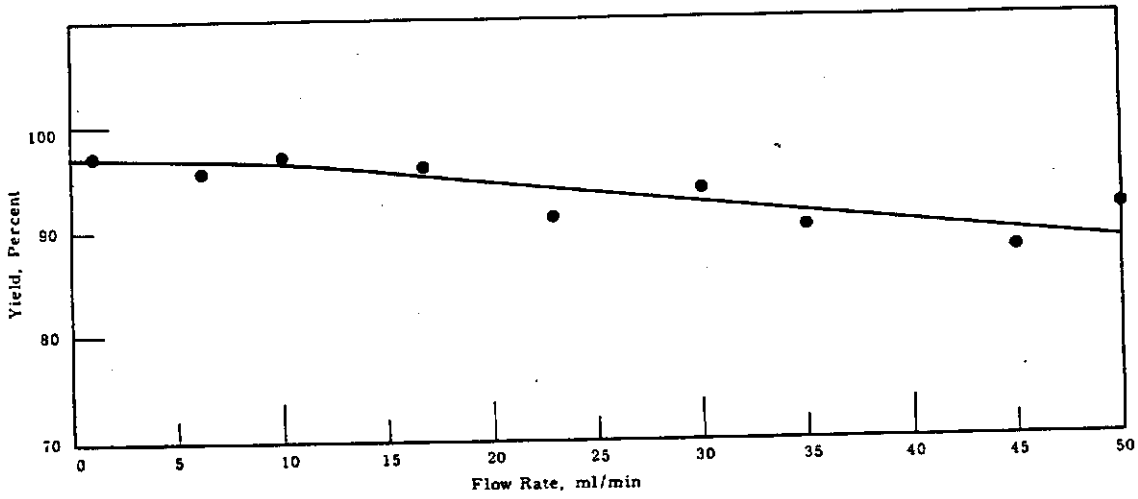

FIGURE 4

Yield Versus Flow Rate
1M HNO_3 Concentration

AEC-GE RICHLAND, WASH.

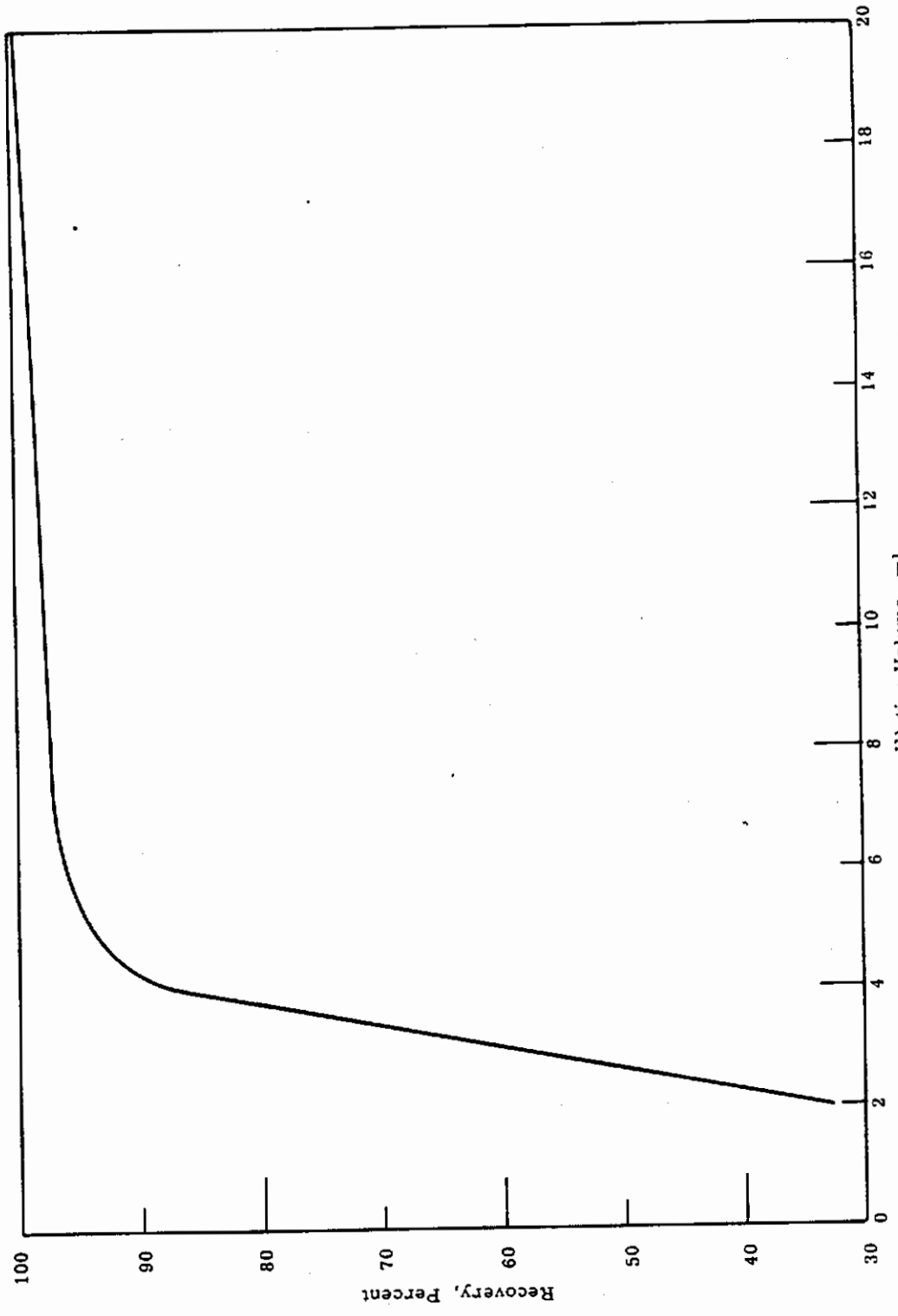

FIGURE 5

Removal of Tri-n-Octyl Phosphine Oxide with Ethanol

The Determination of Cesium-137 in Columbia River Water -
C. W. Thomas

A simplified procedure was developed to determine the Cs^{137} concentration in water samples. Cesium is directly carried on a cellulose filtering aid from 3-gallon samples by using tetraphenylboron. Contaminant interference is eliminated by a basic carbonate scavenge and gamma spectroscopy. The average yield over a range of 1×10^{-7} μc/ml to 1×10^{-9} μc/ml is 70 ± 5 percent.

Several selective and semiselective reagents for determining the concentration of cesium in aqueous samples are available. The most common of these reagents are the silicotungstates, chloroplatinates, perchlorates, and tetraphenylboron. Most cesium procedures use a combination of these reagents (such as the procedure of Sugihara, James, Troianello and Bowen)[2] to eliminate contamination from the other alkali metals and are classified as the "refined procedures". There is, however, an increasing need in the radiochemical field for simple, quick procedures which give very good results since interference from contaminants can be eliminated by decay and/or gamma spectroscopy. Such a procedure was developed to determine the concentration of Cs^{137} in Columbia River water.

The concentration of Cs^{137} in Columbia River water is such that it is necessary to use 3-gallon sample aliquots to obtain a sufficient quantity for measurement. To eliminate the tedious method of evaporation of an aliquot of this size to a volume which can be handled by current methods, a procedure was developed which used directly a 3-gallon aliquot. Tetraphenylboron, one of the semiselective reagents used for the determination of cesium, was added to a slightly acid 3-gallon sample of distilled water in which 100 mg of cesium carrier and sufficient Cs^{137} spike had been added previously. No visible precipitate was noted. However, by adding Super-cell filtering aid, allowing the sample to sit overnight, and then filtering through a Whatman filter, cesium is separated. The recovery of Cs^{137} was 75 percent. To eliminate interferences from some of the activation and fission products present in the Columbia River water, a basic

carbonate scavenge was necessary. This scavenge consisted of adding iron, zinc, chromium, and barium carriers to a sample made slightly basic to phenolphthalein and adding a solution of saturated sodium carbonate. To test this procedure in river water, ten 3-gallon samples were taken from the Columbia River above the Hanford reactors and spiked with varying amounts of Cs^{137}. The results are presented in Table I. Using this procedure the Cs^{137} concentration in the Columbia River below the Hanford reactors was determined on five 3-gallon aliquots. These results are presented in Table II.

In summary, cesium tetraphenylborate can be carried on Super-cell filter aid from 3-gallon size water samples. The average yield over the concentration range 1×10^{-7} μc/ml to 1×10^{-9} μc/ml was 70 ± 5 percent. The concentration of Cs^{137} in the Columbia River below the Hanford reactors was $3.6 \pm 1.4 \times 10^{-9}$ μc/ml.

TABLE I

RADIOCHEMICAL YIELDS USING TETRAPHENYLBORON

Sample	Sample Size, gal	Cesium-137, μc/ml		Yield, percent
		Added	Recovered	
1	3	1×10^{-7}	7.6×10^{-8}	76
2	3	1×10^{-7}	7.3×10^{-8}	73
3	3	1×10^{-7}	7.2×10^{-8}	72
4	3	1×10^{-8}	7.7×10^{-9}	77
5	3	1×10^{-8}	6.8×10^{-9}	68
6	3	1×10^{-8}	6.4×10^{-9}	64
7	3	1×10^{-9}	6.1×10^{-10}	61
8	3	1×10^{-9}	7.2×10^{-10}	72
9	3	1×10^{-9}	7.7×10^{-10}	77
10	3	1×10^{-9}	5.6×10^{-10}	56

TABLE II

CESIUM-137 CONCENTRATION IN THE COLUMBIA RIVER

Sample Number	Sample Size, gal	Cesium-137, μc/ml
1	3	2.1×10^{-9}
2	3	3.3×10^{-9}
3	3	4.5×10^{-9}
4	3	2.5×10^{-9}
5	3	5.4×10^{-9}

Procedure:

1. To 3 gallons of water add 100 mg cesium carrier, 3 ml of 2M HCl, 20 mg each of iron, zinc, chromium and a few drops of phenolphthalein indicator. Mix solution thoroughly.
2. To the solution add 10 ml 2M NaOH and 60 ml of saturated Na_2CO_3 solution. Stir and allow to coagulate for 6 hours.
3. Filter solution and save filtrate.
4. To filtrate add 60 ml of 6M HCl and stir. Adjust acidity to just acid with NaOH.
5. Add 20 ml of tetraphenylboron reagent.* Stir and let stand overnight.
6. Filter solution using Hi-Flow Super-cell filter aid,** count filter using gamma-ray spectrometer.

---

* Tetraphenylboron Reagent: Dissolve 4 grams of sodium tetraphenylborate and 1 gram of aluminum chloride hexa-hydrate in 100 ml of water. Add a few drops of phenolphthalein indicator and 6M NaOH solution dropwise until the solution is just basic. Allow to stand for 3 hours. Filter and dilute filtrate to 200 ml and store reagent in a cool location.

** Johns-Manville Company

The Determination of Palladium-109 and Palladium-112 in Samples Containing Mixed Fission Products and Plutonium - L. J. Kirby

A radiochemical procedure was developed for the measurement of Pd^{109} and Pd^{112} in mixed fission products plus plutonium.* Palladium dimethylglyoxime is precipitated from a citrate medium containing about 1 mg of palladium carrier and microgram quantities of holdback carriers for other fission products. Following dissolution of the precipitate in HNO_3, the solution is evaporated to a small volume. After dilution, palladium is loaded on a Dowex-50 (X8, 100-200 mesh, H^+) column from 0.5M HNO_3 solution. Elution is accomplished with 0.3M HCl; using a 10 mm diameter by 2.5 cm column, the colored palladium fraction is eluted in about 15 drops of eluate. Palladium is recovered as palladium dimethylglyoxime, weighed, and counted as such. The decay is followed by beta-proportional counting, and measurement of Pd^{109} by gamma-scintillation counting. Counting the source with and without suitable absorbers aids in more precise resolution of the 14- and 21-hour components of the decay curve. When the activity of the sample permits, Pd^{112} is measured by gamma-counting its 3.12-hour Ag_{112} daughter.

The Determination of Rare Earth and Yttrium Radioisotopes in Samples Containing Mixed Fission Products and Plutonium - L. J. Kirby

A "carrier-free" procedure, using lanthanum as a nonisotopic carrier for the rare earths and yttrium, is used to separate the rare earth and yttrium radioisotopes produced in plutonium fission. Plutonium and zirconium are removed from the solution mixture by anion exchange. The rare earth-plus-yttrium group is separated from the column effluent and purified by repeated precipitations of lanthamun fluoride, each time after prior treatment of the solution with HNO_3 and $KBrO_3$. A tributyl phosphate extraction removes

---

* Kirby, L. J. To be submitted for publication in Analytical Chemistry

the last traces of contaminating isotopes.[3] The rare earths and yttrium are separated on a Dowex-50 (X8, 16-27 μ, NH_4^+, 2 mm x 9 cm) column maintained at 87 C, using 0.33M lactic acid, buffered with ammonia to pH 4.20, as elutriant. Each drop of the eluate is counted to define the elution curve, and decay measurements on the most active drop of each fraction determine the ratios of individual radionuclides in the fraction.[4] Lanthanum recovery is used to measure the yield of the procedure.

The Determination of Radioactive Antimony by Gamma Scintillation Counting - L. J. Kirby

As a result of experiments to measure concentrations of antimony radioisotopes in mixed fission products plus plutonium, a procedure was devised which should prove useful for routine analysis of control solutions, for following radioactive antimony in biochemical systems, and for other applications. Carrier antimony is initially precipitated as the metal by treating the acidic solution with finely divided tin or cadmium (if tellurium radioisotopes are known or suspected to be present, a prior carrier separation of tellurium metal must be carried out by treating the 9N HCl colution with KI). The antimony metal is dissolved in Br_2 plus HCl; antimony is reduced to the trivalent state and loaded on a Dowex-1 (X8, 100-200 mesh, Cl^-, 2 mm x 3 cm) column. After successive rinses with hot 9N and hot 4.5N HCl, the resin is transferred to a counting dish and radioactive antimony is determined by gamma-scintillation counting.

The Determination of Cadmium Radioisotopes in Samples Containing Mixed Fission Products and Plutonium - L. J. Kirby

Highly purified cadmium sources are obtained from solutions of mixed fission products plus plutonium by combining anion exchange procedures with selected carrier precipitations. The gross solution, made at least 8N in HCl, is passed through a Dowex-1 (X8, 100-200 mesh, Cl^-, 10 mm x 2.5 cm) column. Washing the column with 8N HCl containing a little added KI, with 6N HCl, and with 1N HCl, respectively, removes

potentially contaminating radionuclides (palladium is "removed" by decay prior to starting the separation). Cadmium is eluted with 3N NH_4OH, the solution scavenged with ferric hydroxide, and cadmium separated by electrodeposition or by precipitation as cadmium ammonium phosphate. The measurement of cadmium radioactivity is made by beta-proportional or by gamma-scintillation counting. Decay data are taken to resolve the 54-hour and 43-day cadmium activities.

The Determination of Uranium in Water - C. W. Thomas

A simplified method for determining uranium in 2-liter aliquots of aqueous solutions was developed. The uranium was removed by adsorption on a column of TOPO-coated microbeads from a 3.2M HNO_3 solution at a flow rate of 10 ml/min. The TOPO and adsorbed uranium was removed by eluting with ethanol. The chromogenic reagent dibenzoylmethane and a pyridine buffer in ethanol solution was added to the eluate to produce the characteristic yellow uranium complex the absorbance of which was measured at 405 mμ, the wave length of maximum absorbance. Uranium concentrations in the original sample as low as 1 ppb were analyzed with a standard deviation of ±10 percent.

The Determination of Tritium in Water - J. D. Ludwick

> The measurement of tritium in water is accomplished through the use of liquid scintillation techniques. Water purification to eliminate radioactive contaminants, the use of low-level counting techniques, and new liquid scintillation phosphors resulted in a tritium detection sensitivity of 3×10^{-6} μc per sample.

Studies aiming to improve tritium analysis techniques were continued, with special emphasis on processing water samples to eliminate any extraneous radioactivity, improvement of counting efficiency through use of different solutions of aqueous adaptable liquid scintillators, and reduction of normal background counting rates. These combined efforts have led to improved sensitivity for tritium detection.

The water purification system used in the initial work involved passing the vapor at low pressure over a 400 C zinc bed. The evolved hydrogen gas was then passed through a hot palladium diffusion barrier and subsequently oxidized by passing over a 400 C copper oxide furnace. Because this process required several hours and was subject to contamination in practice, improvements were desired. The improved apparatus for water purification is shown in Figure 6. Starting at the funnel on the left of the figure, the water sample is allowed to slowly drip onto a calcium metal bed. The evolved hydrogen is purified as it passes through two liquid nitrogen traps and a Drierite column.* It is then led into a quartz combustion chamber, through a jet shown on the right. An oxygen atmosphere is maintained in the chamber from a sidearm in the chamber wall through which dried oxygen is admitted. A platinum filament is located in front of the jet and kept red hot to promote controlled reaction. The water product is collected at the end of the chamber, which is maintained at dry ice temperature. This procedure allows recovery of 1 ml of pure water after about 1 hour and can readily be disassembled for decontamination. The previous system required about 3 hours to process 1 ml of water.

Background reduction and efficiency improvements are accomplished through the use of cooled electronic components, massive shielding, coincidence techniques and a light pipe built to accommodate optically coupled samples.

Sample vials are made of polyethylene to further reduce background radiation. The present background for counting 18 ml sample vials is 50 counts/min. Efficiency improvements are also made from the scintillation mixture, which now consists of a 10 percent water sample in a p-dioxane base liquid scintillator containing 100 g/liter naphthalene, 6 g/liter PPO and 0.6 g/liter dimethyl-POPOP. This solution has an efficiency of about 20 percent for tritium beta detection at the aforementioned background.

For sample counting times of 24 hours, a sensitivity of 3×10^{-6} μc is obtained (95 percent confidence level). This constitutes an improvement from the previous 4.5×10^{-6} μc detection level.

---

* W. A. Hammond, Drierite Company, Xenia, Ohio

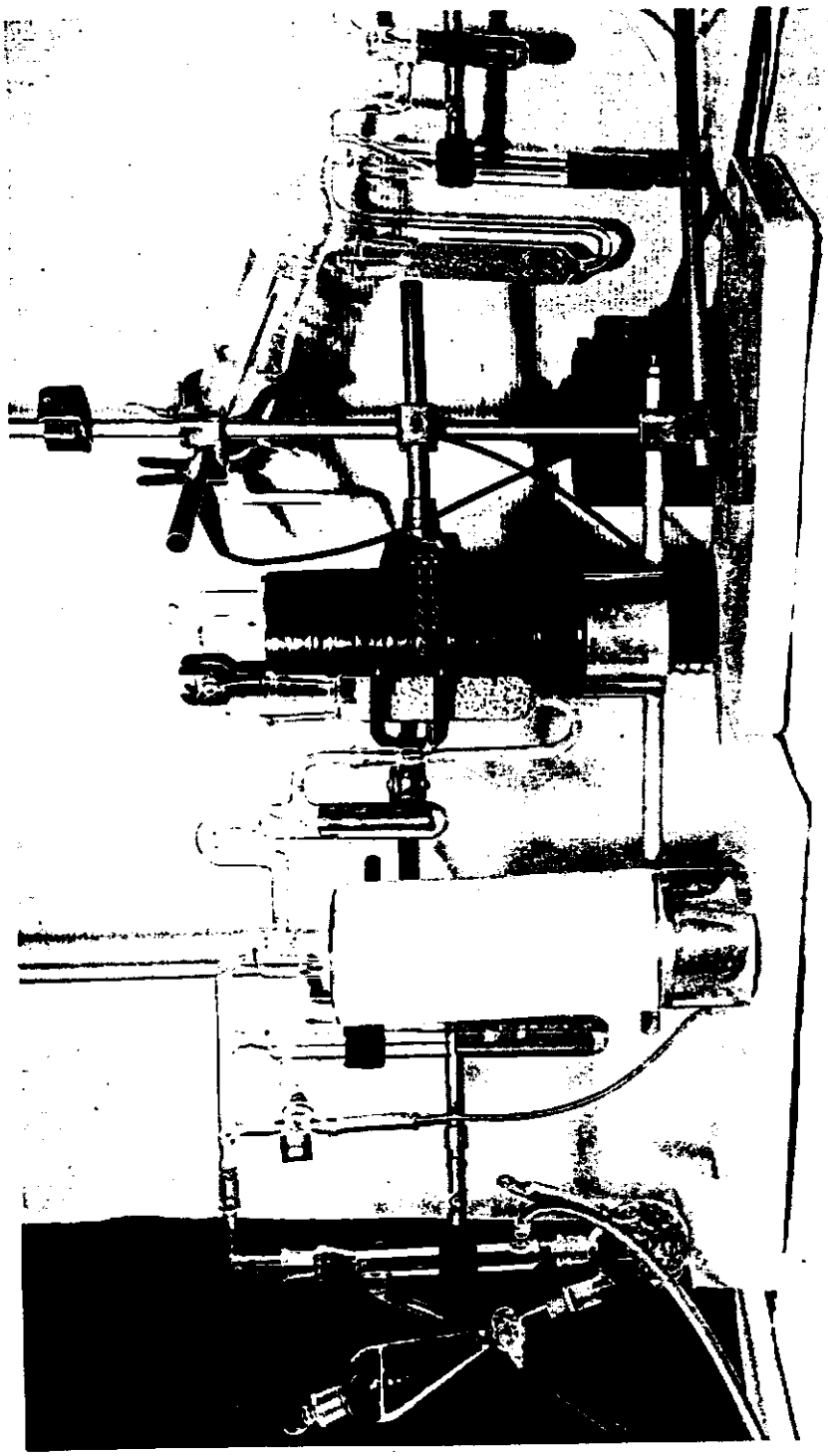

FIGURE 6

Water Purification Apparatus

AEC-GE RICHLAND, WASH

High Sensitivity Gamma Ray Spectrometry[5] - R. W. Perkins

Gamma ray spectrometric methods were investigated with the aim of optimizing both sensitivity and selectivity in radioisotope measurements.

The ultimate sensitivity provided by a neutron activation analysis depends on the sensitivity of the counting equipment used in measuring the product nuclei. Activation analyses have provided sensitivities greater by orders of magnitude than conventional chemical methods for the measurement of many elements; however, many problems arise which require the maximum sensitivities obtainable with activation methods. Gamma ray spectrometric analysis has become the accepted method for measuring many of the product radionuclei produced by activations since it can simultaneously provide a quantitative measurement of a radioisotope and a measurement of its radiochemical purity.

The responses of two high sensitivity gamma ray spectrometer systems were studied. The first system is a summing coincidence spectrometer which uses two large opposing crystals as detectors. The crystals, which are 9-3/8 inches in diameter by 4 inches thick, sandwich the sample between them for the measurements. The signals from the two detectors are summed to provide a "sum spectrum" and are also coincidence analyzed to determine if the total pulse has resulted from simultaneous pulses in each of the two detector systems. The spectrometer system thus permits a sum spectrum and a coincidence sum spectrum to be recorded simultaneously. The sum spectrum is due mainly to radioisotopes emitting one gamma ray per disintegration while the coincidence sum spectrum is due to radioisotopes which emit two or more gamma rays per disintegration. This system aids in the analysis of a mixture of radioisotopes by separating them into two groups characteristic of their decay mode and providing a very low counting background in the coincidence sum mode of operation.

A coincidence summing system which permitted the storage of a coincidence spectrum from two crystals has been described by Miller and Steingraber.[6] Their interests were in the measurement of radium and

thorium in human bone and their evaluation of the system was for coincidence pulses above 0.5 Mev from RaC' and from thorium daughters. The system herein described is similar to the Miller spectrometer but was designed to record both the sum and the coincidence sum spectrum simultaneously and also to permit beta-gamma coincidence counting of the samples.

The second type of high sensitivity spectrometer system studied is the total absorption gamma-ray spectrometer utilizing anticoincidence shielding. A general description and literature review on these instruments has recently been published by the author.[7] This type of spectrometer system employs a large phosphor surrounding the principal detector and operating in anticoincidence with it. The sample to be measured is placed on top of the principal detector (or in its well). The gamma rays which strike the principal detector but which are not completely absorbed are "seen" by the anticoincidence guard phosphor and are canceled. This type of detector system results in a large reduction in the Compton response and in the background.

The use of beta coincidence techniques with both of these detector systems allows further reduction in background and discrimination against nonbeta emitting radioisotopes. An application of this technique is discussed in the next section.

Low Background Gamma Ray Spectrometry by Beta Coincidence Counting of Large-Volume Liquid Samples - R. W. Perkins

The feasibility of using beta coincidence techniques for background reduction in the measurement of radioisotopes in large-volume water samples has been explored. An evaluation of this technique with Columbia River water provided a background reduction of a factor of 40 with an accompanying reduction of gamma-ray counting efficiencies by 30 percent or more, depending on the coincidence beta ray energy.

The measurement of trace amounts of radioisotopes in large samples of water is normally performed by concentrating the sample for gamma-ray spectrometric analysis or by separating the radioisotopes of interest and

counting them in low background counting equipment. The use of a large NaI(Tl) well crystal which holds a 500 ml sample[8] has provided an excellent sensitivity for the direct measurement of many radioisotopes in bulk samples. Although a reasonably high sensitivity is available with direct counting on this instrument, a much better sensitivity could be obtained if the high background counting rate typical of such large detectors could be reduced.

Preliminary measurements have been made on the feasibility of beta coincidence gamma-ray spectrometric measurement of trace radioisotopes in water samples. In this method of analysis, the water sample is mixed with a liquid scintillator, and the mixture is viewed with a phototube while being gamma counted in the well of a large NaI(Tl) crystal (Figure 7). The sample container is a stainless steel cylinder with a quartz window at the photomultiplier tube end and an "O"-ring-sealed screw cap at the other end. The container holds 400 ml and is viewed with a 3-inch DuMont 6363 photomultiplier. The pulses from the large NaI(Tl) well crystal are analyzed with an accompanying multichannel analyzer only when a pulse from the liquid scintillation mixture is received in coincidence. The selection of the liquid scintillation mixture is of course very important for it determines the efficiency with which the beta particles and consequently the gamma-rays are counted. The optimum mixture for this purpose would be one which permitted maximum dilution with sample (water) and maximum counting efficiency. The recipe selected for the initial work was dioxane containing 7 grams PPO/1 and 50 mg POPOP/1. This selection was based on the high solubility of water in the solution and the good counting efficiency in dioxane[9] but it may be far from the optimum mixture.

The counting efficiency of the radioisotope mixture in Columbia River water was measured for a 1:1 volume of the scintillator solution and river water. The gamma-ray spectra obtained with and without the beta coincidence requirement is presented in Figure 8. This beta coincidence method eliminates the photopeaks from K-capture radioisotopes such as Cr^{51} or isotopes which emit a gamma ray without a coincidence beta particle such as Zn^{69}. The gamma ray counting efficiency of Na^{24} (1.4 Mev beta) and As^{76} (2.4 Mev beta) are reduced by factors of about 40 percent and 30 percent respectively

by requiring beta coincidence. Under these same conditions, the integral background counting rate from 0 to 3 Mev is reduced by a factor of 40 in the beta coincidence mode of operation.

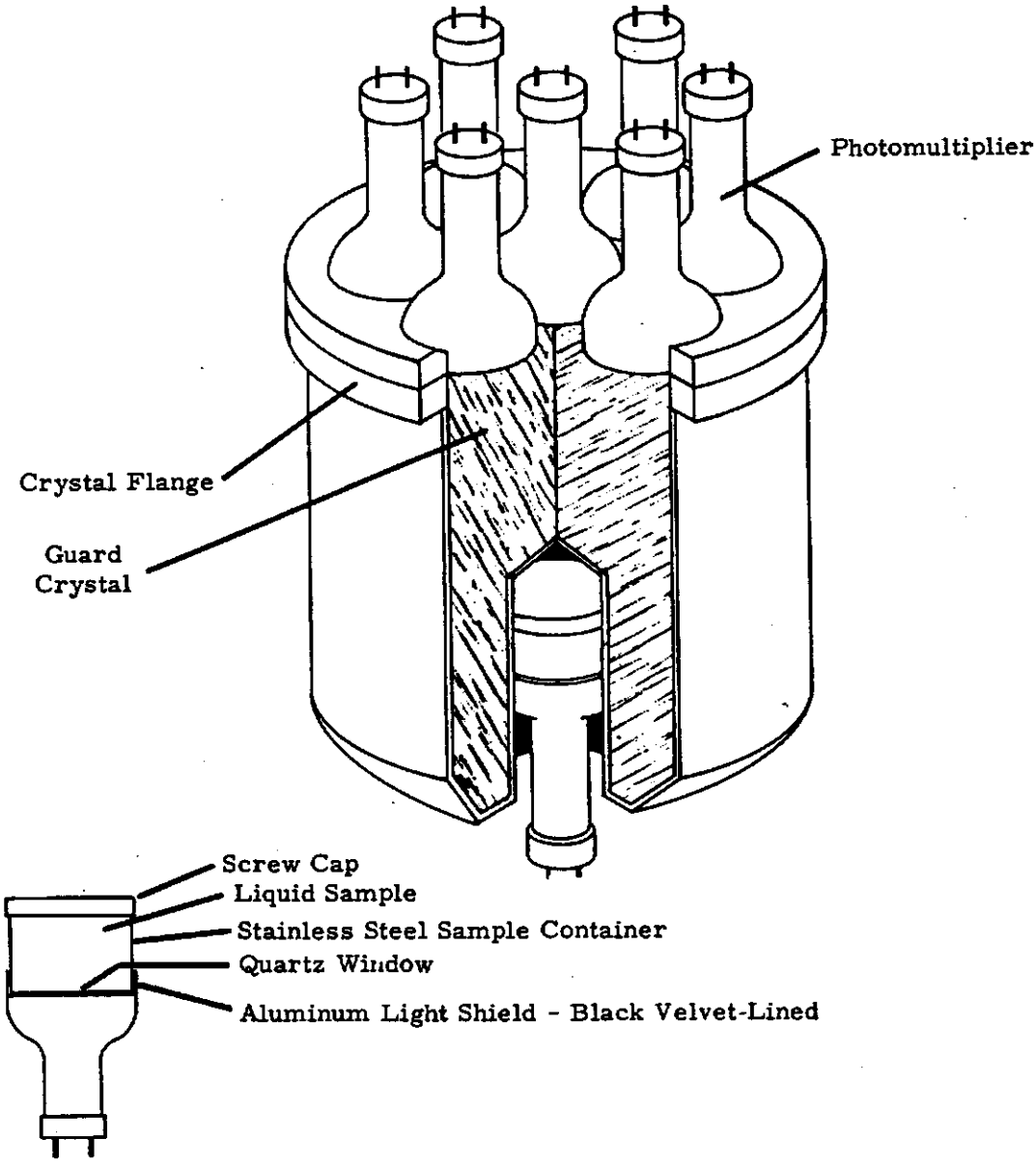

FIGURE 7

Liquid Scintillation Counting Arrangement

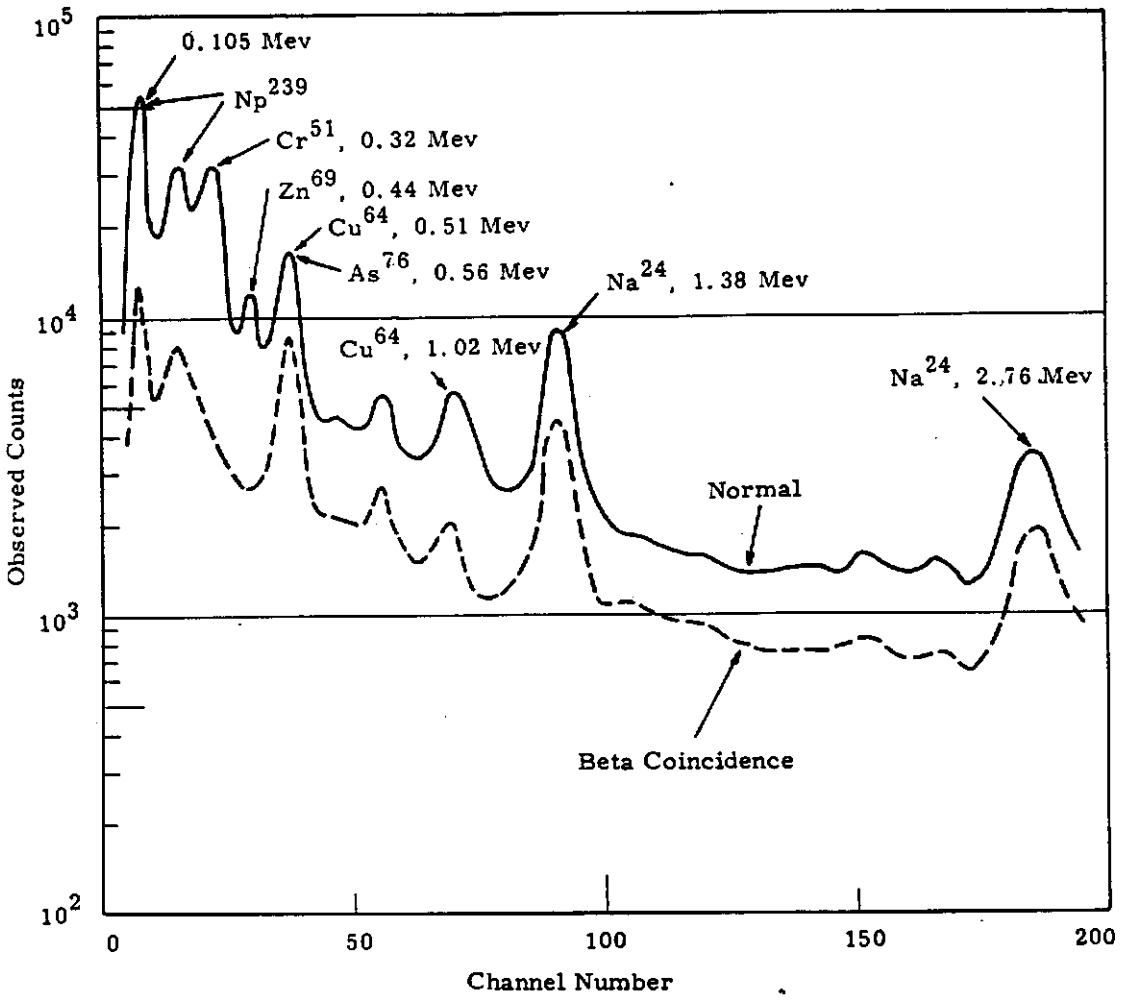

FIGURE 8

Gamma-Ray Spectra of Columbia River Water
with and Without Beta Coincidence

The large background reduction makes this technique rather attractive even with the sacrifice in counting efficiencies. Also, discrimination against nonbeta emitters has advantages in certain measurements. It is planned to investigate scintillation mixtures which will optimize beta counting efficiency at high water concentration.

A High Geometry Gas Cell Proportional Counter* - J. D. Ludwick

A four-chamber proportional counter was built with very thin windows to detect weak beta radiation in an external gas cell. The instrumental design permits relatively high counter efficiencies and an anticoincidence background reduction of cosmic ray-produced events because of the relative positions of the detectors. The instrument is shown in Figure 9 in filling position connected to a vacuum system along with a special scaler used in the detection system. Figure 10 illustrates the internal construction of the counter showing two proportional chambers with thin windows facing the interconnected sample chambers.

Gaseous materials containing the weak beta emitting radioisotopes Kr^{85}, C^{14}, and H^3 have been detected using this instrument. Overall counting efficiencies for these isotopes were 55, 26, and 1 percent, respectively. The specific activity of the material is calculated from PVT data in the sample cell. After calibration, the counter is useful as a means of secondary standardization or where impure gas samples must be tolerated.

* Not supported by Biology and Medicine

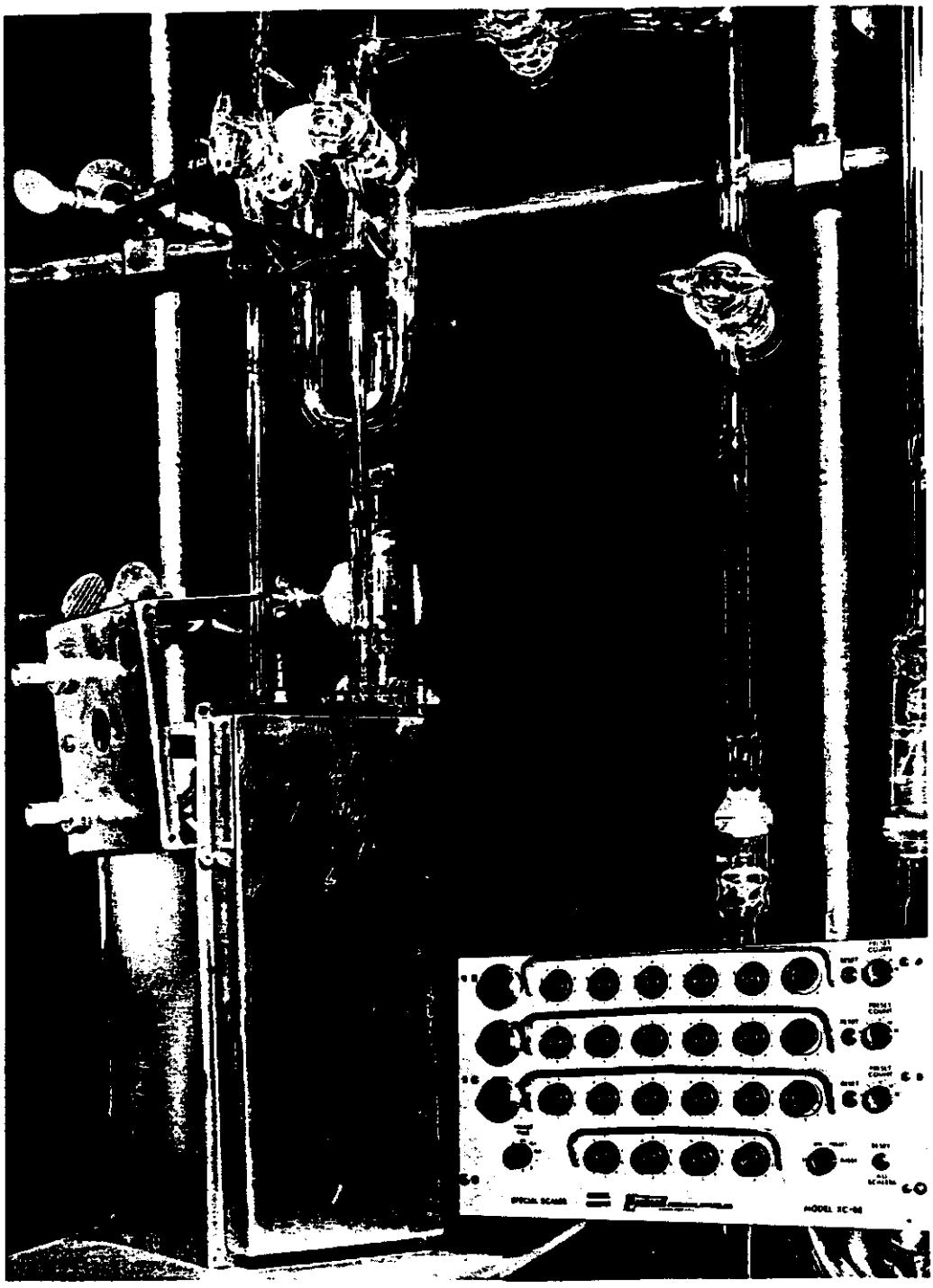

FIGURE 9

Four-Chamber Proportional Counter
Connected to Vacuum Line and Special Scaler Insert

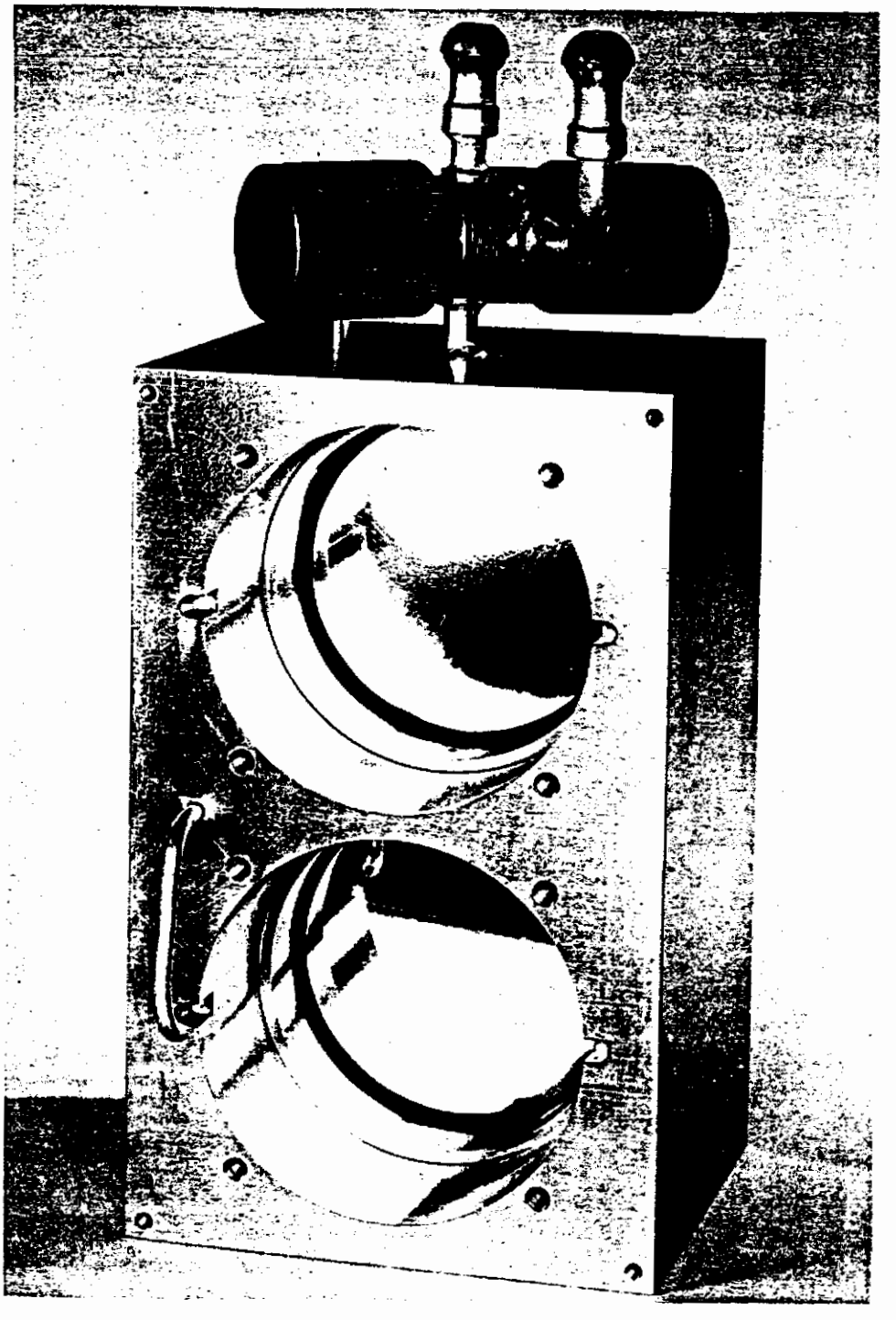

FIGURE 10

Four-Chamber Proportional Counter Internal Construction

The Application of Silicon Surface Barrier Diodes to Alpha Energy Analysis* - R. E. Connally

Silicon surface barrier diode detectors were compared with Frisch grid ion chambers for alpha energy analysis. The diode detectors are especially useful where greater beta tolerance, lower background, or lower initial investment are important requirements

The silicon surface barrier diode has replaced many Frisch grid ion chambers at Hanford. The most commonly used diode is the Ortec** 7 mm by 7 mm diode, guaranteed to give an alpha energy resolution of less than 60 kev (full width of half maximum) for 6 Mev alpha particles. The diode is housed in a brass chamber with the alpha sample; the chamber is evacuated with a mechanical fore pump prior to analysis.

The alpha counting efficiency is dependent on diode and sample diameter, as shown in Table III. The sample is held approximately 2 mm below the diode to protect the diode from mechanical damage and alpha contamination.

TABLE III

COUNTING EFFICIENCY AS A FUNCTION OF SOURCE AND DIODE DIAMETER

Diode Diameter, mm	1/8-in. Diameter Source, %	1/4-in. Diameter Source %
3.5	12	2.5
7	30	10
14	40	30

* Not supported by Biology and Medicine

** Oak Ridge Technical Enterprises Corporation, P. O. Box 524, Oak Ridge, Tennessee

As indicated in Table III, the counting efficiency is less than the 45 to 52 percent obtained with a Frisch grid ion chamber and source preparation can become a problem due to the source diameter limitation. The advantages of the diode over the Frisch grid chamber are lower initial investment, greater beta tolerance and lower background as shown in Table IV.

TABLE IV

COMPARISON OF DIODE AND FRISCH GRID DETECTORS

Performance Measured	Diode	Frisch Grid
Background Count/170 kev/1000 m	1/10-1	5-50
Beta Tolerance for 1% Resolution	>10 rads/hr	<50 mrads/hr
Initial Detector Cost	$100-$500	$2500-$5000

Another advantage of the diode which we have not exploited is the ability to obtain a resolution of 1/3 percent when special very low noise preamplifiers are used with high quality diodes. In our counting applications we find a slight modification of our Frisch grid preamplifier[10] is all that is required to obtain 1 percent resolution. The diode load resistor is 1 megohm and the preamplifier differentiating and integrating time constants are changed from 5 μsec to 1 μsec.

Radiation Chemistry

Kinetics of Radical Reactions in Irradiated Seeds - D. R. Kalkwarf

Introductory electron spin resonance measurements on irradiated radish seeds showed that the signal intensities leveled off with increasing dose and decreased more rapidly at higher temperatures than at lower temperatures over a span of time. A small ESR signal was also obtained from unirradiated radish seeds.

Vegetable seeds are convenient subjects for the investigation of free radical reactions in living tissue since the external environment can be varied greatly and nutrients need not be supplied. In addition, the rates of radical reactions are slower, presumably due to inhibition of diffusion, which

simplifies their evaluation. Radish seeds were used in the present study, which is a prelude to an investigation of the abilities of chemicals to protect the seeds from radiation damage.

Radish seeds were irradiated with Co^{60} gamma radiation at a dose rate of 1.2×10^4 rads·min^{-1}. After irradiation, the seeds were placed in quartz sample tubes and their electron spin resonance absorption was measured with a Varian V-4500 spectrometer and magnet system with 100 kc modulation. When the samples were not in the spectrometer, they were kept in a constant-temperature water bath at 25 or 37 C.

Figure 11 shows typical first-derivative plots of the electron spin resonance (ESR) absorption of the seeds before and 30 minutes after absorbing a dose of 2.2×10^5 rads. The variation of signal intensity with absorbed dose is shown in Figure 12, where samples are compared at equal time intervals after irradiation. Intensities were considered proportional to the integrated area under an absorption band. These were obtained graphically from the first-derivative recordings utilizing the equation,

$$\int_{-\infty}^{\infty} f(x)dx = \int_{-\infty}^{\infty} xf'(x)dx$$

where f'(x) is the first derivative of f(x). As can be seen from Figure 12, the relative signal intensity appears to level off at high doses, indicating approach to a saturated concentration of free radicals in the seeds.

As might be expected, decreases in signal intensity are more rapid at higher temperatures, as shown in Figure 13. For these measurements, the operating controls of the spectrometer were set to give a standard recording of the absorption from a crystalline 1, 1-diphenyl-2-picrylhydrazl sample before measuring the absorption of the seeds. Day-to-day variations in the operation of the instrument were corrected for in this way.

These preliminary measurements show that increased electron spin resonance absorption is exhibited by irradiated radish seeds, indicating the presence of free radicals, although the spectra shows no fine structure to distinguish the chemical form of the radicals. The absorption signals can

be easily evaluated for days following irradiation, making the seeds convenient systems in which to manipulate the kinetics of radiotion-induced radicals. The observation that unirradiated radish seeds give a weak ESR absorption signal may indicate free radical reactions in the normal metabolism of the dormant seed.

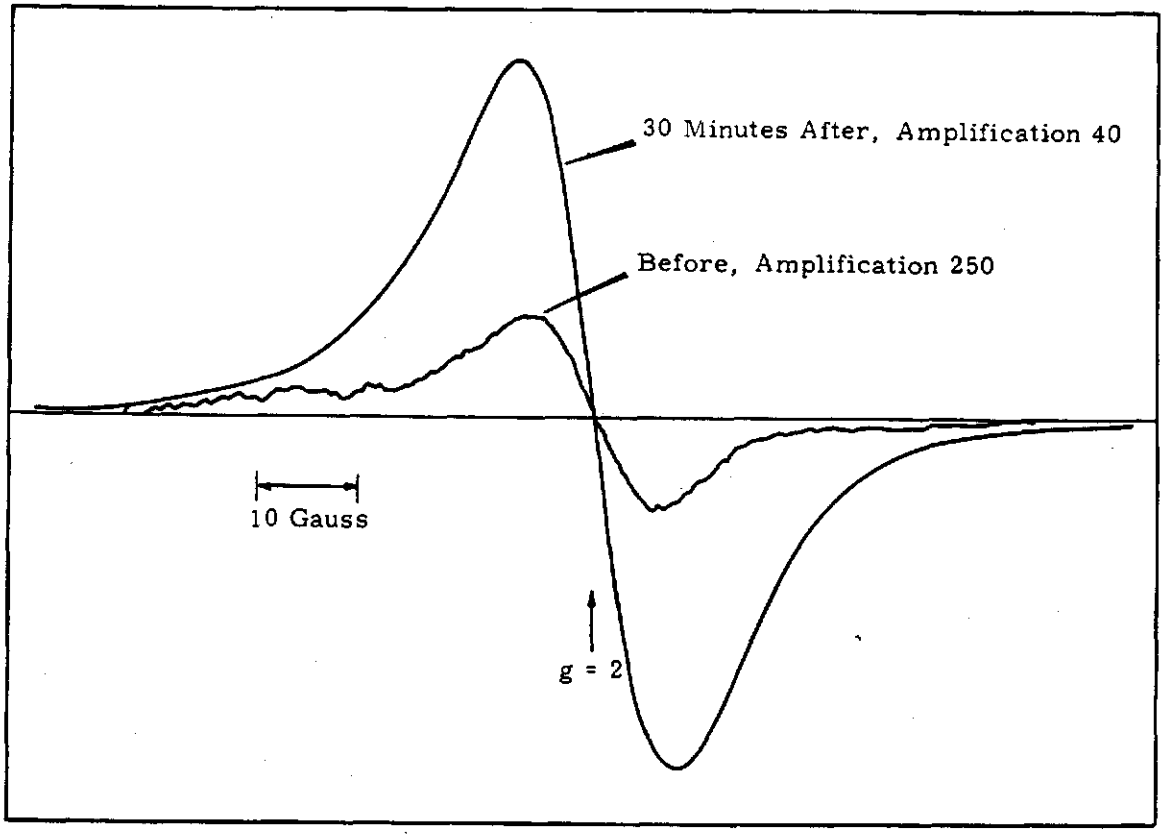

FIGURE 11

ESR Absorption of Radish Seeds
Before and After Absorption of 2.2×10^5 rads

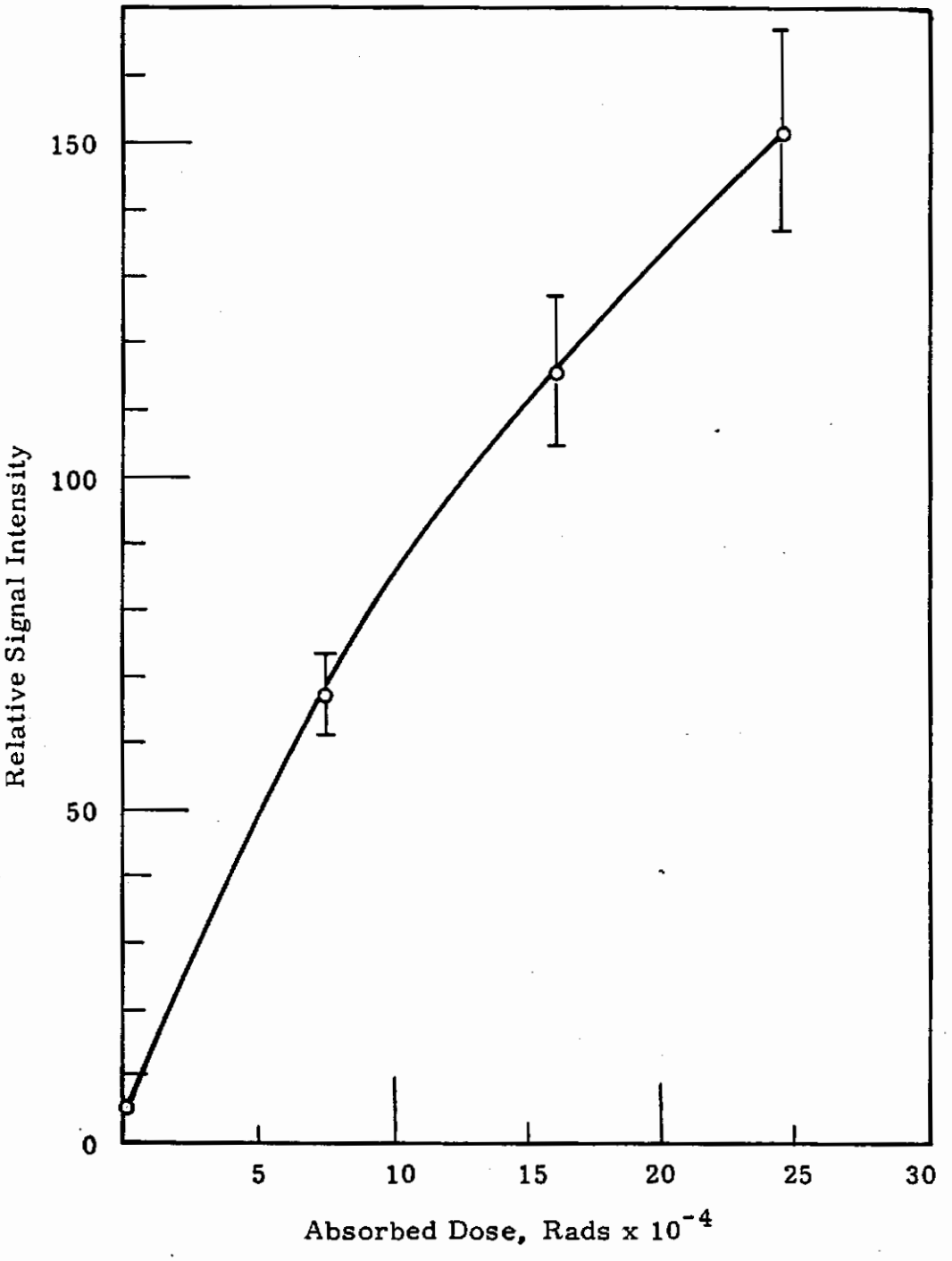

FIGURE 12

ESR Absorption of Radish Seeds
as a Function of Absorbed Radiation Dose

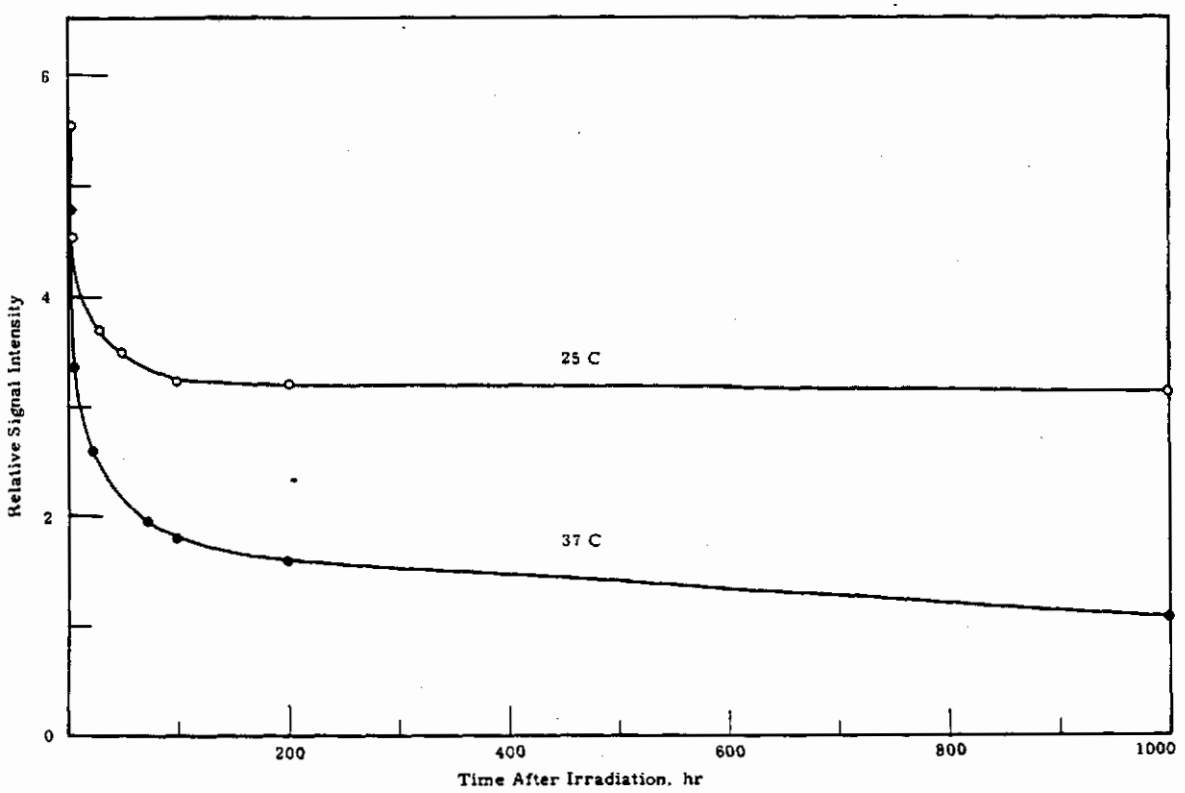

FIGURE 13

Decrease in ESR Absorption
of Irradiated Radish Seeds with Time

Chemical Protection of Red Blood Cells from Radiation Damage - D. R. Kalkwarf and R. W. Henkens

Radiation-induced hemolysis of red blood cells was found to be inhibited by a variety of compounds added to the cell suspensions prior to irradiation. A mechanism was developed which quantitatively describes the process in terms of successive attacks on the cells by free radicals produced in the radiolysis of the surrounding water. The efficiencies of compounds in protecting the cells from hemolysis was found to be directly related to their rates of reactions with these radicals.

Red blood cells in aqueous suspension hemolyze after absorbing ionizing radiation. This damage to the cell membrane was found to be inhibited by a variety of chemicals added to the suspension prior to

irradiation. Red blood cells thus provide a relatively simple biological system for studying the efficiency with which compounds provide radiation protection.

The hemolytic effect of ionizing radiation on red blood cells depends upon the dose absorbed by the suspension (Figure 14). The cells used to obtain the data plotted in Figure 14 were obtained from fresh, human blood and were washed free of other blood consittuents with sterile, isotonic saline (0.16M NaCl). Suspensions of washed cells were prepared with sterile, isotonic solutions containing sodium chloride, protective agent, sodium phosphates to adjust the pH to 7.4, and 0.005M glucose to maintain cell metabolism. The suspensions were irradiated in glass containers at room temperature with Co^{60} gamma radiation (1.3×10^4 rad·min^{-1}). Following this, the containers were placed in a water bath at 37 C and the contents were agitated gently by rotation. Time was counted from immersion in the bath; periodically, samples were removed with sterile hypodermic needles and syringes through puncture seals on the containers. Concentrations of intact cells were measured from photomicrographs of the samples in hemocytometers taken immediately after sampling.

Inhibition of radiation-induced hemolysis by various protective agents is shown in Figure 15. Qualitatively, it can be seen that the degree of protection offered by compounds varies in the order valine < histidine < tryptophan < erioglaucine. This is also the sequential order of these compounds when their rates of reaction with radiation-produced free radicals are compared.[11] For this reason, radical attack on the red blood cell is suggested as the principal mechanism of radiation damage in this system.

In order to discover the actual processes occurring during and after irradiation, hypothetical mechanisms were examined and tested with experimental data. A mechanism which has passed the tests devised so far is described below. This mechanism involves repeated attacks by free radicals, R, on the red blood cells, C_o, converting them successively to C_1, C_2 ----, which are chemically different cells but visually indistinguishable.

The reactions may be represented as follows,

$$H_2O \xrightarrow{\gamma} R$$

$$R + C_o \longrightarrow C_1 + \cdots\cdots$$

$$R + C_1 \longrightarrow C_2 + \cdots\cdots$$

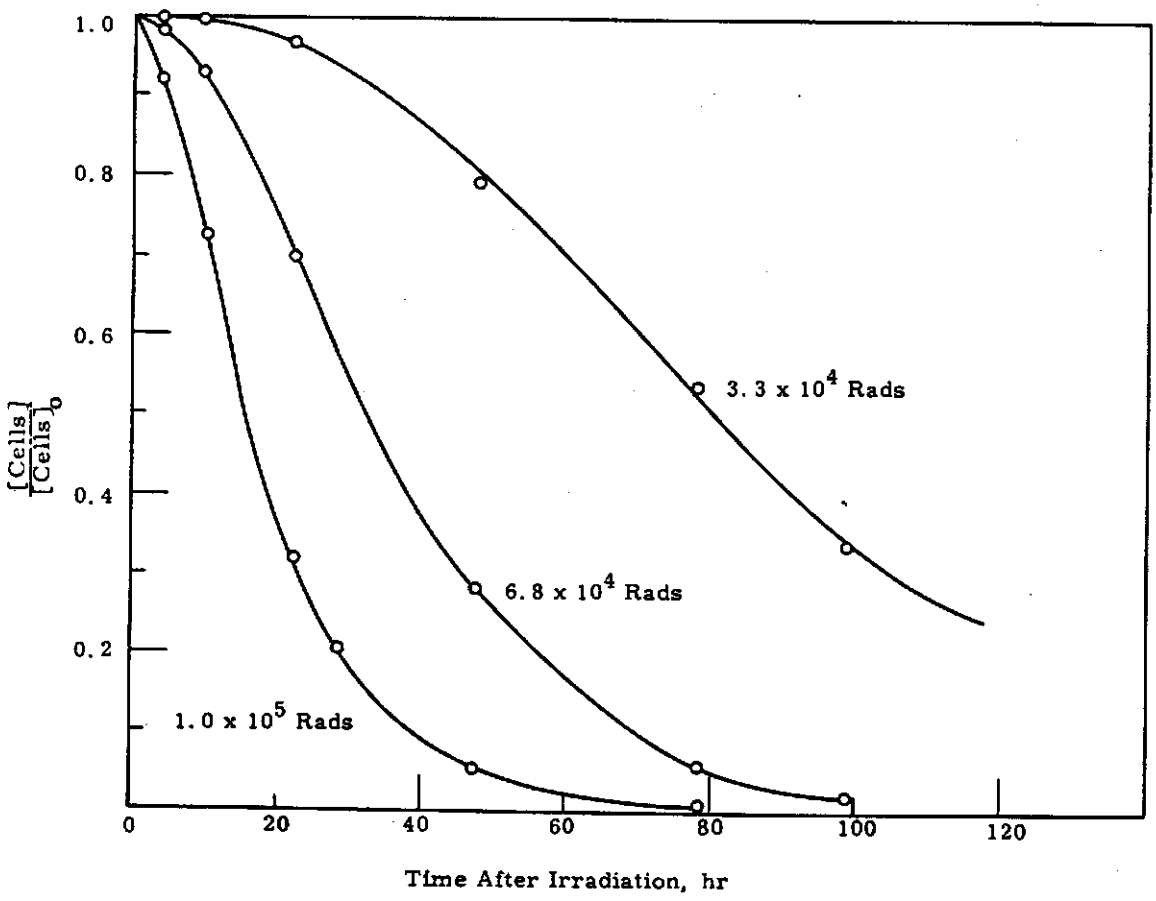

FIGURE 14

Hemolysis of Red Blood Cells at 37 C
After Various Absorbed Doses

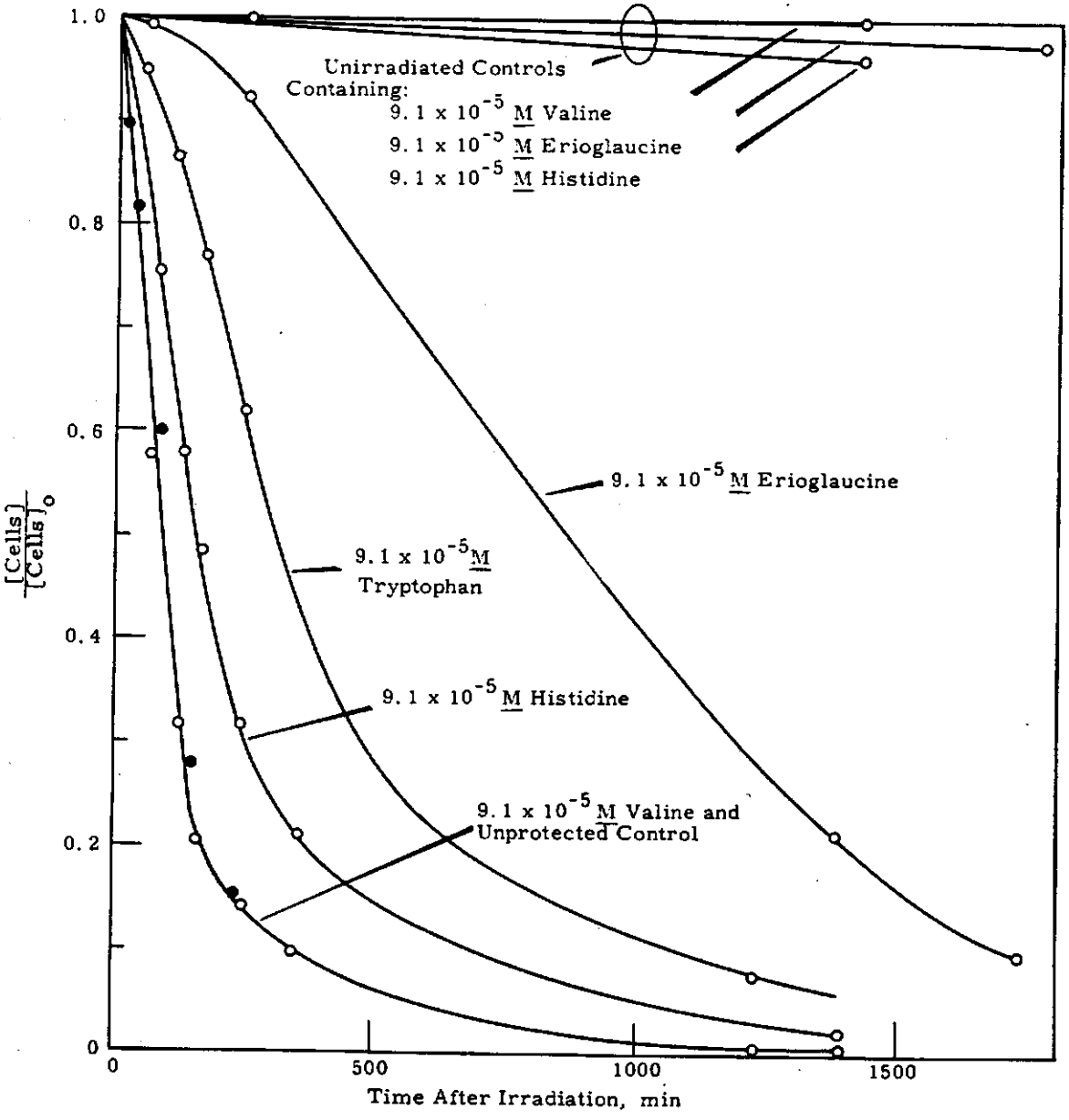

FIGURE 15

Protection of Red Blood Cells from Hemolysis at 37 C Following Absorption of 1.2 x 10^5 rads

AEC-GE RICHLAND, WASH.

If Y is the concentration of radicals produced from water per unit absorbed dose, I is the absorbed-dose rate, t_i is the irradiation time, and all reactions between radicals and cells are bimolecular with equal rate constants k_c,

$$\left.\begin{aligned} d[C_o]/dt_i &= -k_c[R][C_o] \\ d[C_1]/dt_i &= k_c[R]\left([C_o]-[C_1]\right) \\ &\vdots \\ d[C_m]/dt_i &= k_c[R]\left([C_{n-1}]-[C_n]\right) \\ &\vdots \end{aligned}\right\} \qquad (1)$$

Assuming that a steady-state concentration of R is rapidly attained,

$$[R] = IY/k_i[C]_o \qquad (2)$$

where $[C]_o$ is the initial concentration of cells. Substituting (2) into (1), and integrating gives,

$$\left.\begin{aligned} [C_o] &= [C]_o \exp(-IYt_i/[C]_o) \\ [C_1] &= (IYt_i)\exp(-IYt_i/[C]_o) \\ [C_2] &= \left\{(Yt_i)^2/2![C]_o\right\}\exp(-IYt_i/[C]_o) \\ &\vdots \\ [C_n] &= \left\{(IYt_i)^n/n![C]_o^{(n-1)}\right\}\exp(-IYt_i/[C]_o) \\ &\vdots \end{aligned}\right\} \qquad (3)$$

The fraction of cells, F, which have reacted less than n times with radicals is given by,

$$\left.\begin{aligned} F &= \sum_{k=o}^{n-1} \left\{ (IYt_i)^k / k! \left[C\right]_o^k \right\} \exp\left(-IYt_i / \left[C\right]_o\right) \\ &= \sum_{k=o}^{n-1} a^k e^{-a} / k! \ , \ \text{if } a = IYt_i / \left[C\right]_o \end{aligned}\right\} \tag{4}$$

Assuming only that the time required for hemolysis of a cell is a monotonically decreasing function of n, the number of attacks it has sustained, it follows that the cells of all types remaining intact at any time, t, are those for which n is less than some value N, corresponding to a hemolysis time of t. The ratio of the concentration of intact cells to original cell concentration is thus,

$$\left[C\right] / \left[C\right]_o = \sum_{k=o}^{n-1} a^k e^{-a} / k! \tag{5}$$

This series summation has an inflection point at N=a and approaches the value 0.5 when N-a+1/3.[12]

Since the quantity a is large compared with 1/3, the above mechanism predicts that at $\left[C\right]_o / \left[C\right]_o = 0.5$, $N = a = YIt_i / \left[C\right]_o$. (6)

An empirical plot of absorbed dose, It_i, against τ, the time required for $\left[C\right] / \left[C\right]_o$ to reach 0.5, is shown in Figure 16. It indicates that,

$$It_i = \frac{1}{b} \ln (K/\tau) \tag{7}$$

where b and K are constants. Substituting (7) into (6) gives,

$$N = (Y/b\left[C\right]_o) \ln (K/\tau) \ ; \tag{8}$$

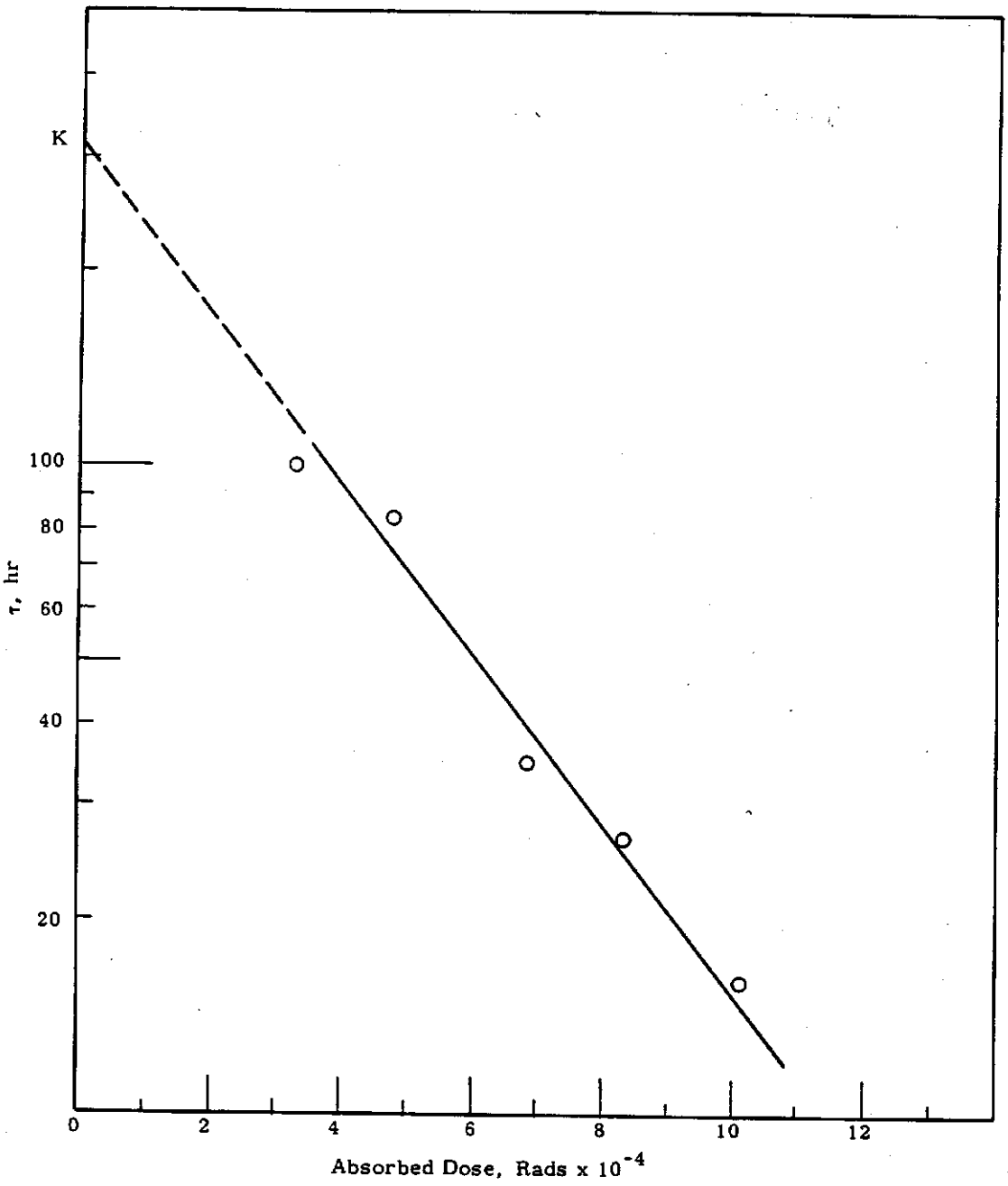

FIGURE 16

Time Required for Hemolysis of Half the Initial Cells at 37 C Versus Absorbed Dose

AEC-GE RICHLAND, WASH.

and since N is not a function of τ, its functional form at τ should also be its functional form at any time t, i.e.,

$$N = (Y/b[C]_o) \ln (k/t) \quad (9)$$

Substitution of (9) into (5) gives $[C]/[C]_o$ explicitly as a function of t.

For large N, the above mechanism predicts that the ratio $[C]/[C]_o$ has an inflection point at some time after hemolysis and that it occurs when the ratio is 0.5. Figure 14 shows that the experimental results verify these predictions.

In the presence of a protective agent, P, additional reactions must be considered of the form,

$$R + P \rightarrow P_1 + \cdots$$

$$R + P_1 \rightarrow P_2 + \cdots$$

$$\vdots \qquad \vdots$$

If these reactions are all bimolecular with rate constants equal to a common value, k_p, the steady-state concentration of R becomes,

$$[R] = IY/(k_c[C]_o + k_p[P]_o) \quad (10)$$

where $[P]_o$ is the initial concentration of protective agent. Solving equations analogous to (1) gives,

$$[C_o]/[C]_o = \exp(-a_p)$$

$$[C_1]/[C]_o = a_p \exp(-a_p)$$

$$[C_2]/[C]_o = (a_p^2/2!) \exp(-a_p) \quad (11)$$

$$\vdots \qquad \vdots$$

$$[C_n]/[C]_o = (a_p^n/n!) \exp(-a_p)$$

$$\vdots \qquad \vdots$$

where $a_p = k_c IYt_i/(k_c[C]_o + k_p[P]_o)$. As a result of these equations, the fraction of cells, F_p, which have reacted less than $\underline{n}$ times with radicals in the presence of a protective agent is given by,

$$F_p = \sum_{k=o}^{n-1} a_p e^{-a_p}/k! \quad ; \tag{12}$$

and by an argument analogous to that given for Equation (5), the ratio of the concentration of intact cells to original cell concentration in the presence of a protective agent is given by,

$$[C]/[C]_o = \sum_{k=o}^{N-1} a_p e^{-a_p}/k! \tag{13}$$

Equation (13) predicts an inflection point at $[C]/[C]_o = 0.5$. If the time at this point is designated τ_p,

$$k_c IYt_i/(k_c[C]_o + k_p[P]_o) = Y/b[C]_o) \ln (K/\tau p) \tag{14}$$

or

$$\left[\ln\left(\frac{K}{\tau_p}\right)\right]^{-1} = \frac{k_c[C]_o + k_p[P]_o}{bk_c It_i[C]_o} \tag{15}$$

The rate constants, k_p, for the reactions between between a protective agent and the radicals produced from irradiated water have been evaluated as relative rate constants, X_p, termed "protection indices".[27] Equation (15), expressed in terms of these protection indices is,

$$\left[\ln\left(\frac{K}{\tau_p}\right)\right]^{-1} = \frac{X_c[C]_o + X_p[P]_o}{bX_c It_i[C]_o} \tag{16}$$

If this mechanism, which pictures radiation damage to the red blood cell as successive attacks of radicals on the cells, is correct, a plot of $\log\left[(K/\tau_p)\right]^{-1}$

versus $X_p[P]_o$ should be a straight line as predicted by Equation (16). Figure 17 shows that this is indeed the case and gives further support to the concept that radiation damage to suspensions of red blood cells occurs predominantly via attacks by radicals produced in the surrounding water.

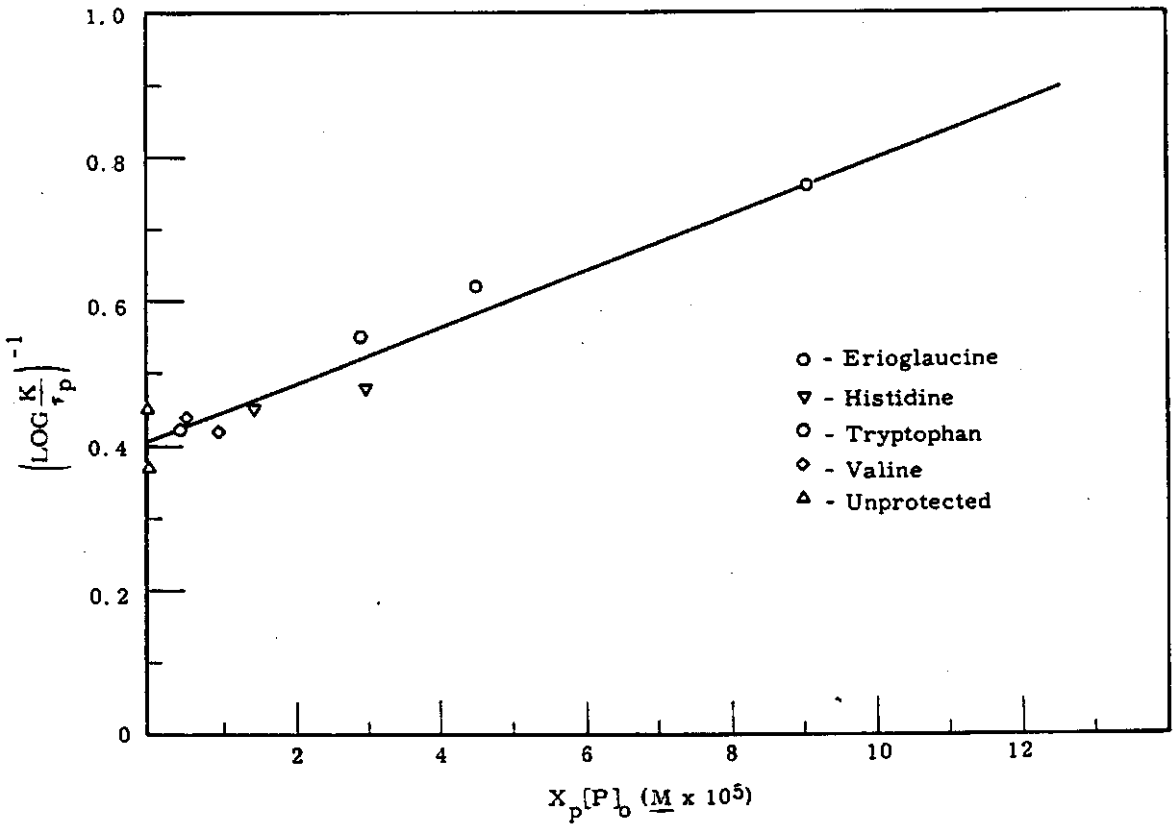

FIGURE 17

Test of the Equation $\left(\ln \frac{K}{\tau_p}\right)^{-1} = \frac{X_c[C]_o + X_p[P]_o}{bX_c It_i[C]_o}$

Interaction of Radiation Protective Compounds and Human Red Blood Cells - R. W. Henkens

The binding of the dyes crystal violet, bismarck brown Y, and erioglaucine by human red blood cells was investigated. Significant amounts of the first two dyes are bound by the cell surface. No binding of erioglaucine was observed, nor was any diffusion into the cell detected. As erioglaucine is very effective in protecting the cell from radiation induced hemolysis, this observation leads to speculation that the site of free radical damage which ultimately leads to hemolysis is on the exterior surface of the cell.

In our studies of chemical protection of human red blood cells from radiation-induced hemolysis (D. R. Kalkwarf and R. W. Henkens, pages 104-113), a knowledge of the nature and extent of interactions between protector and cell is important. Especially intriguing is the possibility of determining the radiation-sensitive structures of a cell through comparison of an unprotected cell with one which has a protector adsorbed or absorbed by a specific structure.

This study describes the binding of the dyes erioglaucine (EGC), crystal violet (CV), and bismarck brown Y (BBY) by human red blood cells. The structural formulas of these dyes are shown in Figure 18. The extent of binding was estimated by suspending washed cells in isotonic saline solution which contained a known concentration of dye, and determining the decrease in free-dye concentration after incubation at 37 C. The cells exhibit substantial binding of BBY and CV. For example, when 7.0×10^{-5} M of CV was added to the cell suspension, 57 percent of this dye was bound, although the volume of cellular material used in the experiments was less than 5 percent of the total volume of the suspension. Both BBY and CV exhibit an increase in binding as the free-dye concentration is increased. However, the rate of increase in binding of BBY becomes less at free dye concentrations above 3×10^{-5} M. At this concentration an average of 8.6×10^{-17} moles or 5.2×10^{7} molecules of BBY are bound per cell. The surface area of the human red blood cell is 1.67×10^{10} sq. Å, and if one assumes that the area occupied by a molecule of BBY lying flat on the cell

surface is about 160 sq. A, it would take roughly 1 x 10^8 dye molecules to cover the cell with a unimolecular layer. As a rough approximation, therefore, the bound BBY at a free-dye concentration of 3 x 10^{-5} M corresponds to a cell 50 percent covered with a unimolecular layer of dye molecules. The rate of increase in binding of CV is roughly constant over the region of free dye concentrations extending from zero to 3 x 10^{-5} M. At 3 x 10^{-5} M about 1.9 x 10^8 molecules of CV are bound per cell.

Erioglaucine Anion

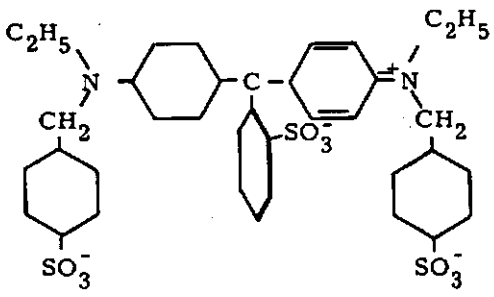

Crystal Violet Cation

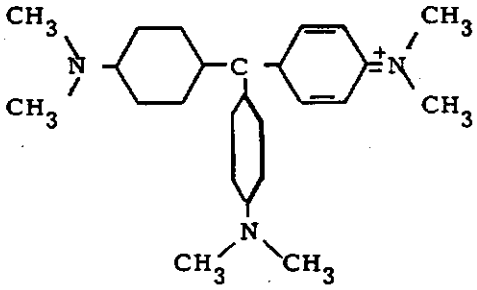

Bismarck Brown Y Cation

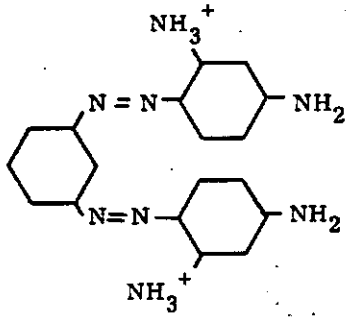

FIGURE 18

Structural Formulas of Erioglaucine, Crystal Violet and Bismarck Brown Y

No binding of EGC was detected either with the procedure used for CV and BBY or when the concentration of cells was increased from 5 to 50 percent by volume and the cells themselves analyzed for the dye, even though the analytical procedure would easily detect the uptake of as little as 1 percent of the dye.

These experiments do not, of course, distinguish between adsorption into the cell. In any case, these results indicate that EGC is neither adsorbed by the cell surface nor does it diffuse into the cell interior. EGC is effective in protecting the red blood cell from radiation induced hemolysis, and from the above observations we can conclude that this protection occurs external to the cell. Therefore the agents responsible for damage exist, at least in part, in the solution external to the cell. This gives additional support to the idea that the damage is done via free radicals formed in the solution, and leads us to speculate that an important site of the free radical damage which ultimately leads to hemolysis is on the exterior surface of the cell.

Relative Electronic Charge on the Different Species of Erioglaucine - R. W. Henkens

A means, based on paper electrophoresis, of determining the relative electronic charges on different species of the same compound is discussed. The relative charges determined for erioglaucine are consistent with a reaction scheme indicated by previous spectrophotometric studies.

Erioglaucine is used as a reference compound for comparing the relative rates at which free radicals react with solutes in aqueous solution.[13] It has also been used as a protector in studies concerning chemical protection of red blood cells from ionizing radiation. Previous spectrophotometric studies have indicated that, in aqueous solution, it consists of two series of dye species.[14] Protolysis reactions within a series are found experimentally to be virtually instantaneous, while hydrolysis reactions between members of different series are measurably slow. Figure 19 shows the reaction scheme.

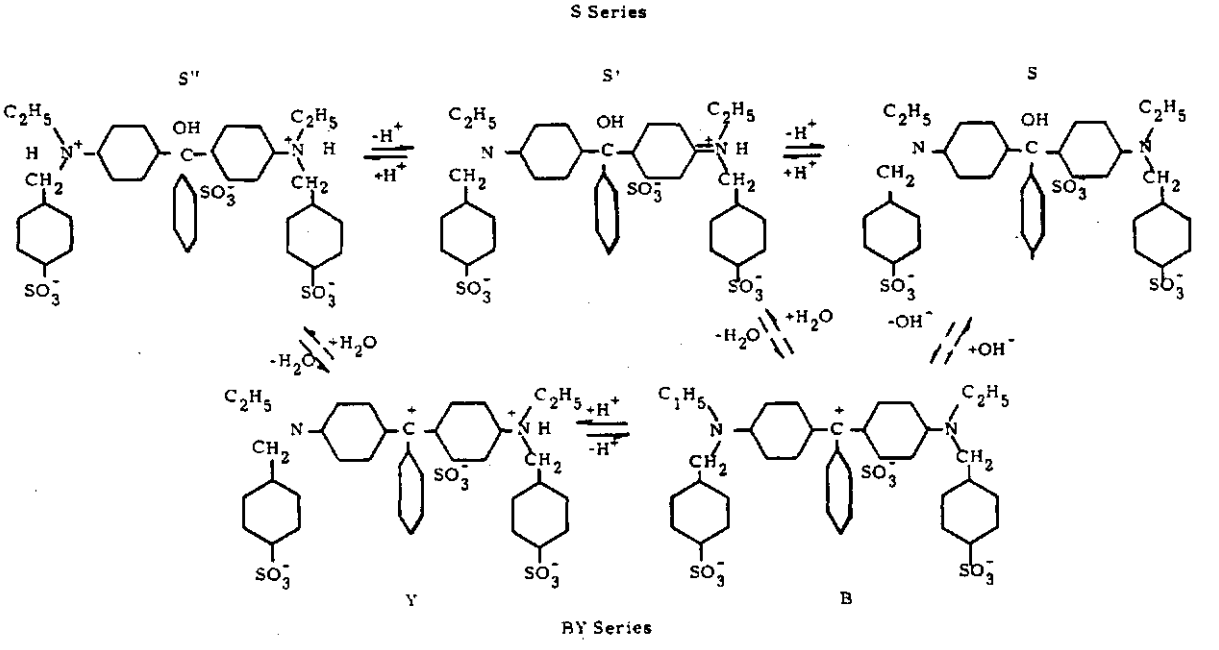

FIGURE 19

Reaction Scheme for Erioglaucine

According to this scheme the net electric charge on the S'', S' and S species is respectively -1, -2, and -3, while the net charge on the Y and B species is respectively -1 and -2. To further test this reaction scheme, a paper electrophoretic study of the relative charges on the various species is in progress. This report discusses the determination of the charge ratio between the S species and the B species.

The limiting free solution mobilities, U_o, of organic ions in water at 25 C are given by[15]

$$U_o = 1.14 \times 10^{-3} \frac{Z}{r_w} \left(\frac{fo}{f}\right) , \qquad (17)$$

where Z is the numerical charge on the ion, r_w is the van der Waals radius, and $\left(\frac{fo}{f}\right)$ is a frictional ratio. If r_w and $\left(\frac{fo}{f}\right)$ are assumed to be the same for the different species of erioglaucine, then the limiting free solution mobility of a given species is

$$U_o = C_1 Z \tag{18}$$

where C_1 is a constant. At a given ionic strength the free solution mobility, U, is, to a first approximation, given by[16]

$$U = U_o - C_2 Z. \tag{19}$$

therefore,

$$U = (C_1 - C_2)Z - C_3 Z. \tag{20}$$

The value of C_2 is not strictly constant but depends to a small degree on U_o. However, for this work the dependence will be neglected. The relationship of the free solution mobility of an ion and its electrophoretic migration distance, d, on paper is[17]

$$U = \frac{dl}{ZE}\left(\frac{l}{l}\right)^{'2} \tag{21}$$

where d is the distance (corrected for electroosmotic flow) which the ion travels in time, t, under a potential gradient $\frac{E}{l}$. The factor $\left(\frac{l}{l}\right)^{'2}$ is a geometrical correction.[17] In the present work the different species of erioglaucine were electrophoretically separated from the same sample, and the factors t, $\frac{E}{l}$, and $\left(\frac{l}{l}\right)^{'2}$ were constant. Therefore,

$$U = C_4 d. \tag{22}$$

From Equations (20) and (22) it can be seen that the charges on the various species are in the same ratio as their migration distances on the paper.

It is not possible, of course, to separate species which are in rapidly established equilibrium; in this condition the species migrate as a group with a mobility intermediate to that of the individual mobilities. Therefore, direct

determination of the charge ratios of erioglaucine species within a series is impossible. However, the charge ratios of species in different series can be determined.

Purified erioglaucine was dissolved in 0.1M NaOH and allowed to stand overnight in order to convert some of the B species into the S species. The solution was then adjusted to pH 9.3 and diluted with DAF pH 9.3 buffer[18] to give a total dye concentration of 8×10^{-4}M. At this pH the rate of conversion of S back to B is very slow (10^5 hours half life), and the solution consists essentially of a mixture of the B and S species.[14] The electrophoretic separations were carried out using DAF pH 9.3 buffer and S and S 2043–a filter paper, with a potential of 100 volts. Riboflavin was used as a zero mobility reference. After electrophoresis the zone corresponding to the colorless S species was detected by heating the paper strip at 100 C to dryness in a vacuum oven. This converted the S to the blue colored B species. Figure 20 shows the paper strip and a densitometer scan of it. Zone 2 corresponds to the B species, and Zone 4 to the S species. Zone 1 is a small amount of impurity which is believed to be an isomer of erioglaucine. Zone 3 is an unknown pinkish colored substance. The ratio of distance traveled by the S species to that traveled by the B species is 3.00:2.06, corresponding to a charge ratio of 3:2. This ratio is consistent with the proposed reaction scheme shown in Figure 19.

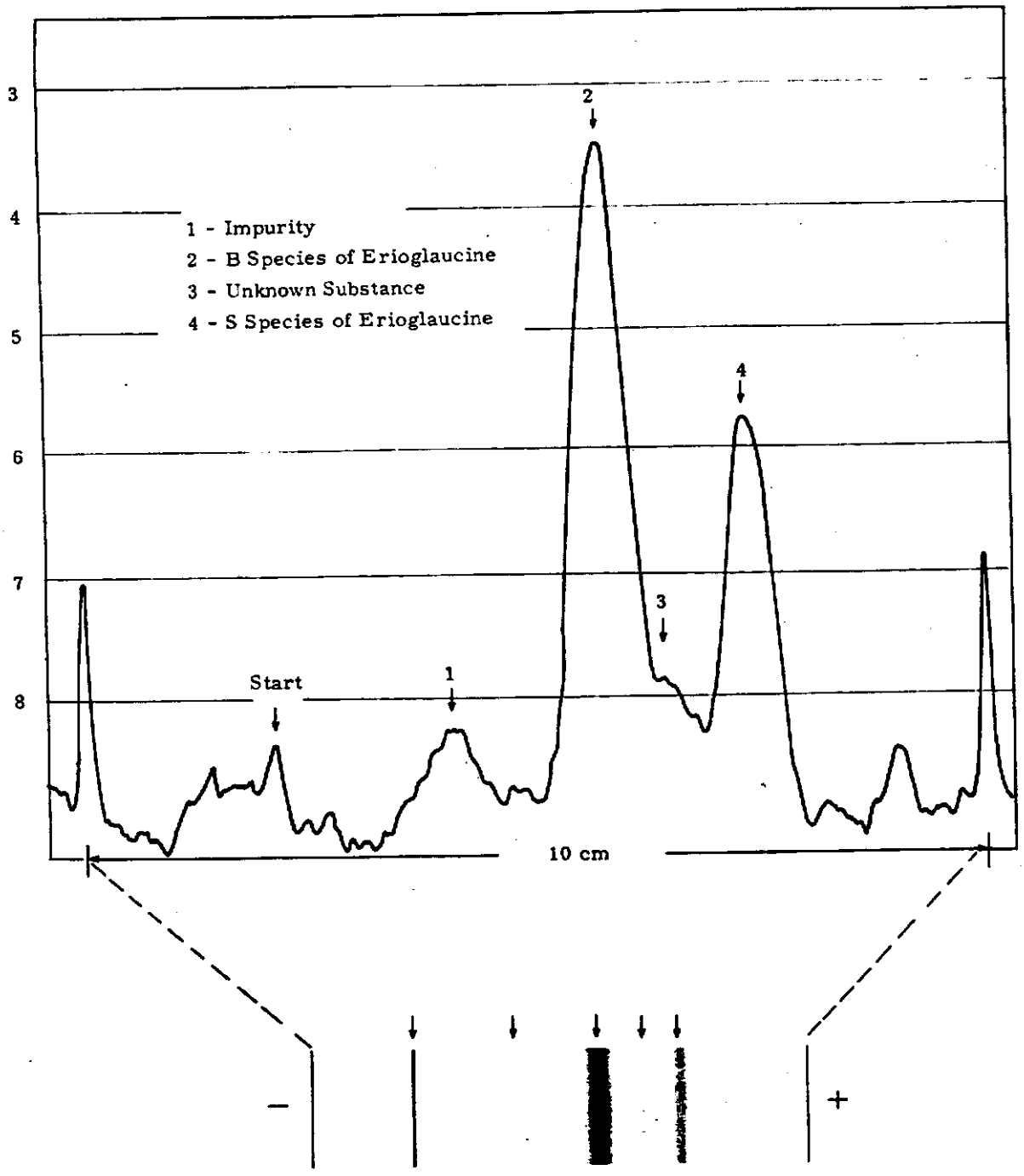

FIGURE 20
Electrophoresis of Erioglacine

Electron Spin Resonance Spectrometer Modifications - R. N. Diebel

A Varian Associates V4500 ESR Spectrometer with 100 kc field modulation is being used to study the electron spin resonance (ESR) signals observed in radiation chemistry and radiation damage studies. The microwave bridge has been modified by replacing the fixed arm with a variable termination in order to provide a leakage current adjustment which was independent of the sample cavity arm.

Measurements of saturation broadening effects have required some modification and additions to the Varian EPR bridge. It is not possible to cover a very wide range of power levels by varying the iris coupling to obtain a constant leakage current. We find that the minimum microwave power necessary to maintain 100 microamperes of leakage is 12 milliwatts, as measured at the 20 db coupler. This leakage was achieved by turning the iris screw on the 100 kc cavity to its clockwise limit, that is, lifting the plastic plunger nearly out of the waveguide. Varying the cavity coupling in this manner results in the signal amplitude being closely related, but not directly proportional, to the square root of microwave power. If the iris coupling screw is turned in the counter clockwise direction so as to increasingly cover the coupling hole, then the relation of microwave power to ESR signal amplitude becomes very obscure. At certain settings of the iris coupling the ESR signal will become zero or have a reversed sign.

A system in which the iris coupling could be left fixed would be desirable. This would allow the cavity Q and coupling to remain constant so that the power incident on the sample would be in constant relation to the power in the sample arm of the bridge. Fixed coupling to the cavity necessitates either an accurate attenuator in the crystal arm of the bridge[19] or a variable termination in what is usually the fixed arm of the bridge.[20, 21] These methods of adjusting the power in the crystal arm are necessary since the crystal current must be kept at a fixed value in order to have a constant sensitivity.

A rigid coaxial fitting has been designed to couple the power from the crystal detector mount of the Varian EPR bridge into an external waveguide.

This permits us to use an attenuator in the crystal arm, or a tunable crystal mount or a balanced superheterodyne mixer whenever the need arises. Figure 22 presents the essential features of this waveguide to waveguide coupler.

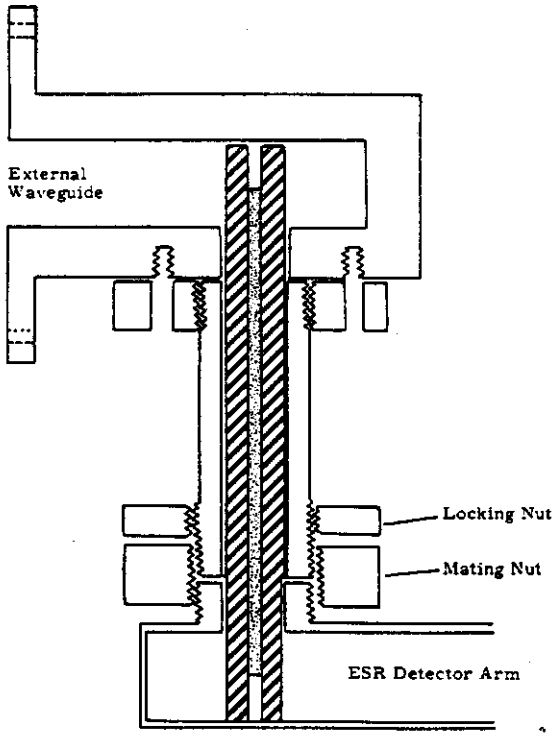

FIGURE 22

Adapter for Connecting Detector Power
of ESR Bridge to External Waveguide

Use of a tuneable crystal mount, Hewlett Packard model X485B, mounted directly on the external waveguide adapter has resulted in improvements in signal amplitude as great as 20 percent. Crystals having the best sensitivity when mounted directly in the ESR bridge gave equally good performance in the external detector mount, while most other crystals gave improved performance in the external tuneable mount.

An important change in the ESR bridge has been made by inserting a variable reflection in place of the original power absorbing termination. A 90 degree waveguide bend was used to make this arm accessible from the

back of the bridge. A level set type attenuator followed by an adjustable short was then attached to terminate this bridge arm. This connection enables one to adjust the leakage current and the reference phase at the detector. Such an arrangement is a portion of the complex reflection coefficient bridge described by Strandberg.[20] The variable short is to be adjusted so that the cavity absorption mode is displayed undistorted, the attenuator being set near the minimum value. The attenuator must be a type which does not exhibit appreciable changes in phase characteristic as attenuation is changed.

The chief advantage of using the variable reflection from the terminated arm of the bridge is the ease with which the leakage current can be adjusted without disturbing the power level in the sample arm of the bridge. The detailed procedure for adjusting the cavity coupling is the same as usually followed for the Varian spectrometer. The coupling iris and reflector voltage are adjusted until the leakage current is zero , than the automatic frequency control (AFC) is turned on (the attenuator in the terminated arm must be at maximum attenuation). The attenuation in the bridge arm is then adjusted to achieve the desired level of leakage current. Using this system of adjusting the leakage current we have been able to operate at half the microwave power level formerly required to achieve minimum leakage current. We also find that the ESR signal level from a well-diluted sample of DPPH in KCl is proportional to the square root of microwave power in the range below about 50 milliwatts of power in the sample arm.

This V4500-30B Varian EPR bridge can also be readily converted into a low power bridge of the type described by Rempel and Weaver.[22] The reference cavity is put in place of the variable short. Actually, the variable short can be made into a cavity by placing a hole in the center of a piece of shim brass which is used as a coupling iris between the waveguide flanges joining the short to the bridge. A fixed value ferrite isolator of about 20 db value can be used in the sample arm where the expense of a variable isolator is not warranted.

In our work with irradiated seeds and with triphenylmethane dyes we find evidence of saturation broadening effects. Since the signals are rather weak we have difficulty in observing the signals at the lowest power levels available in the Varian high power bridge. We could use at least a ten-fold improvement in signal to noise ratio without having difficulties from background due to cavity contamination when operating at low power levels.

The limiting noise in our spectrometer seems to be the input end of the 100 kc receiver and not the detector crystals. The noise level at the receiver output is not altered by turning on the microwave power (when leakage is kept below 100 microamperes) as long as the power is below about 60 milliwatts (microwave attenuator set at greater than 170 dial units). When the power into the bridge is greater than 100 milliwatts the AFC modulation level begins to have an appreciable effect on the noise.

Radiation Chemistry of Fluorinated Hydrocarbons in Aqueous Solutions - C. W. Thomas and D. R. Kalkwarf

CF_2Cl_2 and CHF_2Cl in aqueous solutions were found to decompose into hydrogen, chloride, fluoride and bicarbonate ions following gamma irradiation.

Gaseous CF_2Dl_2 (Genetron-12) and CHF_2Cl (Genetron-22) are often used to test for leaks in closed pipe-circuits through which fluids are to be passed. If these circuits are to be exposed to ionizing radiation, as in a nuclear reactor, traces of the above test gases will decompose upon irradiation, producing products which may corrode the pipe material. In the present experiments, heavy water saturated with either CF_2Cl_2 or CHF_2Cl at one atmosphere was irradiated in glass containers at a dose rate of 1.4×10^4 rads$\cdot$min^{-1}. The products found were D^+, F^-, Cl^- and HCO_3^-. By analogy with the radiation-induced decomposition of $CHCl_3$ in aqueous solution,[23] D_2O_2 was probably formed also, although this possibility was not tested. The concentrations of D^+ in the irradiated solutions were measured with a pH meter, utilizing the equation:

pD = meter reading + 0.40.[24]

The concentrations of F^- were determined colorimetrically[25] whereas Cl^- was determined nephelometrically. No purification of either the gases or the heavy water was attempted, since the yields of the products determined were not very reporducible. For solutions of either gas, however, the yield of each product was of the order of one molecule formed per 100 ev absorbed.

Environmental Studies

Studies of Columbia River Sediments - R. W. Perkins

Preliminary studies of Columbia River sediments with regard to their artificial radioisotope content, particle size distribution and mineralogical composition are described. Age estimates of the sediment layers of a river bottom core sample were made from the ratios of the artificial radioisotopes in the different core layers.

The use of Columbia River water as a coolant for the Hanford reactors and its subsequent return to the river introduces several radioisotopes to the river. Previous studies[26] have shown that substantial fractions of these radioisotopes are removed from the river water by natural self-purification processes as the river water moves downstream to the ocean. A study is being conducted to measure the physical and chemical forms of these radioisotopes, their concentrations in the river water and on suspended particulate material, and to determine their concentrations and the composition of the sediments from the various reservoirs and slack water areas in the Columbia River. Information gained from these measurements will be very useful in understanding the processes involved in the self-purification of the Columbia River and will permit a better estimate of the total radiosiotope content of the river bottom sediments.

Several radioisotopes are discharged to the river in reactor effluents; however, most of these radioisotopes have very short half-lives or are present in extremely low concentrations and cannot be readily traced in the river. The radioisotopes which are most readily traceable in the

river and its sedimenta are given in Table V along with their typical concentrations in river water downstream from the reactors during average river flow.

TABLE V

CONCENTRATION OF THE MAJOR RADIOISOTOPES IN COLUMBIA RIVER WATER JUST BELOW THE HANFORD REACTORS

Radioisotope	Half-Life	Concentration, dis/min/liter
Cs^{137}	30 yr	2.5
Zn^{65}	243 days	375
Co^{60}	5.2 yr	2.3
Mn^{54}	300 days	6.4
Cr^{51}	27 days	11,800
Sc^{46}	85 days	39

Radioisotopes in River Bottom Sediments

A gravity coring tube* modified to collect a 24 inches long by 2 inches diameter core has been used to obtain core samples of river bottom sediment. The sediment cores obtained with this device are cut in 2-inch lengths and their radioisotope contents measured. Since artificial radioisotopes of widely different half lives are present in the cores, it is possible to calculate the ages of core sections from various depths relative to the surface if the relative radioisotope concentrations in river water are assumed to have remained constant.

* Gravity coring tube No. 15M1440, modified Phlager design, G. M. Mfg. Co., 12 East 12th St., New York 3, New York

In Table VI the concentrations of the radioisotopes are presented for a sediment core which was taken in about 100 feet of water, 500 yards above McNary Dam during April of 1961.

Also included in this table are the ages of the various levels relative to the surface sample as calculated from the Zn^{65} to Co^{60} ratio. The age estimates are crude since they compare the lower sections with the thick 2-inch surface section and neglect any change of Zn^{65} to Co^{60} ratio with time.

TABLE VI

RADIOISOTOPE CONCENTRATIONS AND AGE ESTIMATES OF A CORE SAMPLE FROM THE McNARY RESERVOIR

Depth of Sample, in.	dis/min/gram of Sediment					Ratio: $\frac{Zn^{65}}{Co^{60}}$	Relative Age, yr
	Sc^{46}	Cr^{51}	Co^{60}	Zn^{65}	Cs^{137}		
0 - 2	78.6	425	61.5	2360		38.4	0
2 - 4			17.1	380	13.4	22.2	0.6
4 - 6			6.5	71.1	7.6	10.9	1.4
6 - 8			3.5	20.8	5.7	6.0	2.1
8 - 10			1.6	6.5	2.7	4.1	2.5
10 - 12			2.5	7.6	3.1	3.1	2.8
12 - 14			4.7	4.7	5.2	2.6	3.0

More refined age calculations will be made on cores which are sectioned in thinner layers. Other core samples, including some 2 feet long, have been obtained near this location and have shown a factor of about three variation in absolute concentration at the surface.

Core samples are being collected from various locations in the McNary Dam Reservoir to permit an estimate of the total activity in the sediments and to obtain information on the depths and distribution of the sediments. Core samples from above the Hanford project have been collected and measured to obtain background information. Core samples from near the mouth of the river have also been analyzed in preliminary studies.

The radioisotope measurements are being made with gamma ray spectrometric equipment which was designed with sufficient sensitivity to permit measurement of the natural radioactivity in samples.[27]

Particulate Composition of Sediment

Only a crude particle separation of the sediments from the McNary Dam Reservoir has been made. This separation was made by sedimentation from an aqueous slurry and the coarse fraction was washed free of fines by elutriation. X-ray diffraction measurements of the smallest particle fraction showed it to be compsed mainly of montmorillonoids, quartz and feldspar. The material was poorly crystalline. The coarse fraction contained about 50 percent quartz, 40 percent feldspar and small amounts of chlorite and mica. The material consisted of well-crystallized mineral compounds.* Microscopic particle size measurements showed that about 90 percent of the visible particles were less than 20 microns in diameter. But about 50 percent of the sediment weight was estimated to be due to particles of greater than 20 microns diameter. Radioisotope measurements of the fine and coarse fractions showed a greater, by about a factor of 5, specific activity for Zn^{65} and Co^{60} on the finest fraction than on the coarsest fraction.

Association of Radioisotopes with Particulate Material in River Water

Some of the radioisotopes in the Columbia River water become adsorbed on particulate matter and can thus be deposited in river bottom sediments as the river flows to the ocean. The fractions of the various radioisotopes associated with particulate matter in both reactor effluent and river water (after about 35 miles travel in the river) have been measured and reported earlier.[28] The changes which occur as the river water moves downstream are presently being studied to determine the effect of river flow rates, temperature, and turbidity on the amounts of the individual radioisotopes associated with particulate material. In making these studies, the

* Analyses of the X-ray diffraction spectra were made by L. L. Ames of Hanford Laboratories

particulate material is separated from the water by filtration through membrane filters and the fraction of each radioisotope associated with the particulate material is determined by instrumental or radiochemical analyses. To obtain a realistic picture of the changes which occur, measurements over a one year period are planned.

The Concentrations of Certain Chemical Elements in the Columbia River - W. B. Silker

Results of activation analyses of Columbia River salts are presented. Samples were collected along the length of the U.S. portion of the river during different seasons and flow conditions.

The majority of radioisotopes found in Hanford reactor effluent water are formed by activation of impurities in the cooling water. Seasonal fluctuations in the concentration of many of these radioisotopes are well known, but little data are available to relate these changes with the concurrent parent isotope concentrations in the cooling water. In addition, the ultimate source of the parent materials has never been investigated.

An extensive survey is in progress to evaluate the seasonal parent isotope concentration variation from samples of the Columbia River collected pariodically just upstream from the reactors. In addition, five sets of samples were collected from the Columbia River between Hunters, Washington, and Hanford during different river flow conditions. The first and last samplings were made during the low flow periods in March and October, before and after the peak river flow. The third sampling was made during peak flood condition. To augment other studies, the river length covered by these three samplings was extended to Rainier, Oregon, to characterize the concentration variations downstream from Hanford. Two additional samplings were made, before and after the river crested, at the times the flow was about half of the maximum for the year.

All samples were filtered through tared 450 mμ Millipore filters, and the amount of insoluble material was measured by weighing. Aliquots

of the filtered samples were encapsulated in quartz ampules, and placed in the flux zone of one of the Hanford reactors, together with standardized solutions of the elements of interest. After a suitable residence time in the reactor, the samples were removed and analyzed radiochemically for sodium, copper, manganese, arsenic, uranium, lanthanum, iron, cobalt, zinc, and scandium. Subsequent analyses will be made for phosphorus and sulfur. These data, while still partially incomplete, are presented in the following tables. The first two tables contain the analytical results for samples collected just upstream from Hanford during 1960 and 1961. The 1960 samples showed some algae growth by the time analyses were made which may make the results nonrepresentative. This difficulty was not encountered in the 1961 samples. Tables VII through XIV are devoted to the samples from different locations on the Columbia River.

Much information, such as the contribution of tributary streams to the flow of the Columbia River and estimates of the drainage from which these waters were derived, is not available at this writing. Because of these omissions and the incomplete nature of the analytical results, only general comments regarding these data will be made.

The most striking result observed was the influence of the Snake River on the concentration of several materials, notably sodium. The concentration of this material increased as much as a factor of five below the mouth of the Snake River, and lesser, but still significant, changes were observed for several other materials. From the data available, it appears that the Wenatchee River is the only upstream tributary that provided any positive change, that being copper during the high flow periods.

The effects of dilution were noticeable in the sodium, uranium manganese, and possibly zinc concentrations, which would indicate a steady source of these materials. An inverse trend was indicated for arsenic, copper, lanthanum and cobalt, which could reflect high concentrations of these materials in the watersheds supplying the high runoff during flood season.

A complete evaluation of these data will be made when the analytical work is completed. Three upstream samplings are scheduled during 1962 in an attempt to locate the source of the parent materials responsible for the spring increase in reactor effluent radioactivity.

TABLE VII

ELEMENTAL CONCENTRATIONS IN COLUMBIA RIVER WATER COLLECTED FROM 100 B IN 1960*

	Element Concentration in ppb									
Date	Na	Cu	Mn	As	La	U	Zn	Fe	Co	Sc
2/3/60	2200	6.17	0.66	1.46	0.039	0.39	15.0	23.4	0.044	0.002
3/8/60	2200	6.54	1.19	1.47	0.021	0.39	18.6	13.1	0.024	0.004
3/22/60	2300	9.90	0.86	1.29	0.012	0.36	14.7	9.3	0.019	0.002
4/7/60	2500	9.21	1.86	1.62	0.019	0.33	28.7	21.0	0.027	0.002
4/19/60	1890	8.01	1.64	1.66	0.042	0.30	25.4	10.5	0.020	0.003
5/3/60	2110	8.50	1.27	1.43	0.016	0.40	24.5	8.9	0.034	0.003
5/18/60	1720	4.53	1.84	1.51	0.056	0.37	22.1	22.3	0.023	0.003
6/1/60	1740	4.17	0.82	1.27	---	---	14.6	12.6	0.011	---
6/15/60	1400	--	2.89	0.98	0.051	0.35	10.0	16.7	0.035	0.005

* These samples were one year old before received, and most of them contained algae growth which may have affected the results.

TABLE VIII

ELEMENTAL CONCENTRATIONS IN COLUMBIA RIVER WATER COLLECTED FROM 100 B IN 1961

	Element Concentration in ppb									
Date	Na	Cu	Mn	As	La	U	Zn	Fe	Co	Sc
3/3/61	1960	12.9	3.96	1.37	---	---	39.6	17.1	0.011	0.013
3/13/61	2100	6.94	2.68	1.62	---	---	29.0	6.7	0.013	0.014
4/18/61	2370	11.3	3.16	1.90	---	---	32.5	8.6	0.015	0.023
5/2/61	1950	4.18	0.56	1.92	---	---	37.2	--	0.015	0.018
5/10/61	1920	8.18	1.14	1.50	---	---	39.7	9.2	0.016	0.021
5/17/61	1840	4.76	0.86	2.68	---	---	25.1	24.5	0.012	0.020
5/26/61	1660	4.35	0.56	2.11	---	---	24.1	13.8	0.011	0.029
6/2/61	1480	3.96	0.63	1.33	---	---	35.3	12.5	0.014	0.034
6/9/61	1210	4.28	1.41	1.57	---	---	146.9(?)	16.9	0.020	0.041
6/23/61	---	---	---	2.38	0.256	0.39	64.2	35.7	0.100	0.015
7/5/61	1440	5.36	---	1.31	0.054	0.37	6.1	11.4	0.031	0.004
7/7/61	1350	2.28	0.51	1.46	0.057	0.33	10.8	17.4	0.058	0.005
7/14/61	1500	1.57	0.30	1.60	0.058	0.36	8.3	23.4	0.034	0.003
7/21/61	1580	3.95	0.59	1.38	0.045	0.32	4.6	32.5	0.023	0.003
8/4/61	---	---	---	5.45	0.061	0.37	4.8	20.0	0.017	0.003
8/11/61	---	---	---	1.89	0.026	0.37	5.0	19.1	0.026	0.003

TABLE IX

COLUMBIA RIVER SAMPLING LOCATIONS

Sample Number	Sampling Location	Major Tributary Streams Since Previous Station, Rivers
1	Above mouth of Spokane River	- - - - - - - - - - - - - - -
2	1/2 mile below Coulee Dam	Spokane and San Poil
3	Brewster, Washington	Nespelem and Okanogan
4	Chelan Falls, Washington	Methow and Chelan
5	Wenatchee, Washington	Wenatchee
6	Vantage, Washington	- - - - - - - - - - - - - - - - -
7	Vernita Ferry	Crab Creek
8	Sacajawea Park	Yakima
9	Umatilla, Oregon	Snake and Walla Walla
10	Rufus, Oregon	John Day
11	The Dalles, Oregon	Deschutes
12	Warrendale, Oregon	Klickitat and Hood
13	Rainier, Oregon	Willamette, Lewis and Kalama

TABLE X

FIRST COLUMBIA RIVER SAMPLING - LOW FLOW CONDITIONS

Sample	Date Collected	Element Concentrations, ppb									
		Na	Cu	Mn	As	La	U	Zn	Fe	Co	Sc
1	4/17/61	2040	3.4	2.79	1.98	0.070	0.66	89.9	10.7	0.024	0.007
2	4/17/61	2420	3.3	3.56	1.71	0.070	0.62	104.6	16.3	0.023	0.011
3	4/17/61	2790	---	---	---	---	---	---	---	---	---
4	4/18/61	2350	6.8	1.84	1.91	0.082	0.73	80.1	24.6	0.022	0.036
5	4/18/61	2360	2.8	2.09	1.95	0.060	0.67	69.4	14.0	0.020	0.007
6	4/18/61	2340	2.4	1.54	1.70	0.062	0.67	79.8	19.5	0.022	0.011
7	4/18/61	2730	2.2	2.53	---	---	---	---	---	---	---
8	4/19/61	2330	3.0	1.07	1.51	0.54	0.73	63.4	15.0	0.022	0.0080
9	4/19/61	6930	5.9	2.55	2.13	0.106	0.72	48.5	15.4	0.036	0.012
10	4/19/61	6390	3.3	1.51	1.61	0.036	0.73	50.4	17.1	0.049	0.014
11	4/19/61	6400	6.4	1.09	1.84	0.034	0.78	32.4	19.1	0.058	0.011
12	4/20/61	6410	15.6	5.19	1.83	0.039	0.68	242.2	12.7	0.076	0.007
13	4/20/61	5820	13.2	1.89	1.36	0.030	0.52	121.9	25.2	0.045	0.014

TABLE XI

SECOND COLUMBIA RIVER SAMPLING - ONE HALF PEAK FLOW, RIVER RISING

Sample	Date Collected	Element Concentration, ppb									
		Na	Cu	Mn	As	La	U	Zn	Fe	Co	Sc
1	5/18/61	---	14.93	0.84	1.75	0.056	0.033	16.1	17.2	0.023	0.011
2	5/18/61	1860	5.88	0.70	1.91	0.237	0.45	11.6	15.3	0.022	0.006
3	5/18/61	2030	7.53	0.67	1.84	0.044	0.44	14.2	13.2	0.029	0.005
4	5/18/61	2000	3.31	0.56	1.95	0.041	0.41	12.0	52.4	0.026	0.012
5	5/19/61	1710	6.09	9.06	1.56	0.047	0.44	16.4	13.8	0.021	0.004
6	5/19/61	1570	7.58	4.21	1.93	0.052	0.45	13.0	16.1	0.022	0.009
7	5/19/61	1780	26.7	11.81	1.72	0.040	0.49	6.5	23.4	0.019	0.008

TABLE XII

THIRD COLUMBIA RIVER SAMPLING - PEAK FLOOD CONDITION

Sample	Date Collected	Element Concentration, ppb Na	Cu	Mn	As	La	U	Zn	Fe	Co	Sc
1	6/5/61	1380	3.42	2.04	5.11	0.072	0.23	52.1	15.1	0.040	0.033
2	6/5/61	1340	3.85	0.69	4.74	0.063	0.40	23.6	7.8	0.034	0.013
3	6/5/61	1360	3.38	2.87	6.91	0.161	0.34	13.8	13.0	0.039	0.027
4	6/5/61	1250	2.17	1.90	6.15	0.210	0.36	13.0	12.4	0.030	0.018
5	6/6/61	1330	7.64	1.84	7.44	0.079	0.35	33.7	12.5	0.041	0.021
6	6/6/61	1410	4.98	1.69	6.19	0.100	0.34	8.2	12.4	0.045	0.020
7	6/6/61	1440	3.62	1.61	4.97	0.088	0.33	24.3	13.8	0.063	0.022
8	6/7/61	1420	3.38	1.42	5.26	0.094	0.33	16.9	14.8	0.016	0.019
9	6/7/61	1930	3.24	1.72	4.01	0.148	0.25	10.1	14.0	0.013	0.023
10	6/7/61	1910	1.62	1.78	4.97	0.065	0.30	14.6	22.4	0.008	0.034
11	6/7/61	1960	2.44	2.26	3.91	0.059	0.29	11.2	16.2	0.018	0.027
12	6/7/61	2060	2.15	2.15	4.20	0.046	0.26	13.1	10.5	0.013	0.024
13	6/8/61	2210	1.48	1.77	4.54	0.092	0.20	8.3	18.6	0.021	0.041

TABLE XIII

FOURTH COLUMBIA RIVER SAMPLING - ONE HALF PEAK FLOW, RIVER RECEDING

Sample	Date Collected	Element Concentrations, ppb Na	Cu	Mn
1	8/10/61	1290	10.3	2.05
2	8/10/61	1010	3.4	2.53
3	8/10/61	1030	6.2	1.28
4	8/10/61	1140	10.1	2.46
5	8/11/61	1010	11.5	2.84
6	8/11/61	1140	9.1	---
7	8/11/61	1040	5.5	3.76

TABLE XIV

FIFTH COLUMBIA RIVER SAMPLING - LOW FLOW

Sample	Date Collected	Element Concentrations, ppb									
		Na	Cu	Mn	As	La	U	Zn	Fe	Co	Sc
1	10/23/61	---	545.6	0.41	1.56	0.121	0.43	12.89	14.0	0.016	0.006
2	10/23/61	---	21.83	0.43	1.73	0.050	0.39	8.86	17.8	0.019	0.003
3	10/23/61	---	3.21	0.74	1.40	0.074	0.45	15.29	11.7	0.023	0.005
4	10/24/61	---	1.31	0.50	1.62	0.161	0.38	12.71	12.4	0.019	0.007
5	10/24/61	---	1.80	0.46	1.72	0.059	0.41	4.85	11.6	0.017	0.007
6	10/24/61	---	---	---	4.07	0.131	0.40	8.83	15.9	0.017	0.018
7	10/24/61	---	2.31	0.65	3.56	0.086	0.42	11.86	20.8	0.013	0.013
8	10/25/61	1270	6.00	1.09	2.88	0.074	0.48	6.55	13.8	0.011	0.014
9	10/25/61	6130	2.61	3.23	4.48	0.083	0.082	3.66	23.2	0.029	0.025
10	10/25/61	6530	3.42	3.08	4.18	0.053	0.92	1.66	16.1	0.020	0.022
11	10/25/61	6840	7.06	2.82	3.87	0.084	---	2.76	17.7	0.033	0.026
12	10/25/61	6580	6.92	2.27	4.26	0.103	0.91	3.23	17.8	0.051	0.025
13	10/26/61	6190	4.21	27.77	3.99	0.169	0.71	5.80	41.5	0.143	0.068

Ground and Vegetation Effects on Atmospheric Diffusion Experiments - J. D. Ludwick

A study was undertaken to determine the effects of ground cover and vegetation on meteorological diffusion experiments which disperse particulates to the atmosphere. Methods were developed which allow removal and quantitative measurement of the dispersed particles from the vegetation. Results showed that a considerable number of the particles were found on the vegetation. Standing vegetation was found to have about five times as much particulate as ground level samples.

Many meteorological studies concerning atmospheric diffusion and pollution are carried out through dissemination of micron size particles to the atmosphere in the form of zinc sulfide or similar materials. This material is then collected at various sampling locations downwind and quantitative estimates made. For this purpose fluorescence[29] or phosphorescence[30] measurements are used at Hanford.

The present study* was carried out to help elucidate the effects of ground and standing vegetation on diffusion and to extend particle dispersion techniques to deposition studies. Of particular interest in this area is a measure of ground contamination from airborne particulate radioisotopes.

Quantitative estimates of the airborne contaminants are made from experimental models arrived at from normal diffusion studies; however, quantitative ground and vegetation deposition studies are necessary to deduce more accurate estimates of the vertical turbulent flux.

At Hanford the normal downwind terrain from the dispersion point is considered low and rolling and contains sagebrush averaging about 4 feet high in an irregularly distributed manner. In addition, there is some thin cheat grass growing among the sage brush. Since many atmospheric studies

---

* This project was undertaken in collaboration with the staff of Hanford Meteorology.

have been carried out along this course, a knowledge of the ground and vegetation deposition would allow an accurate vertical flux estimate to be made. Also, if the ground-cover had picked up dispersed material from these previous studies, this prior contamination would preclude quantitative measurement of ground and vegetation results from a new field run. It was probable that this would be the case even though weathering would be expected to slowly remove prior contamination.

A cheat grass field was found which was level for several hundred meters. This field had a very dense cover and presented almost a complete blanket of vegetation. The experiment was carried out in late summer when the grass was very dry. The field presented an unusually level vegetation appearance. Techniques were developed to process the material in a manner which would allow quantitative determination of the zinc sulfide on any selected grass sample or on any ground sample. Standard zinc sulfide samples were treated in a similar manner to insure validity of results. Electronic counting of the phosphorescence emission from the zinc sulfide particles was the final step in analysis.

Samples of sagebrush were selected downwind from the meteorology dispersion tower at distances up to about 200 meters. Previous atmospheric dispersion experiments had taken place over this course. Each sample consisted of sagebrush leaves and blossoms weighing about 0.1 gram per sample. The samples were weighed and placed into 2-dram vials normally used for phosphorescence measurements. Small aliquots of ethyl acetate (75 percent) and ethyl alcohol (25 percent) solvent (normally used for zinc sulfide counting) were added to the sagebrush and the sample shaken for about 5 minutes. Several shakings, decantings and counting of the extracting solvent showed that about 85 percent of the zinc sulfide was physically removed in the first pass. It was apparent that this technique was lacking because the density of zinc sulfide (about 4.0 g/ml) was such that some settling was taking place back onto the leaves before it could be decanted. The solvent material was changed to a denser liquid which would float the leaves off the top and allow leaf removal for further extractions. Carbon tetrachloride and chloroform were subsequently used with equal success.

Samples were placed in the vials, solvent added, and the vials shaken for about 10 minutes. The vials were then centrifuged for about 5 minutes. For samples having greater than 1×10^{-7} grams of zinc sulfide, two extractions removed more than 90 percent of the particles. Samples with less than this quantity required three extractions to remove about 90 percent. Sagebrush samples taken several miles upwind from the dispersal tower were treated in the same way and the solvent counted to determine the background phosphorescence. Although it was relatively easy to remove the floating vegetation from the solvent for further extraction, a more convenient and less time consuming method was desirable. A glass sample extraction apparatus was constructed which contained two chambers separated by very fine holes. The sample was placed in the upper chamber and aliquots of solvent added and shaken for one minute each. The extracting solvent and zinc sulfide were collected in the lower chamber while the vegetation was trapped in the upper chamber. A stopcock connection was used to bleed out the extracted material. Four 1-minute extractions removed almost all the zinc sulfide from the vegetation. It was noted that chloroform removed a considerable amount of the green chlorophyll and oil from the sagebrush while carbon tetrachloride was almost as efficient in removing zinc sulfide and extracted very little colored material. This color, when carried into the samples, will absorb the light from phosphorescence emission to some degree. All samples were counted in electronic counting equipment* containing an automatic sample exposure and positioning device as well as a preset delay mechanism.

Typical results of sagebrush extraction with chloroform and carbon tetrachloride are shown in Table XV. It is apparent that the less zinc sulfide particulate on the sagebrush, the more difficult it becomes to remove a large percentage of it.

---

* Tri-Carb, Model 314X Modified

TABLE XV

SAGEBRUSH EXTRACTION RESULTS

Solvent	Mass ZnS, grams		Summed Percent of Total	
	Extraction No. 1	Extraction No. 2	No. 1	No. 2
$CHCl_3$	8×10^{-6}	1.2×10^{-6}	84	96
CCl_4	8×10^{-6}	1.0×10^{-6}	87	98
$CHCl_3$	9.5×10^{-7}	2.7×10^{-7}	75	97
CCl_4	1×10^{-6}	2.5×10^{-7}	77	96
$CHCl_3$	3.5×10^{-8}	1.7×10^{-8}	61	86

Samples of sagebrush over which atmospheric diffusion studies had been carried out contained large amounts of the dispersed zinc sulfide. The results shown in Table XVI for various distances also indicated the wind direction when the studies were carried out. The higher counts at any distance indicated that the sample position was more in line with the wind direction from dispersal point. Comparison of the relative counting rate of air-collected samples with ground samples showed exact agreement. These data demonstrated that quantitative particulate results could be obtained from this type of vegetation.

TABLE XVI

ZnS MASS ON SAGEBRUSH

Sagebrush Sample	Distance, meters	Phosphorescence Counts, 18 sec	Mass ZnS, grams
108	25	760,000	1.0×10^{-5}
102	25	720,000	9.5×10^{-6}
114	50	42,000	1.3×10^{-6}
A	50	30,000	9.5×10^{-7}
120	115	3 900	3.5×10^{-7}
B	115	350	5.5×10^{-8}
132	200	330	5.0×10^{-8}
138	200	250	4.0×10^{-8}
126	200	100	2.0×10^{-8}

Samples of cheat grass were first obtained for experimental purposes from the downwind course beside the Hanford meteorology tower. It was demonstrated that zinc sulfide particles could be determined quantitatively from this type of vegetation.

Initially, the zinc sulfide particulate removal from the grass was carried out in a manner similar to that of sagebrush treatment. Particle removal from this grass was more difficult than from sagebrush. There was the possibility in this case, that the more readily removable particles had already been weathered from the standing grass, since dispersion had taken place several weeks before. The 2-chamber extraction apparatus failed to recover more than 80 percent zinc sulfide for low concentration vegetation samples. A method was developed to remove the grass while the sample was in the glass counting vial, leaving only the zinc sulfide.

A cheat grass field was selected and the dispersion equipment set up about 10 feet above vegetation level. The equipment was placed on the upwind corner of the grass field and sample collection was made downwind in arcs of 10, 50, 100 and 200 meters. Samples were collected from an area of one square decimeter of standing vegetation and comparable samples were taken at ground level. The latter samples were also cheat grass vegetation that was crushed or blown down. These field samples consisted of about 4 grams of grass from which a random aliquot of about 0.18 grams was taken for analysis.

Samples of grass were placed into a weighed 2-dram vial and the vial reweighed to determine the amount of material present. Background samples were obtained several miles upwind of dispersal point and analyzed with the other samples. The samples were inserted into an oven and slowly brought to 380 C and maintained at this temperature for 2 days. This treatment reduced the grass to a very small amount of residual translucent material. At the same time, standard samples of zinc sulfide mounted on millipore filters were placed in vials and also baked. It was necessary to raise the oven temperature very slowly to about 180 C and maintain it there for several hours while oxidizing the millipore filters containing the standard

zinc sulfide. This eliminated the possibility of these filters burning or exploding and ejecting zinc sulfide from the vials.

The standards and samples were cooled and 8 ml solvent (75 percent ethyl acetate - 25 percent ethyl alcohol) added. Vigorous shaking for 10 minutes insured dispersion of the zinc sulfide particulate. Automatic exposure to blue light and counting of the phosphorescence in the dark, after a preset delay, completed the determination of zinc sulfide. Samples containing only residue from the grass were almost clear; however, many samples from the ground cover level had dirt present and corrections for this effect were made with a colorimeter to give quantitative results.

Results and Discussion

When sample vials were counted, it was immediately noted that there was an unusual fast-decaying phosphorescent component present. The standard zinc sulfide samples were then analyzed to see if this could be attributed to the dispersed particulate. A comparison of the new calibration curve with previous calibration work[31] demonstrated that there was no statistically significant difference in the curves; consequently, the phosphor had survived the baking process without change. Background samples of cheat grass showed this same fast decaying component and it was apparent that a longer delay period than normal would be necessary to detect the zinc sulfide. Normally, a 6-second delay was used; however, a delay of about 42 seconds was necessary to reduce the contributed grass phosphorescence to a negligible level (Figure 23). The cause of this grass phosphorescence is not definitely known, but silicates of plant minerals, which probably make up the translucent residue material found after baking, are suspected. In effect, the electronic counting of phosphorescence emission can be used to differentiate two phosphors with sufficiently different decay characteristics. Unfortunately, the necessity for added delay resulted in reduction of the overall sensitivity for zinc sulfide detection.

Results of zinc sulfide analysis for arc No. 1 at 10 meters, which were typical of all arcs, are shown in Table XVII. The summed mass for standing and ground vegetation is multiplied by the aliquot factor to obtain

the final mass of zinc sulfide per square meter of ground at the sampling site. It may be noted that the particles are preferentially found on the standing vegetation. There was approximately five times as much zinc sulfide on the vegetation as on the ground, indicating that the deposition process on standing vegetation is quite efficient.

A typical downwind zinc sulfide deposition pattern is illustrated in Figure 24. This figure also exhibits a shift in wind direction which took place while the experiment was in progress and can be easily recognized.

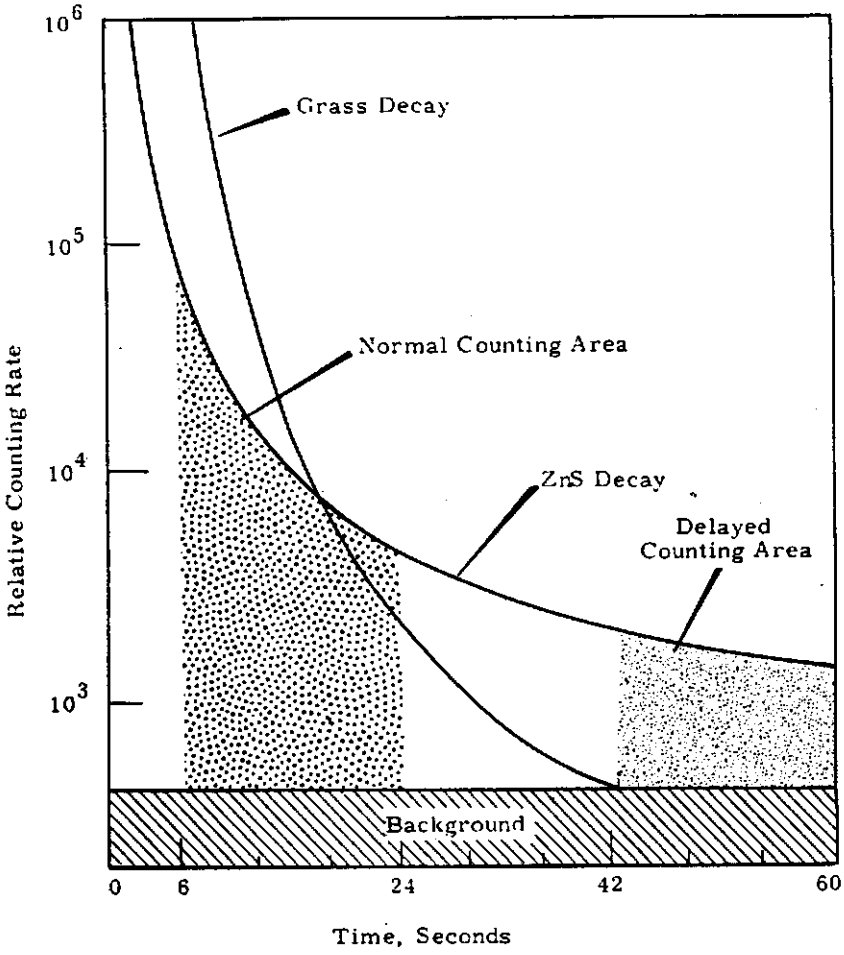

FIGURE 23

Phosphorescence Decay of ZnS and Baked Grass

TABLE XVII

TEN METER ZnS CONCENTRATIONS

Sample	ZnS Mass on Vegetation, grams		Total grams/meter^2
	Standing	Ground Level	
1	2.60×10^{-5}	7.95×10^{-6}	0.041
2	1.43×10^{-4}	3.98×10^{-5}	1.002
3	4.88×10^{-4}	8.65×10^{-5}	1.973
4	4.02×10^{-4}	6.79×10^{-5}	1.091
5	1.62×10^{-4}	3.12×10^{-5}	0.630
6	1.96×10^{-4}	3.94×10^{-5}	0.360
7	7.56×10^{-5}	1.70×10^{-5}	0.174
8	2.12×10^{-5}	7.85×10^{-6}	0.039
9	1.31×10^{-5}	3.22×10^{-6}	0.037
10	1.14×10^{-5}	3.02×10^{-6}	0.045

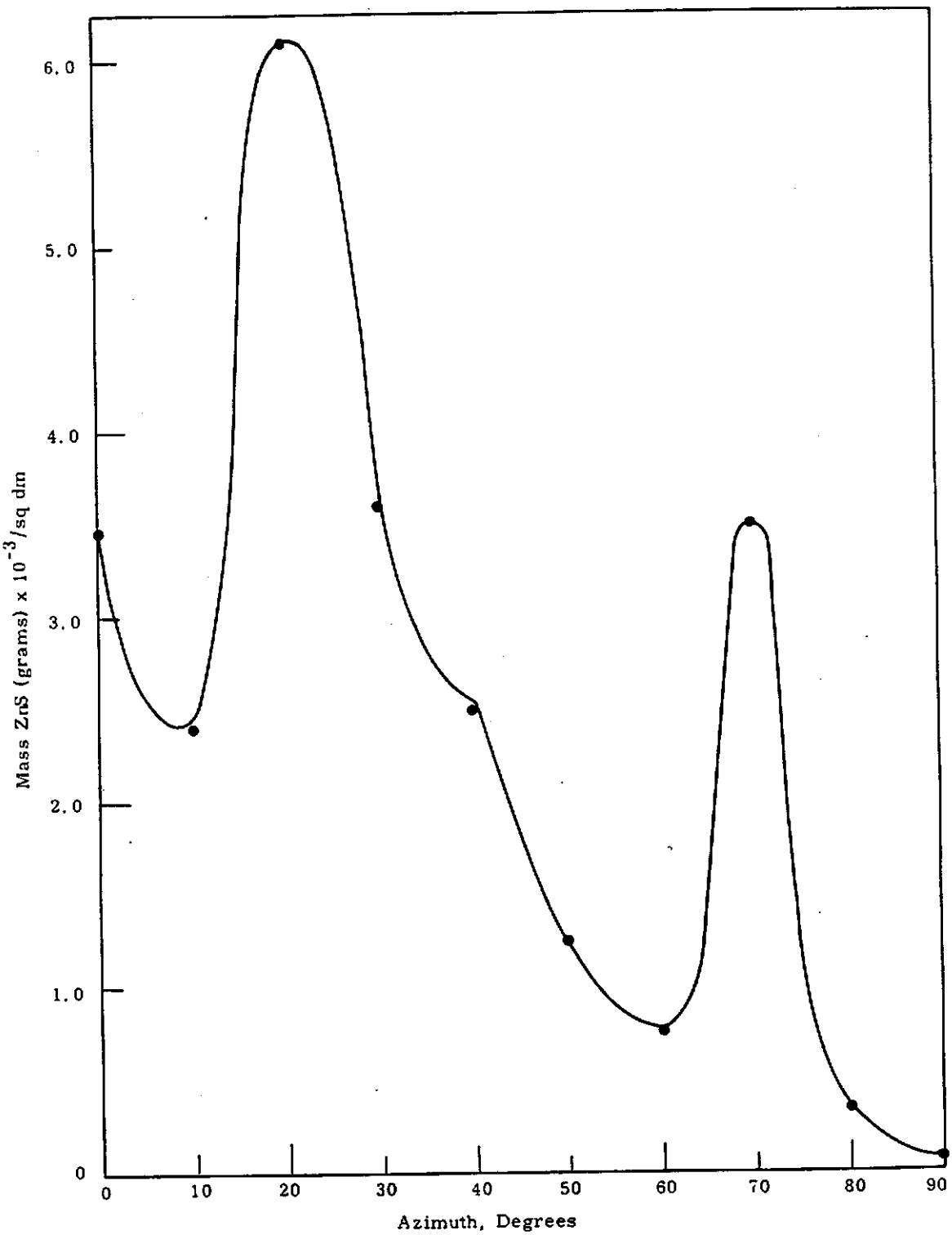

FIGURE 24

Fifty Meter ZnS Deposition Pattern

AEC-GE RICHLAND, WASH.

Reactor Studies

Parent Isotope Concentrations in Reactor Process Tube Film -

R. W. Perkins

The composition of the parent isotopes of most of the major reactor effluent water radioisotopes has been measured in process tube film. The relative rates of formation of the daughter radioisotopes are compared with their observed relative concentrations in reactor effluent water.

Previous studies have shown that only a small fraction of the observed radioisotope concentrations in reactor effluent water is produced from parent material which passes through the reactor in solution in the cooling water.[32] The majority of observed radioisotopes are produced from parent elements which are adsorbed on the surface film of process tubes and fuel elements and from which the activation products are subsequently released.

To study the composition of the film which forms on the surface of process tubes, a sample of film was obtained from a tube which had been in the central flux zone of C reactor for 4 to 5 years. The surface film, which was dark brown in color, was carefully removed by scraping and was used for the measurements herein reported. This brown film was underlaid with a hard gray aluminum oxide coat. The brown film was analyzed by neutron activation analysis for some of the trace elements of interest and the results are given in Table XVIII. The table also lists the daughter radionuclides, their relative rates of formation (for the parent element concentrations in the film) and compares these values with the observed relative radionuclide concentrations in reactor effluent water. If all of the radioisotopes were released immediately upon formation, their observed ratio in effluent water would be similar to the ratio in which these are formed on the film. The extremely large differences in the relative formation rates and observed concentrations reflect the relative affinities of the film for these daughter radioisotopes.

Assuming a similar composition in fuel element jacket film, these data, along with concentrations of both parent material in the influent and

radioisotope content of the effluent, can be used to calculate the fraction of each parent adsorbed. If the parent and daughter isotopes are assumed to act similarly, the elution rates of the parent elements can be calculated.

TABLE XVIII

CONCENTRATION OF THE PARENT ELEMENTS AND FORMATION RATE OF THE DAUGHTER RADIOISOTOPES IN REACTOR PROCESS TUBE FILM

Parent Element	Concentration, ppm	Daughter Radioisotope	Relative Formation Rates of Daughters, dis/min	Relative Concentration of Daughters in Effluent Water, dis/min
Na	0.68	Na*	1	1
P	1000	P^{32}**	16.9	0.025
Cu	920	Cu^{64}	3180	0.87
Ga	20	Ga^{72}	30	0.043
As	56	As^{76}	144	0.41
Sb	2.2	Sb^{122}	0.99	0.0067
La	12	La^{140}	16.6	0.022
Sm	2.3	Sm^{153}	115	0.0087
U	67	Np^{239}	71	0.43

* See Reference (24)

** P^{32} is also formed from S. Measurement of the S to P ratio in tube film showed between 4 and 40 times as much S as P. Most of the P^{32} in the film thus results from the S^{32} (n, p) P^{32} reaction.

Evaluation of the Ferrous-Permanganate System for Water Treatment - W. B. Silker

The usefulness of the ferrous-permanganate system as a water treatment process for removing trace ions was demonstrated using radioactive tracers. Optimum reactant concentrations and pH ranges were determined in static and dynamic systems. Further evaluation in reactor experiments is proposed.

Some reduction in concentration of radioisotopes in Hanford reactor effluent water can be obtained by improvements in water treatment processes. The prerequisite for any treatment process is the capability of producing large quantities of low turbidity water while simultaneously removing the parent materials responsible for radioisotopes of major interest, notably P^{32} and As^{76}. A new water treatment process, which utilizes the products of a redox reaction between permanganate and ferrous iron, was evaluated by laboratory-scale and pilot plant studies. (Application of this system was shown by Rosinski and Nagamoto[33] to be effective in scavenging several radioactive fission and corrosion products from synthetic sea water.) The overall reaction of interest is $3\ Fe^{++} + MnO_4^- \rightarrow 3\ Fe^{+++} + MnO_2$. The trivalent iron hydrolyzes to form hydrous ferric oxide, which, together with the hydrated manganese dioxide, forms a highly sorptive surface for both colloid and ion removal.

Beaker tests were made to determine the optimum reagent requirements for removal of radioactive arsenic. For these experiments a $KMnO_4$:$FeSO_4$ ratio of 1:2.7 was maintained to provide a slight excess of permanganate, and the final pH of the solution was adjusted to 7.5. The solution was spiked with As^{76} and, after the desired quantities of reactants were added, was stirred for 50 minutes. The solution was filtered after a 10 minute settling period, and the filters were assayed to determine the removal efficiencies shown in Table XIX.

To evaluate the effect of pH on the removal efficiencies for both cations and anions, 1.25 ppm of $KMnO_4$ and 3.38 ppm of $FeSO_4$ were added to a solution containing As^{76} and Zn^{65} tracers. The pH of the solution was

adjusted during a 5 minute stirring period, and the solutions were than allowed to stand for 10 minutes, after which time they were filtered. The [redacted] which was determined by comparison of

provided elsewhere.[34] Performance during these investigations was measured by spiking the raw water supply with a radioisotope of interest, and comparing the raw water radioisotope concentration with that in the filtered water.

The removal efficiencies for radioarsenic with 1.25 ppm $KMnO_4$ and 3.38 ppm $FeSO_4$, and postchlorination with 0.5 ppm Cl_2 to insure oxidation, were 97 percent, the pH range of 7.4 through 7.6. In these experiments, 0.02 ppm of Separan 2610* was added to the filter influent as a filter aid.

A series of experiments were performed to appraise the effectiveness of the permanganate-ferrous system in removing phosphate from river water. Radioactive phosphorus in the form of the orthophosphate ion was added to the raw water supply of the water treatment apparatus. At a reactant concentration of 1.25 ppm and 3.38 ppm for $KMnO_4$ and $FeSO_4$, respectively, the removal efficiency was 96 percent, about the same as was observed with radioarsenic. When the reagent concentrations were doubled, the P^{32} removal, under otherwise identical conditions, dropped to 90 percent. This is believed due to the additional load placed on the filter by the increased amount of insoluble materials. When the addition of permanganate and iron was reduced to 0.62 and 1.69 ppm respectively, only 50 to 60 percent of the radiophosphorus was removed in the process. This was probably due to the decreased surface area available for sorption of the radioanion.

After about 50 hours of operation, it was found that an initial breakthrough of P^{32} occurred when a freshly backwashed filter was put in service. Only 90 percent of the P^{32} was removed during the first hour or two of filter operation with 1.25 ppm $KMnO_4$ and 3.38 ppm $FeSO_4$. The removal efficiency increased until a consistent 97 percent removal was obtained during the remainder of the filter run. It was also noted that the sand portion of the filter had become discolored, which indicated that iron or manganese deposition had occurred on the sand. It was first believed that the initial

---

* Separan 2610 is a polycrylamide manufactured by Dow Chemical Company

activity breakthrough was due to gradual passage of the particulates which had not been removed by the previous backwash. That this was not the case was shown when radioactive iron, which was incorporated in the flocculating material, was consistently removed with a 97 to 98 percent efficiency. No tendency toward initial breakthrough of iron was observed in any of the experiments. The difficulty was then ascribed to the conditions which resulted from an attempt to substitute manganous ion for the ferrous ion in a previous experiment. The filter was treated with dilute sulfuric acid until the sand discoloration had been removed, thoroughly washed with water and placed back in service. No premature breakthrough was noted during any subsequent experiments; likewide, no further discoloration of the filter medium was noted.

A series of runs were made in which the pH of the water was varied to check the removal efficiencies under dynamic conditions. The $KMnO_4$ and $FeSO_4$ concentrations were maintained at 1.25 and 3.38 ppm, respectively, and 0.02 ppm Separan 2610 was added to the filter influent. Ninety-eight percent of the radiophosphorus was removed when the pH was maintained between 7.0 and 7.4, and 97 percent removal was obtained at pH 7.6. Filter runs in excess of 7 hours were obtained with no evidence of breakthrough. A filter run of this duration is sufficient to meet reactor area requirements.

This process will be subject to further evaluation when a small water treatment plant in the reactor areas becomes available. This plant is designed to treat a sufficient quantity of water to furnish the coolant to two process tubes in KE reactor. Parameters which will be subject to in-reactor evaluation are: the effect of the process on effluent radioisotope concentrations, the degree of control required during the addition of the reactants, the effect of the process on the film forming characteristics of the water, and effective filter bed life.

Optimum Alum Feed Rates for Reactor Water Treatment - W. B. Silker

The optimum alum feed rates for treatment of Columbia River water for process water use were established by measurement of the zeta potential of the floc. If the zeta potential of the flox is maintained between 0 and -5 mv, optimum removal of both river colloids and anions is obtained.

Measurements of the zeta potentials (ZP) of river colloids and aluminum floc were made at several reactor area water treatment plants in an attempt to relate this measurement to the quality of water produced. The river colloids had a ZP of -16 to -18 mv during the first part of January. Treatment of the water at several reactor areas with 18 ppm of aluminum sulfate (produced by the reaction of sulfuric acid and "raw bauxite") increased the ZP of the colloids to 0 to -8.9 mv. The process was controlled to furnish finished water at a pH of 7.0 ± 0.1. Where the pH of the finished water is maintained at 6.6 to 6.7, 18 ppm of liquid alum provided a floc with a ZP of +7.6 mv, a reversal of the charge of the incoming colloids. This occurs because of the amphoteric nature of the aluminum ion. At reduced pH more aluminum occurs as Al^{+++} than at higher pH values. The net effect is that counterion replacement occurs and the adsorbed anions of arsenic and phosphorus, in particular, are displaced into solution and are not removed by the filtration process. This minimizes the effectiveness of the process in reducing the effluent concentrations of the radioactive daughters of these materials, and explains in part why the reactors using 18 ppm alum and treating water to a pH of 6.7 have not shown a reduction in the effluent radioisotope concentration. Operation of the laboratory water treatment apparatus under these conditions provided a floc with ZP of +8.8 mv. During a 6-hour filter run (with addition of 0.02 ppm Separan to the filter), the arsenic removal efficiency dropped from 80 percent to less than 40 percent. The process was then controlled to provide a final pH of 6.7 and alum was added to control the ZP of the colloids between 0 and -5 mv at the flash mixer. When the process was controlled by ZP adjustment, 94 percent of the radioarsenic was initially removed. This

figure showed a gradual decrease to 88 percent after a 6 hour filter run, with no added Separan. Subsequent runs under the same conditions removed greater than 92 percent of the radioarsenic over the full 6-hour filter run.

The addition of 0.03 ppm Separan to the filter influent appeared to smooth the removal efficiency curve throughout a 6 hour filter run, with no appreciable difference in head buildup. Addition of 0.04 ppm Separan improved the removal efficiency to 95 percent, but a higher rate of head buildup limited the filter run to 5-1/2 hours. Since the filter in this experimental apparatus is operated differently than the production filters, direct comparison between the two systems relative to pressure drop and rate of head buildup is not possible.

These data indicate appreciable cost savings can be effected in plants producing water at a pH of 6.7 by reducing the alum feet rate to provide a floc with a ZP between 0 and -5 mv, by limiting filter runs to produce water with a turbidity reading of less than 0.003 ppm, and by adjusting Separan addition to provide water of this quality.

Measurements of Radioisotopes and Trace Constituents in the PRTR D_2O and Helium Systems* - R. W. Perkins and C. W. Thomas

During the initial testing of the Plutonium Recycle Test Reactor (PRTR) at a power level of a few Mw, rather large amounts of fission product gases were observed in the helium and the D_2O systems. The D_2O system also contained the fission products $I^{131, 133, 135}$ and considerable amounts of Cl^- and F^-. From a survey of possible sources of the fissionable material, including surface contamination of the fuel elements, the ion exchange resins, addition chemicals, and other sources, it was concluded that the observed concentrations of fission products could only arise from a failed fuel element. The Cl^- and F^- concentrations in the D_2O system were attributed to the presence of Freon which was apparently trapped in the system during previous pressure testing.

---

* Published as HW-69924

Radioisotope Concentrations in the PRTR Coolant and Helium Systems During Operation with a Failed Fuel Element(s)* -
R. W. Perkins and C. W. Thomas

Measurements of the radioisotope concentrations in the primary D_2O and helium systems of the PRTR were made during operation with a failed fuel element. The major fission product radioisotopes present in the helium system were Xe^{135} (5.2d), Xe^{135} (9.2 hr), and Kr^{88} (2.8 hr). These radioisotopes were also the major fission product constituents of the D_2O system. However, the iodine radioisotopes, I^{131} (8d), I^{133} (21 hr), and I^{135} (6.7 hr), were sometimes present in large amounts.

Bursts of fission gases following reactor startup or increases in power level were observed. Under the reactor operating conditions these bursts were, at times, equivalent to those produced by fissions in 150 grams of natural uranium (or 870 mg Pu^{239}). These activity bursts frequently increased the specific activity of the helium system by two orders of magnitude (and by an order of magnitude in the D_2O system). During the bursts, the gross gamma activity increased sharply for about 30 minutes and the peak duration was approximately 6 hours. Calculations based on the observed activity increases in the helium system during bursts indicated that the design of a rupture monitor must permit almost instantaneous comparison of the radioactivity in the 85 reactor tubes if it is to be successful in identifying the defective fuel element.

---

* Not supported by Biology and Medicine, published as HW-70980.

REFERENCES

1. Dietrich, W. C., J. D. Caylor, E. E. Johnson. Separation of Uranium from Urine by a Tri-n-octylphosphine Oxide Column and an Automation of the Procedure, Y-1322. December 15, 1960.
2. Sugihara, T. T., H. I. James, E. J. Troianello and V. T. Bowen. "Radiochemical Separation of Fission Products from Large Volumes of Sea Water," Anal. Chem. 31: 44-49. January 1959.
3. Kirby, L. J., W. B. Silker, and R. W. Perkins. Analytical Chemistry in Nuclear Reactor Technology - Instrumentation, Remote Control Techniques, and Nucleonics - Second Conference - Gatlinburg, Tennessee - September 29 - October 1, 1958, TID-7568 PT2. pp. 214-229. September 1958.
4. Alstad, J. and A. C. Pappas. "Radiochemical Studies of Fission Product Lanthanum and Lanthanides - I. Isolation of Trace Lanthanides using Non-Isotopic Carrier and Drop Elution Technique," J. Inorg. Nucl. Chem. 15: 222-236. 1960.
5. Perkins, R. W. "High Sensitivity Gamma-Ray Spectrometry," Proceedings of the 1961 International Conference: Modern Trends in Activation Analysis.
6. Miller, C. E. and O. J. Steingraber. Radiological Physics Division Semiannual Report - July through December, 1958, ANL-5967. p. 129. December 1958.
7. Perkins, R. W., J. M. Nielsen, and R. N. Diebel. "Total Absorption Gamma-Ray Spectrometers Utilizing Anticoincidence Shielding," Rev. Sci. Instr. 31: 1344. 1960.
8. Perkins, R. W. "A Large Well Crystal for the Direct Measurement of Trace Amounts of Radioisotopes in Environmental Samples," Health Physics 7: 81-86. 1961.
9. Davidson, J. D. and Philip Feigelson. "Practical Aspects of Internal-Sample Liquid-Scintillation Counting," Intern. J. App. Rad. and Isotopes 2: 1-18. 1957.
10. Brauer, F. P. and R. E. Connally. The Operation and Maintenance of an Alpha Energy Analyzing System, HW-60974. July 10, 1959.
11. Kalkwarf, D. R. "Radiation Sensitivities of Metabolic Products in Dilute Aqueous Solution," Radiological Chemistry Annual Report - January-December, 1960, HW-68533. January 15, 1961.
12. Furch, R. "Uber die asymtotische Halbierung der Exponentialreihe und der Gammafunktion bei grossem Argument," Z. Physik, 112: 92-95. 1939.

13. Kalkwarf, D. R. "Radiation Sensitivity and Chemical Structure," International Conference on Peaceful Uses of Atomic Energy, 29: 379-384. New York: U. N. Pub., 1958.

14. Kalkwarf, D. R. and R. W. Henkens. "Protolysis and Hydrolysis Constants for Trisulfonated Triphenylmethane Dyes," Radiological Chemistry Operation Annual Report - January - December, 1960, HW-68533. January 15, 1961.

15. Edward, J. T. "The Mobilities of Organic Ions in Paper Electrophoresis," Chem. and Ind. pp. 929-930. 1956.

16. Henkens, R. W. and D. R. Kalkwarf. "The Chemical Form of Radioactive Ions in Dilute Aqueous Solutions," Northwest Regional Meeting American Chemical Society, Seattle, Washington, June 18-19, 1959.

17. Block, R. J., E. L. Durrum, and G. Zweig. A Manual of Paper Chromatography and Paper Electrophoresis, page 505. New York: Academic Press. 1958.

18. Werum, L. N., H. T. Gordon, and W. Thornburg. "Rapid Paper Ionophoresis Using Organic Buffers in Water-Formamide and Water-Urea," J. Chromatog. 3: 125-145. 1960.

19. Goldsborough, J. P. and M. Mandel. "Analysis of a Magnetic Resonance Spectrometer," Rev. Sci. Inst., 31: 1044-1046. October 1960.

20. Strandberg, M. W. P. "Linear, Complex-Reflection Coefficient Bridge," The Microwave Journal, 4: 66-73. June 1961.

21. Weger, M. "Passage Effects in Paramagnetic Resonance Experiments," Bell Sys. Tech. J., 39: 1013-1112. July 1960.

22. Rempel, R. C. and H. E. Weaver. "Low-Power Microwave Reflection Bridge," Rev. Sci. Inst., 30: 137. 1959.

23. Tepley, J. and J. Bednar. "Radiation Chemistry of Aqueous Chloroform Solution," International Conference on Peaceful Uses of Atomic Energy, 29: 71-79. New York: U. N. Pub., 1958.

24. Fife, T. H. and T. C. Bruce. "The Temperature Dependence of the ΔpD Correction for the Use of the Glass Electrode in D_2O," J. Phys. Chem., 65: 1079-1080. 1961.

25. Rodden, C. J. (ed.). Analytical Chemistry of the Manhattan Project, pp. 241-243. New York: McGraw-Hill, 1950.

26. Nielsen, J. M. and R. W. Perkins. The Depletion of Radioisotopes from the Columbia River by Natural Processes, HW-52908. October 4, 1957. (SECRET).

27. Perkins, R. W., J. M. Nielsen, and R. N. Diebel. "Total Absorption Gamma-Ray Spectrometers Utilizing Anticoincidence Shielding," Rev. Sci. Instr., 31: 1344-1349. 1960.

28. Nielsen, J. M. Radiological Chemistry Semiannaul Report - July - December 1959, pp. 39-40, HW-63824. March 15, 1960.

29. Rankin, M. O. Zinc Sulfide Particle Detector, HW-55917. May 1958.

30. Ludwick, J. D. and R. W. Perkins. "Liquid Scintillation Techniques Applied to Counting Phosphorescence Emission. Measurement of Trace Quantities of Zinc Sulfide," Anal. Chem., 33: 1230-1235. 1961.

31. Ludwick, J. D. Dual Atmospheric Tracer Techniques for Diffusion Studies Using Phosphorescence-Fluorescence Analysis, HW-70892. March 1961.

32. Perkins, R. W. Source of Reactor Effluent Water Radioisotopes, HW-69969. May 1961. (SECRET).

33. Rosinski, J. and C. T. Nagamoto. "Scavenging Radionuclides in Substitute Ocean Water," Ind. Eng. Chem., 52: 429-432. 1960.

34. Silker, W. B. The Effectiveness of High Coagulant Feed in Reducing Hanford Reactor Effluent Radioisotope Concentrations, HW-SA-2192. July 14, 1961.

CHEMICAL EFFLUENTS TECHNOLOGY

Soil Chemistry, Geochemistry

Soil Column Breakthrough Curve Analysis - J. L. Nelson

Equations of Mayer and Tompkins, Hiester and Vermeulen, and Glueckauf for prediction of ion exchange column breakthrough curves do not yield consistent results for soil columns of different lengths. Two modifications were found to improve the predictions. The first involves adjustment of the breakthrough curve for the longitudinal dispersion effect as determined by the nitrate breakthrough. The second makes use of the square root of column length rather than column length per se in calculation of plate heights.

The method used at Hanford to predict breakthrough of radionuclides into ground water is a linear extrapolation of breakthrough curves from short laboratory columns.[1, 2] The assumption is made that the slope and position of the curve, i.e., column volumes versus effluent concentration, are the same for short as for long columns. It is known that this assumption is not entirely valid. Attempts to improve the extrapolation have been made by applying chromatographic equations suggested by Mayer and Tompkins,[3] Hiester and Vermeulen,[4, 5] and Glueckauf.[6, 7] In all three methods the assumption is made that the "height of theoretical plate", or the length of the "column capacity parameter", remains the same with changes in column length. It is necessary that this assumption be valid in order to use the results of short-column experiments to predict the breakthrough from longer columns.

Analysis of laboratory data from experiments utilizing columns of various lengths indicated that the height of theoretical plate, or column capacity parameter, consistently increased with column length. For example, Glueckauf calculations are shown in Table I for influents containing 0.08N solutions of Mg^{+2}, Ca^{+2}, and Na^{+} ions in competition with 0.1 ppm Sr^{+2}. Flow rates used were 4.3 ml/cm^2/hr. The soil was presaturated with the major ion. Four to six replicates of each column dondition were found necessary to obtain sufficient precision to delineate the functions involved.

TABLE I

HEIGHT OF THEORETICAL PLATES
CALCULATED FROM GLUECKAUF EQUATIONS

(Strontium Sorption by Hanford Project Soil
in the Presence of the Indicated Accompanying Ion.)

Column Length (cm)	Height of Theoretical Plate (cm) = $\frac{\text{Column length}}{N}$		
	Na^{+}	Mg^{+2}	Ca^{+2}
5	0.29	0.46	0.20
10	0.30	0.75	0.56
20	0.46	1.2	0.37
40	0.64	1.8	0.71
120	2.31	2.9	1.68
360	--	--	4.0
1440	--	--	11.0

The formula used for calculation of the number of theoretical plates per column was:

$$N = \frac{\overline{V}\ V'}{(\overline{V}-V')^2}$$

where N is the number of theoretical plates in the column,

$\overline{V}$ is the throughput volume to 50 percent breakthrough, and

V' is the throughput volume to 15.87 percent breakthrough.

It can readily be seen that the height of the theoretical plate increases with increasing column length. Calculations of similar kinetic parameters using formulas of Mayer and Tompkins,[3] and Hiester and Vermeulen[4] result in approximately the same magnitude of change with column length. It appears obvious that the equations are not applicable to the conditions of the soil columns used at Hanford.

Papers by Glueckauf,[6] and Hiester and Vermeulen,[4] state that at low flow rates and small particle sized, "longitudinal dispersion" may have considerable effect. Hydrodynamic dispersion is probably the principal

mechanism involved. Since these flow rates are impractical for industrial ion exchange resin application, little attention is given to quantitative analysis of this case. The reported particle sizes and flow rates for which "longitudinal dispersion" becomes important are in the same range we encounter in our soil columns, and it is this range in which most flows in field soils occur.

It is desired, then, to obtain a measure of diffusion plus dispersion in the columns and to use this to adjust the calculations of HETP or column kinetic parameters. Nitrate ion has been shown to pass through the soil without being sorbed, so it could be used as a tracer for water. Nitrate breakthrough curves were compared with strontium curves. Easily-compared linear curves were obtained by plotting erf (C/C_o) versus log $V/\overline{V}$; where C_o is influent concentration and C is effluent concentration. Figure 1 shows the Mg^{+2}-Sr^{+2} column breakthrough curves as well as the nitrate curve. It can be seen that the slope of the strontium breakthrough curve increases with increasing column length, approaching that of the nitrate breakthrough curve.

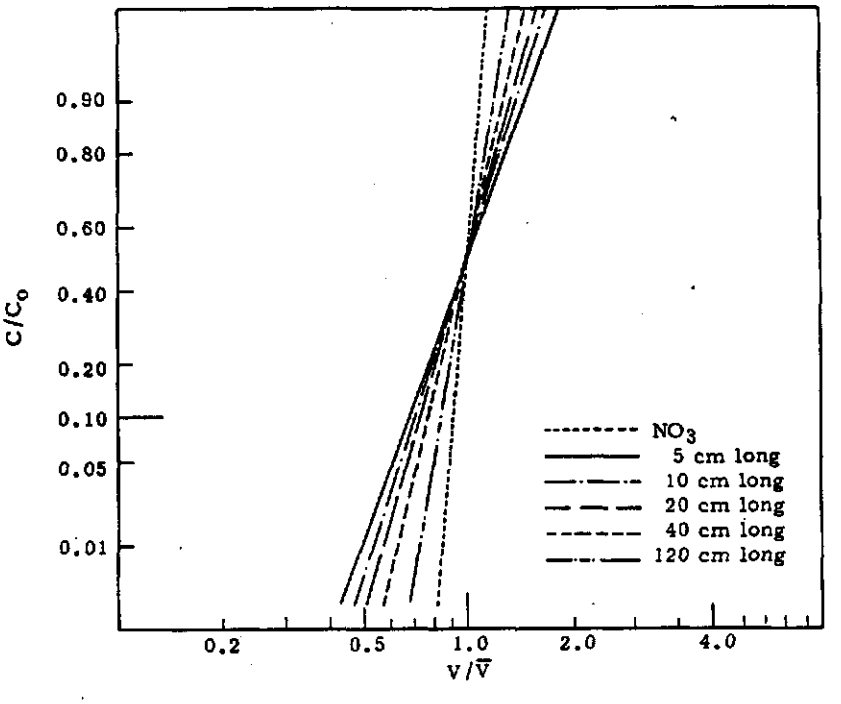

FIGURE 1

Normalized Sr^{90} Breakthrough Curves from Soil Columns of Various Lengths

In order to subtract the dispersion effect, as represented by the nitrate breakthrough curve, Glueckauf's formula was altered to:

$$N = \frac{V'' \; V'}{(V''-V')^2}$$

where V'' is the 15.87 percent breakthrough volume for nitrate. Results of these calculations are given in Table II.

TABLE II

HEIGHT OF THEORETICAL PLATES CALCULATED FROM MODIFIED GLUECKAUF EQUATION

(Strontium Sorption by Hanford Project Soil in the Presence of the Indicated Accompanying Ion.)

Column Length (cm)	Height of Theoretical Plate (cm) = Column length / N		
	Na^+	Mg^{+2}	Ca^{+2}
5	0.15	0.28	0.09
10	0.14	0.43	0.26
20	0.17	0.71	0.11
40	0.22	0.96	0.19
120	0.50	0.59	0.17
360	--	--	0.26
1440	--	--	0.41

The high variability of the data is due to the sensitivity of the equation to experimental uncertainties. The width of a pencil line drawn on the graph can make an appreciable difference. However, the dispersion modification appears to result in nearly constant values of HETP for columns of different length. This indicates that dispersion may be of major significance in soil columns.

Vermeulen[8] suggested that the spreading of a chromatographic zone is directly proportional to the square root of column length. Therefore, another modification was tested in which a kinetic parameter was calculated

from the square root of the column lengths examined. The results of this substitution are given in Table III for the modified Glueckauf derivation.

TABLE III

MODIFIED KINETIC PARAMETER USING GLUECKAUF EQUATIONS AND SQUARE ROOT OF COLUMN LENGTH

(Strontium Sorption by Hanford Project Soil in the Presence of the Indicated Accompanying Ion)

Column Length (cm)	Modified Kinetic Parameter = $\frac{\sqrt{\text{Column length}}}{N}$		
	Na^{+}	Mg^{+2}	Ca^{+2}
5	0.13	0.20	0.09
10	0.10	0.24	0.18
20	0.10	0.26	0.08
40	0.10	0.28	0.11
120	0.21	0.26	0.15
360	--	--	0.21
1440	--	--	0.29

Similar calculations of Hiester-Vermeulen parameters are presented in Table IV. It can readily be seen from either set of calculations that the width of the exchange zone is more closely proportional to the square root of column length than to column length per se. It is quite possible that the square root function is a result of longitudinal dispersion effects.

TABLE IV

COLUMN CAPACITY PARAMETER CALCULATIONS
USING HEISTER-VERMEULEN EQUATIONS
(Strontium Sorption by Hanford Project Soil
in the Presence of the Indicated Accompanying Ion)

Column length (cm)	Mg^{+2}-Sr^{+2} System		Ca^{+2}-Sr^{+2} System	
	Column length / "S" Parameter	$\sqrt{\text{Column length}}$ / "S" Parameter	Column length / "S" Parameter	$\sqrt{\text{Column length}}$ / "S" Parameter
5	0.13	0.060	0.08	0.038
10	0.25	0.075	0.07	0.023
20	0.37	0.083	0.18	0.041
40	0.59	0.093	0.29	0.045
120	0.71	0.064	0.60	0.055
360	--	--	1.33	0.070
1440	--	--	3.60	0.095

Metasomatic Replacement of Limestones by Alkaline, Fluoride-Bearing Solutions - L. L. Ames, Jr.

A laboratory study of the kinetics of limestone replacement by alkaline, fluoride-bearing solutions is presented. Data on the effects of temperature, concentration, pH, calcite surface area, and flow rates on fluoride and strontium ion removal are included.

During a study of the replacement of limestone by phosphorite,[9] fluoride ion was added to the limestone-altering solution as NaF. The presence of fluoride ion did not appreciably change the rate of formation of apatite, but without the presence of phosphate ion, the fluoride caused the alteration of limestones ($CaCO_3$) to fluorite (CaF_2) at a pH less than 10.

Figure 2 is a photomicrograph of an optical grade calcite rhomb partially replaced by fluorite. The replacement was accomplished by placing a calcite rhomb in a 0.2M NaF solution for two weeks. The resulting partially-altered calcite was then sectioned and photographed by reflected

light. The outline of that part of the original calcite rhomb now composed of CaF_2 is well-preserved. The CaF_2 layer is 0.5 mm at its greatest dimension. Much of this replacement layer was torn away during grinding and polishing of the thin section.

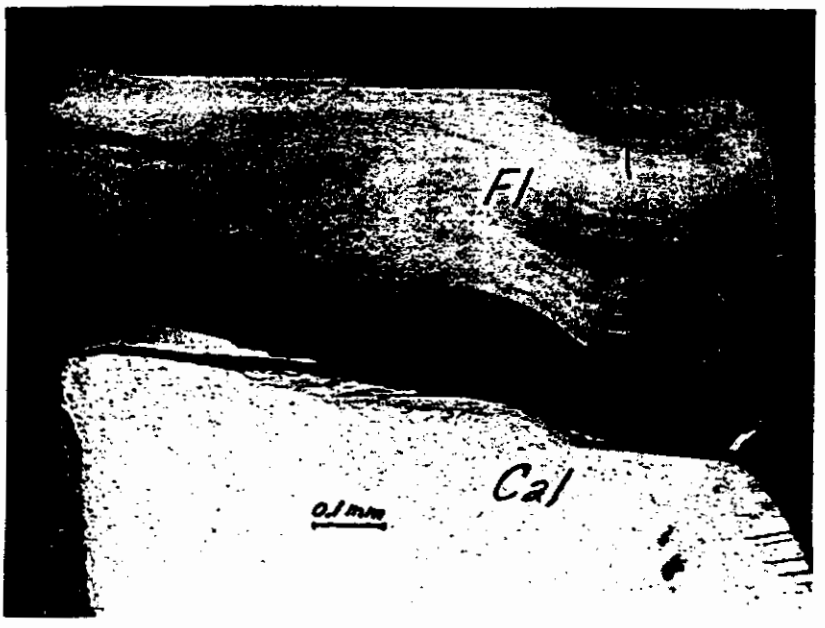

FIGURE 2

A Calcite Rhomb, Sectioned Parallel to $10\bar{1}1$, Showing the Fluorite Replacement Layer

Cal = Calcite Fl = Fluorite

Figure 3, an enlargement of the extreme lower left of Figure 2, shows fluoride replacement along a cleavage crack in the original calcite. Note the vestigial outline of the original calcite crack as preserved in the fluorite. Fluoride ion has diffused down the calcite crack and carbonate ion back out. Material transfer was intercrystalline.

The alteration product was identified as fluorite from X-ray diffraction patterns.

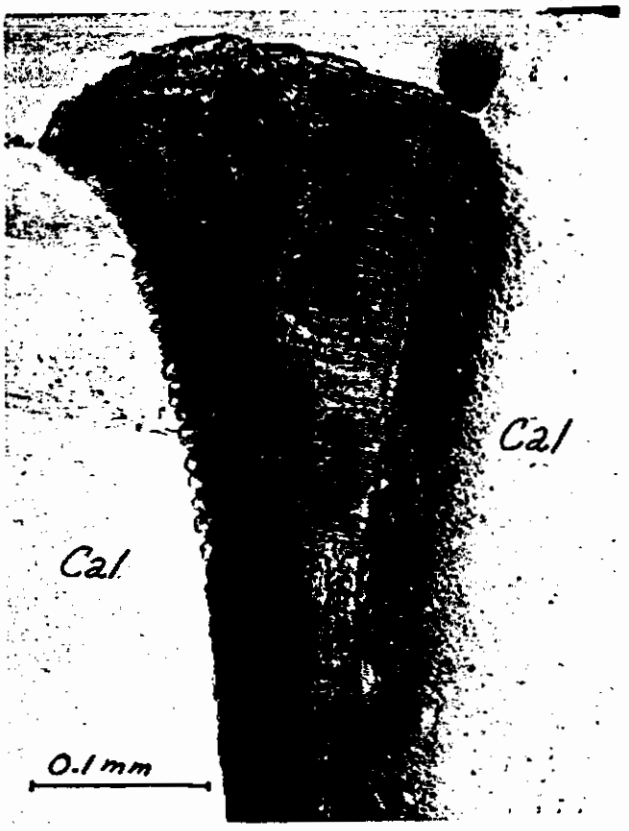

FIGURE 3

Fluorite Replacement of Calcite Along a Cleavage Crack in the Original Calcite

Cal = Calcite Fl = Fluorite

Figure 4 shows the effect of the several indicated variables on C/C_o values for fluoride ion. The relationship between fluoride removal and calcite surface area is approximately linear and directly proportional. Also of interest is removal of fluoride with changing influent pH, which increases with decreasing calcite stability in the system. Standard conditions are indicated on the various scales by the arrow that cuts across them. Only one variable at a time was changed while the rest were maintained at the indicated standard conditions. The failure of these curves to intersect at a single point represents experimental error.

Figure 5 illustrates the effects of the several variables on C/C_o values for strontium removal from solution. The strontium was present in the influent solution along with fluoride ion.

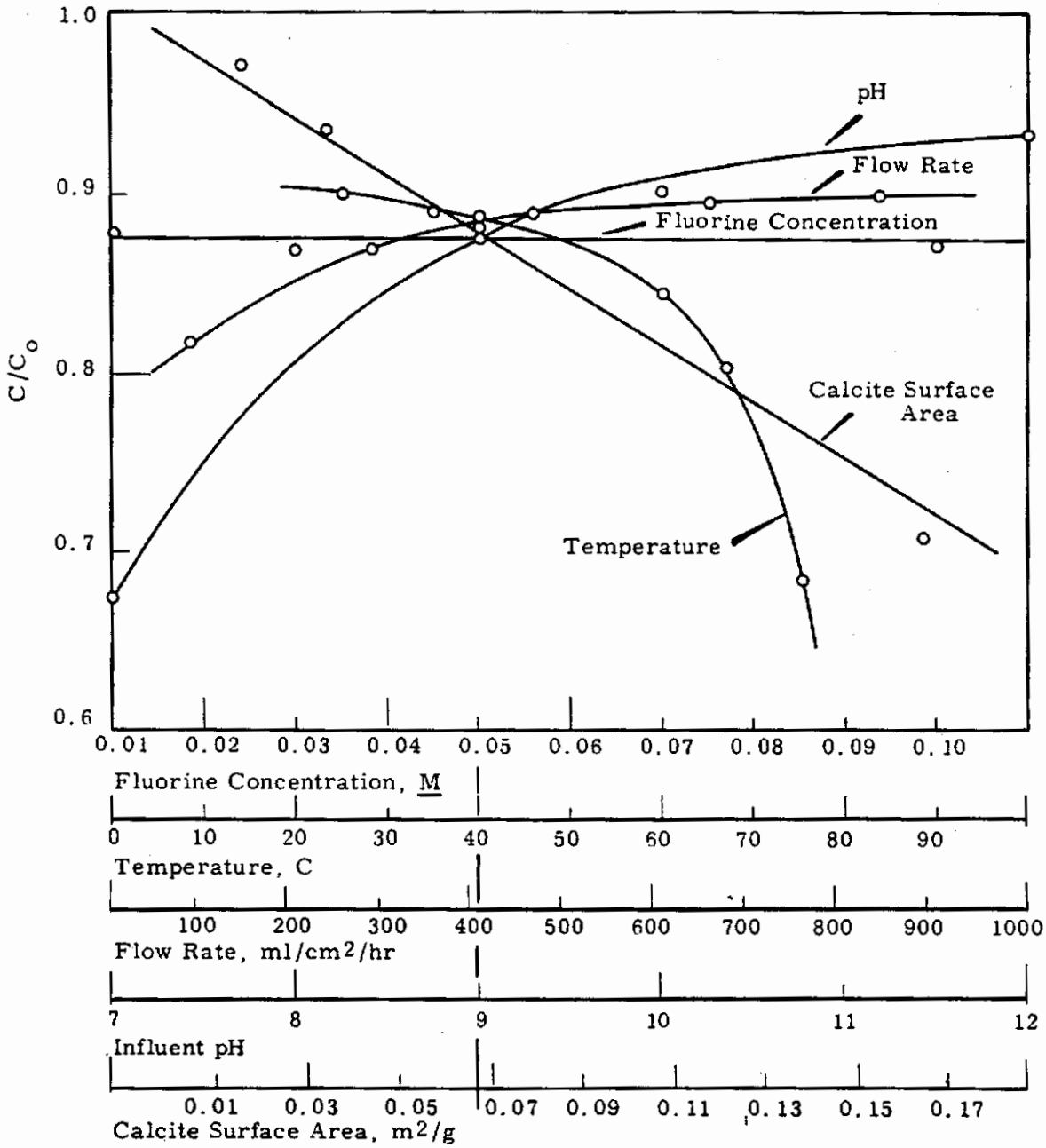

Standard Column Conditions

FIGURE 4

Fluoride Ion Removal During Calcite Replacement by Alkaline, Fluoride-Bearing Solutions. Fifty Gram Calcite Columns were Used to Obtain These Data. All Solutions Contained 1M NaCl in Addition to Their Other Consituents.

AEC-GE RICHLAND, WASH.

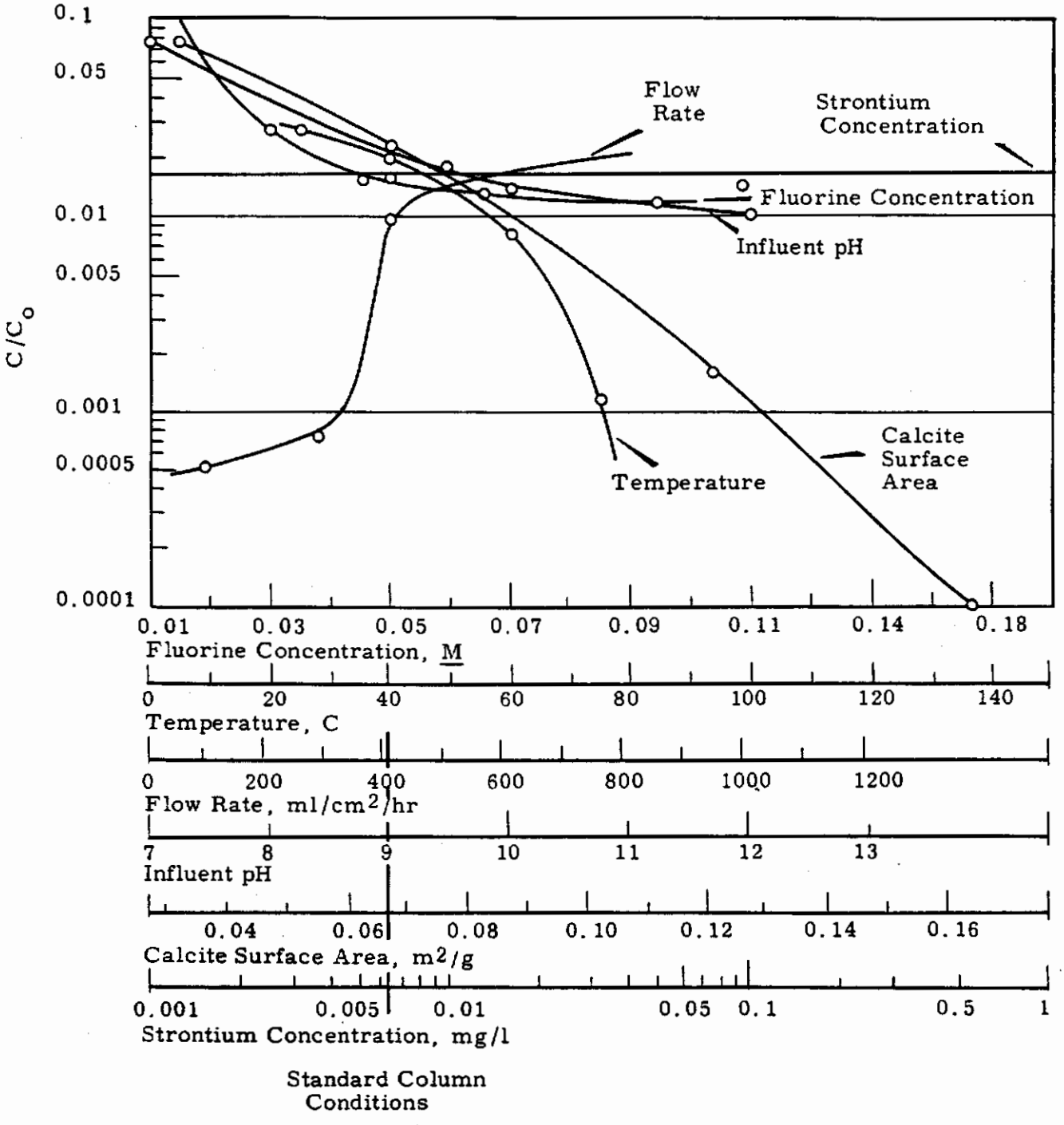

FIGURE 5

Strontium Ion Removal During Calcite Replacement
by Alkaline, Fluoride-Bearing Solutions.
Fifty Gram Columns were Used to Obtain These Data.
All Solutions Contained 1M NaCl in Addition to Their Other Constituents.

Cation Metasomatic Replacement Reactions - L. L. Ames, Jr.

The principles governing cation replacement reactions were investigated, utilizing reactions between calcium-, strontium-, and barium-containing solutions and the minerals calcite-strontianite-witherite and gypsum-celestite-barite. Both the replacement order and rates of replacement are directly related to the difference in solubility between the original mineral and final replacing mineral.

Four cation replacement reactions were studied. The general chemical equations for these reactions can be represented as follows:

1) $CaCO_3 + BaCl_2 \rightleftharpoons BaCO_3 + CaCl_2$

2) $CaCO_3 + SrCl_2 \rightleftharpoons SrCO_3 + CaCl_2$

3) $CaSO_4 + BaCl_2 \rightleftharpoons BaSO_4 + CaCl_2$

4) $CaSO_4 \cdot 2H_2O + SrCl_2 \rightleftharpoons SrSO_4 + CaCl_2 - 2H_2O$

Table V presents column results in which the above reactions occur. Only the least soluble final product is stable in a system containing the constituents for two possible final products with a common anion, both less soluble than the original column mineral. As an example, when an influent containing equal concentrations of Ba^{+2} and Sr^{+2} is passed through $CaSO_4$, only $BaSO_4$ is finally stable in the system.

Figure 6 is a graph of the cation fraction retained on the solid, or original mineral vs. temperature. The original column material is noted in each case along with the reacting cation and radiotracer present in the influent solution. Sample points were comparable between reactions, so that relative reaction rates are indicated as well as order of replacement.

TABLE V

KINETIC PHASE RELATIONS IN SOME CATION-SULFATE AND CATION-CARBONATE SYSTEMS

Influent Solution	Original Column Material	Final Product
0.03M $SrCl_2$	$CaSO_4$	$SrSO_4$
0.03M $SrCl_2$	$CaCO_3$	$SrCO_3$
0.03M $BaCl_2$	$CaSO_4$	$BaSO_4$
0.03M $BaCl_2$	$CaCO_3$	$BaCO_3$
0.03M $MgCl_2$	$CaSO_4$	$CaSO_4$
0.03M $MgCl_2$	$CaCO_3$	$CaCO_3$
0.03M $BaCl_2$	$CaSO_4 + CaCO_3$	$BaSO_4 + BaCO_3$
0.03M $BaCl_2$	$CaSO_4 + SrSO_4$	$BaSO_4$
0.03M $BaCl_2$ 0.03M $SrCl_2$ 0.03M $CaCl_2$	$CaSO_4$	$BaSO_4$
0.03M $BaCl_2$ 0.03M $SrCl_2$ 0.03M $CaCl_2$ 0.03M $MgCl_2$	$CaCO_3$	$SrCO_3$
0.03M $BaCl_2$ 0.03M $SrCl_2$ 0.03M $CaCl_2$ 0.03M $MgCl_2$	$CaSO_4$	$BaSO_4$

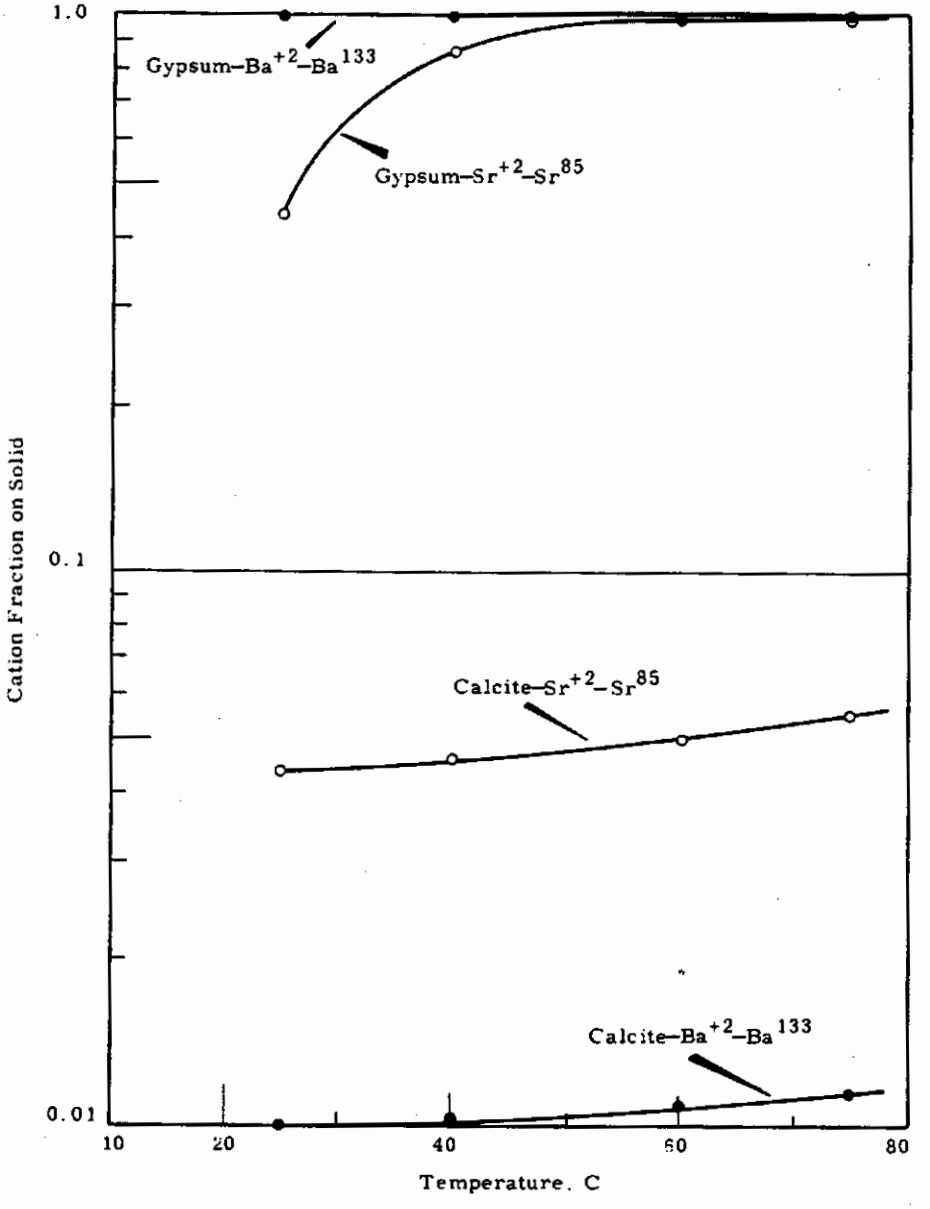

FIGURE 6

A Comparison of the Order of Replacement of Several Cation Reactions

Influent solution	-	1M NaCl, 0.05M other active macroconstituents and tracers as indicated
Influent pH	-	5.0
Common flow rate	-	410 ml/cm^2/hr
Temperature	-	as indicated
Column	-	50 g of calcite ($CaCO_3$) or gypsum ($CaSO_4 \cdot 2H_2O$ as indicated; 0.25 to 1.0 mm diameter

Table VI shows the activity products of possible compounds in the systems studied. The final product of Table V could have been predicted from these data.

TABLE VI

SULFATE AND CARBONATE SOLUBILITY DATA AT 25 C

Compound	Activity Product[10]
$CaSO_4$	3.6×10^{-5}
$SrSO_4$	7.6×10^{-7}
$BaSO_4$	1.5×10^{-9}
$CaCO_3$	4.7×10^{-9}
$SrCO_3$	6.9×10^{-10}
$BaCO_3$	1.6×10^{-9}
$MgCO_3$	7.9×10^{-5}

Volume Relationships During Replacement Reactions - L. L. Ames, Jr.

Replacement reactions and their initial rates are determined by the activities of the system constituents in relation to activity product ratios. Large positive or negative volume changes between initial and final products do not cause or prevent replacement reactions, but may profoundly affect reaction rates.

To ascertain the effect of volume relationships between the initial mineral and the reaction products on replacement reactions and rates, the following reactions were studied:

1) $\underline{CaSO_4} + BaCl_2 \rightleftharpoons \underline{BaSO_4} + CaCl_2$

2) $\underline{CaCO_3} + ZnCl_2 \rightleftharpoons \underline{ZnCO_3} + CaCl_2$

3) $\underline{CaCO_3} + Na_2C_2O_4 \rightleftharpoons \underline{CaC_2O_4} + Na_2CO_3$

4) $\underline{CaCO_3} + SrCl_2 \rightleftharpoons \underline{SrCO_3} + CaCl_2$

5) $\underline{CaCO_3} + BaCl_2 \rightleftharpoons \underline{BaCO_3} + CaCl_2$

Solid minerals retained in a column are underlined.

Figure 7 is a graphic comparison of the initial rates and order of these replacement reactions. Samples were taken for analysis at the same time interval for each reaction, yielding comparative reaction rates.

Table VII presents a comparison of ion fraction reacted, activity product ratios, and volume changes between initial material and final reaction products. The correlation coefficient between volume change and initial fraction of cation reacted is -0.51, while the correlation coefficient between log of activity product ratios and fraction of cation reacted is +0.99. Volume relationships are a result of a given replacement reaction and are apparently without causal efficacy. Volume changes can, however, speed or retard an ongoing replacement reaction by changing the controlling mechanism from free-flowing ion transfer to diffusion transfer, and vice versa. As the replacement reactions (Table VII) proceed, the correlation coefficient between fraction of ion reacted and loss or gain in volume during alteration begins to approach -1 due to the effect of molar volume changes on reaction kinetics.

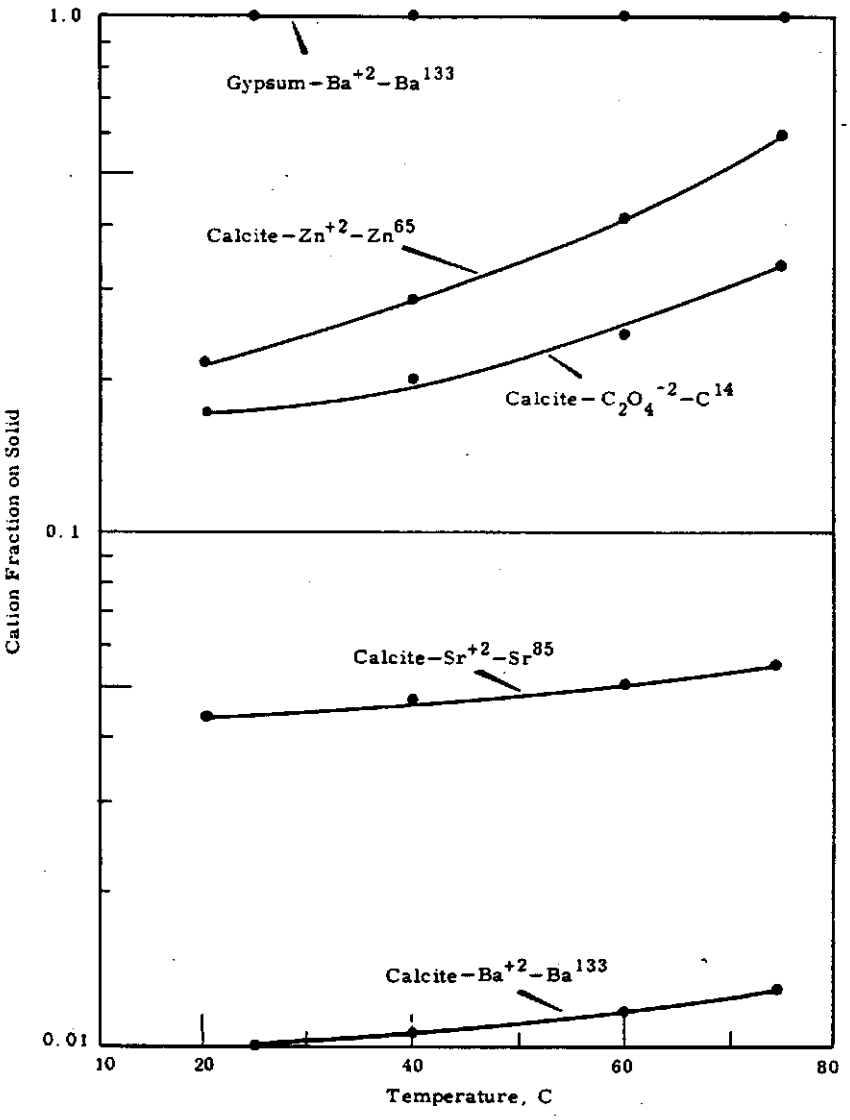

FIGURE 7

A Comparison of the Initial Rates
and Order of Replacement of Several Replacement Reactions

Influent Solution	-	1M NaCl, 0.5M other active macroconstituents plus radiotracers as indicated; the first 100 ml through the column were collected for analysis
Influent pH	-	5.0
Common Flow Rate	-	410 ml/hr/cm^2
Temperature	-	as indicated
Initial Column	-	50 g, 1.0 to 0.25 mm calcite ($CaCO_3$) or gypsum ($CaSO_4 \cdot 2H_2O$) as indicated, 2.84 cm^2 cross sectional area of column.

TABLE VII

CATION REPLACEMENT REACTIONS - ION FRACTION REACTED AND ACTIVITY RATIOS

Reaction	Percent loss or gain in Molar volume	Log [Activity product of original mineral / Activity product of final mineral]	Initial ion fraction reacted at 25 C (from Figure 7)
Gypsum→Barite	-30.2	+4.38	0.999
Calcite→ Smithsonite	-23.6	+1.36	0.223
Calcite→ Whewellite	+80.0	+1.08	0.182
Calcite→ Strontianite	+ 7.9	+0.83	0.044
Calcite→ Witherite	+20.8	+0.47	0.012

Strontium and Cesium Loading Characteristics of a Gel, a Synthetic Zeolite, and Clinoptilolite - L. L. Ames, Jr.

The cation exchange properties of a gel, clinoptilolite, and pelletized Type-A synthetic zeolite were compared in laboratory column studies. The gel, a six-to-one, silica-to-alumina, noncrystalline material, was a superior cation exchanger for cesium and strontium in the absence of macroconcentrations of competing cations. Type A was the most strontium-selective, and clinoptilolite was the best exchange material for cesium removal.

Figure 8 shows the effect of column residence on the strontium breakthrough curves of the gel, clinoptilolite and Type-A synthetic zeolite. Within the residence time range studied, only the slopes of the breakthrough curves were changed. The capacity, as computed at the 50 percent breakthrough volume, was unchanged.

Figure 9 illustrates the superior strontium selectivity of Type A under the listed conditions. The addition of competing calcium rather than sodium leads to the results shown in Figure 10. The strontium capacities of the gel and Type A are nearly the same.

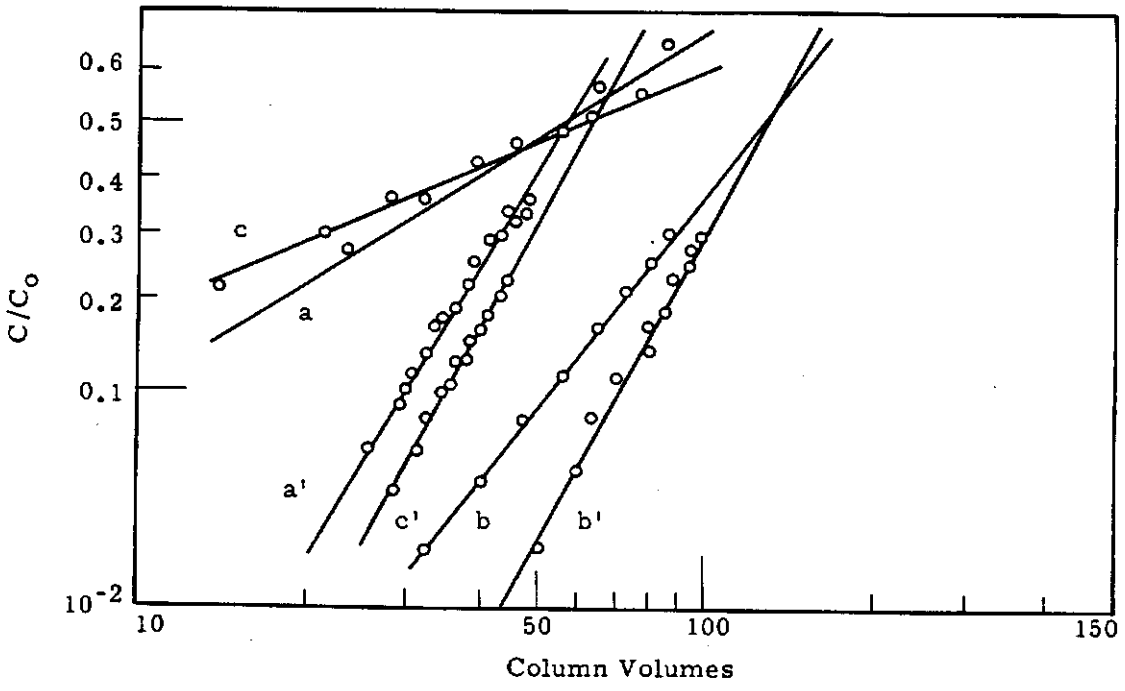

FIGURE 8

The Effect of Column Residence Time on the Slope of Sr^{+2} Breakthrough Curves of Clinoptilolite and Gel

Influent solution - 0.008N Sr^{+2}, 120,000 Sr^{85} d/m/ml, 0.1N mg $(C_2H_3O_2)_2$
Influent pH - 7.0
Temperature - 25 C
Column - 1.0 to 0.25 mm, Na-based gel and clinoptilolite; 1/16-in., Na-based, pelletized Type A
Flow rate - 285 ml/hr and 57 ml/hr
Column residence times - as indicated

Curve Designation	Adsorbent	Residence Time, min	Strontium Capacity, meq/100 g	Surface Area m^2/g
a	Clinoptilolite	1.01	58.4	15-20
a'	Clinoptilolite	5.05	58.4	15-20
b	Gel	1.05	128.0	120-150
b'	Gel	5.25	128.0	120-150
c	Type A	1.18	72.7	10-15
c'	Type A	5.90	72.7	10-15

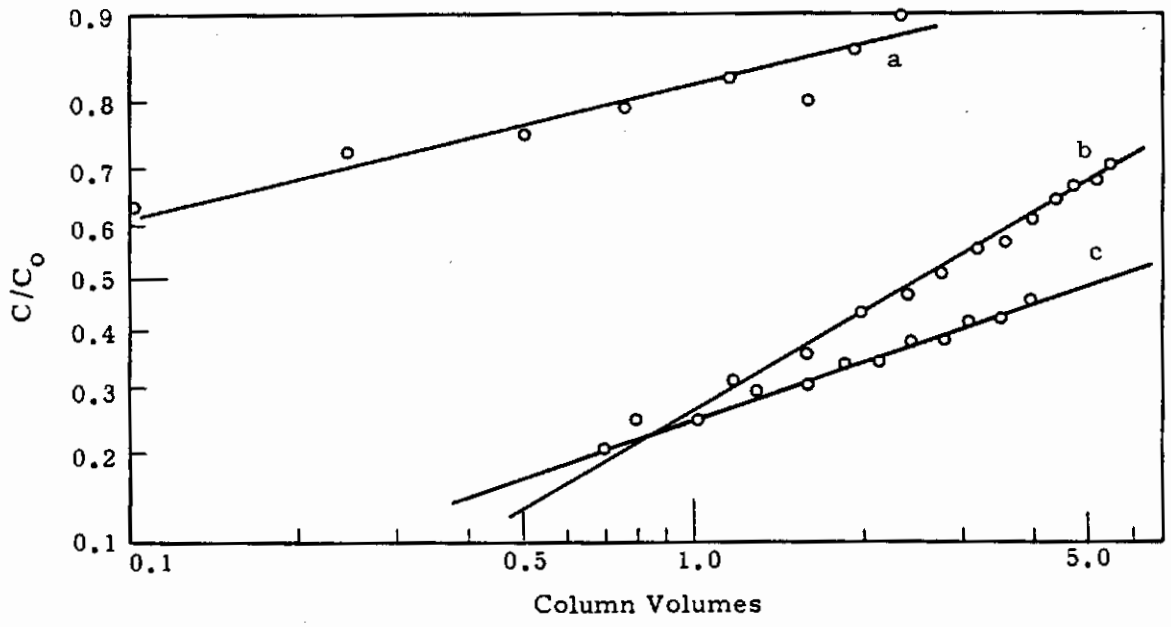

FIGURE 9

The effect of Competing Na^+ on the Sr^{+2} Capacity of Clinoptilolite and Gel. The Breakthrough Curves of Figures 9, 10, and 11 are Directly Comparable to Their Shorter Residence-Time Counterparts in Figure 8.

Influent solution	-	1.0N Na^+, 0.008N Sr^{+2}, 120,000 Sr^{85} d/m/ml, 0.1N mg$(C_2H_3O_2)_2$
Influent pH	-	7.0
Temperature	-	25 C
Column	-	1.0 to 0.25 mm, Na-based gel and clinoptilolite; 1/16-in., Na-based, pelletized Type A
Flow rate	-	285 ml/hr
Column residence time	-	same as lesser values given in Figure 8.

Curve Designation	Adsorbent	Sr^{+2} Capacity, meq/100 g
a	Clinoptilolite	0.03
b	Gel	1.71
c	Type A	12.50

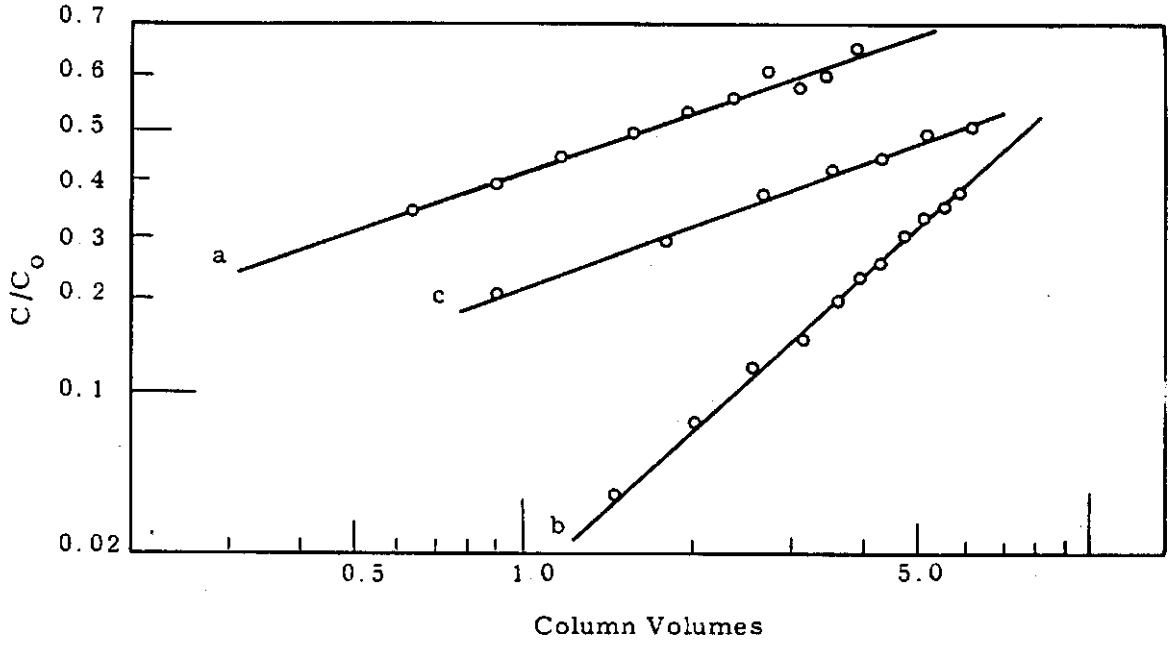

FIGURE 10

The Effect of Competing Ca^{+2} on the Sr^{+2} Capacity of Clinoptilolite and Gel

Influent solution	-	0.4N Ca^{+2}, 0.008N Sr^{+2}, 120,000 Sr^{85} d/m/ml, 0.1$\overline{N}$ mg$(C_2H_3O_2)_2$
Influent pH	-	7.0
Temperature	-	25 C
Column	-	1.0 to 0.25 mm, Na-based gel and cliniptilolite; 1/16-in., Na-based, pelletized Type A
Flow rate	-	285 ml/hr
Column residence time	-	same as lesser values given in Figure 8

Curve Designation	Adsorbent	Sr^{+2} Capacity, meq/100 g
a	Clinoptilolite	1.7
b	Gel	8.0
c	Type A	7.2

The effect of hydrogen ion concentration on the strontium capacities of the gel and clinoptilolite is shown in Figure 11. Type A was not a stable phase in the same environment. The cesium capacities of Type A, gel and clinoptilolite are shown in Figure 12. The cesium capacity of Type A is relatively small even without competing cations. Figure 13 presents cesium capacity data derived from several gel and clinoptilolite cesium breakthrough curves. While the cesium capacity of clinoptilolite is considerably less than that of the gel in the absence of competing sodium, the gel cesium capacity rapidly decreases with increasing sodium concentration, while that of clinoptilolite is much less affected.

For each specific chemical environment, a different exchanger was most selective for a given radioisotope.

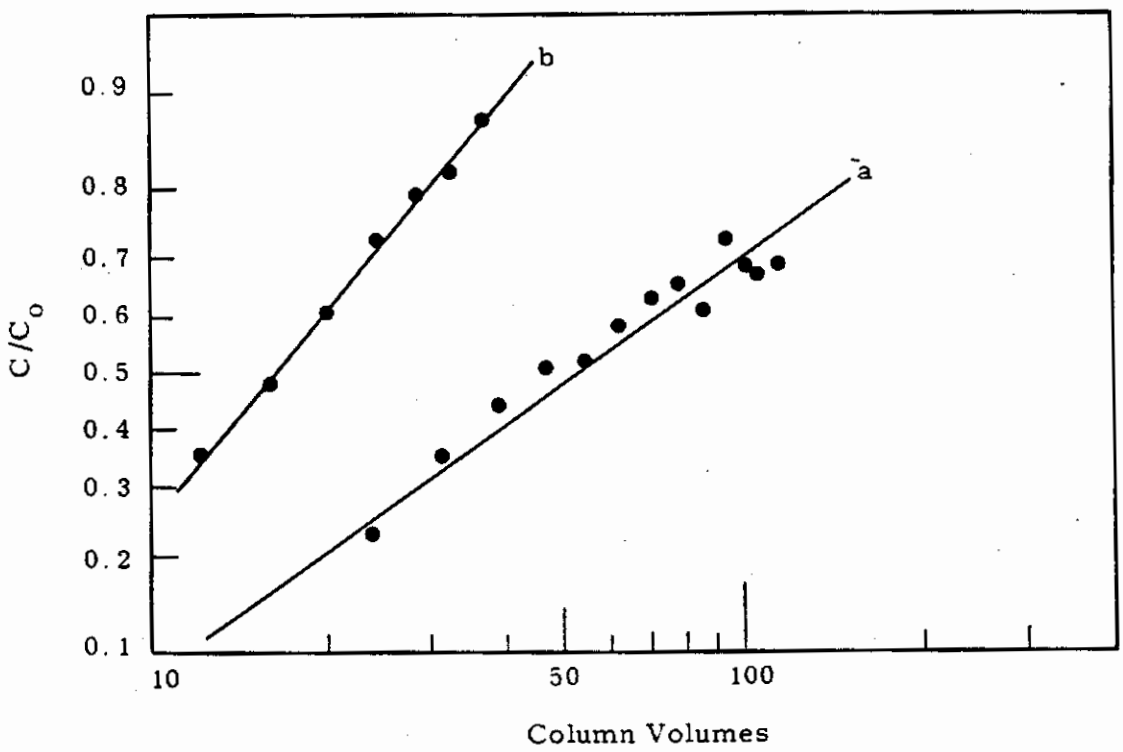

FIGURE 11

The Effect of Competing H^+ on the Sr^{+2} Capacity of Gel and Clinoptilolite

Influent solution	-	0.008N Sr^{+2}, 120,000 Sr^{85} d/m/ml, 0.1N CH_3COOH^-
Influent pH	-	3.0
Temperature	-	25 C
Column	-	0.25 to 1.0 mm, Na-based gel and cliniptilolite
Flow rate	-	57 ml/hr
Column residence time	-	same as lesser values given in Figure 8

Designation	Adsorbent	Strontium Capacity, meq/100 g
a	Clinoptilolite	55.3
b	Gel	16.0

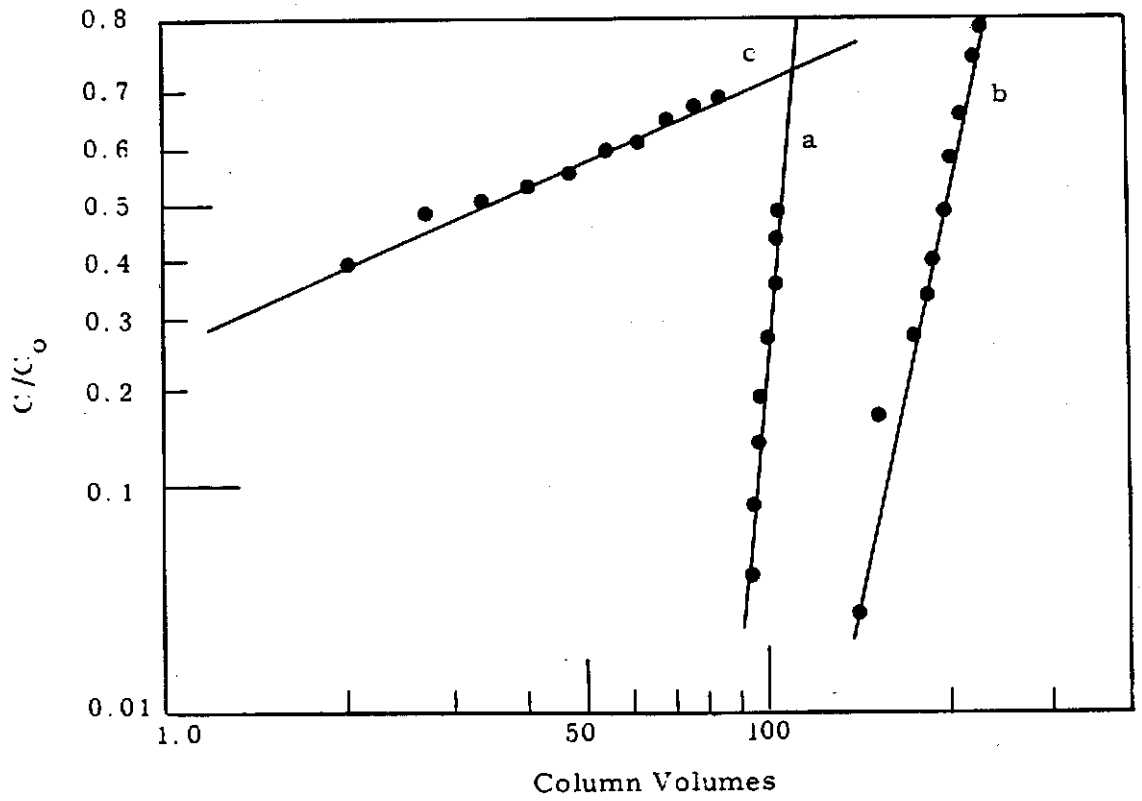

FIGURE 12

Comparative Cesium Capacities of Type A, Clinoptilolite and Gel in the Absence of Competing Cations

Influent solution - 0.01N CsCl, 100,000 Cs^{137} d/m/ml
Influent pH - 6.6
Temperature - 25 C
Column - 1.0 to 0.25 mm, Na-based gel and clinoptilolite; 1/16-in., Na-based pelletized Type A.
Column flow rate - 835 ml/hr

Curve Designation	Absorbent	Column Residence Time, min	Cesium Capacity, meq/100 g
a	Clinoptilolite	0.37	135.2
b	Gel	0.36	250.0
c	Type A	0.39	49.7

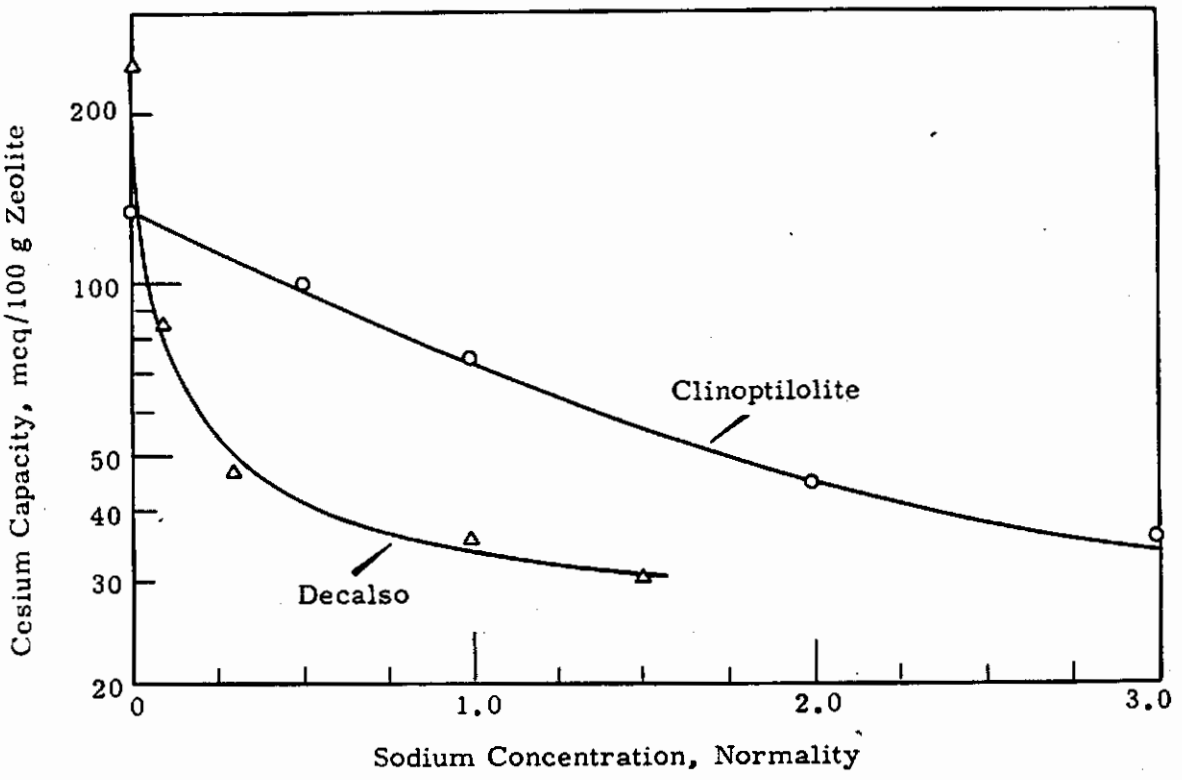

FIGURE 13

The Effect of Competing Na^+ on the Cs^+ Capacity of Clinoptilolite and Gel. Decalso is the Trade Name of the Six-to-One, Silica-to-Alumina Gel Used in this Study.

Influent	-	0.01N Cs^+, 100,000 Cs^{137} d/m/ml, Na^+ as indicated
Influent pH	-	6.0
Temperature	-	25 C
Column	-	0.25 to 1.0 mm, Na-based zeolite
Column flow rate	-	835 ml/hr
Column residence time	-	gel, 0.36 min and clinoptilolite 0.37 min

The Use of Clinoptilolite to Remove Potassium Selectively from Aqueous Solutions of Mixed Salts - L. L. Ames, Jr. and B. W. Mercer

Clinoptilolite was utilized to remove potassium from a solution containing relatively high concentrations of sodium, magnesium and calcium. Column capacities for potassium of the order of 60 meq/100 g of clinoptilolite were obtained. Elution of the K^+ was accomplished with a saturated solution of NH_4Cl in about 8 column volumes.

The possible application of clinoptilolite to recover potassium from mixed salt solutions was indicated during studies aimed at removing cesium from aqueous wastes. Table VIII shows the chemical composition of the salt solution used for the potassium removal study.

TABLE VIII

CHEMICAL COMPOSITION OF THE SALT SOLUTION

Salt	Salt Molarity	Solution pH
NaCl	0.495	
$MgCl_2$	5.32×10^{-2}	
$CaCl_2$	9.97×10^{-3}	6.4
KCl	9.72×10^{-3}	
$SrCl_2$	1.50×10^{-4}	

A potassium loading curve is shown in Figure 14. The constant potassium leakage probably indicated a too rapid flow rate.

Table IX shows the potassium and sodium content of a saturated NH_4Cl eluting solution. The loaded zeolite contains 1.35 parts of potassium to one part by weight sodium after starting with an influent solution containing 37 parts by weight of sodium to one part potassium.

The potassium specificity of clinoptilolite gives it a potential for extraction and recovery of potash from mixed salt solutions.

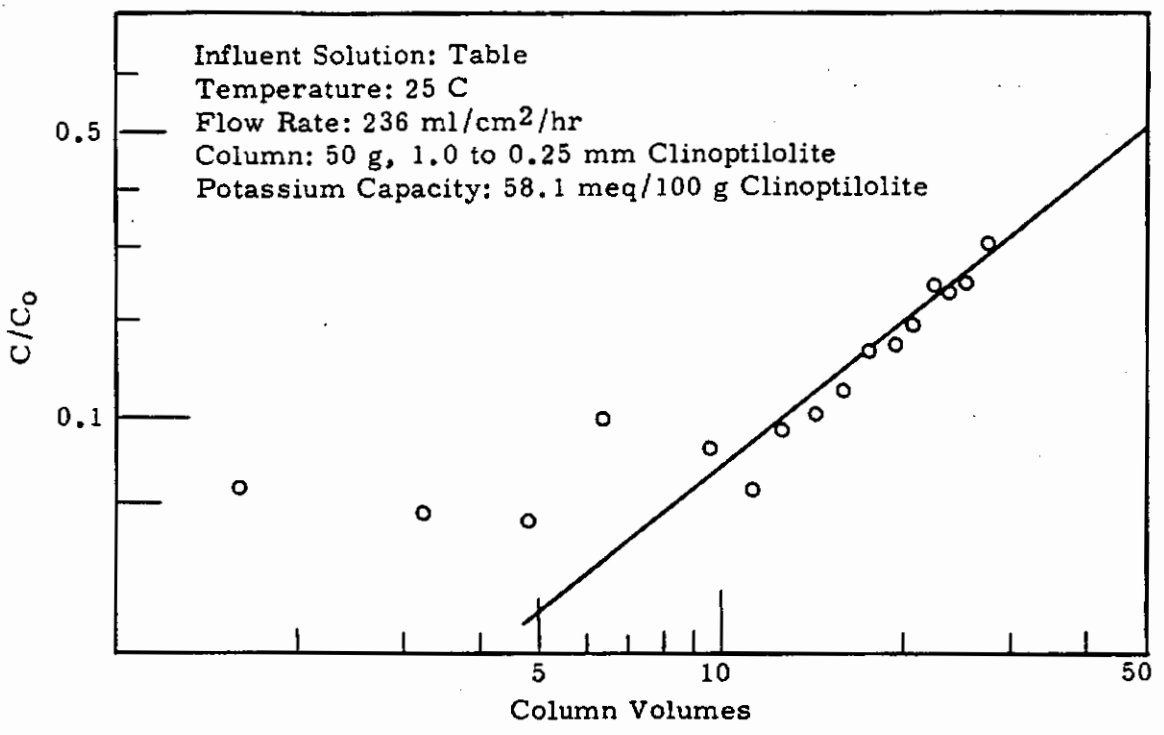

FIGURE 14

Potassium Breakthrough Curve for Clinoptilolite

TABLE IX

SODIUM AND POTASSIUM CONTAINED IN THE ELUTING NH_4Cl SOLUTION FROM COLUMN OF FIGURE 13

Column Volumes	K^+, mg/l	Na^+, mg/l
0.0- 1.6	8660	8510
1.6- 3.2	1950	560
3.2- 4.9	940	100
4.8- 6.4	720	7
6.4- 8.0	103	4
8.0- 9.6	23	2
9.6-11.2	7	2
11.2-12.8	4	2
12.8-14.4	2	2

Effluent solution pH = 6.3

Removal and Recovery of Plutonium from Slightly Acidic Waste with Phosphate Rock - A. E. Reisenauer and L. L. Ames, Jr.

An exchange column of Florida pebble phosphate, a commercially available natural apatite, was found to absorb plutonium from slightly acidic wastes. Approximately 90 percent of the total plutonium content from 400 bed volumes waste was adsorbed on a phosphate mineral bed through which the waste was passed at a flow rate which provided a residence time of 3.25 minutes. Prompt elution of the mineral with 1M Na_2CO_3 recovered more than 90 percent of the adsorbed plutonium in 2.8 column volumes. Elutions performed after a time lapse of three days removed only about 10 percent of the plutonium, probably because of diffusion along radial crystal boundaries. Recharging the pebble phosphate bed with dibasic sodium phosphate was necessary before reloading with plutonium.

Florida pebble phosphate rock is a commercially available variety of the mineral apatite, normally $Ca_{10}(PO_4)_6(OH; F)_2$ in composition. Because the composition and crystal structure of the apatite are very similar to those of bone mineral, the selective adsorption of one of the "bone seekers," plutonium, could be expected.[9]

Preliminary studies indicate selective adsorption of plutonium on Florida pebble phosphate followed by elution with sodium carbonate may be used for removal and recovery of plutonium from dilute solutions.[11] Sump waste from a Hanford plant was used in these experiments. Adsorption of plutonium from slightly acidic solutions was studied within a plutonium concentration range of 0.4 to 4.7 mg/liter. Typical breakthrough data are plotted on logarithmic probability coordinates in Figure 15.

Because of the selective nature of the apatite for plutonium, elution from the apatite by competing cations is not readily accomplished. An alternative to direct elution with competing cations is the alteration of apatite to the corresponding non-Pu-selective carbonate.[9] The apatite is altered to calcite in the presence of a strong carbonate solution according to the reaction:

$$Ca_{10}(PO_4)_6 + 10\ Na_2CO_3 \rightleftharpoons 6\ Na_3PO_4 + 10\ CaCO_3 + 2\ NaOH.$$

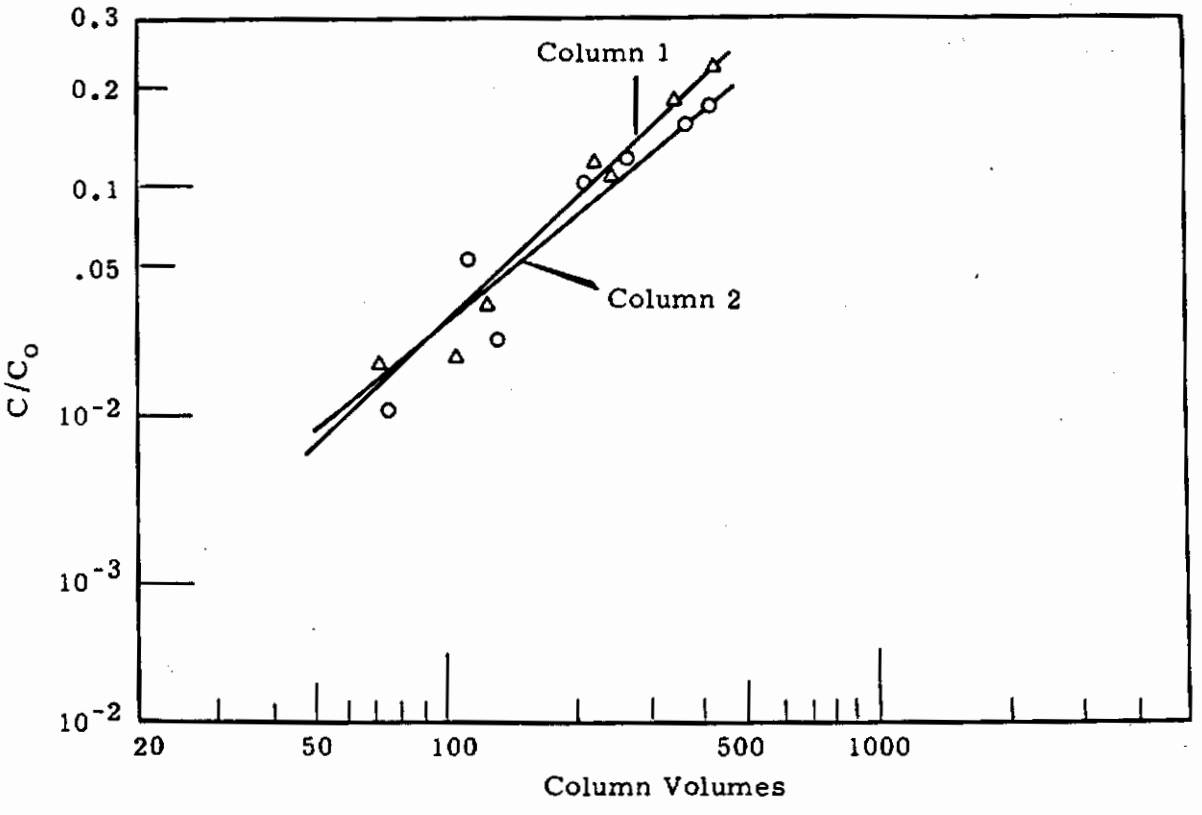

FIGURE 15

Initial Plutonium Breakthrough Curves
for Florida Pebble Phosphate Columns

Column volume	-	11 ml
Column length	-	14 cm
Flow rate	-	4.2 ml/min/cm^2
Residence time	-	1.4 min
Influent	-	0.74 mg/l plutonium (Hanford sump waste)
pH	-	2.1

This replacement reaction proceeds from the exterior of the apatite grain and, in doing so, destroys the plutonium adsorption sites. Thus, by replacing a superficial layer of pebble phosphate with calcite, which has little adsorption capacity for plutonium, the surface adsorbed plutonium is removed. Prompt elution recovered at least 90 percent of the plutonium within 2.8 column volumes. During the preparation of the pebble phosphate surface for further plutonium recovery, the calcite layer on the surface of the mineral was converted back to apatite by reversing the replacement

reaction through the addition of an excess of phosphate ion. Regeneration of the mineral surface actually increases the effective adsorption capabilities for plutonium as is shown in Figure 16.

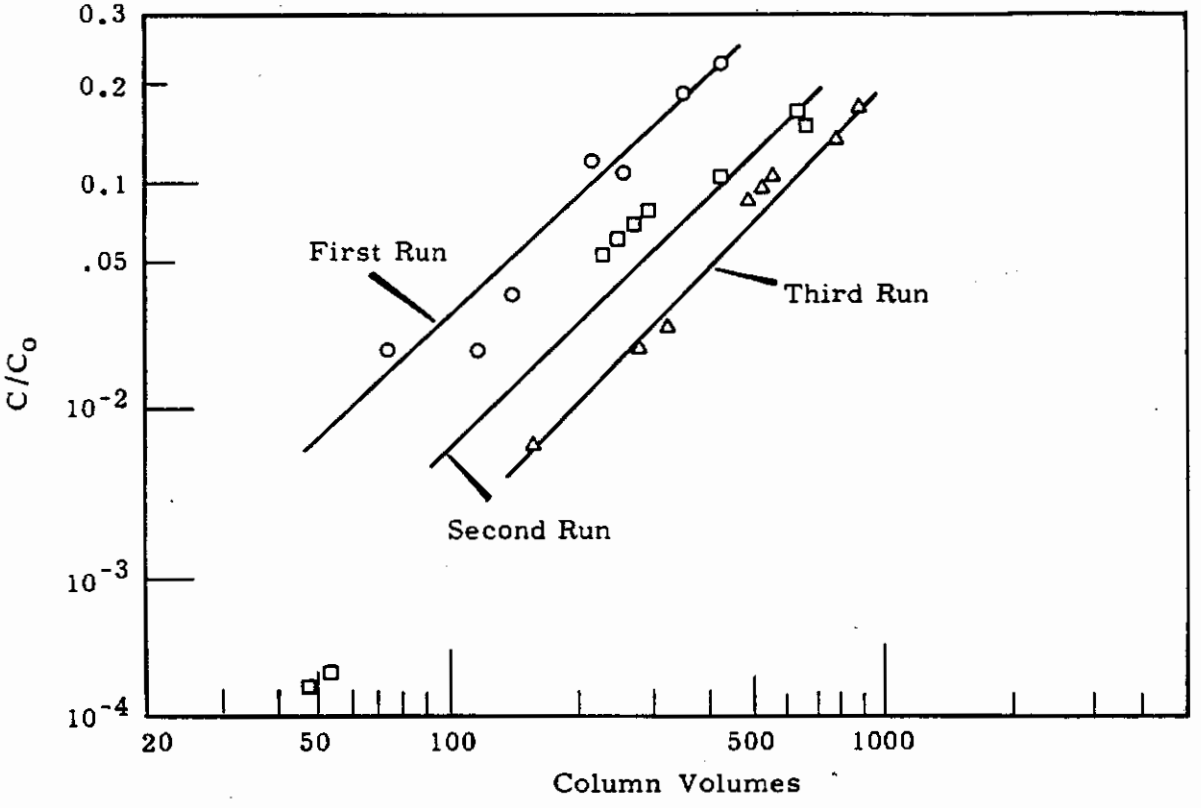

FIGURE 16

Flutonium Breakthrough Curves for Recycled Pebble Phosphate Column

Column volume	-	11 ml
Column length	-	14 cm
Flow rate	-	2.33 ml/min/cm^2 for second and third cycles, first cycle same as Figure 15
Residence time	-	2.7 min
Influent	-	0.74 mg/l plutonium (Hanford sump waste)
pH	-	2.1

When the plutonium-containing apatite bed was permitted to stand for two days, elution with sodium carbonate solution recovered as little as 10 percent of the plutonium. This phenomenon is ascribed to diffusion of plutonium along radial crystal boundaries into the interior of the grains. It is

evident that with the diffusion of the plutonium into the mineral grains permitting only partial elution, an increasing amount of plutonium may accumulate in the pebble phosphate as the mineral bed is used. Dissolution of the bed would be desirable ultimately to recover this plutonium. This is readily accomplished with nitric acid.

Mineral Adsorption of Radionuclides from Simulated Reactor Coolant - Batch Studies - D. W. Bensen

The relative adsorption of P^{32}, As^{76}, Np^{239}, Zn^{65}, and Cr^{51} from tap water was determined by contacting radionuclide solutions with finely ground samples of 25 selected minerals. Phosphorus-32 was adsorbed best by olivine, pyrite, pyrrhotite, fluorite, calcite, galena, dolomite, hornblende, scapolite, goethite, microcline, apatite and epidote. Moreover, olivine and pyrrhotite exhibited good adsorption of arsenic, zinc and chromium. Neptunium adsorption was not significant with any of the minerals.

Low concentrations of certain radioisotopes are released to the Columbia River in the spent cooling water from the Hanford reactors. The radioisotopes are formed by neutron activation of parent isotopes in the water and by neutron-activated corrosion products from reactor hardware.[12, 13] This research was designed to investigate the potentialities of beds of natural minerals for decontaminating reactor effluents. Preliminary batch experiments, employing 25 minerals and 5 radionuclides were performed.

The uptake of radionuclides by selected minerals was determined at 80 C. One gram of mineral with a particle size range of between 0.05 and 0.25 mm was conditioned with 50 ml of tap water at the equilibration temperature and then spiked with the radionuclide being studied. The distribution of the isotope after one hour of continuous shaking was determined.

A summary of the experimental results is presented in Table X. Because of the relative importance of P^{32} in the biosphere, the minerals are listed in decreasing order of their selectivity for that nuclide. Olivine, pyrite, pyrrhotite, fluorite, calcite, galena, dolomite, hornblende, scapolite, goethite, microcline, apatite and epidote were found to offer the

greatest promise for P^{32} adsorption from reactor effluent. Arsenic-76 was also adsorbed well by olivine, pyrite, pyrrhotite, galena and goethite. Arsenic-76 adsorption was less complete, in all cases, than that of P^{32}. Nearly all tested minerals exhibited good adsorption of Zn^{65} and Cr^{51}. Neptunium was adsorbed poorly or not at all by the minerals tested.

The specific mechanisms responsible for radionuclide uptake by minerals are not completely known. The most probable sorption reactions include ion exchange on the unaltered mineral surface and inclusion and adsorption by secondary minerals and precipitation products generated by metathesis of solubilized mineral constituents.

The results of these batch experiments formed a basis for selecting minerals for testing in packed columns. Although batch testing offers a means of screening a large number of candidate minerals in a relatively short time, the results can sometimes be misleading. Moreover, one-hour contact such as that employed in the batch tests was sufficient to provide only a partial measure of the sorption potential of the minerals. Zinc-65, for example, was found to adsorb poorly on pyrite in batch systems, yet a column of pyrite 1 cm in diameter and 34.5 cm long adsorbed virtually all of the zinc from 41 liters (1530 column volumes) of tap water. Thus, minerals such as pyrite, which alter or oxidize slowly and which possess an insignificant inherent capacity to adsorb, can be erroneously rejected solely on the basis of batch testing.

TABLE X

THE ADSORPTION OF RADIOISOTOPES BY SELECTED MINERALS

Experimental Conditions

System - batch
Conditioning - 90 min
Contact - 60 min
Temperature - 80 C

Solution - Tap water
Mineral/Solution Ratio - 1:50

Number	Mineral	Composition	Isotope Adsorption*				
			P^{32}	As^{76}	Np^{237}	Zn^{65}	Cr^{51}
1	Olivine	$(Mg, Fe)_2SiO_4$	VG-E	G	P	E	VG
2	Pyrite	FeS_2	VG	G	N	VP	G-VG
3	Pyrrhotite	$Fe_{1-x}S$	VG	VG	VP-P	G-VG	G
4	Fluorite	CaF_2	VG	F	N	G	F
5	Calcite	$CaCO_3$	VG	F	N	VG	G
6	Galena	PbS	G	G	N	F	E
7	*Dolomite*	$Ca, Mg(CO_3)_2$	G	P	VP	VG	VG
8	Hornblende	$Ca_2Na(Mg, Fe^{+2})_4, (Al\ Fe^{+3}, Ti)_3Si_6O_{22}(O, OH)_2$	G	P	N	VG	VG
9	Scapolite	$(Ca, Na)_4Al_3(Al, Si)_3Si_6O_{24}(Cl, CO_3, SO_4)$	G	F	N	E	VG
10	Goethite	FeO(OH)	G	G	N	G	VG
11	Microcline	$KAlSi_3O_8$	G	F	N	VG	VG
12	Apatite	$Ca_5(F, Cl, OH)(PO_4)_3$	G	P	N	VG	G
13	Epidote	$Ca_2(Al_3Fe_3)(SiO_4)_3OH$	G	P	N	VG	G
14	Anorthite	$CaAl_2Si_2O_8$	F	F	N	VG	VG
15	Labradorite	$(Ca, Na)Al_2SiO_8$	F	F	N	VG	VG
16	Gypsum	$CaSO_4 \cdot 2H_2O$	F	F	VP	F	G-VG
17	Albite	$NaAl_2Si_3O_8$	F	F	N	VG	VG
18	Sodalite	$Na_4Al_3Si_3O_{12}Cl$	F	P	N	E	E
19	Smaltite	$(Co, Ni, Fe)As_3$	F	P	P	VG	VG
20	Vermiculite	$(MgO)_2(Fe_2O_3)_{0.5}(Al_2O_3)(SiO_2)_3 \cdot 2H_2O$	P	P	N	E	F
21	Sphalerite	ZnS	P	P	N	G	VG
22	Green Sand	$K_2(Mg, Fe)_2Al_6(Si_4O_{10})_3(OH)_{12}$	P	P	P	VG	F
23	Biotite	$K(Mg, Fe)AlSi_3O_{10}(OH)_2$	P	P	N	E	VG
24	Erionite	$Na_2O \cdot Al_2O_3(SiO_2)_4 \cdot 6H_2O$	VP	P	P	VG	P
25	Clinoptilolite	$Na_2O\ Al_2O_3(SiO_2)_{8-9} \cdot 6H_2O$	N	N	N	G	F

*Terminology

80-100% removed - E (excellent)
60- 80% removed - VG (very good)
40- 60% removed - G (good)
20- 40% removed - F (fair)
5- 20% removed - P (poor)
0- 5% removed - VP (very poor)
0- % removed - N (none detectable)

Mineral Adsorption of Phosphorus-32 from Simulated Reactor Coolant - Column Studies - D. W. Bensen

Phosphorus-32 adsorption from 80 C tap water by 21 minerals was determined. Eleven of the minerals adsorbed 30 percent or more of the influent P^{32}. Mixed mineral columns were better adsorbents than any of the component minerals alone. The best mineral mixtures, i.e., pyrite-Idaho rock phosphate-calcite, and pyrite-Florida pebble phosphate-calcite adsorbed 65 to 70 percent of the influent P^{32}. The best adsorption by single minerals, i.e., sodalite, epidote, goethite, fluorite, pyrite and pyrrhotite, ranged from 37 to 60 percent.

Reactor coolant water is discharged to the Columbia River containing trace amounts of many radioactive impurities. A method is being sought to reduce the amount of P^{32} and other radiologically significant radionuclides in the waste. Phosphorus-32 is of prime interest because of its accumulation by river biota, especially fish and waterfowl, which are harvested and consumed by a portion of the local population.[14]

Preliminary experiments indicated that certain minerals were capable of adsorbing P^{32}.[15] The purpose of this research was to determine how effectively columns of selected, naturally occurring minerals would adsorb P^{32} from simulated reactor coolant.

Crushed minerals were washed and screened to a particle size range of 0.25 to 1.0 mm and packed in columns 1 cm in diameter and 34.5 cm long. Tap water containing added P^{32} was pumped through the columns at 80 C as shown schematically in Figure 17.

Phosphorus-32 adsorption by 21 columns of minerals is summarized in Table XI. In each of these experiments the flow rate gave a mean residence time of 2.9 minutes.

Breakthrough of P^{32} from most columns occurred soon after start-up, indicating that inherent exchange adsorption was low. However, upon reaching the fraction of breakthrough reported in Table XI, adsorption remained relatively steady and undiminished.

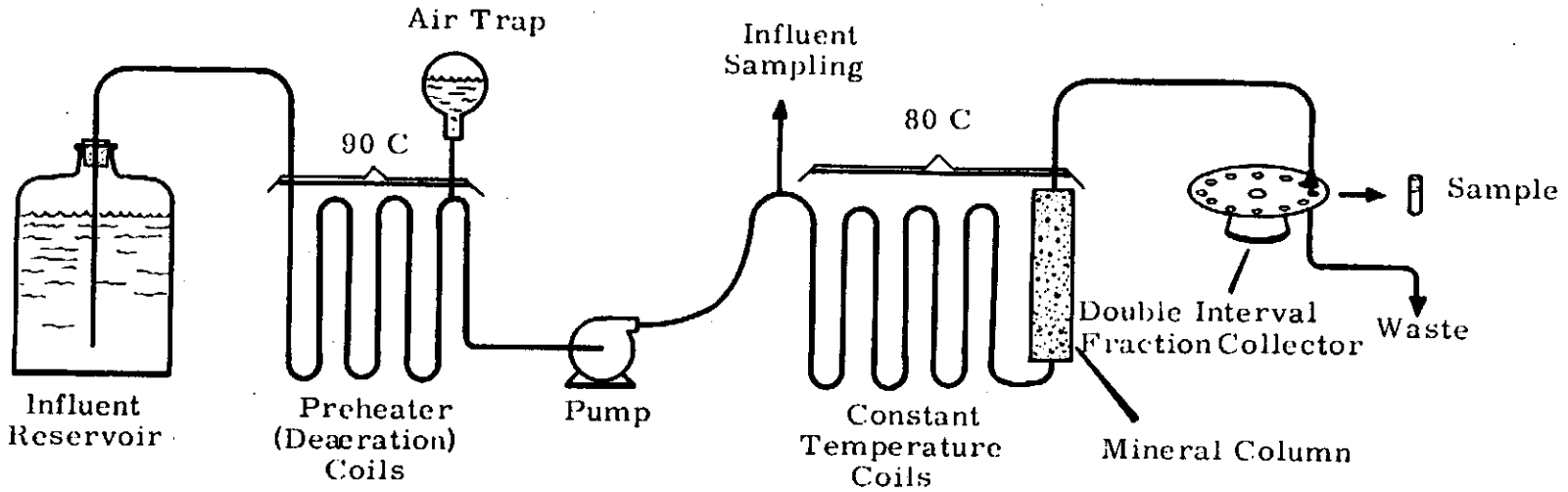

FIGURE 17

Experimental Apparatus Used to Study the Adsorption of P^{32} by Columns of Minerals

TABLE XI

MINERAL ADSORPTION OF PHOSPHORUS-32

Mineral	Formula	Adsorption, avg. %	Total Throughput, column volumes
Sodalite	$Na_4Al_3Si_3O_{12}Cl$	60	3000
Epidote	$Ca_2(Al_3Fe_3)(SiO_4)_3OH$	47	1300
Goethite	$FeO(OH)$	40	1300
Fluorite	CaF_2	40	1900
Pyrite	FeS_2	37	1300
Pyrrhotite	$Fe_{1-x}S$	37	1600
Albite	$NaAl_2Si_3O_8$	34	3100
Smaltite	$(Co, Ni, Fe)As_3$	34	3900
Microcline	$KAlSi_3O_8$	33	1000
Galena	PbS	30	1900
Apatite	$Ca_5(F, Cl, OH)(PO_4)_3$	30	950
Olivine	$(Mg, Fe)_2SiO_4$	18	2200
Scapolite	$(Ca, Na)_4Al_3(Al, Si)_3Si_6O_{24}(Cl, CO_3, SO_4)$	17	1100
Labradorite	$(Ca, Na)Al_2SiO_8$	14	1100
Dolomite	$Ca, Mg(CO_3)_2$	10	900
Calcite	$CaCO_3$	10	1200
Hornblende	$(Ca_2Na(Mg, Fe^{+2})_4, (Al, Fe^{+3}, Ti)_3 Si_6O_{22}(O, OH)_2$	--	500
Anorthite	$Ca\ Al_2SiO_8$	--	1200
Vermiculite	$(MgO)_2(Fe_2O_3)_{0.5}(Al_2O_3)(SiO_2)_3 \cdot 2H_2O$	--	12
Sphalerite	ZnS	--	43
Gypsum	$CaSO_4 \cdot 2H_2O$	(unstable)	3200

The mechanisms whereby minerals adsorb radioisotopes from solution are not well defined but are believed to include replacement of an ion in the mineral lattice with a different ion species from solution,[16] and adsorption or inclusion by alteration products, principally hydrous oxides formed during column operation.[17, 18]

Several mixed mineral beds were tested to determine if pyrite oxidation liberated sufficient acid[19] to stimulate recombination of an adjacent mineral or to dissolve from it the reagent (Fe^{+3} or PO_4^{-3}) necessary to sustain replacement on calcite or galena. In the presence of adequate PO_4^{-3} the following typical replacement reaction occurs:[16]

$$5(CaCO_3)_S + 3Na_3PO_4 + NaOH \rightarrow (Ca_5(PO_4)_3(OH))_S + 5\ Na_2CO_3$$

The results of several mixed bed tests are summarized in Table XII.

TABLE XII

PHOSPHORUS ADSORPTION BY MIXED MINERAL BEDS

	Minerals	Throughput, column volumes	Adsorption, avg. %
1	Pyrite-Florida Pebble Phos-Calcite	600	70
2	Pyrite-Idaho Rock Phos-Calcite	600	65
3	Pyrite-Apatite-Galena	400	57
4	Pyrite-Apatite-Calcite	400	49
5	Pyrite-Siderite-Calcite	600	47
6	Apatite-Calcite	400	35

The residence time was 8.4 minutes in all of these experiments, thus preventing a direct comparison with adsorption by single beds (Table XI). However, the advantage of combining certain minerals may be illustrated by comparing adsorption by the pyrite-apatite-calcite column with the one containing only apatite and calcite. In this case pyrite increased adsorption by the apatite-calcite column from 35 to 49 percent. Phosphorus-32 adsorption by a Florida pebble phosphate-calcite column was similarly increased from 60 to greater than 70 percent by acidifying the influent to pH 3.4 with HNO_3.

Although the nature and timing of the research was such that very little attention was given to determining the mechanism of mineral adsorption, a scan of the mixed mineral columns after completion of the experiments revealed that the bulk of the adsorbed P^{32} was retained by Florida pebble phosphate and Idaho rock phosphate in preference to pyrite or calcite. Localization was not so apparent, however, in the other mixed mineral columns.

Aluminum Bed Decontamination of Reactor Effluent - H. G. Rieck

The percentages of radiologically significant isotopes removed from reactor effluent water by a pilot-scale bed of aluminum turnings are shown to decrease with increased velocity of the coolant through the bed. Qualitative effects on the decontamination efficiencies resulting from changes in chemical concentrations in the coolant are also given.

The use of aluminum beds to remove radiologically significant radioisotopes from reactor effluent water was demonstrated in laboratory experiments.[20] The design of a full-scale bed from laboratory data would require a very large scale-up factor. This scale-up factor was greatly reduced by operating a pilot-scale aluminum bed with a capacity nearly 1000 times that of a practical laboratory bed.

The bed (20 feet long, 6 feet high and 3 feet wide) was operated with reactor effluent superficial velocities of 2.7, 3.8, and 6 ft/min, based on the cross-sectional area of the packed bed. The decontamination achieved for the seven isotopes studied are listed in Table XIII:

TABLE XIII

ISOTOPE REMOVAL BY ALUMINUM BED

Superficial Velocity, ft/min	Isotope, percent removed						
	P^{32}	As^{76}	Zn^{65}	Np^{239}	Cu^{64}	Cr^{51}	Mn^{56}
2.7	55	64	70	36	81	12	89
3.8	45	58	78	11	76	15	--
6.0	37	51	62	16	70	9	71

In addition, the following observations were made:

(1) The maximum radiation intensity of the bed in roentgens per hour was 2.1.

(2) The maximum pressure drop in inches of water per foot of bed was 0.55.

(3) The maximum corrosion rate of the aluminum turnings in mils per month was 0.34.

Additional small-scale experiments were conducted to evaluate the effects of changes in coolant treatment on the decontamination efficiencies of aluminum beds. These experiments showed that:

(1) A reduction in the dichromate concentration of the coolant caused no significant change in decontamination efficiency.

(2) An increase in the alum concentration of the coolant may result in a lower decontamination efficiency.

(3) Aluminum nitrate substitution for the aluminum sulfate addition to the coolant may result in a lower decontamination efficiency.

Aluminum-filled troughs were used to evaluate the effect on the decontamination efficiency of two effluent water pretreatment steps. A reduction of pH by adding sulfuric acid resulted in a slightly improved decontamination efficiency. Reduction of dichromate with bisulfite prior to passage through the bed caused an insignificant change in the degree of decontamination.

Soil Physics

The Computational Accuracy Requirement for a Field Permeability Measurement Method - R. W. Nelson

A computational problem arises from the need to compromise between the accuracy of calculated soil permeability and the ease of performing the calculation. Finite difference methods were expected to provide such a compromise. However, imprecision in numerical differentiation prevented use of the difference method. A study of the accuracy required for measuring permeability indicated that 7.5 times as much variation is allowable in the permeability as in the potential pattern. Since potential patterns are the tools needed to treat practical problems, errors in permeability measurements as great as 37 to 75 percent may be tolerated and still provide answers within the common engineering accuracy range of 5 to 10 percent.

The primary concern of the ground water hydrologist is usually the prediction of the expected potential pattern after structures such as wells, drains or disposal structures are installed. In practice the required level of accuracy is specified in terms of potential distributions. Accordingly, information is needed to change a desirable accuracy level in potential to an equivalent statement in permeability or its reciprocal, the resistance to flow.

In preceding papers[21, 22] theoretical and experimental consideration was given to a method for measuring in-place permeabilities in heterogeneous media. In brief, it was shown that an analysis of the hydraulic head distribution of the existing flow regime, combined with a few in-place permeability measurements used as a boundary condition, makes it possible to determine the permeability distribution throughout the region of interest.

The desirable practical features of the method, other than the capability of considering heterogeneity, are that the piezometric head is rather easily measured and that a very large soil sample, or in a sense the entire soil mass, is utilized in the method. These facts are encouraging and may contribute toward filling a long-recognized need for obtaining

reliable values of permeability. However, solution of the computational problem is required. This paper presents a plausible scheme for overcoming the computational problem.

The problem arises from the measured potential being in tabular form rather than an algebraic function. Yet first and second spatial derivatives of the potential are necessary for solving directly for the permeability distribution. Numerical differentiation lacks the precision needed in this application since a small discrepancy in the potential results in a several-fold variation in permeability. Accordingly, a study was undertaken to determine the accuracy required in the proposed measurement method for permeability.

Electrical conductance paper analogs of the soil water system as described previosly[23] were used to examine the permeability-potential relationship. Since the experimental work was carried out in an electrical system, it is convenient to use resistance, i.e., the reciprocal of conductance or permeability, in the discussion to follow.

The relationship[21] between potential and resistance variation is shown in Figure 18. The dimensionless resistance discrepancies (measured resistance $R_{\mu}/\bar{R}$ minus the calculated resistance $R_c/\bar{R}$), are the maximum discrepancies found along a line approximating a streamline. The potential differences associated with the resistance discrepancies were obtained from the measured potential $\varphi_{\mu}/\bar{\varphi}$ minus the calculated potential $\varphi_c/\bar{\varphi}$. The variables $\bar{R}$ and $\bar{\varphi}$ are the mean resistance and potential, respectively, for the analog on which the discrepancy was observed.

The data shown in Figure 18 provide the needed relationship between resistance and potential error. They are useful for finding the allowable variation in resistance from the known or estimated tolerable limits of error in potential. Interpretation of this data shows that in general only about 2/15 as much precision is required in the resistance determination as in the potential. In other words, 7.5 times as much error can be tolerated in the calculated resistance (reciprocal permeability values) as in the final potential distribution being predicted.

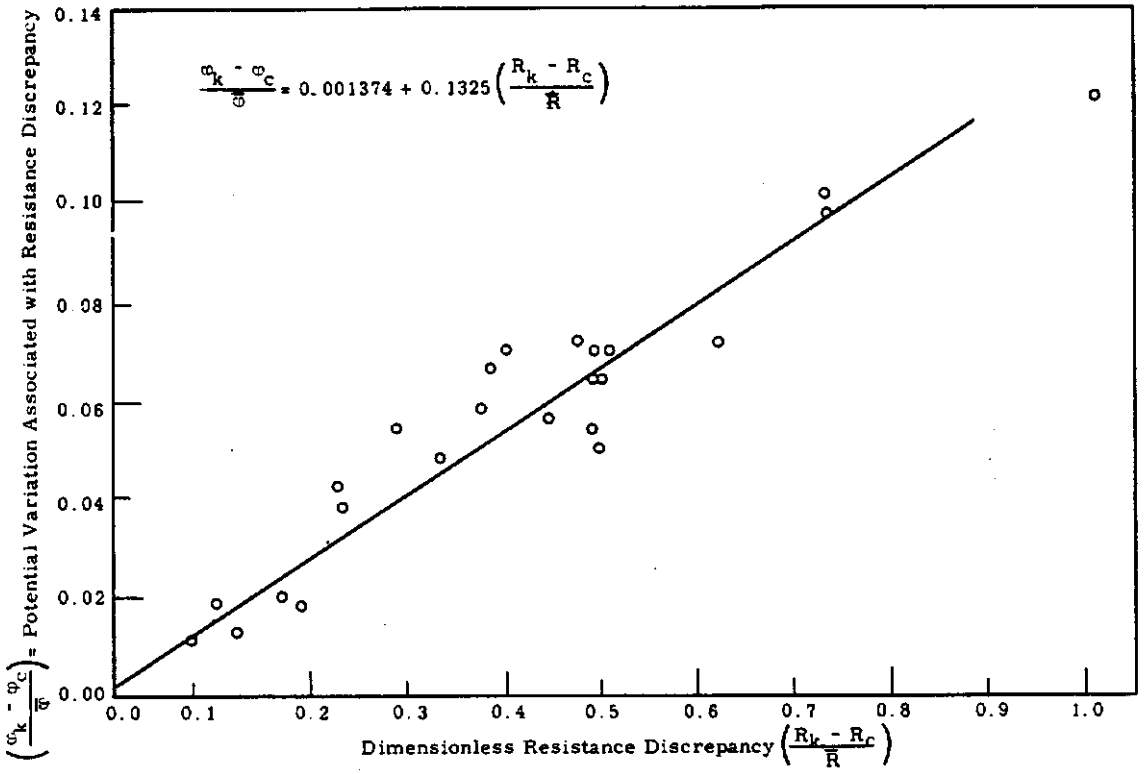

FIGURE 18

Potential Variation as a Function of Resistance Discrepancy for Use in Electrical Modeling of Soil-Water Flow Systems

This result has important practical implications which indicate that extreme precision is not absolutely required in computational schemes which may be devised. This is apparent when the potential pattern answer sought within the common accuracy range of 5 to 10 percent are converted to yield allowable permeability variations of from 37 to 75 percent. Even in waste disposal applications where ground-water velocities are needed and resistance enter directly, these studies show that a computational method giving results with 5 to 10 percent error may well be satisfactory.

An Approximate Method of Computation for In-Place Permeability Measurement - R. W. Nelson

Linear flow approximations are found to be rather reliable in overcoming the computational problems associated with an in-place method of permeability measurement for heterogeneous soils. The geometrical shape of the elements in a properly constructed flow net is used to calculate the permeability. Experimental examination of the method indicates the error to be 8.3 percent in the conductance and 1.12 percent in the potential.

The computational problem associated with an in-place method of permeability measurement was described in the preceding paper along with the general theory of measurement. In this section, linearized approximate method is described which offers possibilities in overcoming the computational problem.

In the linearized flow approach an approximate semigraphical method is simple and may be beneficial in lateral flow systems. Two variations of this method will be considered; in both, a properly constructed flow net is required.

The use of a proper flow net will expedite application of the linearized flow analysis. The commonly accepted practice for drawing flow nets in a uniform medium will provide the basis for constructing a proper flow net for heterogeneous conducting material. These requirements are:

(1) The incremental difference in potential between successive equipotentials is constant.
(2) Streamlines are everywhere orthogonal to equipotentials for an isotropic, heterogeneous medium.
(3) The spacing between streamlines is such that the same quantity of fluid passes between each pair of streamlines making up the flow system.

All these requirements are essentially the same as common flow net convention for a homogeneous medium. As a result of requirement 3, however, the streamlines may have a rather erratic spacing at some places in the flow

net for a heterogeneous medium. Occasionally it is convenient to insert dashed streamlines intermediate to primary streamlines in regions of very low permeability. If this is done, the flow net can no longer be classified as proper but forms a utilitarian flow net which must be used with care. In such cases the discharge in every stream tube is not a constant value, and corrections must be applied when analyzing the geometrical aspects of the resulting flow net elements. The proper flow net provides the basis for the linearized flow approximations which will now be examined.

In the first variation of the linear method, the width, and consequently the area, of any stream tube making up the flow net is assumed to be constant. This is equivalent to assuming strictly one-dimensional flow. Since the rate of flow and the cross-sectional area of the stream tube are assumed to be constant, Darcy's law combined with linear continuity reduces the relationship which states that resistance to flow (reciprocal of the permeability, K) is directly proportional to potential gradient. This may be written as:

$$\frac{K_2}{K_1} = \frac{R_1}{R_2} = \frac{\partial \varphi_1 / \partial s_1}{\partial \varphi_2 / \partial s_2} = \frac{\Delta \varphi_1 / \Delta s_1}{\Delta \varphi_2 / \Delta s_2} \qquad (1)$$

Since $\Delta\varphi_1$ is equal to $\Delta\varphi_2$ by requirement 1 for a proper flow net, Equation (1) reduces to

$$R_1/R_2 = \Delta s_2/\Delta s_1 \qquad (2)$$

where R_1 and R_2 are the resistances at two points along the stream tube, φ_1 and φ_2 are the potentials at these points, s is the distance along a stream tube, and Δs is the incremental distance between equipotentials at the points designated by the subscripts 1 and 2.

The electric conductance paper analogs described elsewhere[23] were used in drawing proper flow nets for the analogs and the incremental distances between equipotentials (Δs_n) were measured along the length of each streamline. The boundary condition[21] was used as the starting value for R_1. The value of R_n (n = 2, 3, 4, etc.) at any point along that

streamline could then be calculated from the measured ratio $\Delta s_1 / \Delta s_2$ using Equation (3). Values of R_n along the streamline were assumed to represent the values of resistance midway between the equipotentials and were plotted on a map of the analog. Lines of equal resistance were drawn by interpolation to form isoresistance maps for each of the analogs. Figure 19 shows such a map for analog 5. The experimentally known resistance map for the same analog is shown in Figure 20.

The isoresistance maps were used to determine the effective resistance for the 2-inch squares for which the resistance had been measured experimentally. The effective resistances were found by multiplying the areas lying between isoresistance lines by the mean resistance of these areas, adding the products for all areas within the 2-inch square, and dividing the total by four.

Comparison of the resistances calculated in the above manner with those measured in the experimental procedure showed the mean absolute difference to be 261 ohms (11.5 percent) for analog 5. The potentials discrepancy associated with this resistance difference is 1.70 percent.

Closer scrutiny of the data for the first approximation showed that the differences were largely for high values of resistance, the computed values being smaller than those measured. The predominant cause for the consistently lower values was found to be the assumption that the area of flow is constant.

A second modification of the linearized flow approximation can further reduce the error by taking into account the change in area along stream tubes. Again assuming only one-dimensional flow and letting Δs be the average incremental distance between equipotentials and b the average width of the stream tube, we can equate the flow at two points along the stream tube and thus modify Equation (2) by the stream tube width. Equation (2) then becomes

$$\frac{K_1}{K_n} = \frac{R_n}{R_1} = \frac{(b_n)(\Delta s_1)}{(b_1)(\Delta s_n)} \qquad (3)$$

FIGURE 19

Computed Iso-Resistance Using the Linear Approximal Method
(Compare with Figure 20)

AEC-GE RICHLAND, WASH.

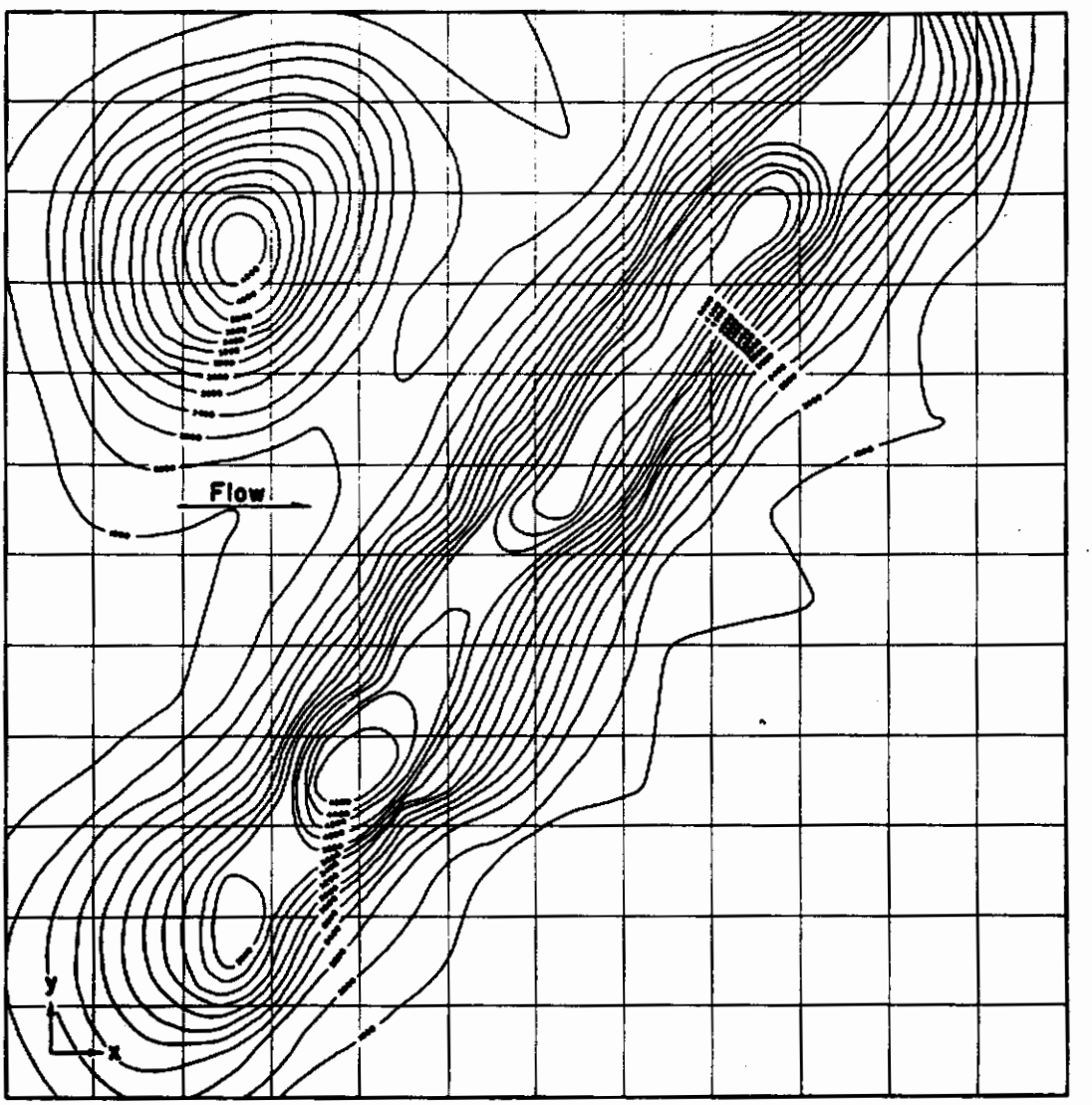

FIGURE 20

Known Iso-Resistance Map for Analog 5

The procedure used with Equation (2) was used again with Equation (3) to get the effective resistance of the 2-inch square. A comparison of resistance values computed with Equation (3) with those experimentally measured gave mean absolute differences of 198 ohms (8.43 percent) for analog 1. The potential discrepancy associated with these resistance differences is 1.12 percent.

Discussion of Linearized Approximations

A thorough understanding of what is implied by assuming linear flow will make it possible to evaluate the error introduced by the approximation. Saying that flow is essentially linear implies that the velocity, v_n, in the direction normal to the general stream tube direction is so small in comparison with the velocity, v_s, along the flow that it can be ignored, i.e.,

$$v_n \ll v_s \tag{4}$$

Then by Darcy's law,

$$\partial\varphi/\partial n \ll \partial\varphi/\partial s \tag{5}$$

where n is the direction normal to the general flow and s is the direction tangential to the flow. If this is the case, then, approximately,

$$\partial\varphi/\partial n = 0 \tag{6}$$

and no energy will be expended in expansion or contraction of flow. If this were strictly true, all stream tubes would of necessity have straight parallel boundaries with the area available for flow being constant. This is the real physical system described by Equation (2). The limitations it contains are:

(1) Any energy utilized in the divergence, convergence, or curvature of flow along the stream tube is negligible when compared with that expended in flow along the stream tube.

(2) The cross-sectional area available for flow along the length of the stream tube is constant.

The first of these limitations is inherent in the application of Equation (3), but not the second. Accordingly, Equation (3) gives a better estimate of experimental results than does Equation (2).

Partially Saturated Flow Studies in Porous Media - R. W. Nelson and A. E. Reisenauer

Basic equations are presented to describe steady, partially saturated flow and its reduced special case of saturated flow in both homogeneous and heterogeneous media. These equations have application in describing the downward flow phenomena which occur in the soil beneath a waste disposal site. The fundamental nonlinearity of the expressions prevent direct analytical solution. Therefore, finite difference methods were utilized and a general computer program was prepared capable of solving 1-, 2-, 3-dimensional and axial-symmetrical problems for up to 8000 grid points. A typical solution using the method is presented for partially saturated flow from a trench. The computed results showed good qualitative agreement when compared with measurements from an experimental field crib.

There are several types of disposal problems where partially saturated flow in soils is important. For example, downward flow of wastes from cribs, trenches, or swamps toward the water table is usually under conditions of partial saturation. The "specific retention" of waste solution above the water table, and transient measurement methods using ring infiltrometers, pumping tests, etc., all involve partially saturated flow. This variety of problems can be compactly formulated in terms of basic expressions. Upon solution of the basic equations, useful information for practical flow systems is obtained.

A macroscopic description of flow in partially saturated, nonhomogeneous media is needed. Precise statements of the properties of the fluid and porous media, along with a characterization of flow, provide the equations of state and dynamics.[24] These two equations, when combined with the equation of continuity, result in a complete hydrodynamic description, yielding the required fundamental expressions.

Partially saturated, nonturbulent flow of an incompressible fluid, which does not interact with the porous medium, is assumed. The medium is considered variable from point to point in the flow system. Accordingly, the permeability or capillary conductivity is a function of the spatial

coordinates as well as a function of capillary pressure. Therefore, the generalized Darcy's law,

$$\bar{v} = -K \operatorname{grad} \varphi, \tag{7}$$

provides a dynamic description of flow on a macroscopic basis. Conservation of mass, i.e.,

$$\operatorname{div} \rho \bar{v} = 0, \tag{8}$$

defines the continuity condition. Substituting (7) into (8) gives:

$$\operatorname{div} \rho(-K \operatorname{grad} \varphi) = 0,$$

$$\operatorname{grad} \varphi \cdot \operatorname{grad} K + K \operatorname{div} \operatorname{grad} \varphi = 0 \tag{9}$$

or, in expanded form,

$$K \left(\frac{\partial^2 \varphi}{\partial x^2} + \frac{\partial^2 \varphi}{\partial y^2} + \frac{\partial^2 \varphi}{\partial z^2} \right) + \frac{\partial K}{\partial x} \frac{\partial \varphi}{\partial x} + \frac{\partial K}{\partial y} \frac{\partial \varphi}{\partial y} + \frac{\partial K}{\partial z} \frac{\partial \varphi}{\partial z} = 0 \tag{10}$$

where:

		Dimensions
$\bar{v}$	is the velocity vector with components in the x, y and z coordinate directions	$L/_T$
K	is the capillary conductivity of the soil. It is a function of capillary pressure, P_c, during partial saturation and becomes the hydraulic conductivity or soil permeability at saturation. Since the soil is assumed to be nonhomogeneous, K is also a function of space, i.e., x, y and z	$L^3/_{(L^2T)}$
$\varphi = \frac{P}{g} + z$	is the piezometric head, hydraulic potential or potential function and	FL/F
P	is the hydraulic pressure	FL/L^3
P_c	is the capillary pressure head and is defined only for negative P	FL/F

		Dimensions
P_d	is the displacement pressure head or the negative pressure head which must be reached in order to empty the first soil pore	FL/F
z	is the position head or potential energy due to location in the gravitational field	FL/F
θ	is the moisture content on a volume basis	L^3/L^3
ρ	is the fluid density	$F/(L^3L/T^2)$
g	is the gravitational scalar	L/T^2

In addition to Equation (10), two other relationships may be written for partially saturated systems. They are:

$$P_c = \frac{-P}{\rho g} = z - \varphi \qquad (11)$$

$$K = f(P_c) \qquad (12)$$

where $f(P_c)$ is the functional relationship of moisture conductance to capillary pressure head.
Therefore, $f(P_c)$ is the function which interrelates the soil properties of capillary pressure head and moisture conductance.
The nonlinearity of the equations suggests the difficulty of obtaining analytic solutions. As a result a numerical solution technique must be applied as a general approach to these problems. Computer methods are helpful in getting solutions for practical problems.[25]

Finite difference methods were applied to the flow-system described by Equations (10), (11), and (12). This reduced the partial differential equations to a system of simultaneous expressions which were then solved iteratively. The conditions of Equations (11) and (12) necessitate an iterative technique rather than a more direct linear method.

The computer program developed at Hanford can handle 1-, 2-, and 3-dimensional and axi-symmetrical problems with up to 8000 grid points. For this purpose a program was prepared for application to an IBM 7090

computer. Three 8000-word matrices are stored so that access is immediate during all calculations. This results in a very efficient computation with an average rate of 370 grid-point calculations per second. Even at this rate very large problems can require 30 to 50 minutes of computer time; however, this is the exception and the average problem requires 6 to 10 minutes. Methods to further shorten computation time by hastening convergence are being examined.

The full range of boundary conditions that may be needed for various problems is available and only minimum input effort is required to designate the boundary types. The system is completely flexible and every grid point can be individually controlled for boundary type.

The soil need not be homogeneous since descriptive data for up to 15 different soils can be included in any one flow problem. In each case the soils data (Equation (12) for as many soils as are being used are input to the computer. The different soils can be repeated at as many locations in any problem as may be desired. This is accomplished through a soils-type matrix, which designates the soil for every spatial grid point. A merging method allows both the type of calculation and soil identification matrices to be stored in a single computer work. This saves considerable case storage, facilitating solution of the large 8000 grid-point problems.

Other problems for which solutions can be obtained involve combined partially saturated and saturated flow.[26] This is possible as a direct result of the reducibility of partially saturated flow to the special case of saturation as shown through inspection of Equation (7). In such flow systems the solution proceeds smoothly with no concern about the water table location. The latter is located after the whole solution has been accomplished. Such a procedure is easier and at the same time is more descriptive of nature than are the free-boundary type solutions usually sought when considering only a saturated system.

A typical application of the methods described illustrates the solutions that are obtained. Figure 21 shows the calculated flow pattern for an experimental disposal trench. The equipotential lines and streamlines indicate

the spread below the trench. It is interesting to compare the conservative "column volume" used at Hanford to estimate crib capacity with the actual flow pattern. The volume of soil used in Hanford crib evaluations is that contained in a column having the cross-sectional dimensions of the crib and extending to the water table. The values shown on the streamlines indicate the percent of the total flow leaving half of the trench. For example, 10 percent of the flow leaving half of the crib passes from the crib downward to the water table between the streamlines labeled 0.5 and 0.6. Figure 22 shows the moisture distribution beneath the trench obtained in the course of the problem solution. The definite zone of lower moisture content below the crib is consistent with the pattern found under a field test crib at Hanford, using a neutron probe. Further application of these techniques for solving actual plant disposal problems is planned.

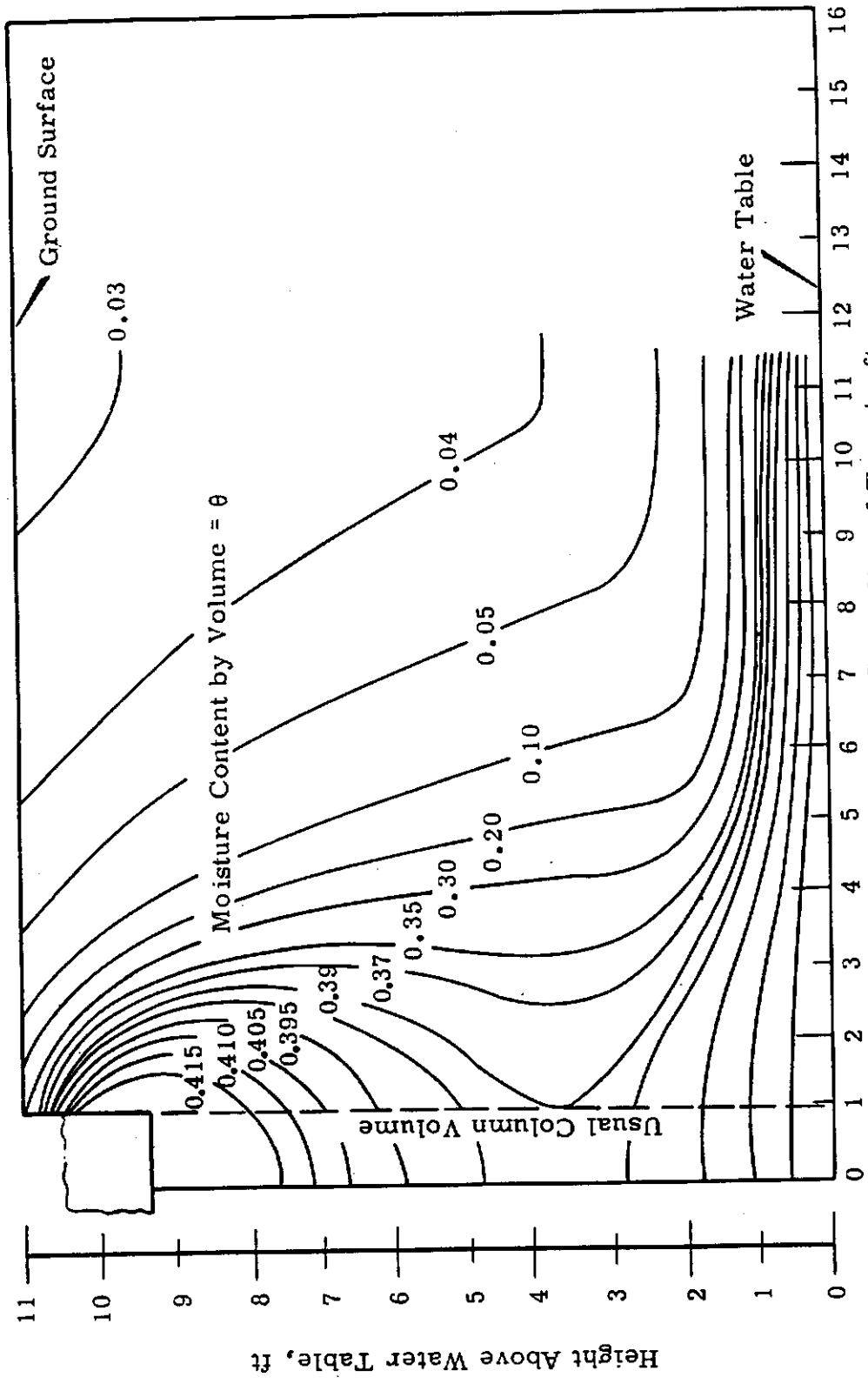

FIGURE 22

Moisture Distribution Below a Two-Foot Disposal Trench

Geology

Geologic Features and Ground Water Flow at Hanford - R. E. Brown

Geological studies show hydrologic continuity between the upper part of the Columbia River basalt series and the postbasalt sediments. The movement of ground waters in three dimensions is thus more critical than if the basalt series terminated downward movement of the higher waters. Hydrologic continuity results from the similarity of geologic structures in the two major units and reflects the importance of even minor structures in directing the flow of ground waters.

The break or contrast between the basalt flows of the Columbia River basalt series and the postbasalt sediments is generally sharp. However, geological studies show that sufficient hydrologic continuity evidently exists between the two major units that they need be treated as one for the determination of ground water movements in the dimension of depth.

Structural studies continued to confirm the general conformability of basalt flows and overlying Ringold Formation sediments. Topographic highs on the eroded Ringold Formation surface overlie structural highs on the underlying basalt, suggesting lithologic control of the erosion. Inasmuch as ground waters flow most rapidly in the channels in the Ringold Formation surface, structural control of ground water flow has occurred there.

The absence of indicated angular unconformities between flows and interbedded sediments of the basalt series and the Ringold Formation sediments implies no major differences in the behavior of ground waters in the two major units. However, numerous disconformities (local erosion surfaces) between horizons are now recognized. These represent old Columbia River courses which are now gravel-filled channels or gravel trains. These channels represent potentially rapid flow paths for ground waters at many different levels and in somewhat different directions, depending on the particular orientation of each stream course.

The Ringold Formation section terminates downward in a sandy gravel that evidently is an alluvial fan deposit laid down by an eastward-flowing stream at its junction with the Columbia River. Although the fan

thins eastward and appears to pinch out, to east and west it evidently passes beneath a later basalt flow. Hence, ground waters beneath Hanford have a means of entering aquifers continued within the basalt series under the proper piezometric head conditions.

Erosion of the basalt by the Columbia River also was demonstrated. Adjacent to a chemical separations plant area a channel nearly 100 feet deep was eroded through the topmost basalt flow into an underlying interbed. Flow of ground waters into or out of the basalt series is possible in this area with proper piezometric heads.

Geology Underlying Hanford Reactor Areas - D. J. Brown

> There are three distinct geologic units beneath the reactor areas: the Columbia River basalt, the Ringold Formation, and the glaciofluviatile sediments. The Columbia River basalt series forms the bedrock beneath the reactor areas and is generally compact, hard, and dense. The Ringold Formation is a lacustrine and fluviatile deposit of sand, silt, gravel, and clay which conformably overlies the basalt. Unconformably overlying the Ringold Formation is a sedimentary deposit of coarse outwash sands and gravels locally referred to as glaciofluviatile sediments. The structure of these rocks underlying the reactor areas reflects the tectonic deformation which has been going on continuously in this region for the last several million years. The lower beds of the Ringold Formation exhibit the greatest degree of conformity to the basalt.

A comprehensive study is in progress which should extend, detail, and refine the conceptual understanding of the geology underlying the Hanford Project and the region immediately surrounding it. Certain regions and geologic horizons of the project are being studied first because of their more immediate interest. A general overall report will combine and incorporate the reports covering these selected regions and problem areas. This section summarizes the data and the latest concepts of the geology underlying the Hanford Reactor Areas. Its basic purpose is to provide working maps and information on the geologic structure and stratigraphy beneath the reactor areas as well as to describe the general influence of the geology on ground water movement.

The bedrock beneath the reactor areas is a vast series of basaltic lava flows and related rocks known as the Columbia River basalt (Figure 23). In the western portion of the region in which the reactors are located, the first 100 feet of basalt are essentially continuous, with no apparent interbeds. To the east, however, there are numerous interbeds within the upper portion of the basalt series. The interbedded materials are predominantly sand, gravel, clay, and volcanic ash. The surface of the basalt is vesicular to scoriaceous while samples obtained from depths of more than 10 feet beneath the surface are hard, dense, dark gray in color, fine textured, but similar in composition to surface samples.

Directly overlying the basalt bedrock is an extensive lacustrine and fluviatile deposit of sand, silt, gravel and clay known as the Ringold Formation. Over much of the Hanford Project, three members of the Ringold Formation are distinguishable; however, beneath the reactor areas these three members are not distinct from each other and can not be readily differentiated. In the northwestern region of the Hanford Project the Ringold Formation is dominantly coarse material such as sands and gravels. Farther to the east it grades into sand and coarse silt, and on the northeastern margin it is mostly silt and coarse clay. Where the middle member of the Ringold Formation can be distinguished, it is generally cemented with calcium carbonate.

Fluviatile and glaciofluviatile sediments brought down from the north by the Columbia River overlie the Ringold Formation. These materials were laid down unconformably on top of the erosion surface of the formation. In the region around the reactor areas these materials consist of sand, gravel, and boulders, although some lenses of fine, well-sorted materials have been observed. The coarse materials are also more abundant in the northwestern section of the project, grading into finer materials to the east and south.

Tectonic deformation in the region of the Pasco Basin has resulted in the warping and folding of the underlying basalts and the sedimentary deposits which lie above them. Figures 24 and 25 are contour maps of the surface of the basalt bedrock and the surface of the Ringold Formation,

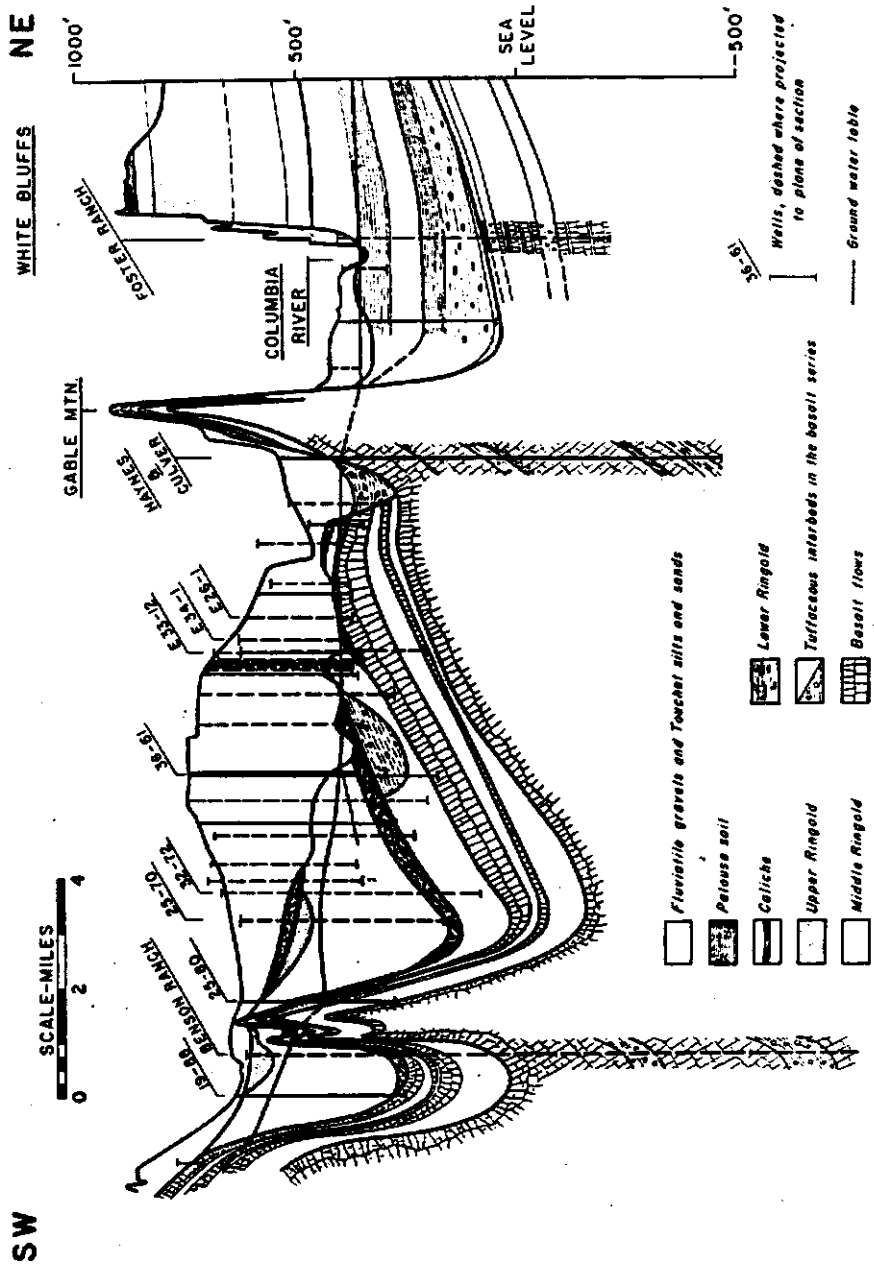

FIGURE 23

Geolgic Cross Section
Hanford Works

AEC-GE RICHLAND, WASH.

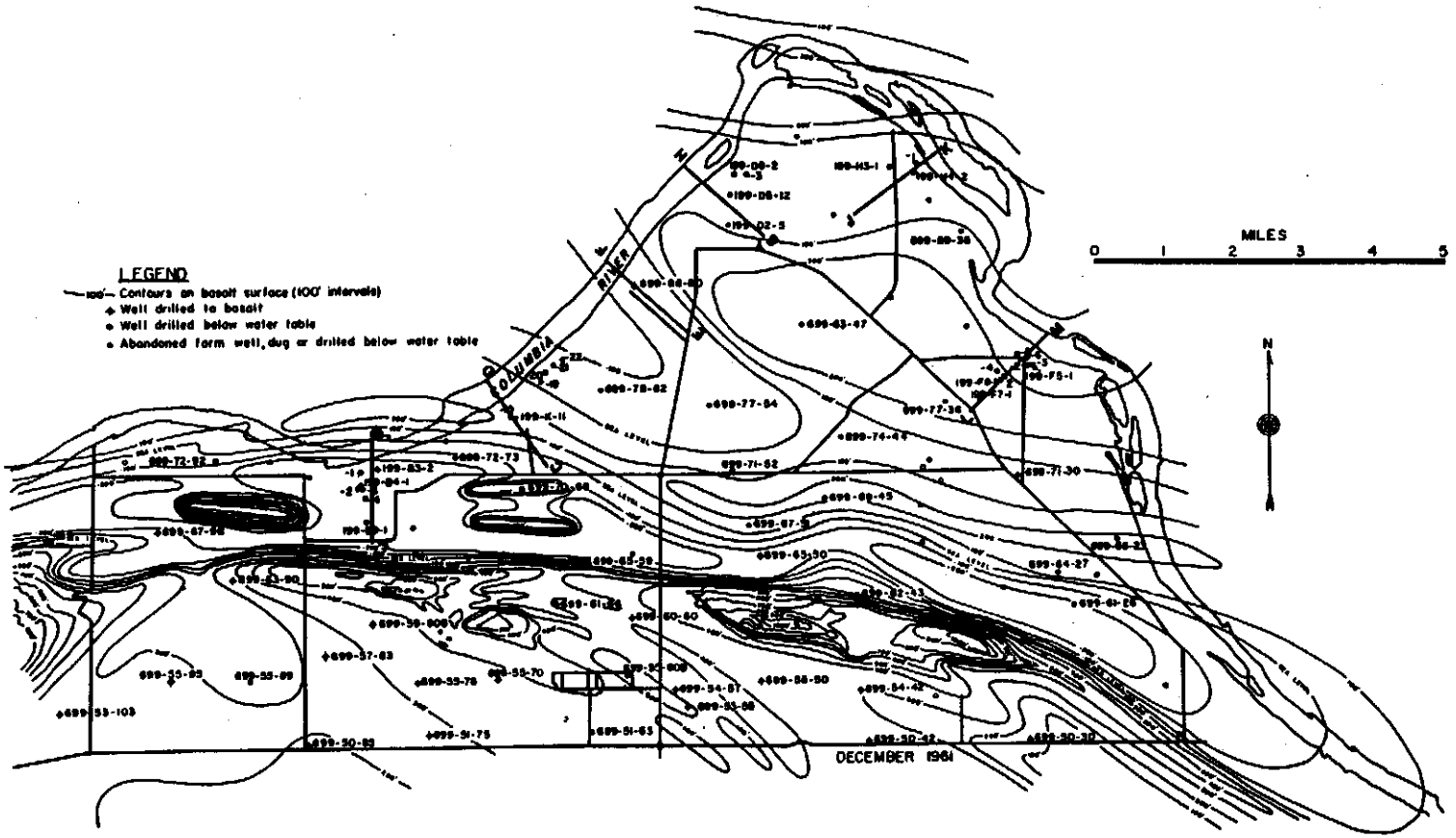

FIGURE 24

Contour Map of the Basalt Surface Underlying the Region of the Hanford Reactor Areas

1102697

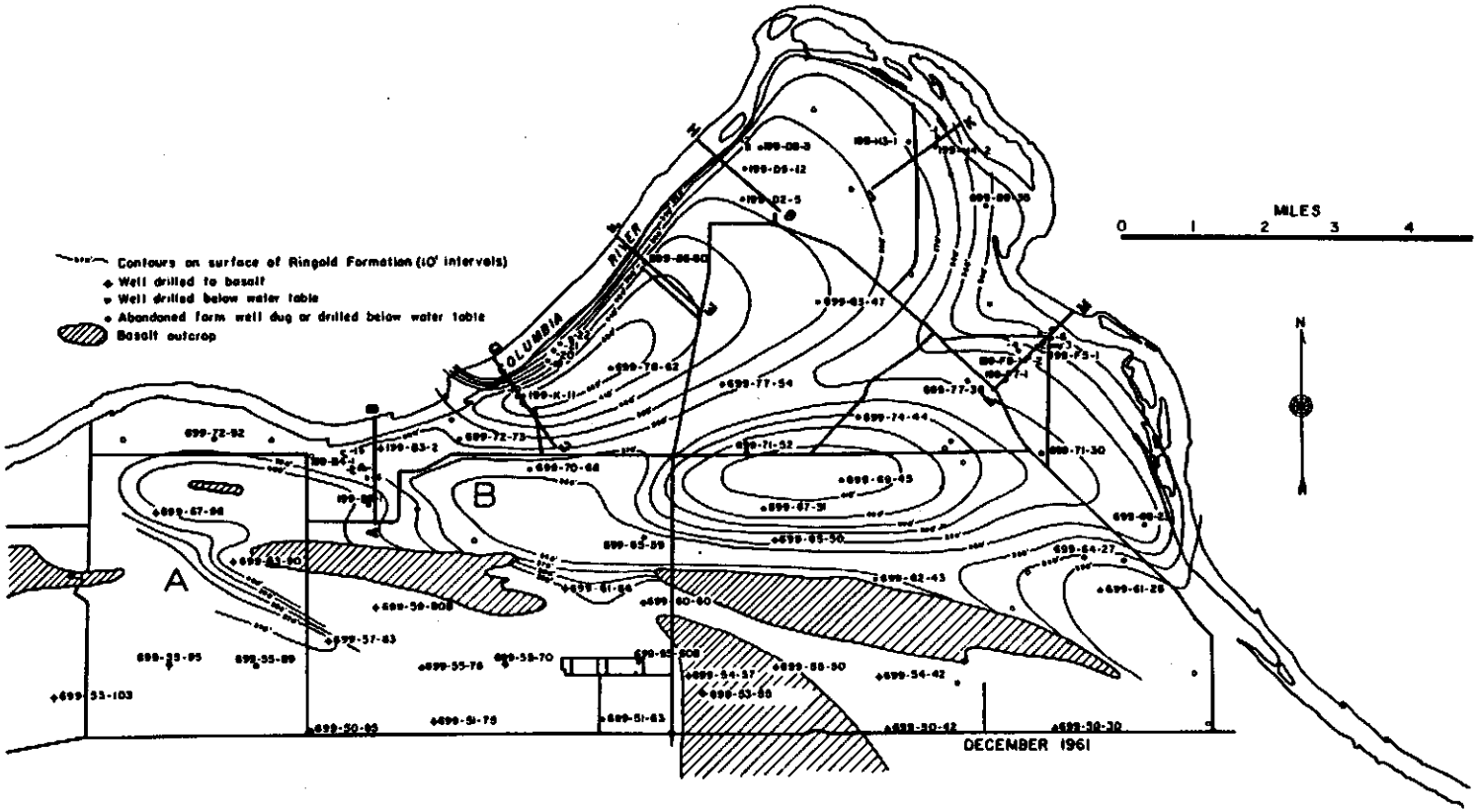

FIGURE 25

Contour Map of the Surface of the Ringold Formation Underlying the Region of the Hanford Reactor Areas

respectively. The relief features shown on the basalt contour map resulted primarily from folding of the basalt flows with essentially no erosion. All of the Ringold surface shown on the contour map of the Ringold Formation has been eroded by the Columbia River. There are, however, several topographic highs on this contour map which have resulted primarily from structural control of the Ringold beds. These topographic highs coincide with highs located in the same position on the basalt contour map.

The water table beneath the reactor areas lies at an average depth of 100 feet. Figure 26 is a contour map drawn on the water table beneath the reactor areas for the month of December 1961. This map shows the general ground-water contour pattern beneath the reactor areas, except for seasonal fluctuations which occur adjacent to the Columbia River in the late spring. The recharge of the ground water is normally from the high-land areas to the south and southwest.

Several small ground-water mounds along the Columbia River are shown on the ground-water contour map. These mounds represent small recharge areas. The source of this water is retention basins and cribs which receive the cooling water from the reactor buildings.

The permeability normal to the surfaces of the basalt flows is generally very low, particularly in comparison to the lateral permeability of the interflow zones. Hence, ground waters within the basalt series are quite separate and distinct from those in the postbasalt sediments. The materials which make up the Ringold Formation are either fine-grained or so poorly sorted that they have a relatively low permeability; generally this ranges from 10 to 10,000 gal/ft^2/day. The fluviatile and glaciofluviatile sediments are coarse-grained and generally highly permeable. Permeabilities range from 10,000 to 50,000 gal/ft^2/day, or from 10 to as much as 5000 times those of the Ringold Formation sediments.

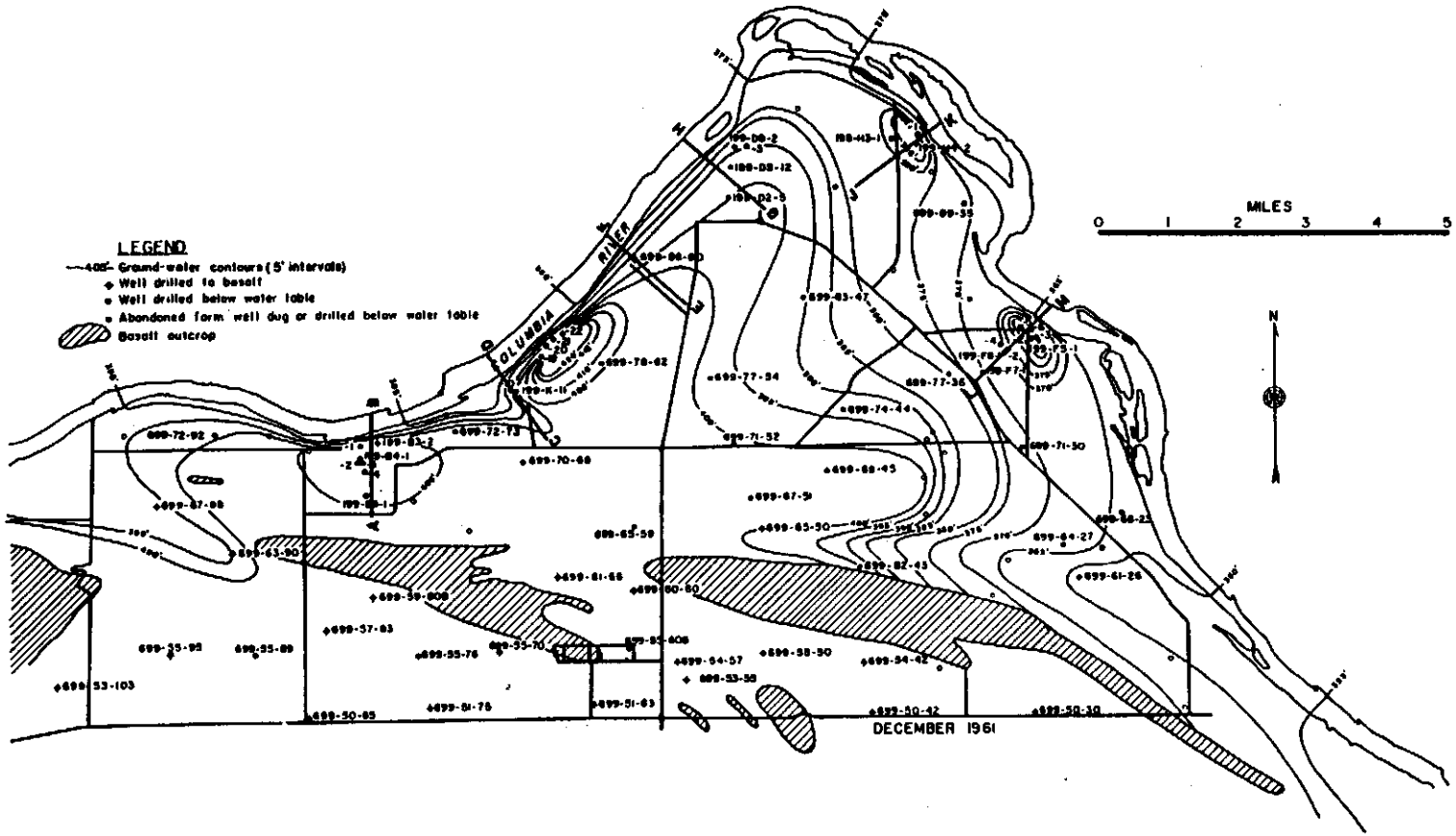

FIGURE 26

Ground-Water Contour Map of the Water Table Underlying the Region of the Hanford Reactor Areas, December, 1961

Disposal of Reactor Wastes at Inland Sites - R. E. Brown

Disposal of New Production Reactor decontamination wastes to ground at an inland site is planned to help minimize Columbia River contamination by neutron-activated isotopes. Disposal will be at a site from which the direction of flow to the Columbia River will assure entry of parent materials into the river downstream from all reactors. Sorption on earth materials and increased decay resulting from longer travel times to exposure points also will deplete the radiocontaminants in the wastes. Success in disposal probably will be followed by similar disposal of other waste streams.

Plans were made to minimize Columbia River contamination by neutron-activated isotopes in reactor effluent by the discharge of a New Production Reactor (NPR) waste stream to ground at an inland site. Success in the disposal of this stream, containing H_3PO_4 decontamination waste, at a site remote from the Columbia River is expected to be followed by similar disposal of additional streams.

Successful disposal of the H_3PO_4 waste to ground requires that the wastes enter the Columbia River at a point downstream from all reactor water intakes so the phosphorous will have no chance of being activated to P^{32}. Additionally, sorption processes in the ground and increased travel times to use points, hence greater decay, than available with current practices will largely deplete radiocontaminants prior to river entry. A site about 5 miles from the NPR reactor was selected, where ground water assuredly flows into the Columbia River downstream from all the reactors. The distance from the river to this site is the maximum possible in the required flow path and it therefore provides a maximum time of travel to the river. Based on drawdown, step-drawdown, and recovery rate tests in wells, an average travel time of ground water from this site to the Columbia River is estimated at 2 to 2.5 years. In tracer tests between wells, flow rates were measured up to 3.5 times faster, suggesting travel times of 200 to 250 days.

Instrumental Techniques

A Logging System for Well-Water Temperature Measurement -

J. R. Raymond

A well-water temperature logging system was developed and is described. The sensing element is a glass-wall thermistor supported in a cage. The thermistor response is measured in a bridge circuit at the surface. A "Widco" electric logger is used for raising and lowering the probe, and a Brown recorder plots the temperature as a function of depth. The sensitivity is about ±0.1 C and the long-term accuracy is ±0.5 C.

Measurement of ground-water temperature variations can give information on aquifer sources, paths of water travel, and, the influence of geologic structures. Where large volumes of thermally hot water are introduced into the ground water (as occurs at Hanford), well temperature surveys may be used to trace the water movement.

A well logging system was devised to study ground-water temperature on the Hanford reservation. The system consists of a sensing probe, bridge circuit, 1000 feet of armored wire line, recorder and cable hoisting equipment. The probe is 18-inches long and consists of 1-inch diameter stainless steel pipe (Figure 27). A Victory Engineering Corporation type 51-A1 glass rod thermistor having a nominal resistance of 100k-ohms at 25 C and a resistance change of 3 percent per degree C is used for the detector. The thermistor is "potted" in a 3-inch section of 3/8-inch stainless steel tubing with a thermosetting resin, and the tubing is connected to the probe end with a compression type fitting. A wire guard protects the exposed thermistor. The thermistor lead is extended through the probe and affixed to a water-tight cable connector which is coupled to the wire line cable head. The thermistor is used as one leg in a deflection bridge circuit with surface controls to allow adjustment of bridge balance and sensitivity. A "Widco" model XMVA-12 electric logger is used for raising and lowering the probe (Figure 28). A modified Brown recorder measures the bridge unbalance and the recorder chart drive is coupled to the cable drum to record depth.

FIGURE 27

The Hanford Ground-Water Temperature Probe

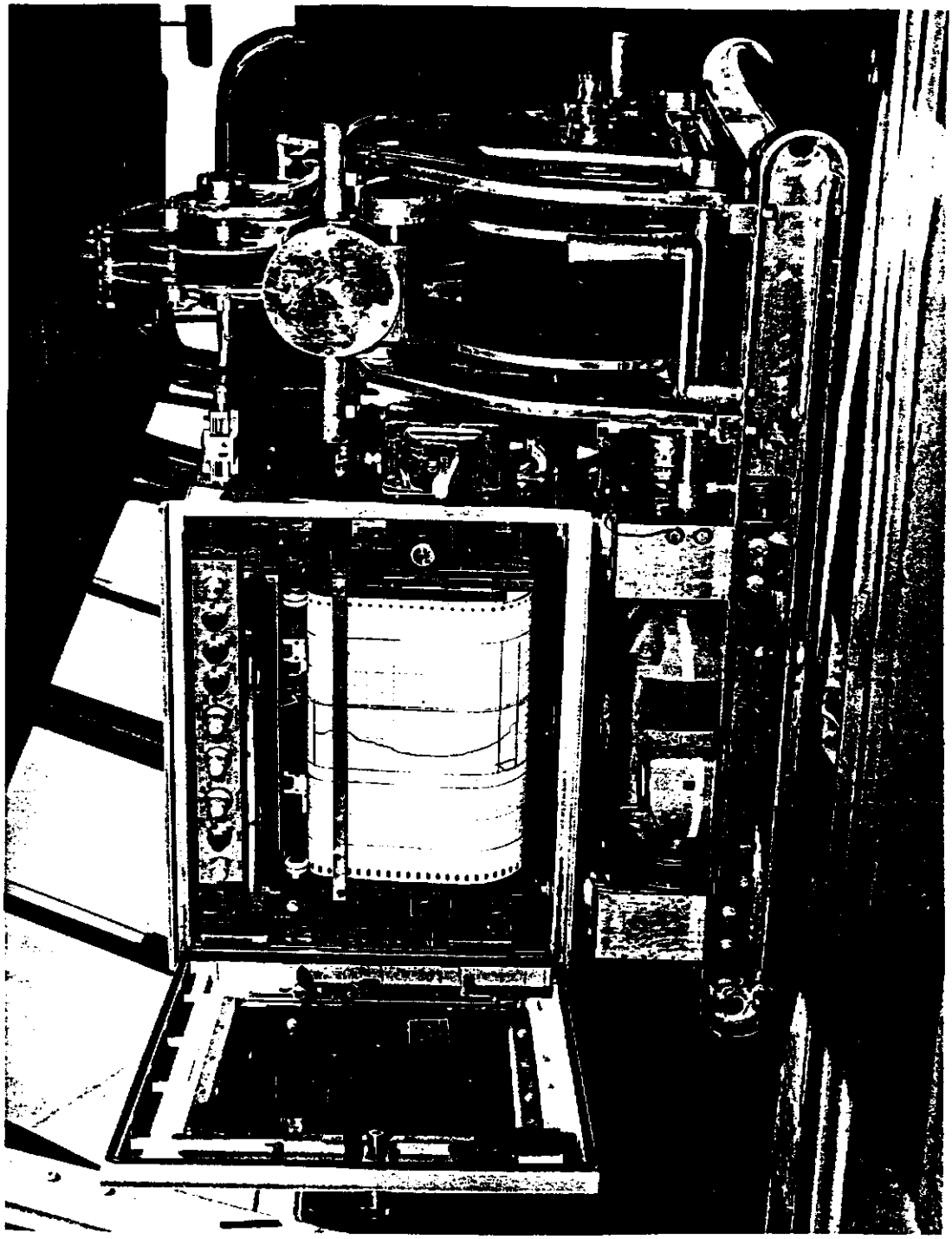

FIGURE 28

Electric Logger and Recorder Used in Temperature-Probe Surveys

A separate odometer is also provided for depth measurement. The equipment is mounted in the back of a four wheel drive, 1/2 ton truck, and a 1500 w light plant is mounted on the front of the truck for power for the logger and recorder.

Instrument range is from 0 to 80 C. Sensitivity is about ± 0.1 C and long term accuracy is ±0.5 C. Figure 29 shows the equipment in use.

FIGURE 29

Hanford Temperature Probe in Use

Flow Meter for Vertical Well Currents - J. D. McCormack

A highly sensitive flowmeter for measuring vertical currents in project wells was developed. The meter employs an orifice diaphragm with a novel pressure differential sensing element, the diaphragm itself. The displacement of the diaphragm resulting from a pressure drop across the orifice is detected by a linear differential voltage transformer, whose armature moves with the displacement of the diaphragm. An electrical signal at the surface can be interpreted as a velocity; the polarity of the signal indicates whether flow is up or down the well. A sensitivity of 30 cc/min, or about 4.4 ft/day was obtained.

Basic analog studies have shown that significant piezometric head differences in the vertical direction are possible, particularly in the vicinity of ground-water recharge points. Marked differences in piezometric head in formations penetrated by a well should result in significant vertical flows since such wells would provide a low-resistance path between horizons of differing head. As the anticipated flows are small, a sensitive flowmeter is required to determine the magnitude and direction of the vertical flow in shallow, cased wells.

The required flowmeter was to be used in 8-inch diameter wells, have low pressure drop, and be remotely operable via 1000 feet of single conductor cable. An orifice was selected as the flow-sensing element and while this enables two-directional flow measurement, the desirability of low pressure drop through the meter requires a sensitive pressure measuring system. In order to avoid problems associated with an air-water interface (problems with level changes, bubbles, and surface tension), the orifice pressure-sensing diaphragm was made to operate completely submerged in the water and to be filled with water. As a further simplification the orifice was incorporated into the pressure-sensing diaphragm, eliminating the need for tubing to connect the orifice and the diaphragm. The motion of the diaphragm is restrained by leaf springs which cause the diaphragm motion to be proportional to the pressure drop developed across the orifice. This motion is measured with a battery-powered linear variable differential transformer (LVDT) whose output voltage and polarity indicate the water velocity.

The assembled meter is shown in Figure 30. Its associated control panel and power supply are located in the truck. Use of the meter in a well necessitates sealing of the unit within the well so that the flow will be directed through the orifice. An innertube, visible in Figure 30, is used as an inflatable seal or packer. The inflation of the packer is accomplished with a small reversible pump which is powered from the surface and is controlled by a voltage-sensitive relay. The pump, control relays and batteries for the LVDT are all contained within the water-tight housing.

The measuring circuit is a zero-center voltmeter with a zero adjustment and range switch. The unit was calibrated for up and down flow over the range of 30 to 600 cc/min (4.4 to 88 ft/day) in a mock well in the laboratory. In the field, uncertainties in zero and cable noise limit the precision to ± 30 cc/min.

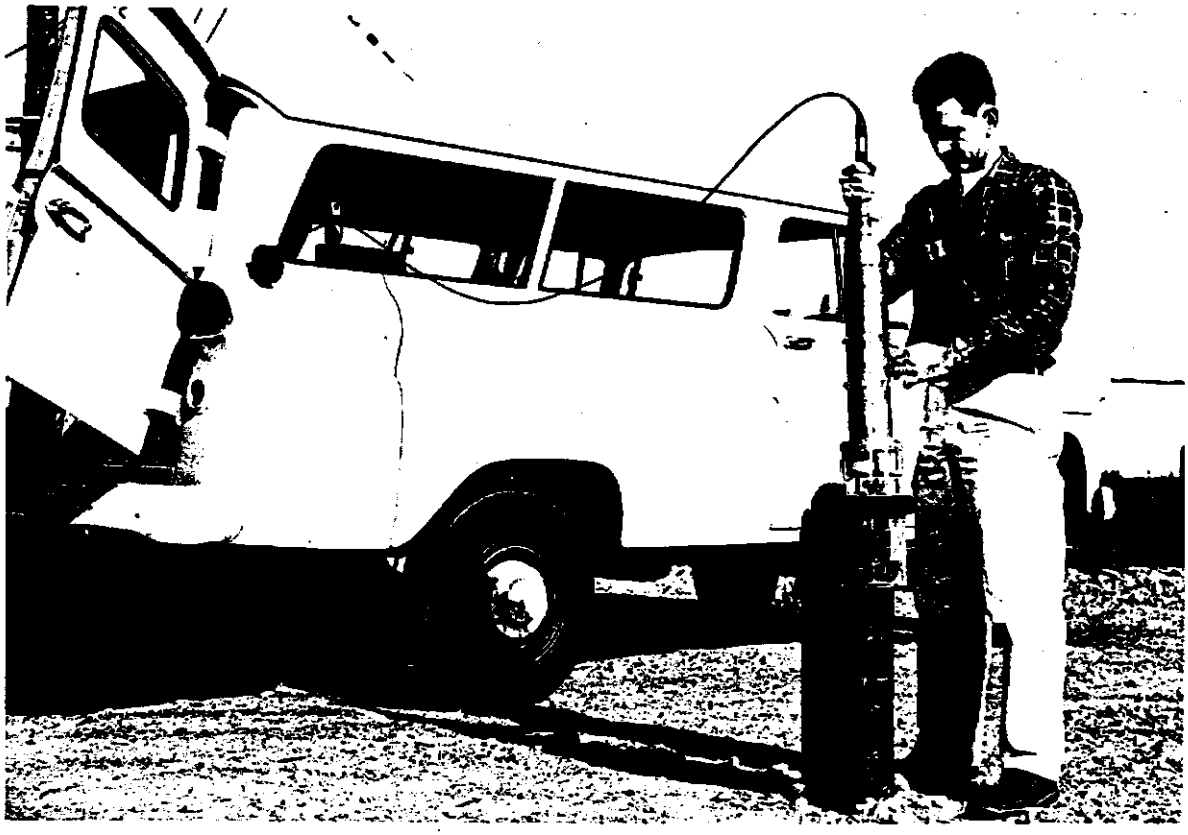

FIGURE 30

Hanford Flow Meter for Vertical Well Currents

Field testing the instrument has resulted in the checking of 22 project wells for flow. Vertical flow was definitely found in 12 wells, usually in the downward direction. Upward flow has been noted in three wells. Performance has been satisfactory although improvement of the "potting" of the LVDT to permit operation in deeper water and protection of the LVDT armature from sand would be desirable.

A more complete description of the instrument has been reported in HW-71388.

Uranium Oxidation and Fission Product Volatility

Particulates Generated from Uranium Burning in Air - L. F. Coleman

The uranium oxide particles generated when a uranium specimen was heated in air were studied. Submicron particles produced at temperatures above 1000 C were found to result from a sublimation-condensation sequence. The distribution of contained fission products among uranium oxide particles of different sizes was also examined.

The effects of temperature and air velocity on uranium oxide particulate production and entrainment were investigated. The results show an increase in the mass median particle size with increasing temperature in the range 400 to 1300 C. The amount of entrained oxide reaching a point 51 cm downstream from the oxidizing specimen (1/4-in. diameter by 3/4-in. long) was greatest at the higher temperatures when low air velocities (8.3 to 33 cm/sec) were employed. At temperatures below 1000 C few submicron particulates are produced. The greater release at high temperatures is associated with submicron particles resulting from a sublimation-condensation process. The rate of uranium release as oxide particulates at 1200 C varied from 7 to 80 μg/min at air velocities from 8.3 to 66.4 cm/sec. Material collections were made 51 cm downstream from 1/4-in. diameter by 3/4-in. long cylindrical specimens oxidizing in a 27 mm tube.

Four experiments were conducted to determine the size of particulates with which certain radionuclides were associated when irradiated uranium

was oxidized in air at 1200 C and with an air velocity of 8.3 cm/sec. More than 95 percent of the Cs^{137}, $Zr\text{-}Nb^{95}$, and Te^{132} activities were associated with submicron particulates. Ru^{106} and Sr^{90} activity was found in high percentage throughout the 5-stage impactor unit employed, 70 and 50 percent, respectively, being classified in the less than one micron fraction. It was not determined whether the observed deposition was due to inertial impaction as anticipated or whether other deposition forces were operative.

Fission Product Release from Irradiated Uranium - R. K. Hilliard and D. L. Reid

The fractional releases of radionuclides from small uranium samples heated to high temperatures are presented as a function of irradiation level. The measured higher release fraction for some of the radionuclides with irradiation level is explained as either the result of a higher uranium oxidation rate or a concentration increase.

The fractional release of fission-product elements from irradiated uranium during reactor disaster conditions was investigated. Uranium cylinders weighing 11.5 grams were irradiated to various levels and heated by induction under controlled conditions. The exposures ranged from an integrated thermal neutron flux of 2×10^{14} to 4×10^{20} nvt. The fractional releases of ten fission-product elements and neptunium, plutonium, and uranium were measured and the results are given in Table XIV.

The information in the table shows that the combination of irradiation structural damage plus higher fission-product concentrations did result in higher releases for some of the elements. About three times more xenon, iodine, cesium, strontium, and barium were released at the highest burnup than at the lowest burnup. No effect was noticed for tellurium, zirconium, cerium and neptunium. Ruthenium and molybdenum release was greatly accelerated at the highest irradiation levels, being about 50 times greater at 4×10^{20} nvt than at 10^{18} nvt. The volatility of these two elements depends on their oxidation to ruthenium tetroxide and molybdenum trioxide.

TABLE XIV

EFFECT OF IRRADIATION LEVEL ON RELEASE OF FISSION PRODUCTS FROM IRRADIATED URANIUM

Element	Fraction Released from Specimen[a]		
	10^{14} nvt	10^{18} nvt	4×10^{20} nvt
Xenon	0.70	0.95	1.0
Iodine	0.60	0.80	0.98
Cesium	0.25	0.50	0.80
Tellurium	0.65	0.65	0.65
Strontium	0.002	0.004	0.008
Barium	0.002	0.004	0.008
Ruthenium	0.001	0.001	0.05
Molybdenum	0.001	0.001	0.04
Zirconium	0.0003	0.0003	0.0003
Cerium	0.0001	0.0001	0.0001
Neptunium	(b)	0.0008	0.0008
Plutonium	(b)	(b)	0.0003
Uranium	(b)	(b)	0.0003

(a) Heated 24 minutes in air at 1200 C

(b) Not analyzed

Releases of ruthenium greater than shown in Table XIV were obtained in tests using trace irradiated metal under conditions where the uranium was completely oxidized.[27] The percent of the uranium oxidation in 24 minutes at 1200 C increased from 69 ± 4 percent at 10^{14} to 92 ± 4 percent at 4×10^{20} nvt, with all the increase occurring at irradiation levels about 10^{18} nvt. From these last two observations it is concluded that the 50-fold increase in release of ruthenium and molybdenum is chiefly an oxidation effect rather than a result of high irradiation level.

Three series of tests were made at different temperatures: 1000, 1200 and 1440 C. The results for 1000 and 1440 C showed similar "burnup effects" to those at 1200 C.

Rare gases were found to be released as a burst from highly irradiated specimens at the time the uranium melted. Trace-level specimens continued to release xenon during the entire heating period. The difference is believed to be caused by the formation of small bubbles of gas at intergranular defect points during the relatively long in-reactor period required for the highly irradiated metal. These bubbles coalesced and migrated to the surface as soon as the specimen was liquified. At trace irradiation levels, in the order of 10^{14} nvt, the concentration of xenon is about one atom per 10^{10} uranium atoms. At this extremely dilute concentration, formation of bubbles is improbable during the very short irradiation period required. Rare gas atoms probably escaped from the uranium by the relatively slow process of atomic diffusion and uranium oxidation.

Special Fission Product Release Studies - Shipping Hazards - D. L. Reid, R. K. Hilliard, and L. F. Coleman

The percent release of purified Sr^{89+90}, $Ce^{141+144}$, and Cs^{137} from their respective chemical shipping forms is presented for postulated accidental firing conditions. Some particle size, density, and solubility information is also presented for evaluating hazards resulting from explosions or inundation in a river.

The shipment of large quantities of purified radionuclides involves a potential accidental release of the material in a form readily available to the biota. Abbreviated studies directly related to shipment of three radionuclides were made in support of hazards evaluations associated with accidental firing, spilling, explosion or water immersion of the material enroute. Strontium-89 + 90 carbonate,[28] sodium cerous-141 + 144 sulfate,[29] and Decalso-adsorbed Cs^{137} [30] were the three materials of interest. A minimal number of tests were made to supply information not available in the literature. There was no lengthy exploration of variables in order to refine the data or to confirm our understanding of the controlling phenomena.

The materials tested for all three shipments were simulated products [redacted]

TABLE XV

PERCENT RELEASE OF RADIONUCLIDES
FROM SIMULATED PRODUCT MATERIAL AT ELEVATED TEMPERATURES

Test Conditions	Atmosphere and Flow	Cesium-Decalso	Strontium Carbonate	Sodium-Cerous Sulfate			
		Cs	Sr	Ce	Ru	Zr-Nb	Sr
Programed temperature increase to 1500 C in 2 hours	He 0.15 mph	0.31					
	Air 0.15 mph	0.25	0.05				
Programed temperature increase to 1450 C in 1 hour plus 1 hour at 1450 C	Air 0.15 mph			0.02	0.3	0.02	0.34
Isothermal at 1350 C for 2 hours	He 0.15 mph	0.73		0.005	0.4	0.1	0.004
	Air 0.15 mph	0.35	0.14	0.005	0.5	0.1	0.03
Room temperature	Air 0.15 mph		0.05				
	Air 1.23 mph		0.7				
	Air 2 mph			<0.0002	<0.09	<0.006	0.006

Micromeritics

The Deposition of Particles in Circular Ducts Due to Thermal Gradients - A. K. Postma and L. C. Schwendiman

Particulates carried in a gas stream may be deposited on the walls of the conduit by forces resulting from thermal gradients. An analysis has been made of thermal deposition based on a simplified model, and an equation derived which expresses the resulting change in particulate concentration. For 0.1 μ particles moving in a conduit with a 150 C difference between gas and the ambient temperature, about 8 percent will be lost to the walls. The conclusion is reached that in most particulate sampling arrangements thermal deposition will be minor.

Particles may deposit on the walls of a conduit as a result of various mechanisms such as turbulent impaction, gravitation, electrical precipitation and from forces caused by thermal gradients. A knowledge of the magnitude of particle removal to walls is important in establishing the transport efficiency of a conduit used in sampling, or in determining the likelihood of radioactive particle build-up in ducts.[31, 32]

The purpose of this study was to develop a simplified model of, and to derive equations for, aerosol deposition on a conduit wall caused by temperature difference between the carrier and the surroundings near the conduit.

We propose a model which assumes a central region in the conduit of constant temperature, and a laminar sublayer near the tube wall through which a temperature gradient exists. We assume the temperature distribution in the sublayer to be that postulated by the Reynolds analogy.[33] For flowing fluids with Prandtl numbers near unity the velocity and temperature distributions will be the same.[34] With these assumptions a heat balance equation was written and, with substitutions of equivalent terms, we arrived at the following expression for the temperature gradient across the laminar sublayer in terms of measurable variables:

$$-\frac{\partial T}{\partial r} = \frac{\mathrm{Re}\, f\,(T_o - T_w)e^{-\frac{2fX}{d_w}}}{2d_w}, \qquad (13)$$

in which

T = absolute temperature of gas at the point in question,
r = radial distance from conduit centerline to point in question,
Re = Reynolds number,
f = Fanning friction factor,
T_o = inlet temperature, K,
T_w = wall temperature, K,
X = distance along conduit to point in question,
d_w = diameter of the conduit.

A particle in a thermal gradient of $\frac{\partial T}{\partial r}$ will move with a velocity, U_{tr}, given by

$$U_{tr} = -\frac{3\mu K_g K_m}{2(K_g + K_p)\rho T}\frac{\partial T}{\partial r} \qquad (14)$$

(see Reference 32).

in which

μ = gas viscosity,
K_g = gas thermal conductivity
K_m = Cunningham's correction for Stokes's law,
K_p = particle thermal conductivity,
ρ = gas density.

Substituting (13) in (14) yields an expression,

$$U_{tr} = \frac{3f\mu K_g K_m \mathrm{Re}\,(T_o - T_w)e^{-\frac{2fX}{dw}}}{4(2K_g + K_p)\rho\, T\, d_w} \qquad (15)$$

Using the expression for U_{tr}, we can write a material balance equation for the particles entering, leaving, and deposited in a differential element of the conduit.

An expression is then derived for the change in particle concentration:

$$\frac{C_\infty}{C_o} = \exp\left[-\frac{3K_g K_m (T_o - T_w)}{2(2K_g + K_p)T_w}\right]. \qquad (16)$$

C_∞ is the particle concentration after the aerosol has passed through an infinitely long conduit; C_o, the entering concentration. When $\frac{X}{d_w}$ equals about 100, the concentration becomes C_∞ for all practical purposes.

As an example of the significance of thermal deposition, we calculated the ratio $\frac{C_\infty}{C_o}$ for a 150 C temperature difference and for 0.1 μ particles. For these conditions about 8 percent of the particles would be deposited in the first 8 feet of the conduit. Since the assumed conditions in the example may be regarded as an extreme case, we conclude that thermal deposition in the usual sampling line will be negligible in most practical situations.

REFERENCES

1. Reisenauer, A. E. A Procedure for Estimating Capacity of a Ground Disposal Facility for Radioactive Waste, HW-57897. May 4, 1959.
2. Rhodes, D. W. and J. L. Nelson. Disposal of Radioactive Liquid Wastes from the Uranium Recovery Plant, HW-54721. June 3, 1957.
3. Tompkins, R. W. and S. W. Mayer. "Ion Exchange as a Separations Method. Parts III and IV," JACS 69: 2859-2874. 1947.
4. Hiester, N. K. and T. Vermeulen. "Saturation Performance of Ion-Exchange and Adsorption Columns," Chem. Eng. Prog. 48: 505-516. 1952.
5. Vermeulen, T. and N. K. Hiester. "Ion-Exchange Chromatography of Trace Components," Ind. and Eng. Chem. 44: 636-651. 1952.
6. Glueckauf, E. "Principles of Operation of Ion-Exchange Columns," pp. 34-46. Ion Exchange and its Applications, London, Soc. Chem. Ind. 1955.
7. Glueckauf, E. "Theory of Chromatography, Part 9. The 'Theoretical Plate' Concept in Column Separations," Trans. Farady Soc., 51: 34-44. 1955.
8. Vermeulen, T. "Separation by Adsorption Methods," Adv. in Chem. Eng. 2: 147-208. 1958.
9. Ames, L. L., Jr. "Some Cation Substitutions During Formation of Phosphorite from Calcite," Econ. Geol. 55: 354-362. 1960.
10. Latimer, W. M. The Oxidation States of the Elements and Their Potentials in Aqueous Solutions. Prentice-Hall. 1952.
11. Ames, L. L., Jr. The Removal of the "Bone-Seeking" Group of Radioisotopes from Solution by a Calcite-Phosphate Reaction. HW-60412. June 1, 1959.
12. Reisenauer, A. E. and L. L. Ames, Jr. Removal and Recovery of Plutonium from 234-5 Building Sump Waste with Phosphate Rock, HW-70041. June 16, 1961.
13. Ewing, R. E. The Origin of Certain Radioisotopes in Hanford Reactor Cooling Water - Interim Report, HW-49485. April 24, 1957. (SECRET).
14. Hall, R. B. Personal communication. June 11, 1958.
15. Nelson, I. C.,(ed). . Evaluation of Radiological Conditions in the Vicinity of Hanford, April - June, 1961, HW-70552. August 15, 1961.
16. Bensen, D. W. Mineral Adsorption of Radionuclides in Reactor Effluent, HW-69225. April 6, 1961.
17. Church, T. G. "Formation of Radioactive Surface Films on Minerals," Canadian J. Res. 28(a): 164-167. 1950.

18. Nash, V. "An Experimental Investigation on the Surface Reactions of Feldspars," Doctoral Dissertion Series No. 14,965. University Microfilms, Ann Arbor, Michigan. 1955.

19. Sato, M. "Oxidation of Sulfide Ore Bodies, II. Oxidation Mechanisms of Sulfide Minerals at 25°C," Econ. Geol. 55(6): 1202-1231. 1960.

20. Silker, W. B. The Decontamination of Reactor Cooling Water with Aluminum, HW-59029. January 28, 1959. (CONFIDENTIAL).

21. Nelson, R. W. "In-Place Measurement of Permeability in Heterogeneous Media. I. Theory of a Proposed Method," J. Geophys. Res. 65: 1753-1758. 1960.

22. Nelson, R. W. "Theory for In-Place Measurement of Permeability in Heterogeneous Media," Research and Development Activities in the Radiological Sciences - Physical Sciences Portion - January Through December, 1960, HW-70050. January 16, 1961.

23. Nelson, R. W. "In-Place Measurement of Permeability in Heterogeneous Media. II. Experimental and Computational Considerations," J. Geophys. Res. 66: 2469-2478. 1961.

24. Nelson, R. W. Steady Darcian Transport of Fluids in Heterogeneous Partially Saturated Porous Media - Part 1 - Mathematical and Numerical Formulation, HW-72335 PT1. January 16, 1962.

25. Nelson, R. W. "Comparison of Theoretical and Experimental Analysis of Partially Saturated Flow," Research and Development Activities in the Radiological Sciences - Physical Sciences Portion - January Through December, 1960, HW-70050. January 16, 1961.

26. Nelson, R. W. and A. E. Reisenauer. Hanford Studies on Flow in Porous Media, HW-SA-2251. August 10, 1961.

27. Hilliard, R. K., C. E. Linderoth and A. J. Scott. "Fission Product Release from Overheated Uranium - A Laboratory Study," Health Physics 7: 1-10. December, 1961.

28. Reid, D. L., R. K. Hilliard, and L. F. Coleman. The Release of Radiostrontium from Strontium Carbonate, HW-69692. June 1, 1961.

29. Junkins, R. L., D. L. Reid, E. C. Watson, and L. L. Zahn. The Consequences of Accidental Releases During Shipment or Radioactive Cerium, HW-72163. To be published.

30. Hilliard, R. K. and D. L. Reid. The Release of Radiocesium from Decalso at Elevated Temperatures, HW-69274. April 20, 1961.

31. Postma, A. K. and L. C. Schwendiman. Studies in Micromeritics. I. Particle Deposition in Conduits as a Source of Error in Aerosol Sampling, HW-65308. May 12, 1960.

32. Postma, A. K. Studies in Micromeritics. II. The Deposition of Particles in Circular Conduits Due to Thermal Gradients, HW-70791. October 1, 1961.

33. Knudsen, J. G. and D. L. Katz. Fluid Dynamics and Heat Transfer, New York: McGraw-Hill Book Co. 1958.

34. McAdams, W. H. Heat Transmission, New York: McGraw-Hill Book Co. 1954.

INSTRUMENTATION

Contaminated Air Monitoring Techniques

A Coincidence-Count Alpha Particulate Air Monitor - M. O. Rankin D. P. Brown, W. G. Spear, and C. D. Boyne

Detection of the Pu^{239} maximum permissible air concentration (MPC)* of 2×10^{-12} μc/cc is complicated by varying background of natural alpha emitters. The air concentration of radon and thoron (and radioactive daughters) in particular, varies considerably with atmospheric conditions. Since 1 MPC of airborne Pu^{239} is only 4.44×10^{-6} dis/min/cc, it is necessary to integrate the activity on a fixed filter to obtain adequate measurement sensitivity. Radon and thoron (and radioactive daughters) are also collected on the filter, and at times their activity levels may accumulate to several hundred times the required detection level for Pu^{239}. An instrument was developed which can detect continuous airborne Pu^{239} concentrations of 2×10^{-11} μc/cc in less than 90 minutes and 2×10^{-12} μc/cc in less than 900 minutes. These detection levels can be obtained with background radon and thoron concentration levels exceeding 2×10^{-10} μc/cc. Coincidence counting techniques are used to compensate for background levels.

A scintillation detection instrument, using coincidence counting techniques, was developed to measure Pu^{239} air concentration levels. In the decay chain for radon, Radium C decays by beta emission to Radium C', which decays by alpha emission with a half-life of 163 μsec; in the similar thoron chain, Thorium C decays by beta emission to Thorium C', which decays by alpha emission with a half-life of 0.3 μsec. Delayed coincidence-counting techniques are used to identify counts due to radon or thoron decay, and these counts are subtracted from a total alpha count to provide a measurement of airborne Pu^{239}.

The system block diagram is shown in Figure 1 and a photograph of the instrument in Figure 2. Airborne particulates are collected at a 15 CFM rate through a 5-inch diameter filter. The alpha and beta activities

---

* Handbook 69, Maximum Permissible Body Burdens and Maximum Permissible Concentrations of Radionuclides in Air and in Water for Occupational Exposure, U. S. Department of Commerce, June 1959.

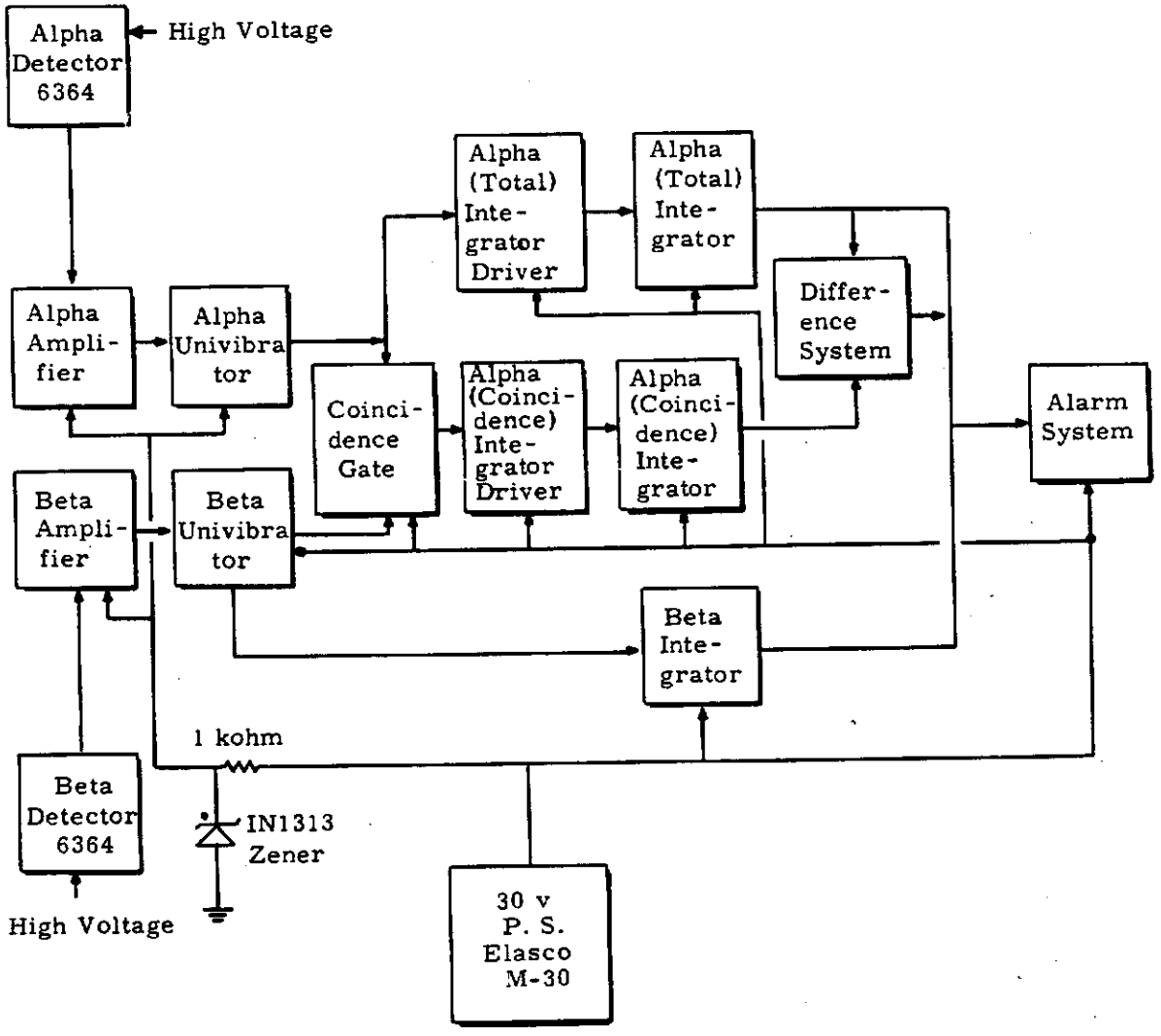

FIGURE 1

Block Diagram Coincidence Alpha Air Monitor

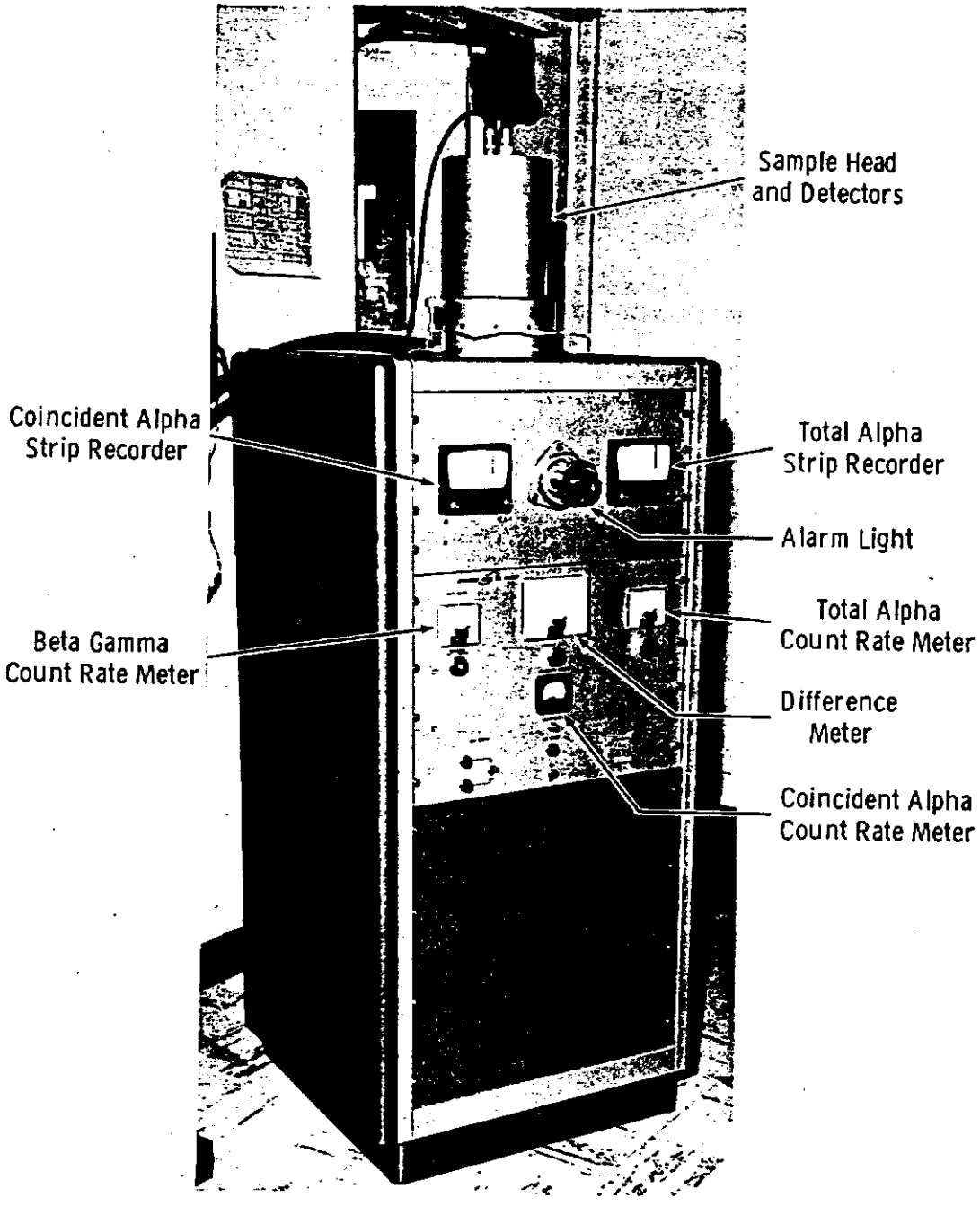

FIGURE 2

Coincidence-Count Alpha Particulate Air Monitor

are measured by two (5-inch diameter) scintillation detectors. After amplification, discrimination, and pulse shaping, the beta pulses open a gate for about 200 μsec. If an alpha pulse appears during the time the gate is open, the event is counted as a coincidence event.

Since the ratio of the total alpha count rate to coincidence count rate is about 8 to 1, the sensitivities of the two count rate meters are adjusted to have this same ratio. Thus, during periods when there is no airborne Pu^{239} present, the difference between the two meters is essentially zero. If Pu^{239} alpha activity is present, a difference signal is sensed by a meter-relay. This activates an alarm through appropriate circuitry.

The following table shows the results obtained with the laboratory experimental system which has now operated satisfactorily for about 4 months:

TABLE I

Airborne Concentration Pu^{239}, μc/cc	Alarm Time, min
2×10^{-9}	0.9
2×10^{-10}	9
2×10^{-11}	90
2×10^{-12}	900

At present a field model is being fabricated for use in the various Hanford plant buildings. Most of the circuitry used in the instrument is transistorized.

A Radionuclide Cell Exhaust Monitoring System - M. O. Rankin

An instrument was developed to sample and monitor filtered hot cell exhaust gases for radioactive particles. The system will alarm in less than 19 minutes if the airborne concentrations of mixed fission product beta emitters in the stack exhaust exceed 6.2×10^{-9} μc/cc or if alpha emitter concentrations exceed 1.2×10^{-11} μc/cc. For a particular installation in Hanford's Radiochemistry Building, continuous exhaust activity at the above concentrations will cause an alarm before the total activity released from the exhaust exceeds 1.8×10^{-4} curies for mixed fission products and 5.6×10^{-7} curies for alpha emitters.

Aerosols of uranium, plutonium, and americium radionuclides were considered the possible airborne alpha hazards, with plutonium the most important of these.

During atmospheric temperature inversions, alpha activity from natural radon and thoron and radioactive daughters is deposited on the filter. To provide better sensitivity, a system was developed to compensate for this varying background. Previous tests showed that the maximum total deposition from natural radioactivity on a 4- x 4-inch filter with 5 cfm flow does not exceed 10,000 dis/min alpha activity; the maximum rate of buildup on the filter from such radon and thoron air concentrations, using the sampling rate, does not exceed 3700 dis/min/hr. The alpha monitor portion of the developed system alarms when the total deposition exceeds 10,000 dis/min or when the buildup rate exceeds 3700 dis/min/hr for more than 10 minutes. A block diagram of the complete system is shown in Figure 3, and a photograph of the electronics system is shown in Figure 4.

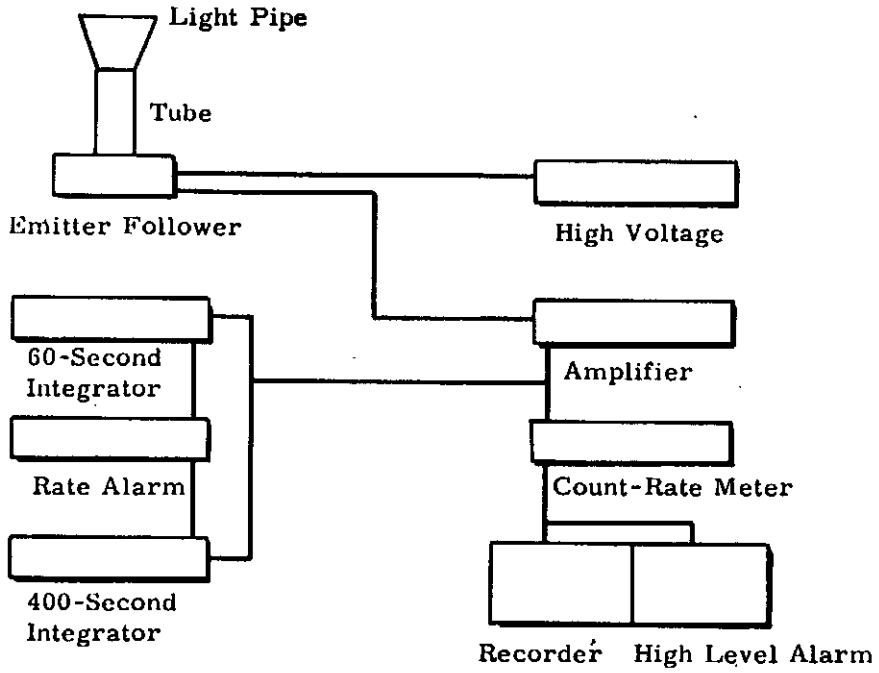

ALPHA CHANNEL

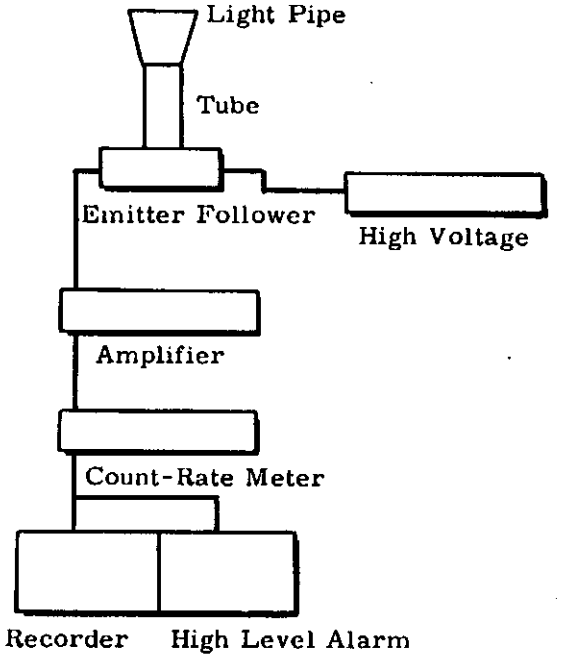

BETA CHANNEL

FIGURE 3

A Radionuclide Cell Exhaust Monitor

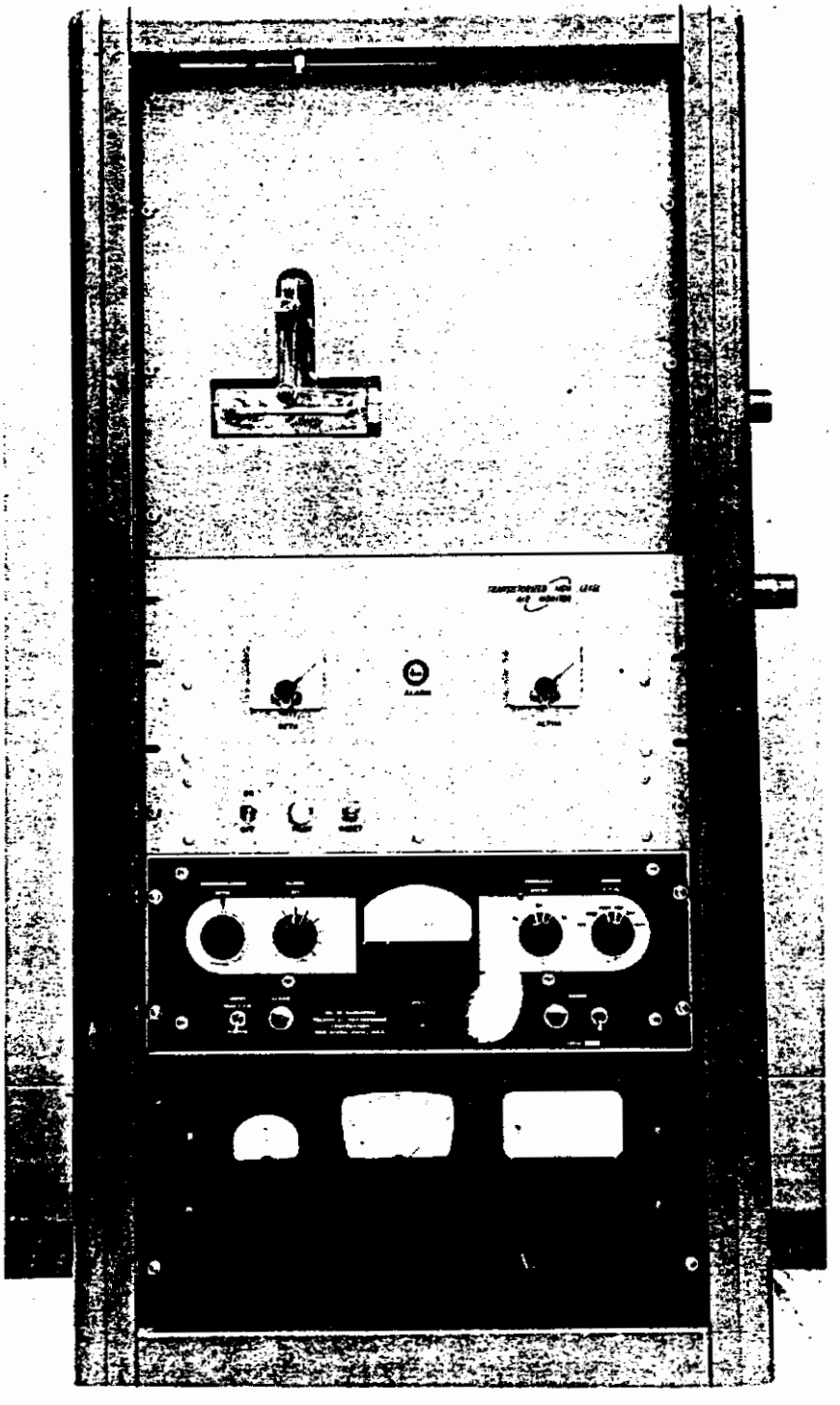

FIGURE 5

A Radionuclide Cell Exhaust Monitoring System

Filter-collected alpha emitters cause scintillations in the silver-activated ZnS attached to the 4- x 4-inch Lucite light pipe. The light photons emitted from the phosphor strike the phototube cathode to produce photoelectrons. Subsequent phototube current amplification, by a multiple secondary emission process, results in the production of electrical pulses which are amplified to drive transistorized and modified vacuum tube count-rate meters. The modified count rate meter has two integrating circuits with different time constants to average the incoming signal pulse rate. The faster integrating circuit has a 60-second time constant sufficient to reduce meter fluctuations caused by low-rate signals but which permits the meter to easily follow a generally increasing or decreasing signal rate. The other integrating circuit has a time constant of 400 seconds. Since the two integrating circuit time constants are different, a changing input pulse rate causes current, which is proportional to the rate of change of the input signal, to flow in the interconnected contact meter relay. If the rate of change current exceeds a preset level, the alarm is energized. In addition to the foregoing, the alpha-caused pulses drive a transistorized count rate meter which drives a chart recorder and activates another alarm called a High Level or Gross Alpha Alarm.

All mixed fission product radionuclides were considered as possible airborne beta-gamma hazards. All are beta as well as gamma emitters with average beta energies ranging from 0.07 to 0.99 Mev. A 0.125-inch-thick terphenyl-in-polyvinyltoluene organic detector was found to provide the best sensitivity for these beta energies. This approach provides the best signal-to-background ratio with the least lead shielding surrounding the detector.

The detector is attached to the 4- x 4-inch Lucite light pipe which in turn is optically coupled to the phototube. As with the alpha channel, the phototube-produced pulses are amplified to drive a count rate meter and a second recorder. Contribution from natural background beta emitters deposited on the filter and from the surrounding gamma background cause

a maximum meter reading of 5000 counts/min, which is one-half full scale. The unit is designed to alarm when the count rate exceeds 10,000 counts/min or full-scale. Calculated average beta detection efficiency is about 5 percent; therefore, 10,000 counts/min, or twice background, is equivalent to a contamination level of 1×10^5 dis/min on one-half of the filter.

The detection sensitivity values are shown in Table II.

TABLE II

Air-Borne Concentration at Sampling Point curies/cubic centimeter	Alarm Time minutes	Total Emission Before Alarm* curies
Alpha		
2×10^{-17}	1500	8.7×10^{-6}
2×10^{-16}	10	5.66×10^{-7}
2×10^{-15}	1.5	8.5×10^{-7}
Beta		
1×10^{-15}	645	1.82×10^{-4}
1×10^{-14}	64.5	1.82×10^{-4}
1×10^{-13}	6.45	1.82×10^{-4}

* For the particular air sample flow rates used in a system installation for the High Level Cells of the Radiochemistry (325-A) Building.

Medium Level Continuous Alpha Air Monitor - M. O. Rankin

A scintillation alpha air monitor was developed and fabricated which will alarm in 10 minutes if the detection head is exposed to a continuous Pu^{239} airborne concentration of 2×10^{-10} μc/cc, and will alarm in 1.5 minutes for a concentration of 2×10^{-8} μc/cc.

This article was published in complete detail in the following journal: Health Physics, Pergamon Press, 1961, Volume 4, pp. 293-311.

Biology Support Instrumentation

Self-Powered Radiation Monitor and Analyzer - D. P. Brown and E. M. Sheen

A radiation monitor and analyzer instrument was developed and fabricated to aid in field studies conducted by the Hanford Biology Operation. This instrument includes detectors, circuitry, and readout for general radiation monitoring for alpha-, beta-, gamma-emitting radionuclides, and it also includes both a pulse height selector circuit for gamma energy analysis and a scaler. Several special detector probes were developed and fabricated for use with the instrument. The instrument incorporates a rechargeable battery, which permits at least 40 hours of continuous operation and a method for direct 110 VAC line use. Total power drain is approximately 2.8 watts.

Radioecology studies by the Hanford Laboratories Biology Operation required a portable instrument suitable for general radiation monitoring for various alpha-, beta-, and gamma-emitting radionuclides and for gamma energy analysis. The developed instrument provides these features with both count-rate meter and scaler presentation of data. It can be powered with an incorporated rechargeable battery in the field, or be operated from the line in the laboratory. This instrument will be used in field studies both at Hanford and in Alaska for Project Chariot.

All circuitry is solid state for low power dissipation and reliable operations. Circuits include preamplifiers, a linear amplifier, pulse height selector, count-rate meter, scaler, basic power supply with automatic battery recharger, and a blocking oscillator-corona regulated 1000 v DC-DC converter. The complete block diagram is shown in Figure 5.

The main amplifier consists of three common emitter stages followed by a conventional emitter follower output. The amplifier, designed for negative input pulses, has a voltage gain of approximately 250 with a linearity of ± 6 percent for output pulses from 0 to 10 volts. The gain stability is

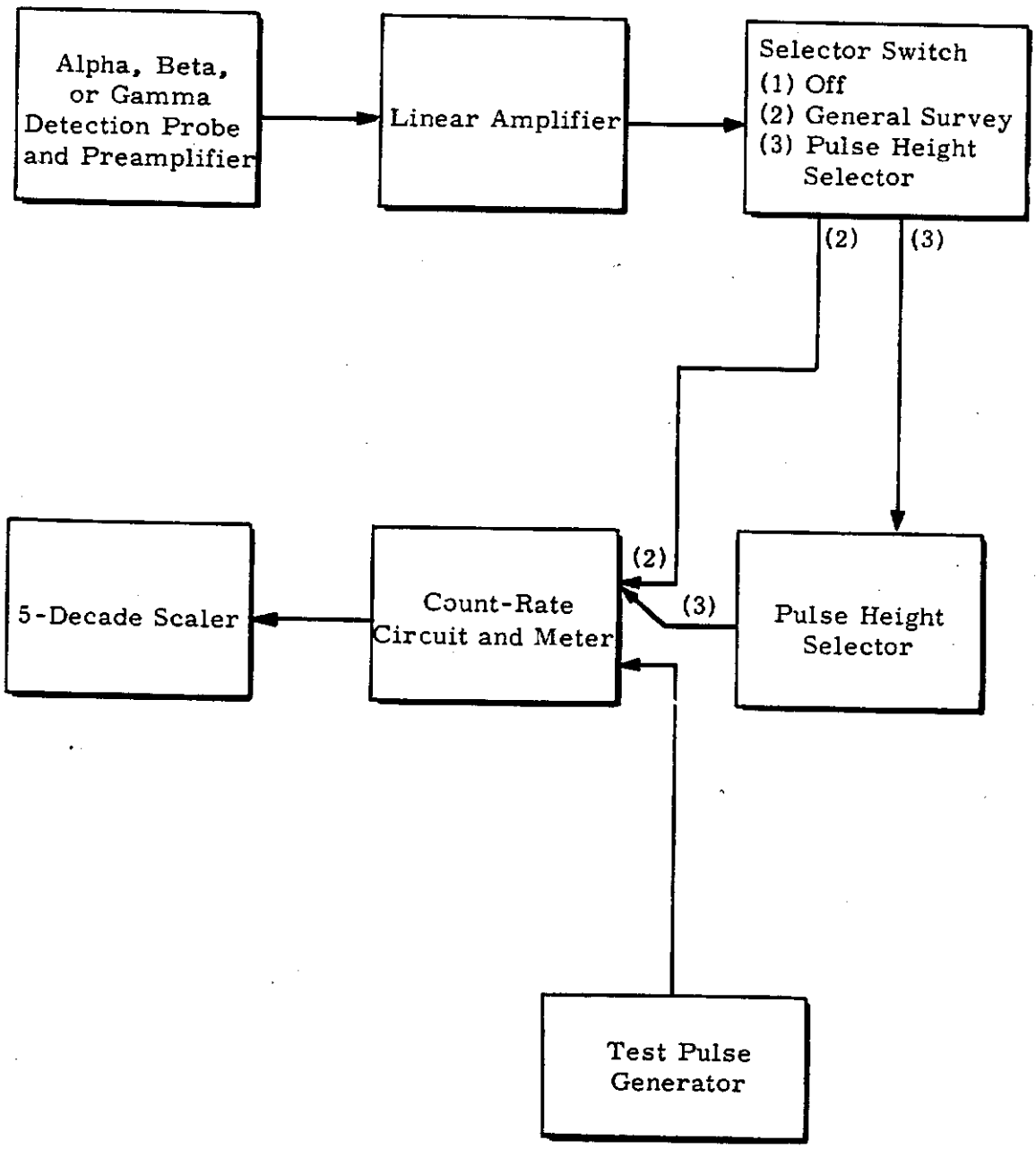

FIGURE 5

Block Diagram of the System

± 1 percent from 0 to 150 F. The first two stages form a voltage feedback amplifier with a low operating voltage for low-noise operation. The pulse height selector uses the switching action of tunnel diodes. Biasing a tunnel diode, which is connected in the switching mode, to currents below the intersection of the load line and the peak current point of the tunnel diode will result in a device which acts as a switch for pulses above a given height. A diode biased to a low value of current will require a larger pulse to cause switching than one biased to a higher current. This effect happens because switching occurs when the load line is raised above the I_p value of the tunnel diode, and a diode that is biased higher than another does not require as much additional current from a pulse to reach the switching level. By using two parallel-driven tunnel diodes in the switching mode, with one biased slightly lower than the other, a larger pulse will be required to switch both diodes than to switch only the diode with the larger bias current. The signals from the two diodes are coupled to a logic gate which produces a signal if the first tunnel diode has an output but not if both diodes have output signals. In the foregoing manner, the logic for a pulse height selector was developed.

Transistorized test pulse generator and count-rate circuits are included in the instrument. The test pulse generator is a General Electric Unijunction transistor oscillator for a pulse rate of 100 pulses/sec. This pulse generator is not intended to give a pulse rate of high stability but is to be used to check the scaler and count-rate meter for proper operation prior to instrument field use. A two transistor count-rate meter circuit is used. The circuit is a monostable multivibrator with three selectable ranges of 0 to 1000, 0 to 10,000, and 0 to 100,000 counts/min. Full rate on each range drives the 100 microampere meter full scale and the meter stays off-scale and the meter stays off-scale for an input rate of 5×10^6 counts/min or 50 times full scale on the highest range. The main selector switch changes the count-rate circuit to drive the scaler with a 5 microsecond pulse, disconnects the count-rate meter from the circuit, discharges the meter time

constant capacitor, and energizes the scaler by applying B+ voltage. The amplifier pulses or pulse height analyzer pulses, depending upong selector switch position, are applied to the base of an inverter transistor which inverts the positive main amplifier output voltage pulses to drive the count-rate circuit. The scaler consists of five solid-state decades with transistor drivers between decades. The circuit was designed to operate from 12 volts DC and a meter indication was developed to conserve power for portable operation. Total power dissipation is about 200 mw/decade. The meters offer the advantage of being readable in bright sunlight whereas miniature neon or incandescent lamps are not. The transistor decade circuit uses binary-quinary logic and will operate at a 150 kc/sec rate. The scaler indicates the total count on five meters on the front panel. Each meter scale is marked in steps from zero to nine and the meters are labeled units, tens, etc. Each scaler meter is short-circuited when the selector switch is in the "off" position to damp the meter during movement of the instrument. The high voltage supply is a single transistor blocking oscillator, corona-regulated type, used in HAPO portable instruments. The circuit was modified to operate from a B+ voltage supply instead of the B- normally used. Other circuits, such as a reset pulse generator for the scalers and several low voltage power supplies are incorporated.

Various types of scintillation detector probes can be used with the instrument and the same high voltage and input connectors are used with all probes. Transistor preamplifiers are included in the beta-gamma probes to drive the connecting cable.

The gamma and beta probes are shown in Figure 6. The lead-shielded gamma probe includes a 2 x 2-inch NaI and phototube integral assembly.* This assembly is mounted in a 6.5-inch diameter by 10-inch-long aluminum container along with a 1.5-inch-thick lead shield. The assembly is shock mounted and thermally insulated with foam rubber.

---

* Integral NaI and phototube, Type 8S8, Harshaw Chemical Company, Cleveland, Ohio.

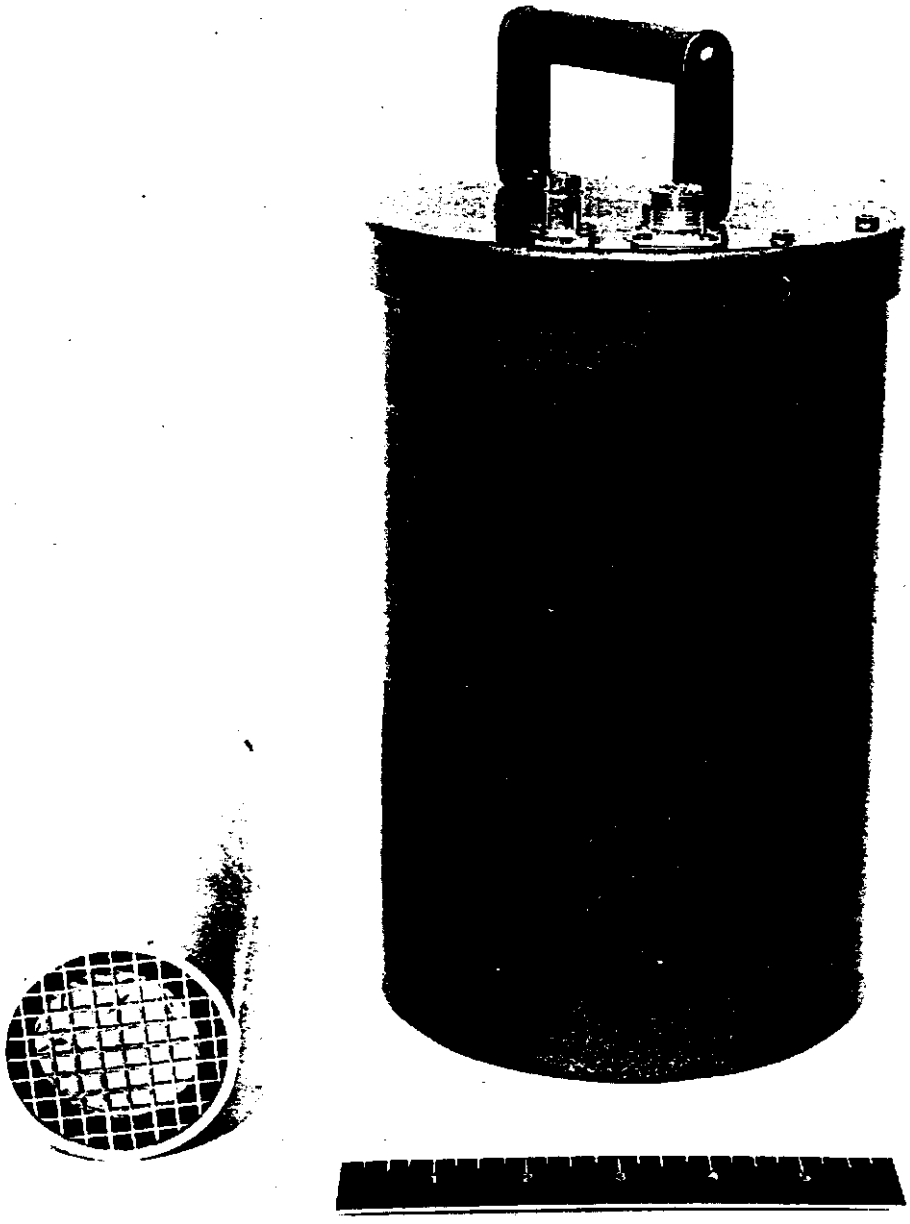

FIGURE 6

Mesh-Protected Beta Probe and Lead-Shielded Gamma Detection-Probe

The beta probes utilize 0.125-inch-thick by 2-inch diameter terphenyl-in-polyvinyltoluene* scintillators optically coupled to RCA-6655A phototubes. Two layers of 0.9 mg/cm^2 double-aluminum coated Mylar cover the scintillator. The beta detector assembly is contained in an aluminum tube housing 2.5 inches in diameter by 9 inches long. A transistor preamplifier is included in the base of the probe to drive the connecting cable.

A miniature beta probe was also fabricated. It uses a 0.125-inch diameter x 4-inch-long polished quartz light pipe to optically couple a 0.125- x 0.125-inch-long NE-102 scintillator to an RCA 6199 phototube. Several types of previously developed scintillation alpha detecting probes, which are now in standard use at Hanford, can also be used.(1)

The complete instrument shown in Figure 7 requires only 2.8 watts of power for operation and will operate continuously for 40 hours on the included rechargeable nickel-cadmium battery. During 110 VAC line operation, the battery is automatically recharged. The instrument weighs 35 pounds and will operate properly in temperatures from less than 0 to +150F.

Dosimetry Instrumentation

Experimental Personnel Radiation Dosimeters - D. P. Brown and M. O. Rankin

Two experimental pocket-size radiation dosimeters were developed. One alarms audibly after a predetermined dose has been accumulated. The second provides digital indication of the received dose on a miniature register. Each uses a modified pencil ionization chamber as the basic detector, and both are adaptable to radiotelemetry methods of information transfer.

The dosimeter which audibly alarms is shown in block diagram form In Figure 8 and in a photograph in Figure 9. With a modified standard pencil

---

* NE-102 Scintillator, Nuclear Enterprises, Ltd., Winnipeg, Canada

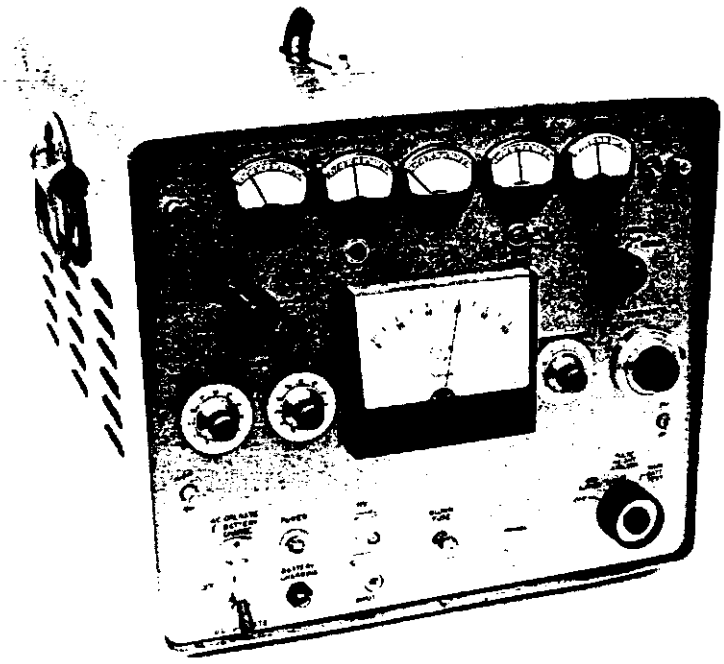

FIGURE 7

The Self-Powered Radiation Monitor and Analyzer

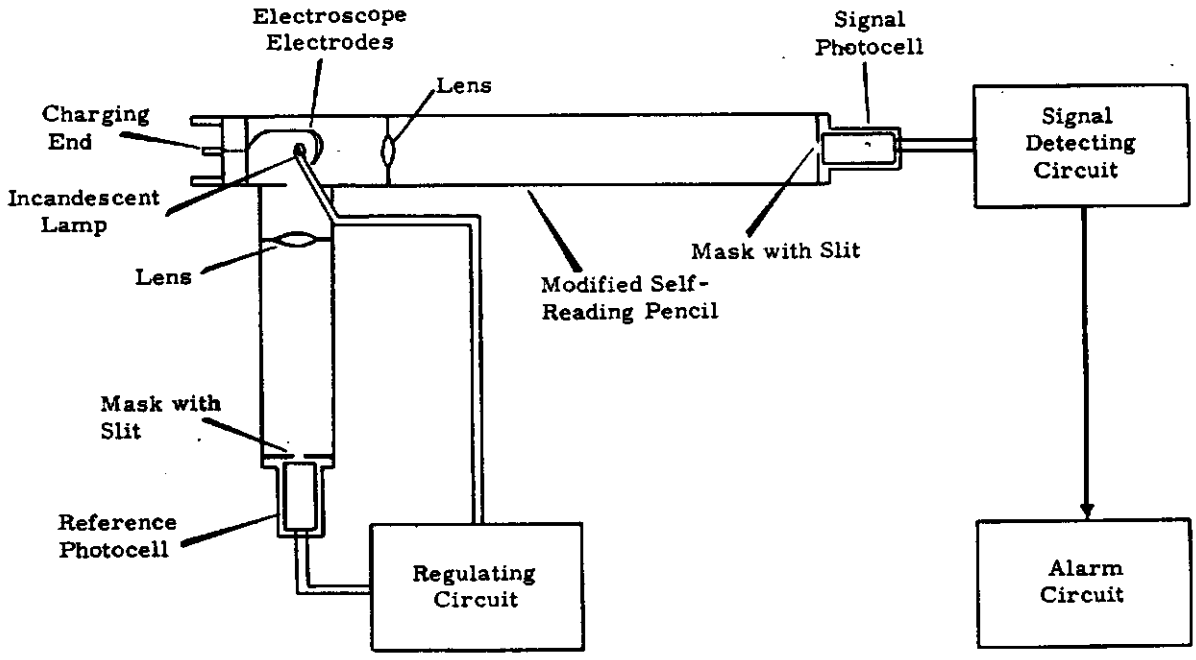

FIGURE 8

Block Diagram of Alarming Type Pocket Radiation Dosimeter

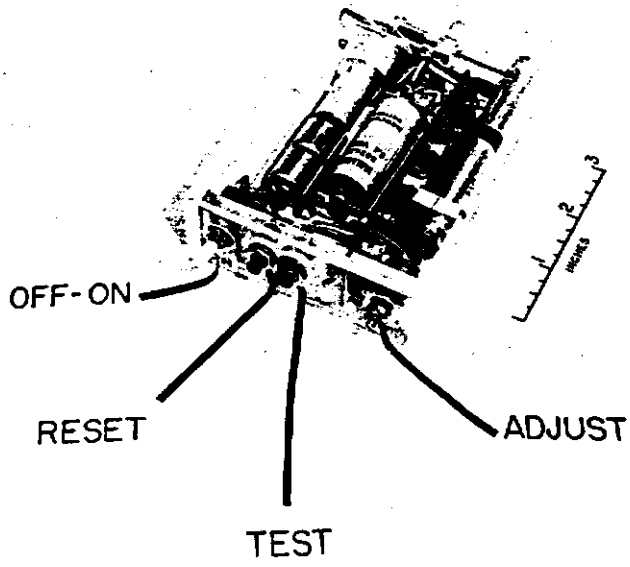

FIGURE 9

Experimental Personnel Radiation Dosimeters

dosimeter, the range of alarm point settings is 0 to 200 milliroentgens; however, with different pencils, this range can extend to 600 roentgens. The sensor modifications include an illuminated quartz fiber, an optical system with slit, and a CdSe light detector. By proper charging with a standard pencil dosimeter charger, the unit can be adjusted to provide a suitable signal from the CdSe cell after the predetermined dose is exceeded. The cell signal drives transistorized circuitry for alarming and a second light sensor is included for temperature compensation. For the 0 to 200 milliroentgen ionization chamber, the alarm point can be adjusted for any level from 10 to 200 milliroentgens. The accumulated dose can be read out at any time with a standard charger-reader.

Operational tests on the experimental model indicate that continuous operation battery life is greater than 60 hours. Fail-safe features incorporated into the design include an audible alarm when the voltage of either of the small batteries falls below a preselected level or when the lamp fails.

The third battery, which is used only as a power supply for the alarm, is tested automatically each time the unit is energized.

The second experimental dosimeter also uses a pencil ionization chamber sensor which has been modified to permit automatic recharging.(2) The pencil has been divided into two sections separated by an insulating holder. The upper section is the sensing chamber and the lower section is an electrostatic shield. A 1 mm diameter graphite coated quartz rod and an 8-micron diameter conducting quartz fiber are arranged in an assembly inside the electrostatic shield. The quartz rod extends up into the sensing chamber. The normal resting position of the fiber is about 1 mm from one rod. When a potential is applied between the fiber contact and the chamber wall, the chamber will charge by causing the fiber to move to the rod by electrostatic forces; thus, the circuit will be completed from the battery to the rod. The rod and the fiber are at the same potential and the fiber will return to its resting position as the rod collects charge due to ionizing radiation since the rod and fiber will develop a difference of potential to cause the fiber to gradually approach the rod. When the fiber touches the rod, the rod will be automatically recharged and the cycle will repeat.

During the recharging a pulse is produced which is amplified by a transistor amplifier to drive a miniature register incorporated in the instrument. This pulse can also activate associated telemetry circuitry. The instrument circuit is shown in Figure 10 and the laboratory model instrument is shown in Figure 11.

The source of energy for the recharge cycle is capacitor C shown in Figure 10. This capacitor, which is charged by a suitable battery, will store enough energy for continuous operation over an 8-hour (one shift) period.

Figure 12 shows a response curve for various dose rates. As shown on the curve, the maximum field application rate is about 4 r/hr. This limiting rate is determined by the register drive circuit time constant. With

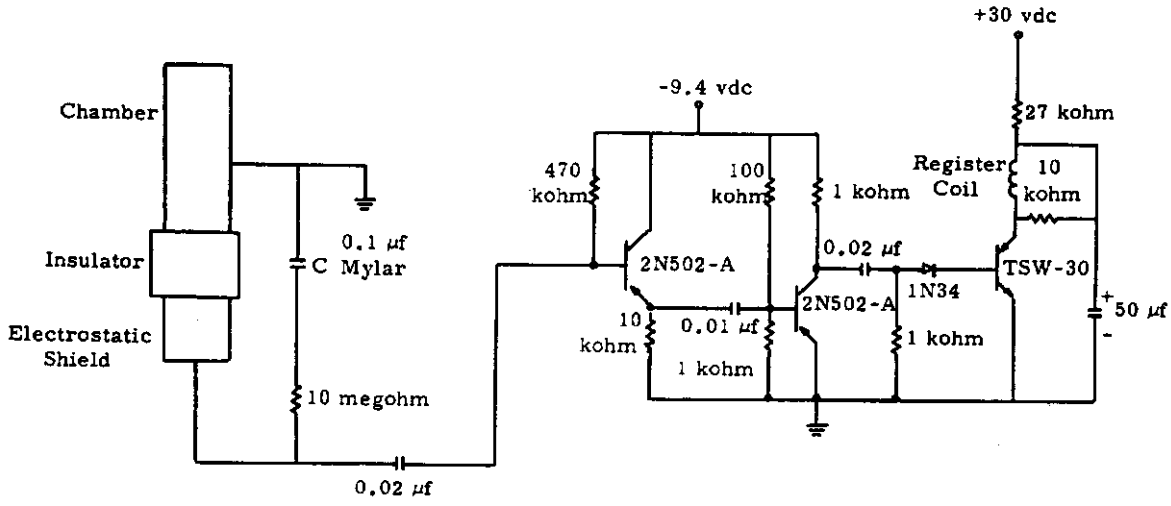

FIGURE 10

Circuit For Register-Indicating Pocket Dosimeter

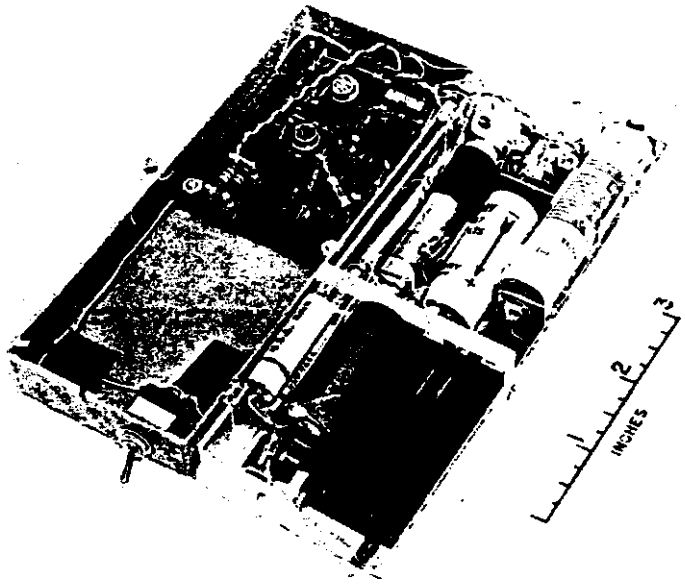

FIGURE 11

Miniature Dosimeter With Register Readout

a different register circuit, this maximum rate could be extended. The included circuit batteries will operate the instrument for about 50 hours.

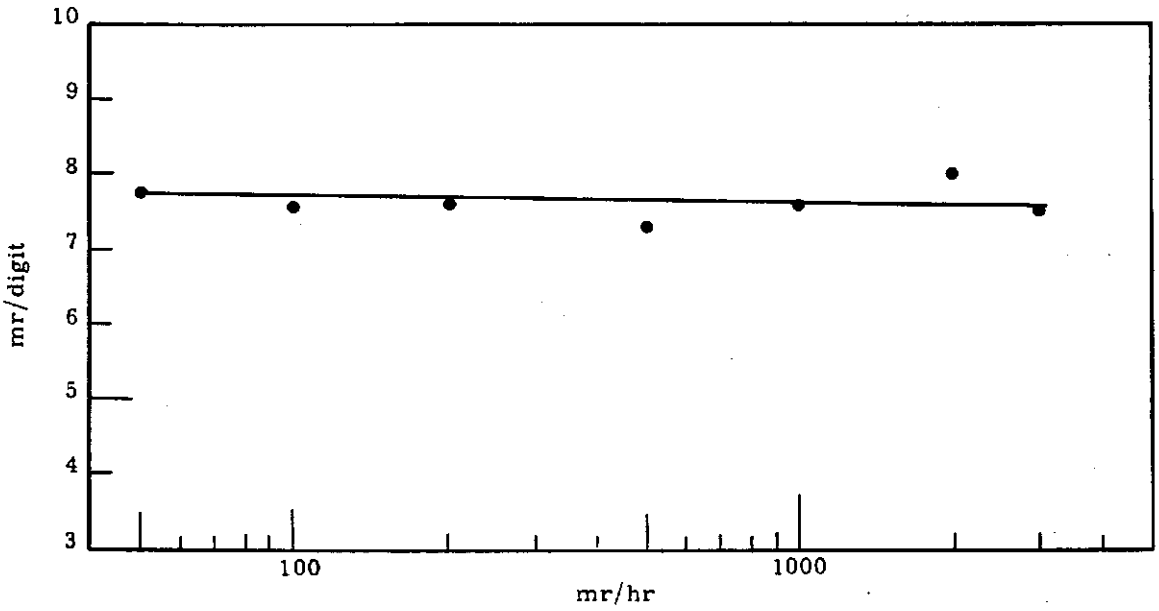

FIGURE 12

Milliroentgens Per Hour

Both of these dosimeter units are still in the laboratory experimental stage. Further circuit development work is planned to improve the performance and reliability. In addition, circuitry is being developed to permit either unit to be used for direct radiotelemetry of accumulated dose information to a suitable central station. Bids are being solicited for commercial fabrication of six of the units for field testing.

Thermoluminescent Dosimeters Proposed Band Structure of CaF_2:Mn

D. E. Hegberg and H. A. Treibs

Interest in the optical properties of CaF_2:Mn arose during research on use of this material for thermoluminescent dosimeters. Transmission absorption spectra were obtained from phosphor crystals taken directly from the melt and ground to 10 to 100 micron size particles. This report describes a method which has been used to obtain high resolution transmission absorption spectra from polycrystalline CaF_2Mn, and discusses the spectra in terms of band structure. Measurements were made for wavelengths from 200 to 700 mμ.

A 3 percent mole weight of ammonium manganous fluoride was introduced into the fluorite lattice of prepared CaF_2. The mixture was fired in a platinum dish at about 1000 C in a high vacuum (10^{-6} mm mercury). The phosphor was cooled slowly from 1000 C to room temperature in about one hour and kept in an evacuated glass dessicator using anhydrous $CaSO_4$ as a dessicant. The phosphor, ground to fine particle size, was exposed several times directly to the air at room temperature for no more than several minutes. Absorption spectra were measured with a Model 12M Cary Recording Spectrophotometer, Applied Physics Corporation.

Samples were prepared by milling the phosphor with Dow-Corning DC-200 fluid (10^6 centistokes viscosity). The mixture was placed between two plates of optically clear quartz, 1/16-inch thick with a 0.030 inch shim of black polytetrafluoroethylene determining cell thickness. The high viscosity of the suspending fluid prevents excessive settling of the phosphor. The cells were wrapped in aluminum foil to avoid light exposure between measurements. The Dow-Corning DC-200 fluid exhibits little obsorption in the visible region and no serious absorption in the ultraviolet at wavelengths greater than about 215 mμ (Figure 13). The spectrum for DC-200 is subtracted from the combined CaF_2:Mn–DC-200 spectra. A cell containing only DC-200 fluid was used in the spectrophotometer reference beam. Results of typical measurements are shown in Figure 14.

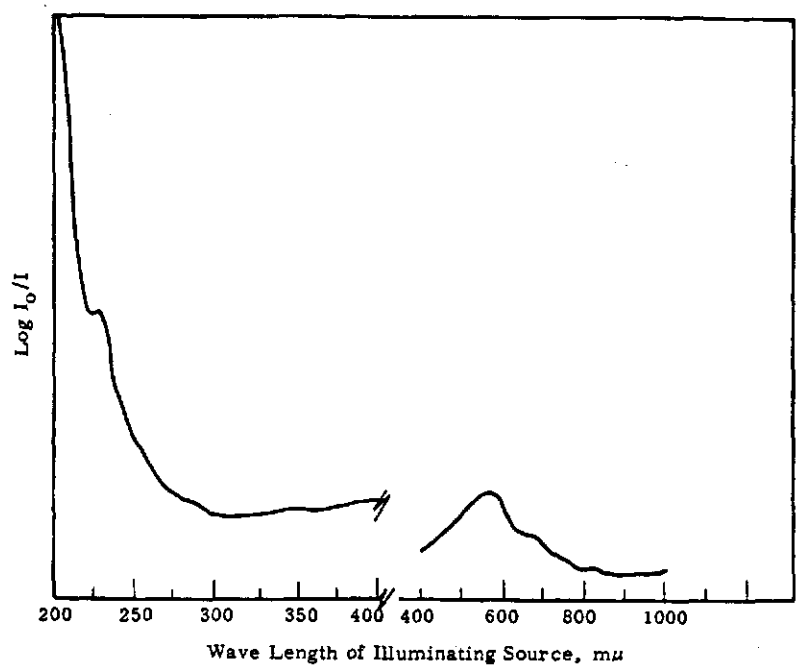

FIGURE 13

Calibration of DC 200 and 2/16-Inch Optically Pure Quartz Versus Air in Cary Recording Spectrometer

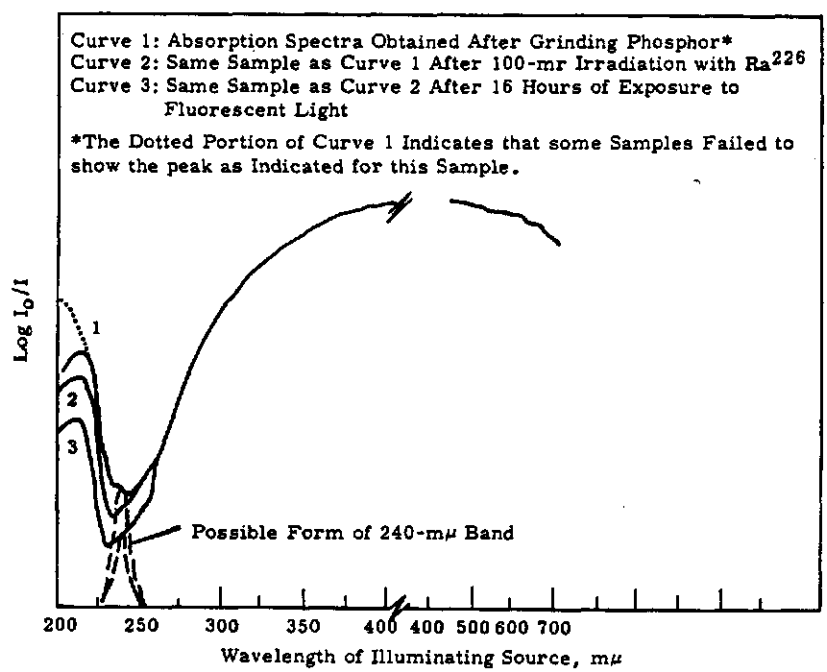

FIGURE 14

Absorption Spectra of CaF_2:Mn Obtained at Room Temperature (20C)

Sample grinding caused electron traps to be filled with valence electrons, and this effect produced a thermoluminescence response equivalent to a Ra^{226} gamma dose of several roentgens. In addition, the DC-200 is a strong absorber of secondary electrons produced in the glass slides by the gamma irradiation. The obtained spectra appear to resemble an F center absorption band at 450 mμ, and V center bands at 215 and 240 mμ. Some doubt is cast on the location of the absorption band at 215 mμ as this is very near the ultraviolet cut off of the DC-200 fluid. Bonfiglioli, Bruoutetto, and Cortese published a paper describing the emission and absorption spectra of thermoluminescent phosphors to which the reader is referred for details.(3)

We propose that the observed 215 mμ band is due to the Mn activator which is present in the fluorite lattice predominantly as interstitial divalent manganese. The ability of Mn^{+2} to accept the hole produced in the valence band and subsequently trapped at an F center depends upon the strong affinity of fluorine atoms for electrons, the relative ease of stripping electrons from divalent manganese, and the mobility of the electron holes in the fluorite lattice. Once Mn^{+2} has lost an electron to the valence band, this ion has become an electron acceptor with an associated narrow and localized energy band (Z bands) which should show absorption characteristics to radiation of suitable wavelength.

The strong F-center like band at 450 mμ is postulated as due to the increase in negative ion vacancies which frequently occurs when a stoichiometric excess of an ion is present and conditions are conducive to crystal growth. The concentration of the Mn^{+2} activator suggests close donor or F center and acceptor sites, and it is possible that the trapped electrons and holes interact to form excitons, which are free to migrate over the crystal domain and remove electrons from traps by energy transfer.

The small absorption band at 240 mμ could be a type of Z center, a V center, or a combination thereof. Dislocations corresponding to the 240 mμ band may have an effect similar to manganic acceptors in forming mobile

excitons. The ease of bleaching the 240 mμ band centers suggests these as a mode of losing trapped electrons. In terms of the proposed mechanisms and experimental data, the band structure of CaF_2:Mn has been sketched in Figure 15. The forbidden energy gap was approximated by a value of 9.48 ev (132 mμ) corresponding to optically pure CaF_2. The first absorption band of natural fluorite has been measured as about 10 ev or 124 mμ.

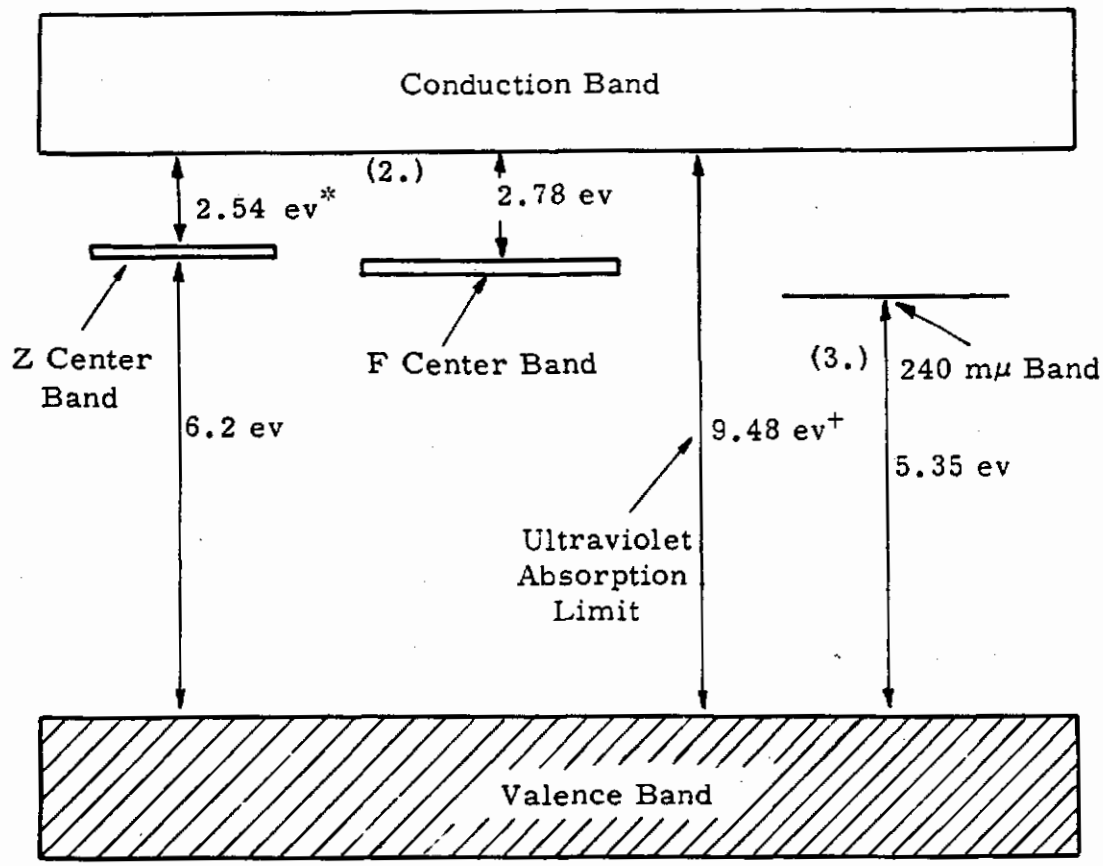

FIGURE 15

Proposed Band Structure of CaF_2:Mn

Radiation Detector Development

Solid State Surface Barrier Diode Detectors - E. M. Sheen

Experimental solid state surface barrier detectors were fabricated from 1100 ohm-centimeter single crystal silicon. The method used in fabricating the detectors is described and the experimental results obtained from typical detectors are given. The best detectors gave energy resolutions for 5 Mev alphas of 1.4 percent for 3.1 cm^2 area diodes and 0.9 percent for 1 cm^2 area diodes expressed in terms of the full peak width at half-maximum height. Several experimental diodes have been applied to portable alpha survey instrument use.

Twenty-five experimental silicon surface barrier diode charged-particle detectors were fabricated with sensitive areas ranging from 0.25 cm^2 to 3.1 cm^2.

The methods used in fabricating the diodes were similar to those used by Blankenship and Borkowski;[4] however, the Hanford method avoided reactions between the etching chemicals and the potting compound by potting the detector after etching and used epoxy material instead of coil dope for protection of the diode edges. This method provided a larger number of useful diodes from each batch of cut wafers.

For the Hanford diode preparation, silicon ingots of 1100 ohm-cm resistivity (n-type) were sliced to wafers of 0.050 inch thickness using a diamond-impregnated steel abrasive disc with distilled water as a lubricant and coolant. The wafers were lapped with 600 grit silicon carbide, thoroughly washed with distilled water and nickel plated using the standard electroless method.[5] A silver plated copper wire was soldered to one side of the wafer to form an ohmic contact. The nickel on the face opposite the ohmic contact was stripped with HNO_3, and this side was lapped with 800 mesh silicon carbide in a water slurry until a fine matte finish was obtained. After thoroughly washing the wafer in running distilled water, the nickel-stripped face of the wafer was etched with CP-4* until a smooth

* CP-4 Solution: 5 parts (Vol.) Concentrated HNO_3; 3 parts Vol. 49.6% HF: 3 parts glacial acetic acid; 10 drops of Bromine for each 50 cc of solution.

specular surface was obtained. The wafer was then potted in Ciba "Araldite" epon resin number 502 with the edges of the etched silicon covered to reduce surface leakage current across the edges of the space charge region. A thin layer of gold (50 to 100 $\mu g/cm^2$) was deposited by vacuum evaporation onto the entire surface of the assembly, thus covering the silicon and plastic with a conductive sheet and making an electrical connection to the brass ring or case. Stable diode characteristics were obtained by permitting the detector to remain in laboratory ambient conditions for 3 days.

A diode holder was designed to minimize handling during the potting process, and to provide a rugged mount for eventual use in portable radiation monitoring instruments. Figure 16 shows 3.1 and 1.0 cm^2 diodes mounted in brass holders. After the diodes were aged in the laboratory for more than 3 days, the reverse current characteristics were checked. The 1 megohm resistor was placed in series to limit the current when the knee of the back resistance was reached. During the checking procedure, care was used to prevent illumination of the surface of the diode since light greatly increases the reverse current. In counting applications where the diode would be exposed to light, a light shield of 0.9 mg/cm^2 double-aluminum coated Mylar* is applied over the gold covered face of the diode. For alpha energy analysis, the diode is used in a light-tight evacuated housing so that no extra Mylar light shield is needed.

Table III shows the experimental results obtained from nine detectors with sensitive areas of 3.1, 1.8, 1.7, and 1.0 cm^2. The resolutions obtained with a number of the diodes, especially the large area units, were better than for commercial units at the time of the experimental work.

An experimental alpha survey monitor utilizing a 1.8 cm^2 area diode detector is shown in Figure 17. The transistorized instrument is compact and has a triggered tone generator and resonant air column aural output.

---

* Wakefield Industries, Skokie, Illinois

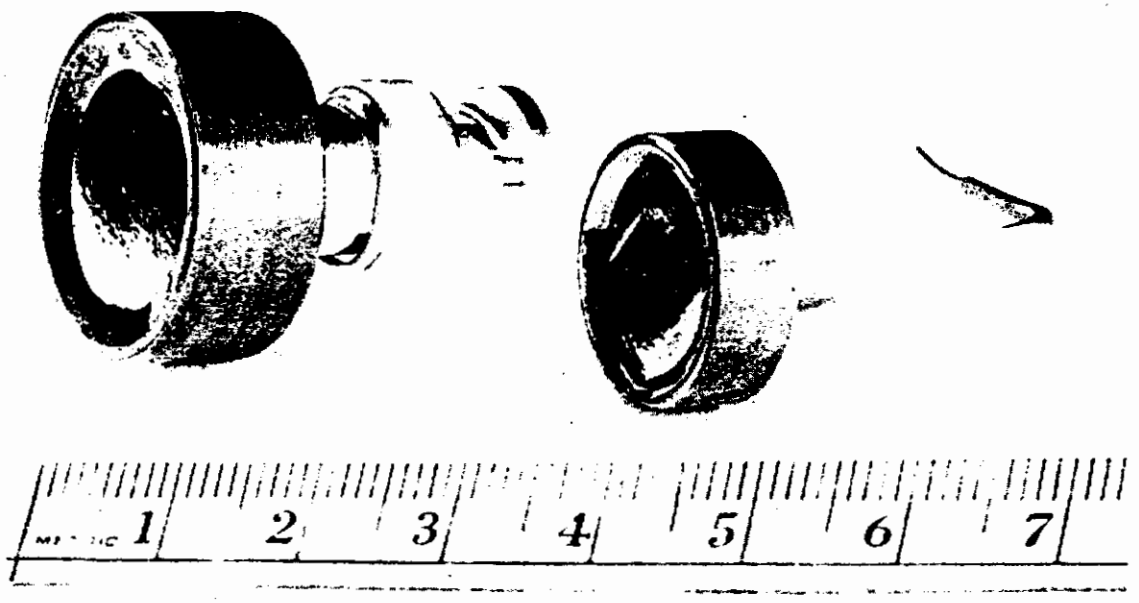

FIGURE 16

One- and Three-Square cm Experimental Detectors

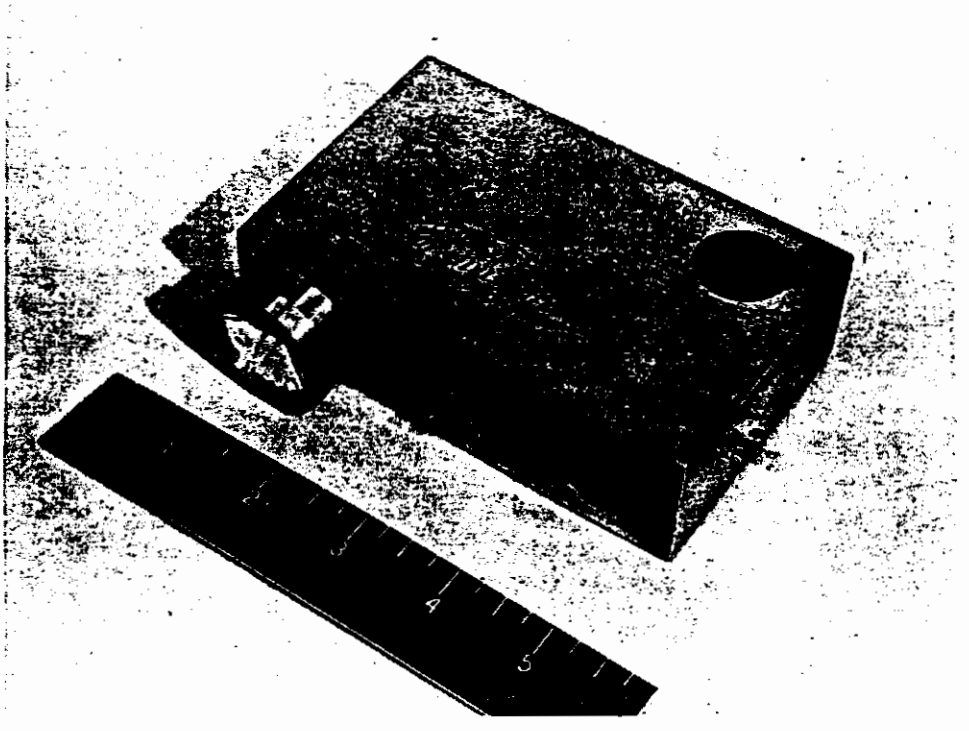

FIGURE 17

Experimental Alpha Monitor Utilizing Surface Barrier Detectors

TABLE III

OBTAINED EXPERIMENTAL DATA

Number of Diode	Dimensions (Area-Effective)	Time Etched in Minutes	Lap Grain Size	Reverse Current in Microamperes at Various Bias Voltages					Percentage Resolution for 5.15 Mev Alphas at Various Bias Voltages			Percentage Resolution for 5.48 Mev Alphas at Various Bias Voltages		
				3 VDC	6 VDC	9 VDC	16.5 VDC	22.5 VDC	10 VDC	20 VDC	30 VDC	10 VDC	20 VDC	30 VDC
1	3.1 cm^2	6	600	0.2	0.2	0.4	0.7	1.1	1.8	2.1	- -	1.8	2.1	- -
2	3.1 cm^2	- -	600											
3	3.1 cm^2	5	800		0.1	0.2	0.2	0.5	2.0	1.7	1.8	2.1	1.9	1.9
4	3.1 cm^2	15-18	800	0.1	0.1	0.1	0.2	0.2	2.0	- -	1.4	1.9	1.5	1.6
5	1.8 cm^2	5	800	0.2	3	4	0.5	0.6	2.1	3.7	- -	2.5	3.2	- -
6	1.7 cm^2	4	800	0.6	1.0	1.4	2.1	2.6	2.3	1.7	1.7	2.9	1.8	1.8
7	1 cm^2	4	800	0.1	0.1	0.2	0.3	0.4	1.1	1.1	1.2	1.1	1.0	1.2
8	1 cm^2	4	800	0.1	0.2	0.3	0.4	0.6	1.1	- -	- -	1.0	- -	- -
9	1 cm^2	3	800	0.1	0.2	0.2	0.3	0.3	0.0	0.9	- -	1.1	0.9	- -

Since a number of manufacturers are now selling quality silicon diodes of both the surface barrier and junction types, further Hanford experimental diode fabrication will be limited to applications with special requirements which cannot be met with standard commercial units.

Plutonium Wound Monitor - D. P. Brown

A monitor for detecting plutonium in wounds was developed, fabricated, and is in routine Hanford use. The instrument detects and counts the 17 kev X-rays from the imbedded Pu^{239}. The monitor can detect less than 1000 dis/min of Pu^{239} through 0.125 inch of Lucite or through an equivalent thickness of flesh. This depth corresponds to a typical puncture wound.

The detection of Pu^{239} in wounds was accomplished by counting the characteristic 17 kev X-rays. This was done with a 2-inch diameter by 1-mm thick NaI crystal and a multiplier phototube, an RCA-6655-A selected for low noise and a high signal to noise ratio. The detector probe is used with an amplifier and single channel pulse height analyzer adjusted to count the pulses resulting from the 17 kev X-rays. A scaler is used to indicate the number of counts received for the particular counting time. A count-rate-meter cannot be satisfactorily used because of the very low count-rates normally encountered.

The geometry, or counting efficiency, was measured to be 1 count/min from a 250 dis/min Pu^{239} source with a 0.125-inch thick Lucite plate between the detector and the source. The geometry was obtained with 850 VDC high voltage and a 3 kev window width centered at 17 kev on the single channel analyzer. With the 0.125-inch thick Lucite between source and detector, it is possible to determine, within 96 percent confidence limits, the presence of less than 1000 dis/min of Pu^{239} with a counting time of 10 minutes and a normal background counting rate of 6 counts/min.

A photograph of the complete monitor, which is in routine use at Hanford, is shown in Figure 18.

FIGURE 18

Plutonium Wound Monitor

General Radiological Monitor and Circuitry Development

An Area Radiation Monitor With Logarithmic and Linear Ranges - W. G. Spear

An area radiation monitor which incorporates both logarithmic and multidecade linear ranges was developed, and two experimental instruments have been thoroughly tested and evaluated for 9 months. One of the scintillation transistorized instruments has linear ranges of 0 to 10 mr/hr decaded to 0 to 10 r/hr and a logarithmic range from approximately 1 mr/hr to 10 r/hr. Other ranges, either more or less sensitive, can be incorporated by detector and/or calibration changes. The two prototypes performed satisfactorily under test conditions involving line voltage variation, vibration, temperature variation, accuracy, drift, and detector aging. The instruments have scintillation detectors, electromechanical choppers, transistorized amplifiers, meter readout, both low and high level adjustable alarming functions, and recorder driving capabilities. The detector can be connected to the main instrument through as much as 500 feet of inexpensive standard coaxial shielded cable. Calibration is not affected by the length of the interconnecting cables.

Each unit has a scintillation detector, cable length as desired, a chopper, a transistorized amplifier, meter readout, adjustable alarming circuitry, recorder driving capability, a high-voltage supply, and a low-voltage supply. The complete circuit diagram is shown in Figure 19. An RCA 6655-A phototube was used since it has a high gain and acceptable signal-to-noise ratio. An alternate phototube, which has exceptionally stable characteristics, is the EMI-9536-B. The RCA 6655-A noise level permits system operation to 60 C without difficulty at the high voltage employed. The high gain permits use of a thin detector of 0.062 to 0.125-inch-thick terphenyl-in-polyvinyltoluene.* This detector provides gamma energy response independence to ±10 percent from about 80 kev to 3 Mev with good response to less than 20 kev.(c) The detector is formed as a hollow hemisphere around a solid Lucite hemisphere to obtain a good 2π

* NE-102, Nuclear Enterprises, Ltd., Winnipeg, Canada

response. In addition, the light-shield weight of about 4 mg/cm^2 permits beta response if desired; however, for the typical application for gamma monitoring, the complete detector is enclosed in a sealed thin-wall aluminum housing.

The detector, cable, and main instrument are nonmicrophonic. The cables used with the prototype units are standard, inexpensive Amphenol RG-58 A/U, and the cables can be as much as 500 feet long without change of calibration or degradiation of system performance. The high-voltage supply is a simple half-wave rectifier, RC-filter, and corona-regulator type. Line voltage changes from 100 to 130 VAC and temperature extremes to +60 C cause no measurable high-voltage changes.

The calibration circuitry is simple. On any linear range, the high voltage to the phototube is merely adjusted as required for calibration. On the log range both high voltage and log diode adjustments are used. The two prototype instruments were calibrated for typical Hanford applications. One instrument was calibrated for linear ranges of 0 to 5 mr/hr (X-1) decaded to 0 to 5 r/hr (X-1000) with a corresponding log scale coverage, and the second was calibrated for 0 to 10 mr/hr decaded to 0 to 10 r/hr with similar log coverage. Other ranges can be calibrated as desired for any particular application by a simple reduction of the amount of scintillator or by a high-voltage change.

The general input circuitry includes the log diode, the chopper, and the various input adjustments. Phototube gain changes caused by high anode currents were essentially eliminated by using current-limiting series resistors in both the linear and log input circuits. The maximum phototube anode current possible on any linear range under any condition of dose-rate is in the order of 3×10^{-7} amperes. A similar situation exists for the log scale, which is current-limited to a maximum of about 5×10^{-6} amperes. For the log range on the 10 r/hr full scale instrument, the input current is only about 5×10^{-7} amperes for a dose-rate of 2 to 3 r/hr.

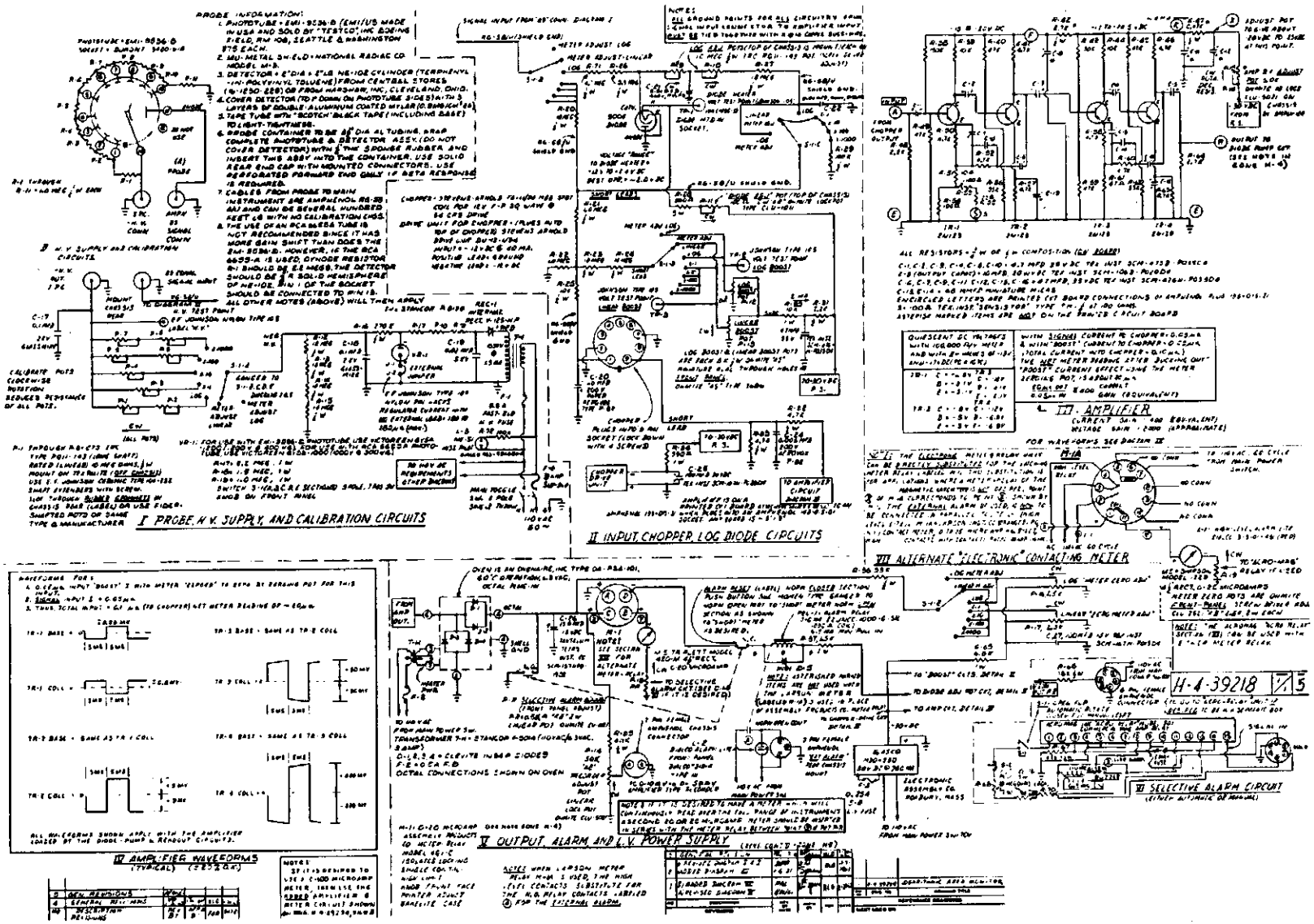

FIGURE 19

Linear and Logarithmic Area Monitor Diagram

A 9004 diode, which has an adjustable heater current obtained from the regulated -30 VDC power supply, was used to obtain the appropriate log scaling characteristic. Adjustment of the diode heater voltage, typically from -1.6 VDC to -2.2 VDC, and adjustment of the potentiometers provide the desired log characteristic. For the two prototype units, the log scale response was adjusted to be accurate to ± 20 percent from about 10 to 20 mr/hr to full scale values of 5 r/hr and 10 r/hr, respectively. The lower ends of the log curves, from 1 mr/hr to about 20 mr/hr, are compressed while retaining reasonable meter indication at these low levels.

The chopper is a commercial, electromechanical type driven at 94 cycles/second rate. Extensive experimentation and tests showed available semiconductor choppers to be too noisy and unreliable for use with the minimum signal levels of 10^{-9} to 10^{-8} amperes. The utilized chopper and pickup noise level is less than 10^{-10} amperes. The original test circuit chopper operated continuously for more than nine months without any change in noise level and without degradation of performance, and the choppers in the prototypes are still operating correctly after similar use.

The Linear Boost and Log Boost potentiometers, which are adjusted only during initial calibration, supply a small current to drive the output diode pump circuit to the correct operating point. Typical "boost" currents are 5×10^{-9} to 10^{-8} amperes to the chopper. Logically, such an operation slightly reduces the optimal signal-to-noise ratio; however, the over-all system performance is improved.

The transistor amplifier employs two feedback doublets in cascade. Decoupling is used in the supply voltage circuit between the two doublets. With the input and output resistors shown, the amplifier is stable with a voltage gain of about 2000 and an equivalent current gain of about 400. The maximum input signal voltage level is about 1 millivolt for an output of 2 to 3 volts. With the germanium transistors used, gain variation is less than ± 3 percent from 0 C to 60 C.

The diode pump circuit, driven by the amplifier, was selected as a convenient and inexpensive method of obtaining meter-driving current. As mentioned earlier, a selected level of input boost current is used for the linear and log ranges to raise the diodes to an appropriate operating point. The diode pump circuit is contained in an inexpensive thermostat-controlled oven rated 60 C and operated from the 110 VAC mains. The oven should be located away from the signal input circuitry to minimize noise pickup effects. Since the oven holds the diodes at + 60 C, temperature effects are nil to + 60 C and the oven is effective down to -20 C.

The meter circuit consists of either a 20 or 25 μa meter, a shunting capacitor, the recorder adjustment potentiometer, and a potentiometer used to drive a supplemental mag-amp relay. Circuit response time to 90 percent of final reading is 2 to 4 seconds. The meter-relay can be either a single high level latching type or one with two adjustable alarm level points of the nonlatching type. The nonlatching Larson contact meter has a transistor amplifier which is used to energize two integral spdt relays with contacts rated 10 amp at 110 VAC.* The two included relays provide low and high level adjustable alarm trips of the nonlatching type. Addenda relays can be used to supply latching alarm trips as desired.

The linear range and log range meter zeroing adjustment potentiometers compensate for pickup noise level and the input boost currents, and only the true detector signal effect is noted as an upscale meter reading. This zeroing can be checked and adjusted without calibration change, at any time by switching to either the Log Meter Adjust or the Linear Meter Adjust positions. Such switching removes the phototube high voltage; thus, effective instrument zeroing can be accomplished whether or not the probe is in a radiation field.

The addenda selective alarm circuit, which uses a modified commercial magnetic amplifier and transistor trip unit, is also shown.** Either

---

* Larson Instrument Company, Orangeburg, New York

** Model 301 "ACRO-RELAY", Acromag Company, Inc., Southfield, Michigan

automatic nonlatching or latching relay functions can be used. The alarm point can be set by adjusting the Selective Alarm Adjustment potentiometer and the adjustable alarm for this added unit can be any point from about 20 percent of full scale to full scale on any selected instrument range.

The two prototype instruments were thoroughly tested and evaluated over a 9-month period. The performance was found to be satisfactory for all tests. No components failed and no performance characteristics changed during the operational period. The multiplier phototubes continue to perform correctly, and long-term drift reading errors for the instruments have been less than ± 10 percent per month. In addition, the probes were test-operated at + 70 C with negligible degradation of performance and no permanent effects. As discussed, a wide variety of operating ranges, both linear and logarithmic or either type singly, can be used as desired for the particular application. In addition, a multiplicity of relaying and alarming functions, either latching or nonlatching as desired, can be obtained. Figure 20 shows a photograph of one complete system, including probe, main instrument, extra alarm-relay box, and a single point chart recorder.

A Recorder Driving Amplifier - J. L. Stringer

A transistorized operational amplifier was developed to drive a 1 ma type chart recorder from a 100 μa full scale count rate meter circuit. The linearity and gain stability of the amplifier-recorder combination is ±5 percent over a temperature range of 0 to + 150 F. The recorder response time (per movement) from 10 to 90 percent of full scale is 0.6 second. The required battery supply is ±9 VDC and the quiescent current drain is 5.2 ma total from both batteries. Full scale recorder deflection requires 6.2 ma from the positive battery. This instrument was developed for radiological survey work from boats, cars, and especially airplanes.

A recorder-driving transistor operational amplifier was developed and fabricated to drive a 1 ma Esterline-Angus chart recorder from a 100 μa full scale count-rate-meter. Previously, the instrument utilized

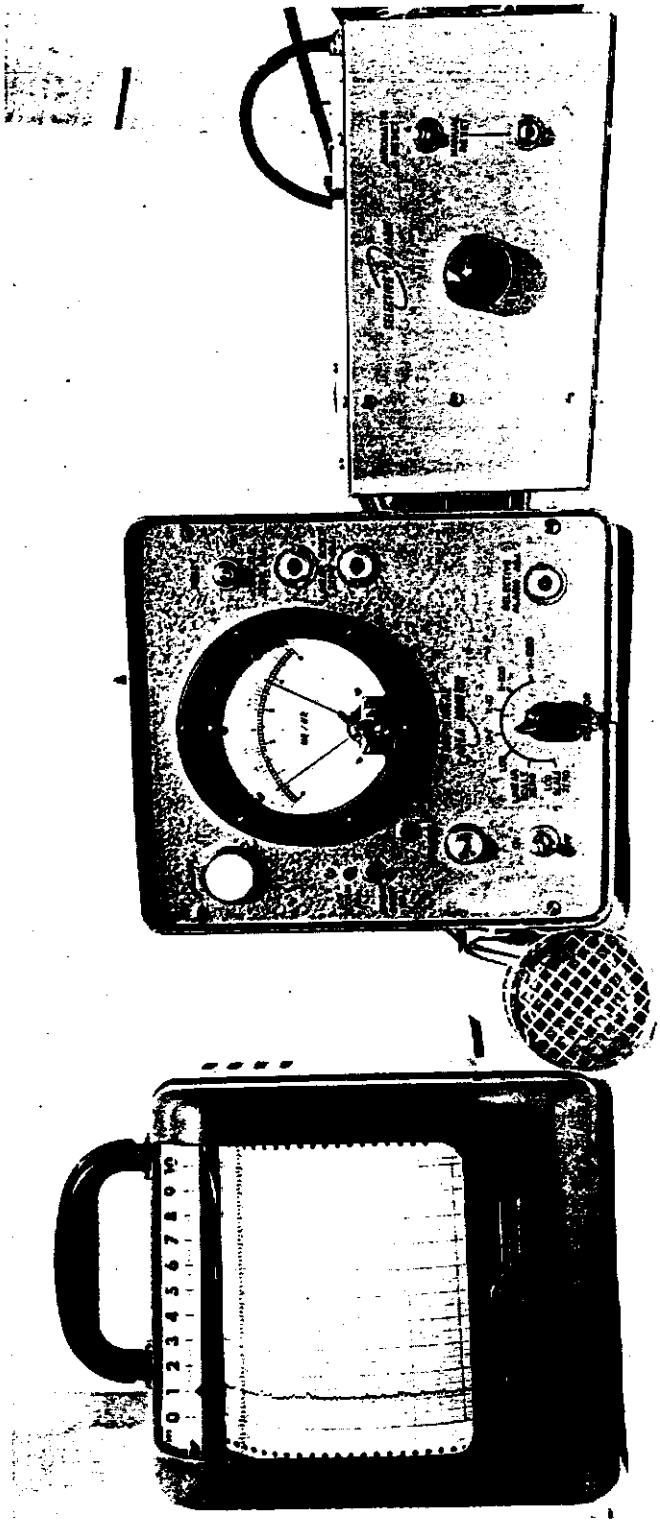

FIGURE 20

Complete Log and Linear Response Scintillation Area Monitor

a 1 ma count-rate-meter which drove the recorder directly; however, this method was poor due to slow combined recorder and circuit response. The Esterline-Angus 1 ma recorder has an inherent response time of 0.5 second when driven from a constant current source. Therefore, it was necessary to develop a circuit which would approach the constant current condition during a step input. The circuit also required linearity and stability of ±5 percent for temperatures from 0 to +150 F.

The final circuit is based on some previous experiments[7] and consists of the transistorized differentially-connected direct-coupled amplifier shown in Figure 21. Feedback is used to achieve linearity and stability and the positive and negative inputs are compared to produce an output error signal. Normally, the amplifier will use a resistive element in the feedback loop to obtain a fast response. In this case, however, the high inductance driving coil of the chart recorder is used as the feedback element. When a 0 to 100 percent current-step is applied to the positive input, a momentary maximum error signal is developed and the full amplifier output voltage of about 8.5 volts is applied to the recorder drive coil. As current starts flowing through the coil, the error signal reduces gradually over a 0.6 second period to zero. When a full scale to zero current-step is applied, the amplifier output goes to zero and the error signal is returned to zero through the 1 kohm resistor and diode D_2. The recorder coil stored energy is removed through the action of diode D_1, and the recorder pen moves toward zero as the energy is removed. The time required for the recorder to move fully down scale is about 0.8 second.

The gain control potentiometer, P-1, is adjusted to provide a full scale recorder deflection for a 100 μa input signal. The balance control potentiometer, P-2, is adjusted to provide a zero output voltage for no input signal. Fewer adjustments are required if the balance control potentiometer is adjusted first.

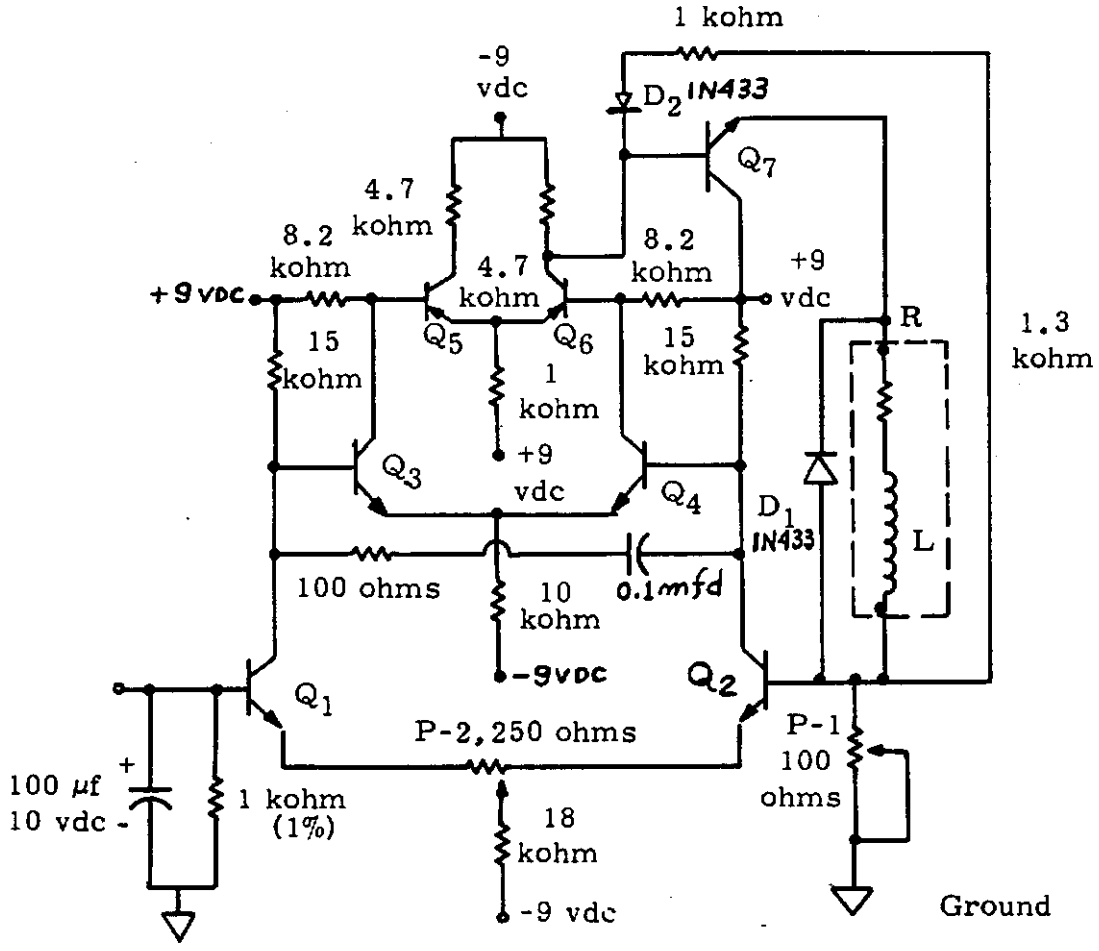

All Transistors Matched for Beta and Icbo

Q_1 and Q_2 - 2N338 Mounted in a Common Heat Sink
Q_3 and Q_4 - 2N337 Mounted in a Common Heat Sink
Q_5 and Q_6 - 2N43A Q_7 - 2N169A
P-1 Gain Control (Voltage) Carbon Pot
P-2 Balance Control Carbon Pot
R - Esterline - Angus 1-ma Recorder
L - Electrical and Mechanical Inductance ≈5000 Henries

FIGURE 21

Recorder-Driving Amplifier

The transistor amplifier consists of three direct-coupled differential stages with an output emitter follower, Q_7, used as a current amplifier. Transistors Q_1 and Q_2, Q_3 and Q_4, and Q_5 and Q_6 are pairs matched for beta values and for leakage currents over the operating current and voltage ranges required. Each matched pair is mounted on a common aluminum heat sink.

The integral linearity of the circuit was measured as ±1.2 percent at a constant temperature, and the gain stability was within ±5 percent over a 0 to 150 F temperature range. The short-term zero stability was within ±1 percent for 2 hours of continuous operation. The amplifier, which is incorporated in a transistorized aerial radiological survey instrument[8], has operated satisfactorily for 1 year and no maintenance, other than routine battery changes, has been required.

A Tunnel Diode Pulse Height Selector - D. P. Brown

A pulse height selector circuit using tunnel diodes was developed for use in both portable and line-operated radiological monitoring instruments. The circuit utilizes the switching characteristics of tunnel diode to form the logic for a pulse height selector. The circuit operates over a temperature range from 0 to +150 F and has a base line linearity of ±5 percent. Total power required is 130 mw.

Two parallel-driven tunnel diodes operating in the switching mode are used to develop the logic for a pulse height detector circuit. If one diode is biased slightly below the other, it will require a larger pulse to cause proper switching action; thus, for small pulses, neither diode switches and for larger pulses, both diodes switch. But the incoming signal pulse is of the proper magnitude, only one diode will switch. When either diode switches, a positive potential appears at its anode. By coupling these potentials to a gate circuit where one tunnel diode controls the gate and the other tunnel diode supplies the signal to be either passed or rejected, a gate pulse output is obtained only for the switching action of one tunnel diode. Thus, a particular signal pulse magnitude can be selected.

An input emitter-follower circuit, which includes a multi-turn potentiometer for back-bias adjustment, provides the required base-line set point or adjustment. The reference voltage circuit, used to supply the back-bias voltage, includes temperature compensation to compensate for change in the emitter-base forward voltage characteristic. With this circuit provision, a wide temperature operation range is possible. The determined limits are 0 to +150 F.

The complete circuit diagram is shown in Figure 22, and a graph of input pulse height versus base-line setting is shown in Figure 23. The linearity with base-line setting is better than ±5 percent as determined by precise pulse measurements. The complete system operates from +12 VDC and requires 130 mw of power. The small size and low power drain make the circuit suitable for portable battery-operated radiological instruments and for similar use in line-operated transistorized instruments.

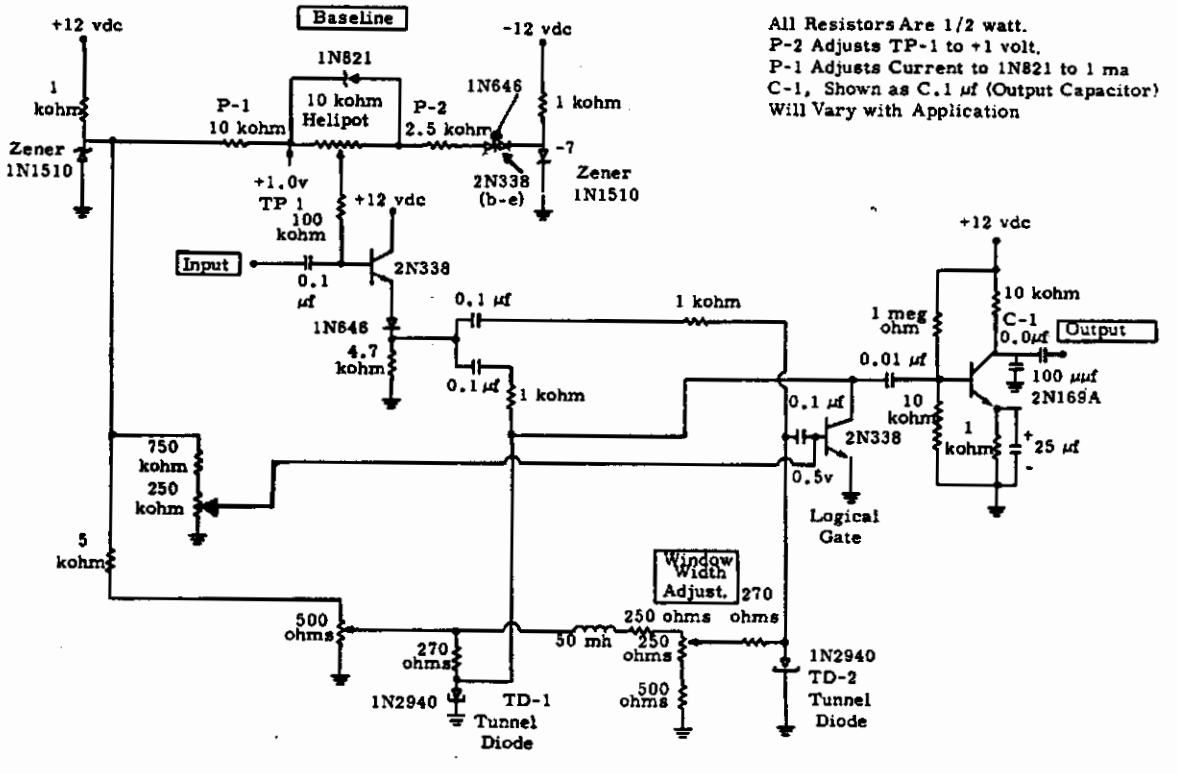

FIGURE 22

Circuit Diagram

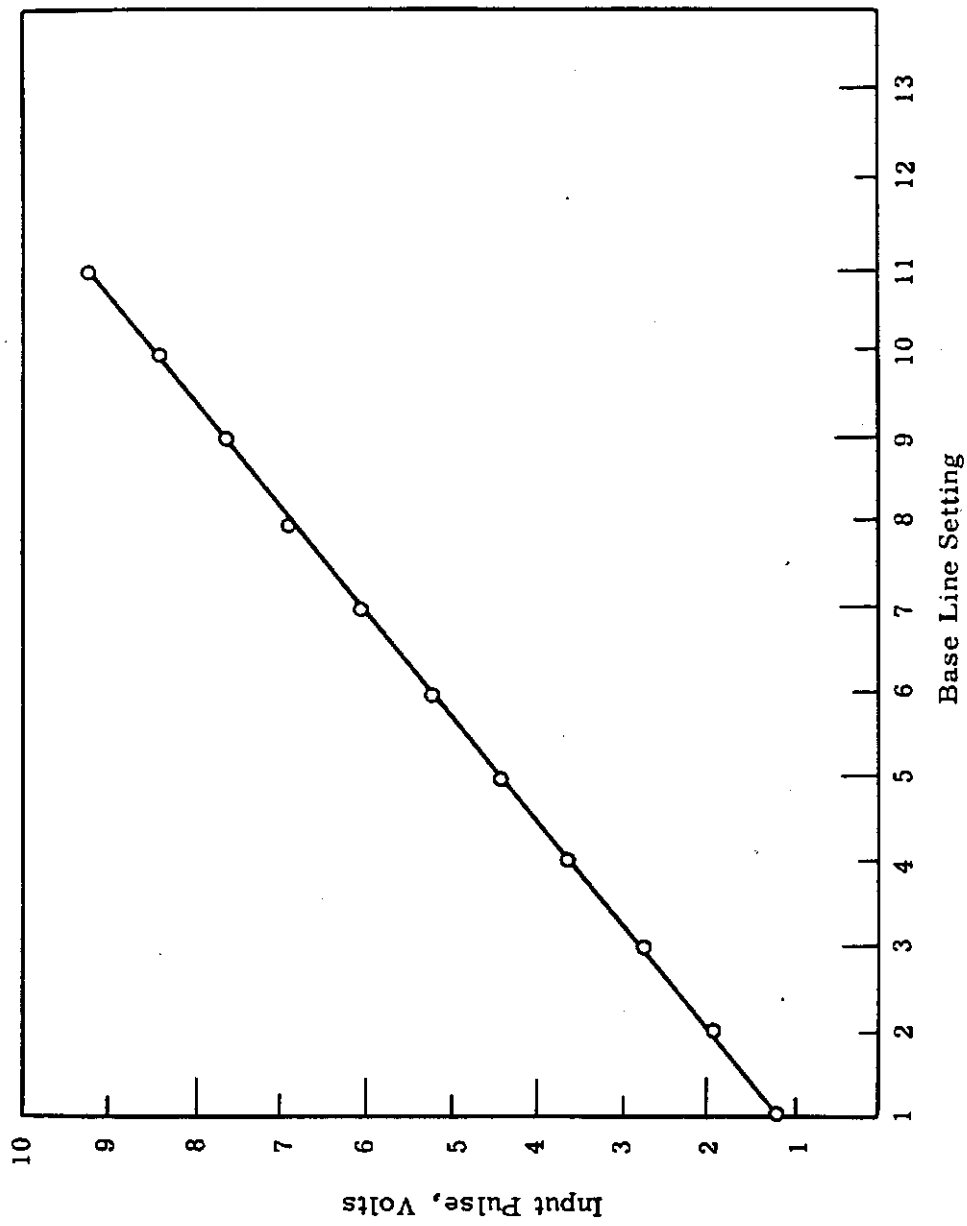

FIGURE 23

Input Pulse Height to Obtain Pulse Output Versus Baseline Setting

Radiation Monitoring Instrument Annunciators - E. M. Sheen

An annunciator, producing a standing sound wave in a short closed pipe, was developed for use with portable radiation monitoring instruments. The annunciator uses the output voltage pulse, which normally energizes the standard headphones, to drive the transistorized circuit, and this provides an audio output tone for a nominal period of 50 msec/trigger pulse. The frequency of the note is approximately 3 kc, and the note sounds like a gated whistle. As the counting-rate increases, the audio output changes from discrete, gated notes to a modulated 3 kc tone at about 600 pulses/min. Above 3600 pulses/min the output changes to a continuous note. The annunciator aural output is adequate for a high background noise area. For applications where larger volume speakers are required, a weatherproof magnetic "howler-type speaker" can be substituted for the smaller resonant column unit. A higher powered circuit is described which is suitable for use with line-operated monitoring instruments in high ambient noise locations.

Figure 24 shows the circuit diagram for a pulse triggered tone generator used with portable battery-powered instruments. This circuit requires approximately 2 ma of current at 10 to 12 VDC at high pulse repetition rates. At very high pulse rates, the output tone becomes a modulated continuous audio level. This circuit was satisfactorily temperature tested from 0 to +150 F (the frequency will shift slightly at low temperatures due to decrease of the mercury cell terminal voltage).

In Figure 24, transistors Q_1 and Q_2 form a monostable multivibrator with Q_1 normally saturated into full conduction or on. Transistor Q_1 is held on by the base current through resistor R_1 from B^+. Transistor Q_2 is normally nonconducting or off because its base voltage is clamped to ground by resistors R_3 and R_4. Resistor R_3 couples the positive collector pulse of Q_1 to the base of Q_2 after an input pulse to the base of Q_1. The input pulse must be greater than a negative 1 volt in magnitude and 1 msec wide or wider. Capacitor C_2 starts discharging through the loop network

composed of C_2, R_5, Q_2, and diode D_1 after input pulse, and this discharge clamps the base voltage of Q_1 at zero and holds Q_1 off during the discharge which saturates Q_2 on. The collector voltage of Q_2 is essentially zero during the discharge time period and B^+ voltage appears across the two bases of the double-base diode Q_3, a General Electric 2N489 Unijunction transistor, and it also appears across resistor R_7 and the potentiometer P_1. Capacitor C_3 charges from B^+ through R_7 in series with P_1 and discharges periodically through the emitter of Q_3. The sawtooth voltage is coupled to the base of an audio amplifier, Q_4, through capacitor C_4, and the frequency, which is controlled by P_1, is tuned to the mechanical resonance frequency of the "howler" unit, M_1, or to the resonant frequency of the closed-end pipe. Capacitor C_5, across M_1, is used for L-C tuning to provide an approximate sinusoidal collector wave form of Q_4. Capacitor C_6 provides an AC bypass across R_{10} which is used for thermal stability, and resistors R_8 and R_9 provide bias voltage and current for Q_4.

The high-level tone generator circuit diagram for line-operated radiation instruments is shown in Figure 25. The action of transistors Q_1 and Q_2, the monostable multivibrator, is the same as previously described. A single transistor audio oscillator composed of R_6 to R_8, L_1, C_3, C_4, and Q_3 is the load for the normally off transistor, Q_2, of the monostable multivibrator. This circuit generates a 45 msec audio tone for each input pulse of 1 μsec or greater width and 1 volt or more in magnitude. The audio tone is direct-coupled through P_1 and R_9 to the base of the audio amplifier power transistor Q_4. The collector load of Q_4 is transformer T-1 which drives the same type of weatherproof "howler" used for the circuit of Figure 24. The output volume is controlled by P_1. Inductor L_2 provides a low resistance DC path to hold Q_4 cut off except during the tone generation period. The silicon diode D_2 prevents base to emitter reverse bias voltages greater than 1 volt at Q_4. The frequency is adjusted by varying L_1. This circuit will provide high aural power outputs considering the compact size and number of components. The circuit has been temperature tested, and will operate properly from 0 to +130 F.

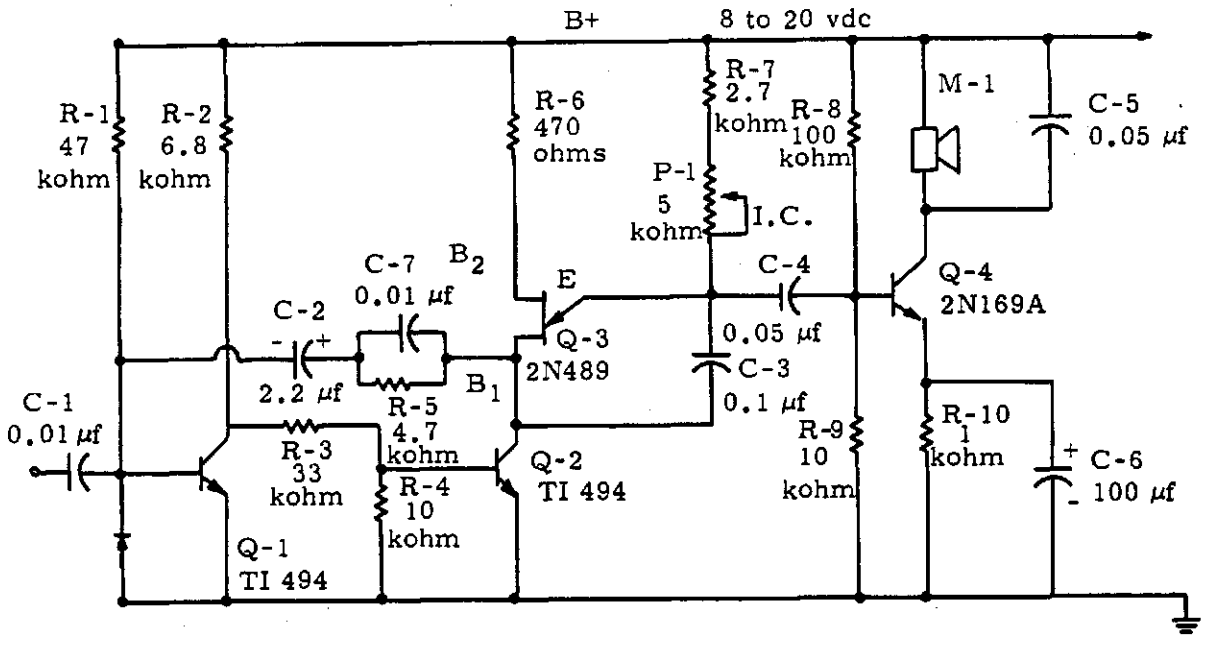

1. All Resistors are 1/4 watt, ± 10 Percent, Composition
2. Capacitors C-1, C-5, and C-7 are Ceramic; C-2 and and C-6 are Tantalum; C-3 and C-4 are Metallized Paper.
3. Input Pulse is -1.5v and 1 μsec or Greater.
4. M-1 is a United States Instrument Corporation type VA-1614-9, or Telex type HFX-91 with 1/2 inch Diameter by 1 M inch long Closed end Resonant Column.

FIGURE 24

Diagram For Low-Power Annunciator

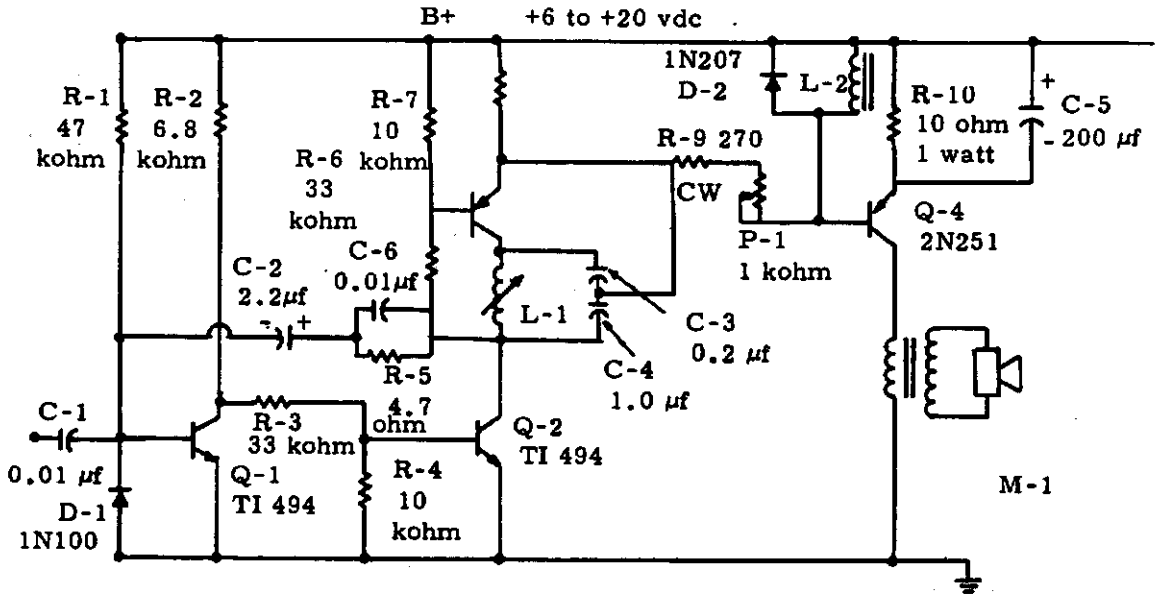

1. All Resistors 1/4 watt ± 10 Percent Composition Except as noted.
2. C-2 and C-5 are Tantalum; C-1, C-3, and C-4 are metallized Paper.
3. L-1, is a UTC Type HVC-3; L-2 is a 3-Henry Choke
4. P-1 is a 1-K, 2-Watt Volume Control
5. T-1 is a Stancor-Type P-6469
6. M-1, United States Instrument Corporation Type UA-1614-9

FIGURE 25

Diagram For High Power Annunciator

Figure 26 shows a photograph of a self-powered annunciator which utilizes a closed-end resonant column speaker, and is suitable for use with portable radiation survey instruments that normally do not provide aural output.

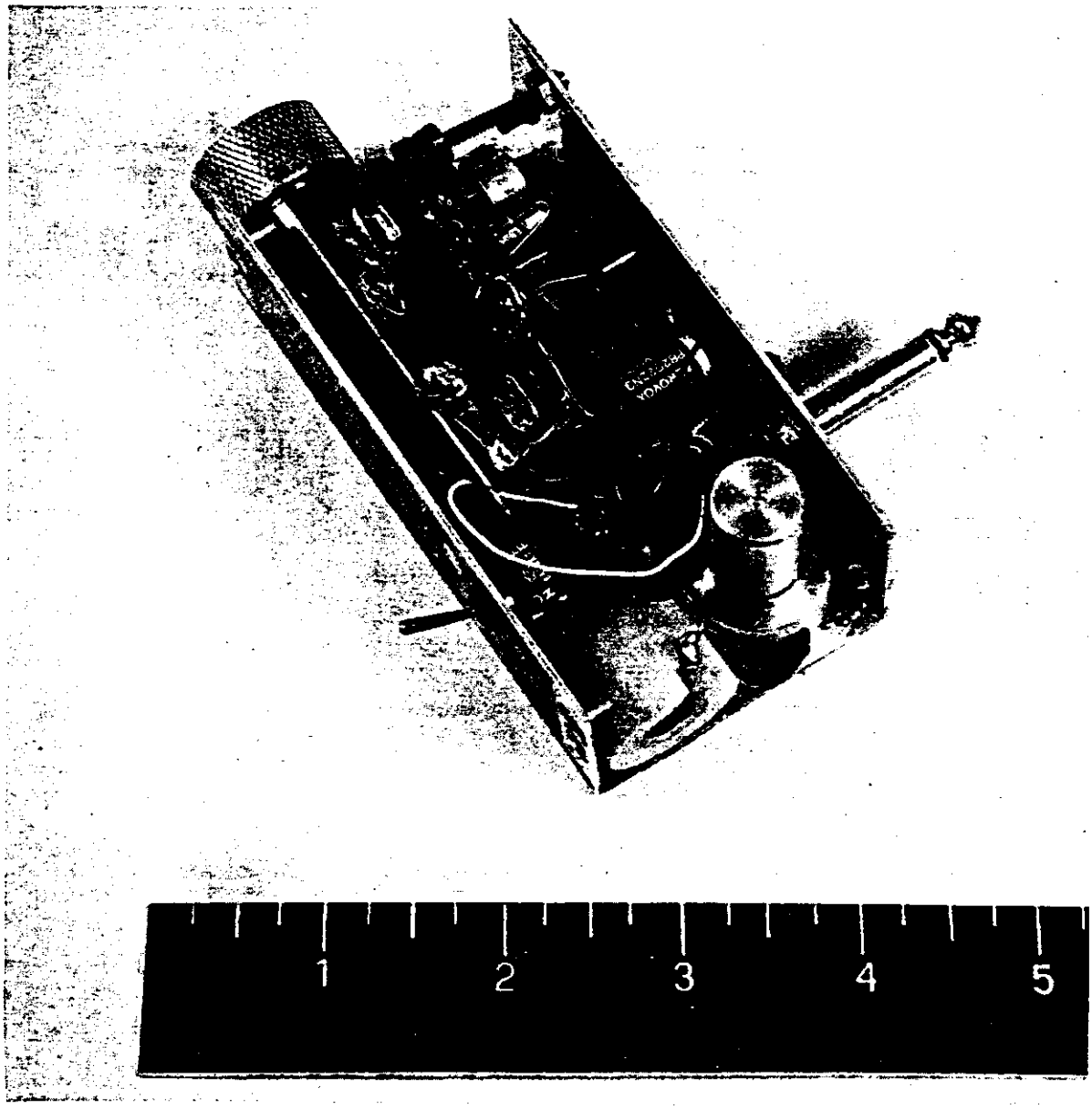

FIGURE 26
Prototype Annunciator

Hand and Shoe Radiological Monitor Development - W. G. Spear

A scintillation beta-gamma monitor for counting hands, shoes, and clothing was developed and fabricated. This prototype, transistorized unit compensates for general gamma background. For a background level of about 1 mr/hr, the hand probes can detect and cause alarms to be energized for a 22,000 dis/min Ra D-E-F source distributed over a 4- by 8-inch area. The shoe probes, which are more exposed, have one-half the sensitivity of the shielded hand probes. The system is linear and a background level of only 0.1 mr/hr would permit reliable alarming at one-tenth the radionuclide source value listed.

A second transistorized combination instrument (alpha-beta-gamma hand and shoe) in prototype use at Hanford was modified with developed discriminator and scaling circuits to provide better alpha detection sensitivity. This instrument, developed for use in gamma backgrounds of 0.1 mr/hr or less, has beta-gamma sensitivities similar to the other instrument and will indicate three times the normal reading levels for a 200 dis/min Pu^{239} alpha source distributed over a 4- by 8-inch area.

Figure 27 shows the circuit diagram for the gamma background compensating monitor used for beta-gamma detection on hands, shoes, and clothing. Two scintillation detectors are used for monitoring each hand and the two output signals are summed. One detector is used for each shoe and the other two shoe probe signals are added for a single presentation. A cable-connected scintillation beta-gamma probe is attached to the instrument for clothing and object monitoring with presentation both aurally and by count-rate-meter. A single fixed scintillation probe is attached to the instrument to provide the required background level signal used for subtraction or compensation. This probe and its electronics channel can also energize appropriate alarms to indicate a background level excursion and can drive a recorder.

The hands, shoes, and background channels employ identical electronics. A six-transistor amplifier is used in each of the five channels. Each main channel has a two-transistor, 1 ma count-rate-meter circuit

with selectable ranges of 3000, 10,000, and 30,000 counts/min full scale. In general operation, depending upon the gamma background level, the four count-rate-meters are switched to the same ranges. The background channel CRM drives a contacting-meter which contains two spdt 10 ampere relays having trip-points selected by meter-face controls. The three main channel CRM circuits use standard meter readout.

All four CRM circuits have potentiometers from meter to ground to provide appropriate voltage signal levels for compensation purposes. The potentiometer voltage levels, proportional to the particular counting rate, are coupled to sensitive 25 μa contacting-meters, termed difference meters, which incorporate one spdt power relay with the trip level controlled by a meter-face knob. The difference meters for right and left hand and shoes channels are connected between the hands and shoes CRMS and the general background CRM. The potentiometers for the four channels are adjusted to compensate for the particular background level. When properly adjusted, the sensitive difference meters read slightly upscale from zero. The adjustments are made so that, as the background level fluctuates within each of the three available basic CRM ranges, the sensitive meter net readings remain slightly upscale with fluctuations of about ± 15 percent of full scale. If beta-gamma contamination equivalent to 22,000 dis/min of Ra D-E-F is introduced into a hand assembly while the instrument is operating in a general background level of 1 mr/hr, the CRM will rise in counting rate, the voltage level at the potentiometer will increase, and current will flow through the appropriate sensitive contacting-meter coil to cause a major upscale deflection. Such a source will cause the meter to exceed the alarm set-point, which is generally set at about one-half to three-fourths of full scale. As the set-point is exceeded, the incorporated spdt relay will close to provide a visual alarm light or audible signal, if desired. For the corresponding shoe probes, this alarm sensitivity level is about 44,000 dis/min of Ra D-E-F for a general background level of about

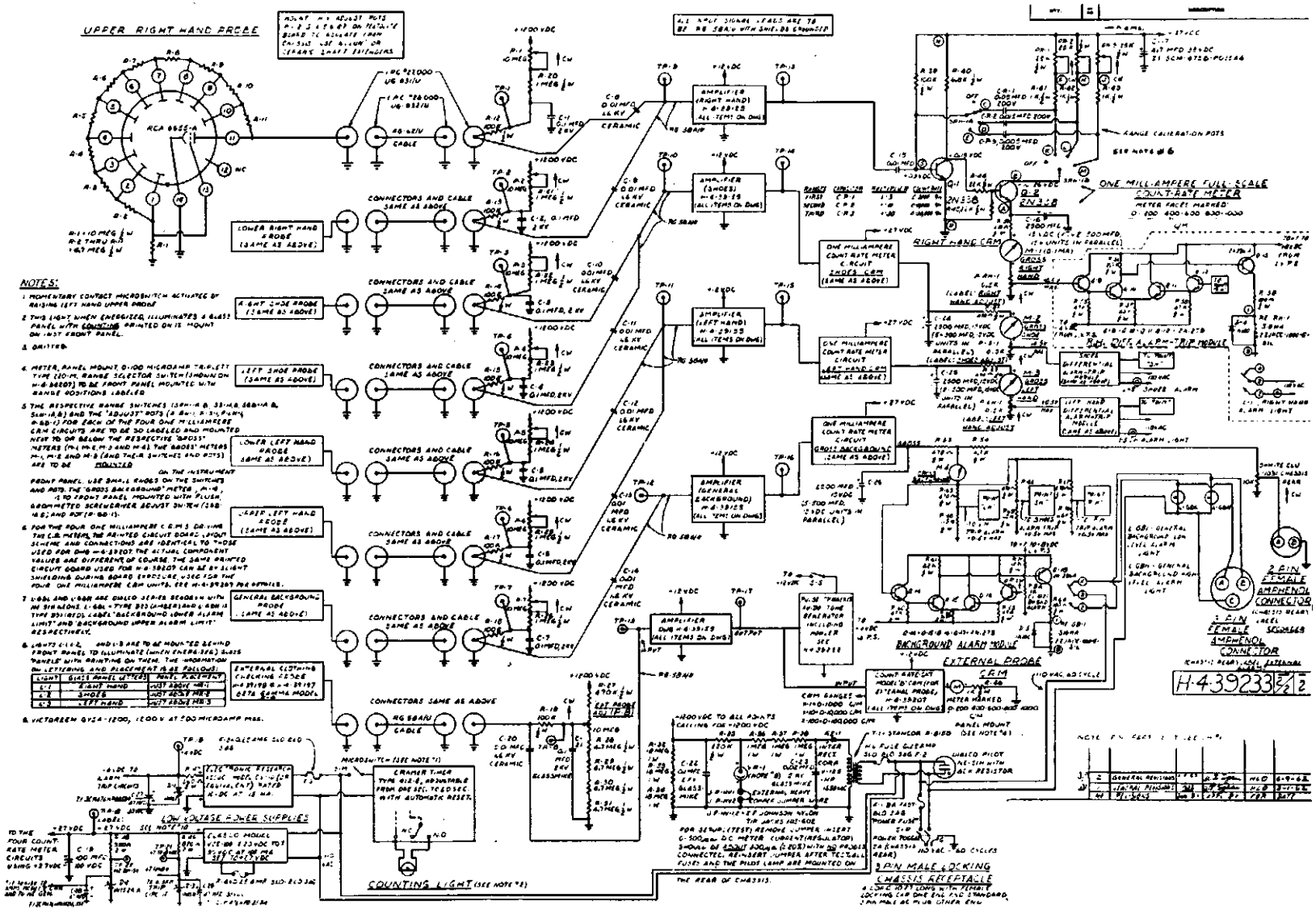

FIGURE 27

Beta-Gamma Hand and Shoe Counter Circuit Diagram

1102771

1 mr/hr. For a background of 0.1 mr/hr, the difference meters alarm-point sensitivities can be set for about 2200 dis/min (Ra D-E-F) for the hand probes and 4400 dis/min for the shoe probes.

In addition to the stated circuits, the cable-connected beta-gamma clothing probe can be used. It drives both a count-rate-meter and a pulse-triggered tone generator (loudspeaker) circuit. A timer is also used in the instrument to indicate to personnel the length of time, generally 15 seconds, to use the instrument. The scintillating material used for all probes is terphenyl-in-polyvinyltoluene (NE-102)* with 0.010 to 0.020-inch-thick sheets of 4- by 8-inch areas for hand probes, 5- by 14-inch areas for shoe probes, and a 2- by 7-inch area for the cabled clothing probe. A 2-inch diameter by 2-inch-long NE-102 cylinder is used for the gamma background probe. With a light-shield covering of three layers of 0.9 mg/cm^2 double-aluminum coated Mylar used on the hand, shoe, and clothing probes, excellent beta sensitivity is obtained, including C^{14} and S^{35}. Other detectors such as halogen-quenched Geiger-Mueller tubes could be used throughout with the transistorized circuits; however, the general performance for the same gamma background would not be as good as can be obtained with the thin scintillators.

The experimental gamma background compensating instrument has successfully performed in field tests for 4 months at Hanford. Standard Hanford drawings have been prepared for the complete instrument. Figure 28 shows a photograph of the prototype instrument being used with the cable-connected probe.

Electronic circuity development and fabrication was also completed on a second type of hand and shoe monitor termed a scintillation transistorized combined alpha-beta-gamma hand and shoe monitor. The general techniques and methods utilized for the detectors and circuits for this monitor were previously developed in basic form;[9] however, progress was made in the past year in improvement of the alpha detection sensitivity and in methods of presentation.

---

* Nuclear Enterprises, Ltd., Winnipeg, Canada

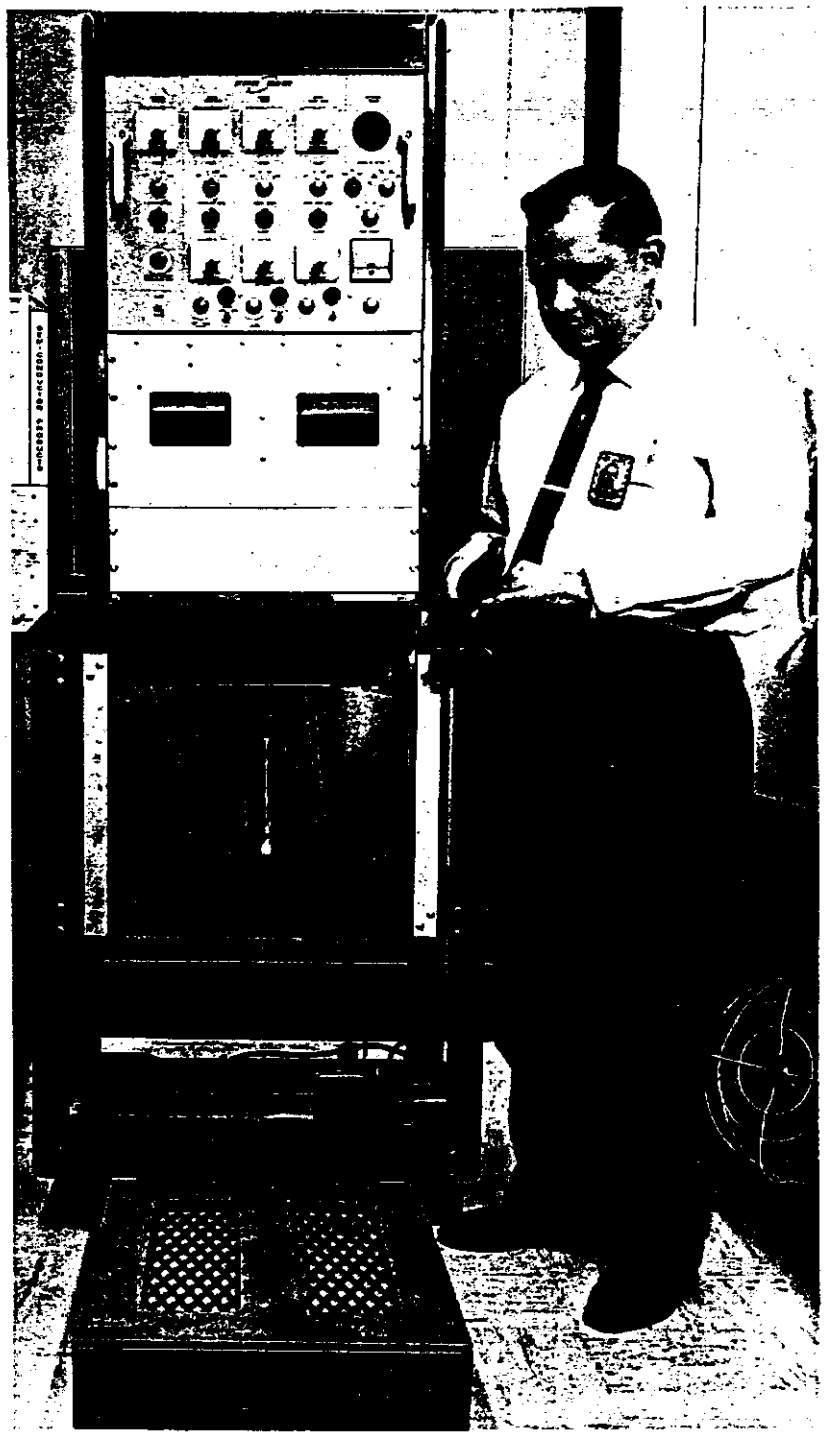

FIGURE 28

Gamma Background Compensated Beta-Gamma Scintillation
Transistorized Hand and Shoe Monitor

AEC-GE RICHLAND, WASH.

The general electronic circuit diagram is shown in Figure 29. The instrument uses combination scintillation detectors for alpha, beta, and gamma detection by the four hand probes. The shoe probes are for beta-gamma detection. An external cable-connected probe is included which can be used, by scintillator selection, for alpha-only or beta-gamma detection. The basic hand probes are mechanically identical to those used for the previously described gamma background compensating monitor for beta-gamma hand and shoe counting, and the shoe probes are completely identical in both instruments. The hand probes of the alpha-beta-gamma monitor use 0.010- to 0.020-inch-thick NE-102; however, the outer surfaces of these scintillator sheets are covered with silver-activated zinc sulfide* for alpha detection. The light shield covering for each hand probe consists of two layers of 0.2 mg/cm^2 aluminum leaf which in turn is covered by one layer of 0.9 mg/cm^2 double-aluminum coated Mylar**.

The two hand probes for each hand drive both a beta-gamma amplifier and a dual alpha amplifier and discriminator. Since the resultant alpha-caused pulses are two to four times the height of the largest beta-gamma caused pulses, the discrimination is relatively simple. Thus, the two amplifiers provide appropriate pulse separation and amplification. The output of the alpha amplifier consists of only alpha-caused pulses which were above the desired discrimination level, whereas the beta-gamma amplifier output includes all pulses. Since the normal pulse rate of beta-gamma caused pulses is several hundred times any alpha-caused pulse rate, the few additional alpha pulses in the beta-gamma channel are quite immaterial. The shoe probes drive a single beta-gamma channel amplifier. The beta-gamma amplifiers drive a series of five binary circuits in each channel to obtain a pulse rate suitable for driving the three electromechanical registers, which are limited in drive-rate to about 10 digits per second.

---

* Alpha decals, "Alpha-Cals", from HAR-D-CAL, Inc., Williston, South Carolina

** Wakefield Industries, Skokie, Illinois

The two alpha-channel amplifiers drive the alpha-decade circuits (transistorized binary-quinary (decade) scalers) which provide signals to drive standard 50 μa meters. As the scaler "counts" progressively, proportional currents are successively added through the meter to move the meter pointer in accurate steps with each step or digit equating to 5 μa. Thus, a scaler "count" of five is indicated as 25 μa or mid-scale. The meter faces aremarked to show 10 segments. This drive and presentation method is both inexpensive and easy to read. Each of the two decade alpha-channel scalers drives an alarm circuit adjusted to alarm at the count of 8 or 40 μa. If the alpha alarms energize, the scalers continue to count progressively in a repetitive fashion.

The external cable-connected probe, used for either alpha or beta-gamma detection on clothing, or objects, drives an amplifier (shown as an alpha type) and an audio-pulse circuit with an indicating triggered tone generator to provide an aural indication of the detected contamination. The monitor also includes a simple high-voltage supply, probe calibration components, various low-voltage supplies, a timer generally set to 15 seconds, register and reset circuits, and alarm units.

Since this monitor does not contain gamma background compensation circuits, the application is for locations where the general background level does not exceed about 0.1 mr/hr. For such a background level, the lead-shielded hand probes will detect and cause indication of twice normal reading for a 22,000 dis/min Ra D-E-F source distributed over a 4- by 8-inch area which is the approximate effective detection area of each of the four hand probes. Since the shoe probes are necessarily less well-shielded, their sensitivities are about one-half that of the hand probes. For lower gamma background levels, the sensitivity is, of course, improved. Each alpha channel has a normal "count" of about two digits in 15 seconds, the regular counting, and will indicate six or more digits for a Pu^{239} source of 200 to 250 dis/min distributed on disks over a 4- by 8-inch area. The usual "alpha warning" levels are generally stated as six digits on the scaler-meter.

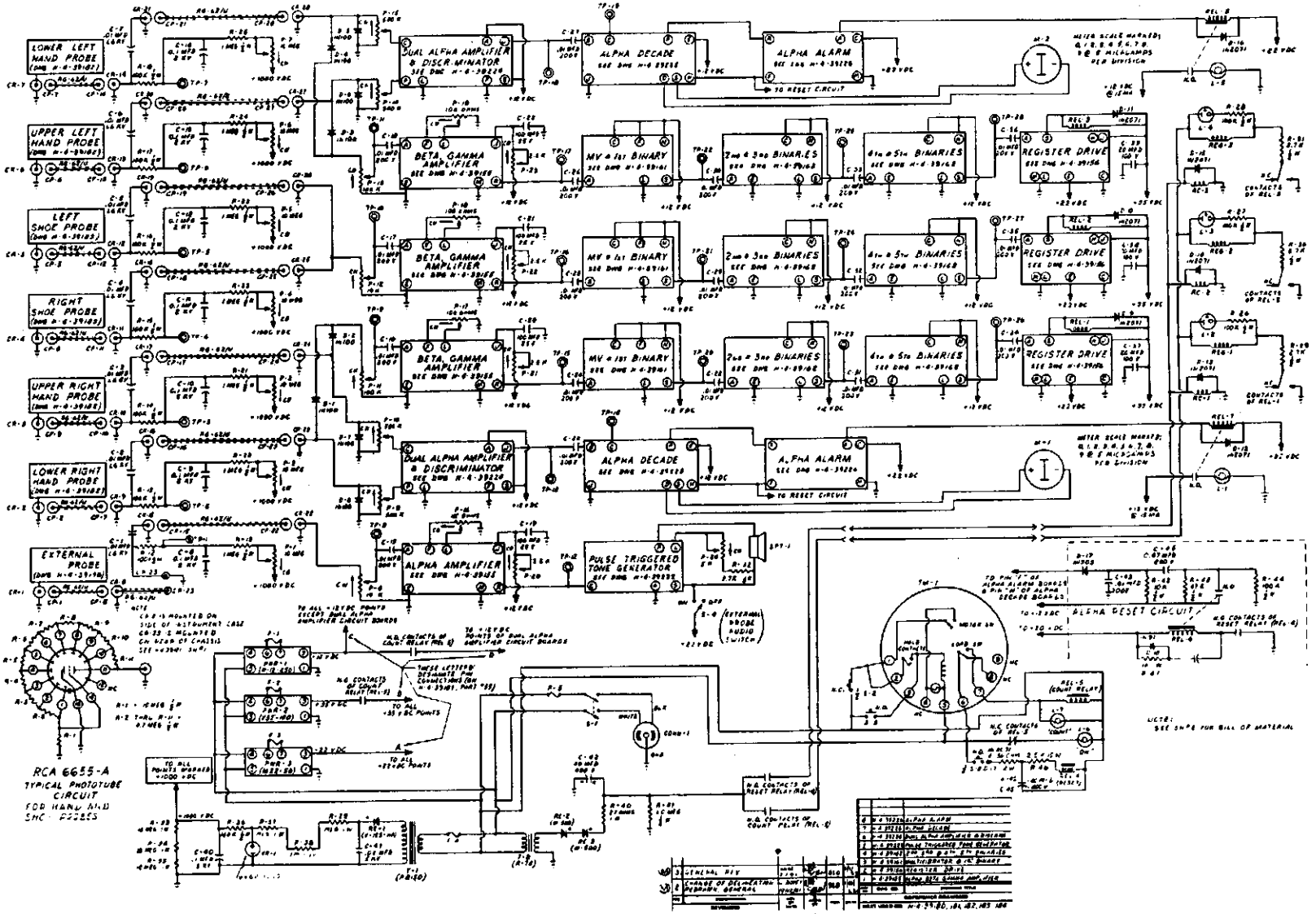

FIGURE 29

Circuit Diagram

1102716

1102777

The prototype combined alpha-beta-gamma monitor has performed satisfactorily for 6 months in Hanford plant tests. Complete drawings have been prepared and approved for all electronic and mechanical portions of the monitor. Figure 30 shows a photograph of the combination instrument. As an added point, the alpha channels of the second instrument can be simply and easily added, with hand probe scintillator changes, to the gamma background compensating beta-gamma monitor to provide another type of combined alpha-beta-gamma hand and shoe monitor with beta-gamma channel background compensation. The two prototypes were purposely devised to permit simple fabrication of such a monitor.

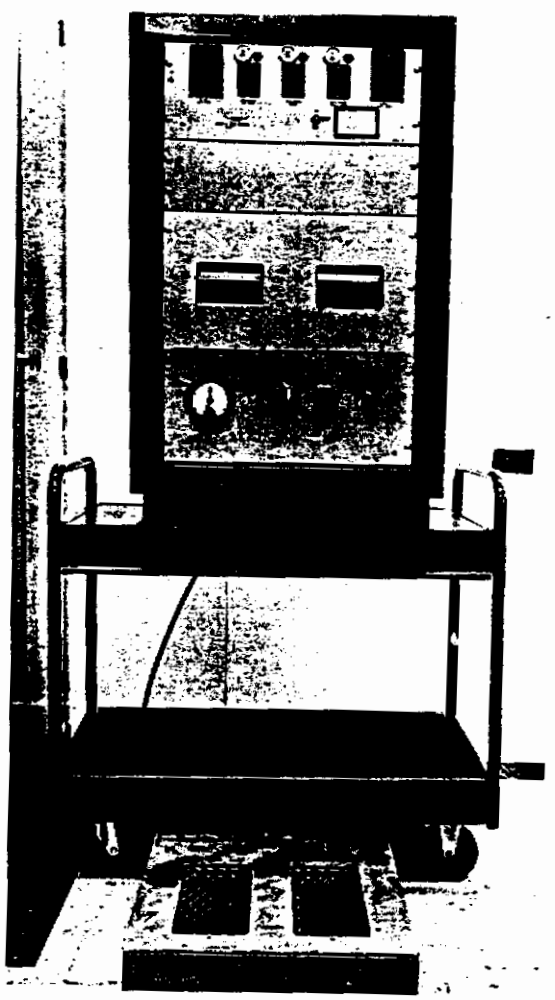

FIGURE 30

Scintillation Transistorized Alpha, Beta, Gamma Hand and Shoe Monitor

Automatic Monitoring and Recording Methods

An Automatic Reader For Personnel Dosimeter Films - C. A. Ratcliffe

An instrument system for automatically reading personnel dosimeter films at Hanford has been fabricated and placed in service. This system consists of a mechanism for transporting and manipulating the film, an optical mechanism to direct light through the film in order to obtain payroll number and optical density information, and electronic circuitry for reading and decoding the payroll information, measuring and digitizing the optical density (dose) information, and controlling the system operation. An IBM printing card punch records the information on a standard IBM card and copies common information, such as date and work area, from card to card.

The block diagram shown in Figure 31 illustrates the system concept used in the instrument. The processing table contains a positioning mechanism, a light source, and a photocell detector head. The mechanism consists of a table, motor, electric clutch, and gears for moving the tray containing the films; a motor, electric clutch, scotch yoke mechanism and clip for taking the film from the tray and inserting it into the light source-photocell head; a microswitch which senses the presence of a tray; a microswitch senses if the tray is in the correct position relative to the films; and a blower to cool the lamp. The light source consists of a lamp, mirror, and collimator. The photocell head contains four photocells for reading the optical density of the film and 20 photocells for gathering payroll number information.

The payroll data from the photocells are suitably amplified and translated for presentation on a payroll number display and for punching onto the IBM card.

The optical density data from the photocells are digitized by an electronic digital voltmeter. The data are accumulated in a temporary storage and then punched onto the IBM card. These data are also presented on the front panel display of the voltmeter.

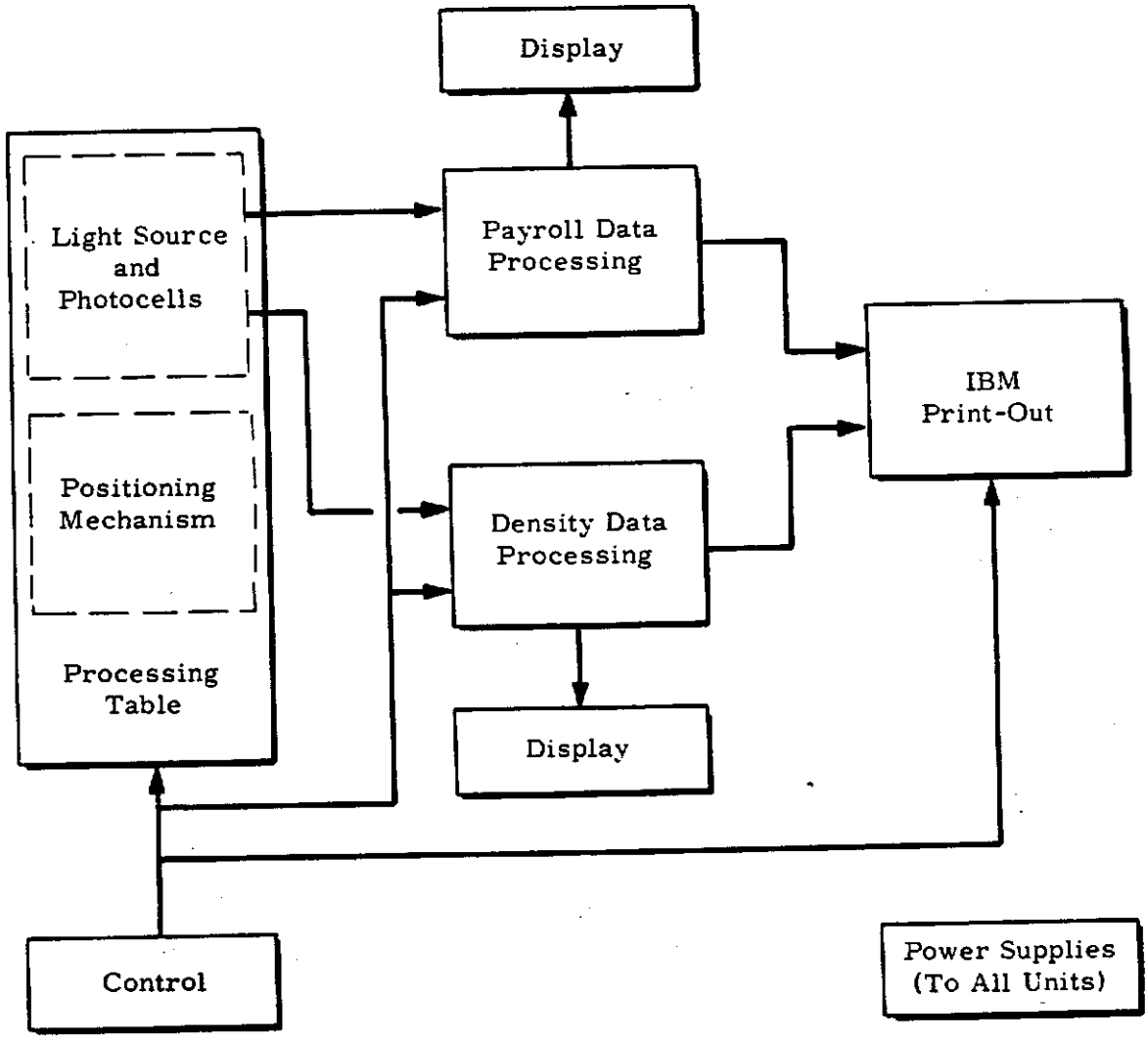

FIGURE 31

Automatic Film Reader System Block Diagram

The control unit governs the positioning of the tray and the films, sequences the translation and display of the payroll number information, sequences the digitizing and display of the optical density information, and governs the card punching of these data by the IBM machine. The control unit also stops the machine at the end of a tray if a film becomes bound in the photocell head, if a nonvalid payroll number appears, or if a radiation overexposure is indicated.

The IBM card punch is programmed to automatically copy common data from one card to the next. Such information is the processing date, work locations of the personnel wearing the film dosimeters, and the production lot number for the dosimeter film.

The project was completed in cooperation with Radiological Development and Calibrations, Radiation Protection Operation. Portions of the system were developed and fabricated by both cooperating groups.

Solar and Sky Radiation Integrator - D. P. Brown and R. A. Harvey

An integrator has been developed which automatically and periodically records the weighted average solar radiation from the previous period. The instrument is used to obtain a measure of the average solar radiant energy per day. This measurement was previously obtained by manual–and often tedious–graphical analysis.

Theoretical considerations involving averaging by passive networks are presented with experimental results which show the accuracy of the instrument.

This article was published in complete detail in the following journal: Bulletin of the American Meteorological Society, Vol. 42, number 5, pages 325 to 332, May, 1961.

REFERENCES

1. Kent, R. A. R. Scintillation Alpha Detection Probes, HW-66837. September 12, 1960.
2. Neher, H. V. "An Automatic Ionization Chamber," Rev. Sci. Instr., Vol. 24, No. 2, 99-102. 1953.
3. Bonfiglioli, G., et al. "Thermoluminescence and F- Centers. I. Theory, II. Experimental," Phys. Rev., 114: 951-960. 1959.
4. Blankenship, J. L. and D. J. Borkowski. "Silicon Surface Barrier Nuclear Particle Spectrometer," Inst. Radio Eng, Transactions on Nuclear Science, Vol. NS-7. September, 1960.
5. Sullivan, M. V. and J. H. Eigler. "Electroless nickel plating for making Ohmic contacts to silicon," J. Electrochem. Soc., 104: 226-230. 1957.
6. Spear, W. G. and L. V. Zuerner. An Experimental Scintillation Dose-Rate-Meter, Model II, HW-55633. June 2, 1958.
7. Slaughter, D. W. "Feedback Stabilized Transistor Amplifier," Electronics, 28: 174-175. May, 1955
8. Spear, W. G. A Sensitive Gamma Scintillation Transistorized Monitor, HW-57507. April 21, 1959.
9. Spear, W. G. A Scintillation Transistorized Alpha-Beta-Gamma Hand and Shoe Counter, HW-60631. July 27, 1959.

INTERNAL DISTRIBUTION

Copy Number	
1	F. W. Albaugh
2	W. J. Bair
3	C. A. Bennett
4	O. E. Boston
5	J. E. Brown
6	L. K. Bustad
7	J. J. Davis
8	I. H. Dearnley
9	R. F. Foster
10	P. A. Fuqua
11	J. J. Fuquay
12	P. F. Gast
13	W. A. Haney
14	F. P. Hungate
15	E. R. Irish
16	W. E. Johnson
17	R. L. Junkins
18	A. R. Keene
19	H. A. Kornberg
20	C. E. Linderoth
21 - 25	J. M. Nielsen
26	W. D. Norwood
27	P. A. Olson
28	R. F. Palmer
29	H. M. Parker
30	R. S. Paul
31	W. H. Reas
32	W. C. Roesch
33	L. C. Schwendiman
34 - 36	R. K. Sharp
37 - 38	W. G. Spear
39	R. C. Thompson
40	M. T. Walling
41	W. K. Woods
42 - 43	Biology Library
44	300 Files
45	Record Center
46 - 220	Extra
221	Technical Publications

EXTERNAL DISTRIBUTION (Special)

Copy Number	
222 - 223	duPont Company, Aiken Attn: W. B. Scott
224	duPont Company, Wilmington Attn: V. R. Thayer
225	G. E. Technical Data Center, Schenectady
226 - 227	Hanford Operations Office Attn: K. L. Englund
228	Hanford Operations Office Technical Information Library
229	Savannah River Operations Office Attn: K. K. Brown
230	U. S. Public Health Service Division of Health Mobilization Washington 25, D. C. Attn: J. J. Lang Acting Chief, Research Branch

EXTERNAL DISTRIBUTION

Number of Copies	
4	Aberdeen Proving Ground
1	Aerojet-General Corporation
5	Aeronautical Systems Division
2	Air Force Special Weapons Center
1	Armed Forces Radiobiology Research Institute
5	Argonne Cancer Research Hospital
10	Argonne National Laboratory
1	Armed Forces Institute of Pathology
4	Army Chemical Center
1	Army Chemical Center (Taras)
1	Army Chemical Corps
1	Army Environmental Hygiene Agency
1	Army Medical Research Laboratory
1	Army Ordnance Missile Command
1	Army Signal Research and Development Laboratory
2	Atomic Bomb Casualty Commission
1	AEC Scientific Representative, France
1	AEC Scientific Representative, Japan
3	Atomic Energy Commission, Washington
4	Atomic Energy of Canada Limited
3	Atomics International
2	Battelle Memorial Institute
1	Borden Chemical Company
2	Brooke Army Medical Center
4	Brookhaven National Laboratory
1	Bureau of Medicine and Surgery
1	Bureau of Ships (Code 1500)
1	Bureau of Yards and Docks
1	Chicago Patent Group
1	Colorado State University
1	Columbia University (Rossi)
1	Committee on the Effects of Atomic Radiation
3	Defence Research Member
1	Defense Atomic Support Agency, Washington
2	duPont Company, Aiken
1	duPont Company, Wilmington
1	Edgerton, Germeshausen and Grier, Inc., Goleta
1	Edgerton, Germeshausen and Grier, Inc., Las Vegas
1	Frankford Arsenal
2	General Dynamics/Fort Worth
2	General Electric Company, Cincinnati
1	General Electric Company, St. Petersburg

EXTERNAL DISTRIBUTION (Contd.)

Number of Copies	
1	General Scientific Corporation
1	Hughes Aircraft Company
1	Iowa State University
1	Journal of Nuclear Medicine
1	Knolls Atomic Power Laboratory
2	Los Alamos Scientific Laboratory
1	Lovelace Foundation
1	Martin-Marietta Corporation
1	Massachusetts Institute of Technology
1	Mound Laboratory
1	National Academy of Sciences
2	NASA Scientific and Technical Information Facility
1	National Bureau of Standards
1	National Cancer Institute
1	National Lead Company of Ohio
1	National Library of Medicine
1	Naval Hospital
1	Naval Medical Research Institute
1	Naval Ordnance Laboratory
1	Naval Postgraduate School
2	Naval Radiological Defense Laboratory
1	New Jersey State Department of Health
1	New York Operations Office
1	New York University (Eisenbud)
1	Office of Assistant General Counsel for Patents (AEC)
10	Office of Naval Research
1	Office of Naval Research (Code 422)
1	Office of the Chief of Research and Development
1	Office of the Surgeon General
2	Phillips Petroleum Company (NRTS)
4	Pratt and Whitney Aircraft Division
2	Public Health Service
1	Public Health Service, Las Vegas
1	Public Health Service, Montgomery
1	Quartermaster Research and Engineering Command
1	RAND Corporation
1	Research Analysis Corporation
1	Sandia Corporation, Albuquerque
2	School of Aviation Medicine
1	Second Air Force (SAC)

EXTERNAL DISTRIBUTION (Contd.)

Number of Copies	
1	Strategic Air Command
1	Strategic Air Command (OS)
1	Surgeon General
1	Union Carbide Nuclear Company (ORGDP)
5	Union Carbide Nuclear Company (ORNL)
1	Union Carbide Nuclear Company (Paducah Plant)
1	United Nuclear Corporation (NDA)
1	U. S. Geological Survey, Denver
1	U. S. Geological Survey, Menlo Park
1	U. S. Geological Survey, Naval Weapons Plant
1	U. S. Geological Survey, Washington
1	U. S. Weather Bureau, Washington
3	University of California, Berkeley
1	University of California, Davis
2	University of California, Livermore
1	University of California, Los Angeles
1	University of California, San Francisco
1	University of Chicago, USAF Radiation Laboratory
1	University of Hawaii
1	University of Puerto Rico
1	University of Rochester
1	University of Tennessee
1	University of Utah
1	University of Washington
1	Walter Reed Army Medical Center
1	Wayne State University
4	Western Reserve University
1	Westinghouse Electric Corporation
1	Westinghouse Electric Corporation (NASA)
325	Division of Technical Information Extension
75	Office of Technical Services, Washington